Vortex interactions with topographic features in geophysical fluid dynamics

David C. Dunn

Ph.D. Thesis
1999

Department of Mathematics
University College London

Supervisors
Prof. E.R. Johnson
Dr N.R. McDonald

ProQuest Number: 10797842

ProQuest 10797842

Abstract

There are regions in the abyssal ocean where sharp topographic gradients occur, for example escarpments, canyons or seamounts. In such regions the contribution of the topography to the ambient potential vorticity dominates over the ubiquitous effects of planetary curvature, and may play an important part in steering abyssal eddies, such as those affecting the dispersal of newly formed bottom water. This thesis studies some models of vortex motion near a topographic escarpment. The topography produces a restoring mechanism for wave generation, and acts as a wave guide, i.e. the topographic wave phase and energy travels parallel to the isobaths with shallow water on the right in the Northern hemisphere. The ratio, S, of the time scale for topographic wave generation to the time scale for the vortex circulation, is a measure of vortex intensity. If the two scales are well separated, i.e. $S \gg 1$ (a weak vortex) or $S \ll 1$ (an intense vortex), analytical progress is made. For a moderate intensity vortex ($S \approx 1$) the wave-vortex interaction is nonlinear and the contour dynamics algorithm is adopted to study the vortex motion in this regime.

In Chapter 1 some examples of geophysical vortices are described, along with their significance. Chapter 2 gives a brief summary of the mathematical preliminaries. Chapter 3 constitutes a review of the relevant work, namely vortex motion over varying topography in quasigeostrophic dynamics. Of interest is vortex motion on the β-plane, since the methods employed in such studies can be adapted for the present work.

In Chapter 4 the results of McDonald (1998) for the motion of an intense singular vortex near an escarpment are extended to cover the full range of vortex intensities. Analytic results indicate that a weak singular vortex moves parallel to the escarpment in the sense of its image in the escarpment. The vortices which travel in the same direction the phase of the topographic waves radiate waves and experience motion perpendicular to the isobath as a result of energy loss. Numerical results for moderate intensity singular vortices show that the motion is characterised by dipole formation. The primary vortex pairs up with an opposite signed patch of relative vorticity which has been produced as a result of cross escarpment advection. An anticyclone located on the shallow side of the escarpment or a cyclone located on the deep side cross the escarpment as a result. A cyclone located on the shallow side of the escarpment or an anticyclone located on the deep side are reflected away from the escarpment.

Chapter 5 is an investigation into the motion of an initially circular vortex patch near an escarpment. It is found that weak vortex patches behave as if the escarpment were a wall. At large times weak vortices which travel in the same direction as the topographic wave phase radiate wave energy, and are destroyed as a result of topographic wave radiation. Analytical results show that an intense vortex patch moves in the same manner as an intense β-plane vortex, i.e. cyclones move along curved northwest trajectories and anticyclones move southwest. Numerical studies for moderate intensity patches show that the motion is again characterised by dipole formation.

Finally, Chapter 6 considers the motion of a singular vortex near a coastal ridge, i.e. an escarpment running parallel to a wall. It is shown that weak vortices behave as if the escarpment were a plane wall. In the cases where the vortex travels in the direction of the topographic wave phase radiate wave energy, and the vortex drifts towards the escarpment as a result. Numerical studies are presented in the cases of intense and moderate vortices.

Contents

Chapter 1

Introduction

Many parts of the oceans and atmosphere are characterised by the presence of strong, isolated, swirling currents, or vortices. These structures exist over a wide range of length scales and are often long lived. Whilst it is not on the Earth, the Great Red Spot of Jupiter has become almost the canonical example of such a vortex in a planetary atmosphere. The Great Red Spot, known to exist since the invention of the telescope in 1610, was first described by Robert Hooke in 1665, and continues to swirl to the present day. Figure (1.1) shows a picture of the Great Red Spot taken in 1979. The Great Red Spot is 14,000 km across in the east-west direction and 40,000 km across in the north-south direction. It swirls anticlockwise and is located in the upper atmosphere in the southern hemisphere of Jupiter, which means that it is an area of high pressure or an anticyclone. Wind speeds in the Great Red Spot are up to 360 km/hour.

In 1961 Raymond Hide described the origin of the Great Red Spot in the popular science journal *Nature* (Hide, 1961). Unlike fluid which is free to move in three dimensions in an arbitrary way, the Jovian atmosphere is confined to a thin spherical shell in which vertical velocities are negligible compared to horizontal velocities. A remarkable feature of such fluids is the emergence of large localised laminar vortices from the background small scale turbulent flow (see e.g. McDonald (1999) and references therein). Figure (1.1) illustrates this well. There are several (smaller) white vortices to the south of the Great Red Spot, and the motion in between is rather turbulent. The longevity of the Great Red Spot is due to opposing shear on the north and south sides, and the rapid rotation of Jupiter which has a day of length 9.6 hours.

The earth's atmosphere and oceans share the quasi two-dimensionality of the Jovian atmosphere and
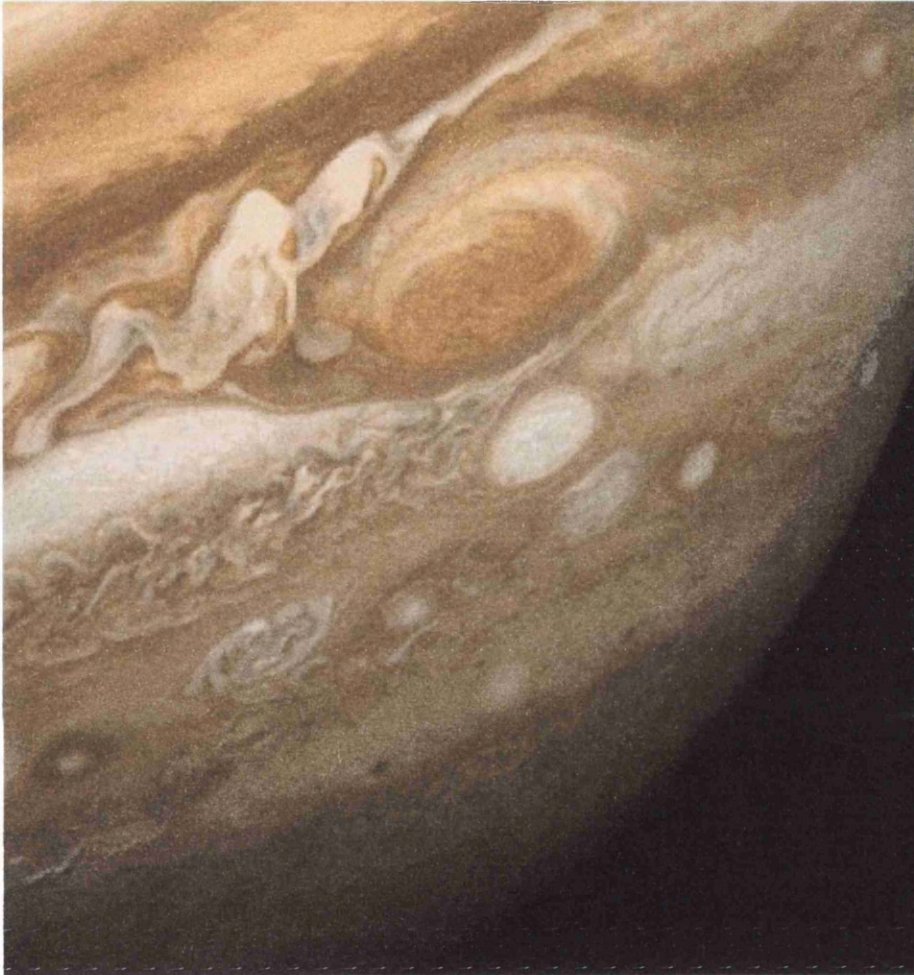
Figure 1.1: The Great Red Spot of Jupiter. The picture was taken by the NASA spacecraft Voyager 1 on 25th February 1979. The bottom of the picture is south and the top is located roughly at the equator of Jupiter.

each gives rise to similar isolated vortices. For example, there is the wintertime polar vortex, located in the stratosphere, and which in effect is isolated from the rest of the atmosphere, enabling the chemistry of ozone depletion to take place (McIntyre, 1995). Tropical cyclones are further examples of intense atmospheric vortices, and which are capable of causing devastation and great cost to human life.

Vortices are equally prolific in the ocean. They are, for example, produced by instabilities in separated intense western-boundary currents. The Gulf Stream is an example of such a current, which spawns vortices when its meandering becomes sufficiently large. These vortices are lenses of anomalous warm water and are known as *Gulf Stream Rings*. Figure (1.2) shows a satellite image of the sea surface temperature off the northeast coast of America. The warm Gulf Stream separates from the western boundary of the Atlantic and its meandering motion is evident. Note the warm rings near the large meander. Gulf Stream rings are typically a few hundred metres deep and 50 to 200 km in diameter. They move southwest in to the surrounding cold water until they interact with the shelf or the Gulf Stream itself. Most of the rings have a lifespan of 1-3 months and are eventually reabsorbed by the Gulf Stream. Similar vortices are shed from the Agulhas current at the tip of South Africa and the Kurushio current off the east coast of Japan.

All of the Gulf, Agulhas and Kurushio rings exhibit a strong surface signature. However oceanic vortices aren't exclusively surface phenomena. For example the Mediterranean salt lenses (*meddies*) are large flat discs which form 1000 m below the surface in the Mediterranean sea and move out into the Atlantic Ocean. Meddies can be 100 km in diameter and about 800 m in vertical extent. Moreover, they have a lifetime of up to 2 years and travel up to 2000 km into the Atlantic ocean - a speed of about 2 cm s^{-1}. Recent evidence also suggests that in the abyssal ocean, deep bottom water formed in the polar oceans is dispersed by vortices rather than continuous currents (see references in McDonald (1999)).

One of the most important characteristics of geophysical vortices is their ability to self propagate on a rapidly rotating planet. Coupled with their longevity this gives vortices the ability to transport passive scalars, such as momentum, salt, heat and biota, over distances much larger than their characteristic size. For example the water, in the core of a meddy is up to $4^{o}C$ warmer than the surrounding Atlantic water and 1 part per thousand saltier; hence meddies are responsible for the dispersal of a large amount of heat and salt throughout the north Atlantic. Similarly Agulhas eddies

7
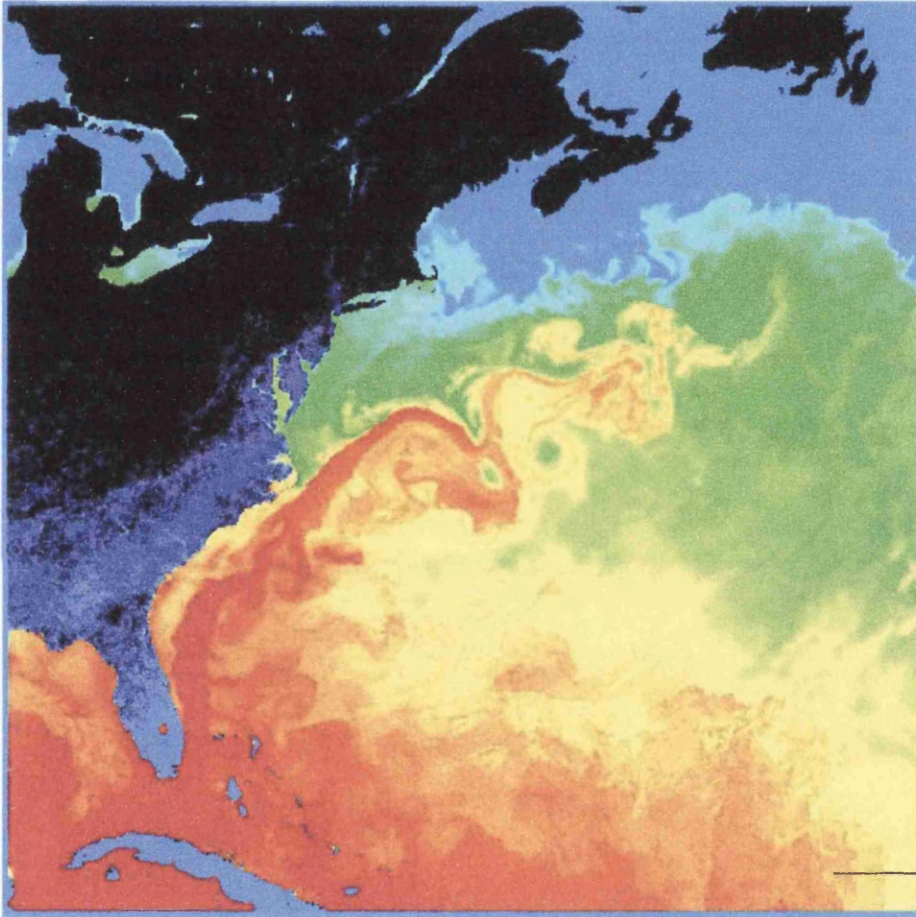
Figure 1.2: Satellite image of a part of the Gulf Stream. See text for further comments.

transport at least 2.2×10^{20}J yr^{-1} of heat and 14×10^{12}kg yr^{-1} of salt from the Indian ocean to the Atlantic ocean. Vortices form an important link in the global circulation of the oceans, and the manner by which they redistribute salt and heat is an important factor in determining the climate and weather. Unfortunately their lengthscales are too small to be resolved by global climate models and so their effects need to be accurately parametrised in such models. It is of considerable importance therefore to understand the behaviour of geophysical vortices through simplified models.

Vortices are also important from an environmental point of view. For example the northern 'wall' of the Gulf Stream meets the Labrador current which brings a high concentration of phytoplankton from the nutrient rich polar waters. In turn this provides a happy feeding ground for fish and larger sea life, and consequently the Nova Scotia and Newfoundland fisheries are rich in marine life. In addition, the water in the Gulf Stream Rings is not only warmer than the surrounding water, but the biology is also different. It has been observed that springtime blooms occur at different times in the warm rings than in the neighbouring cold water. Some of the biota present in the rings originate in the warm Sargasso sea and are not otherwise seen in the cold shelf waters. See Davis and Weibe (1985). At a smaller scale, surf zone vortices near coastlines may be important in the dispersal of pollutants.

As alluded to before, geophysical vortices are not simply pushed around by prevailing currents, but have the ability to self-advect. It is of particular importance to be able to predict the trajectories and longevity of vortices. This is a complex matter since planetary rotation, thermodynamics, shearing currents, neighbouring vortices, friction and bottom topography all contribute to the motion. This thesis examines the effect of sharp topographic gradients on the motion of vortices. Sharp topography exists in the deep ocean and may have a considerable effect on the motion of vortices. For example McDonald (1993) modelled the dispersal of newly formed bottom water from polar regions along mid ocean ridges by cold eddies. The continental slope affects the trajectories of the Gulf Stream rings and the Walvis ridge considerably affects the motion of Agulhas rings. Before proceeding with the study the next chapter presents some of the theoretical background to the present thesis.

Chapter 2

Preliminary considerations

In this chapter and the next some background theory necessary to the present work is considered without derivation. The details can be found in Pedlosky (1979), Chapter 3. In chapters 4 through to 6, quasigeostrophic dynamics of a single layer fluid on an f-plane is modelled. This model ignores the effects of planetary curvature (usually represented by the β-plane), which are assumed negligible, at least locally, compared to the effect of sharp topographic gradients. Vertical structure is trivial, since it is the dynamics of abyssal eddies that are of interest, and the deep ocean can be thought of as a layer of relatively dense fluid lying under an infinitely deep layer of fluid of much lower density. Future work could include the β-effect, more general topography or the effects of stratification. Such work is likely to be numerical in nature. The simple model problems considered in this thesis admit analytical solutions in certain limits. Moreover, when taken in conjunction with existing analytical, numerical and experimental studies of vortex-topography interactions it may be possible to identify some general features of a wide class of geophysical vortex dynamics, an important concern for mesoscale modelling in general circulation models.

2.1   Shallow water theory

In shallow water theory the dynamics of the atmosphere and oceans are modelled by a single "thin" layer of homogeneous (constant density, ρ), inviscid fluid, rotating at constant angular velocity Ω about the vertical z-axis. The motion is governed by the *shallow water equations*, which in a frame of reference rotating with the fluid are

$$\mathbf{u}_t + (\mathbf{u}.\nabla)\mathbf{u} + f\mathbf{k} \wedge \mathbf{u} \;=\; -g'\nabla h \qquad (2.1)$$

$$H_t + \nabla.(\mathbf{u}H) = 0. \tag{2.2}$$

The first equation is the momentum equation, and the second is the equation of mass conservation. Here the dependent variables are $\mathbf{u} = (u, v)$, the horizontal velocity of the fluid, and $H(x, y, t)$, the thickness of the fluid layer. The latter quantity can be written

$$H(x, y, t) = h(x, y, t) - h_B(x, y), \tag{2.3}$$

where h is the deviation of the free surface from its level position at any point and h_B is the equation of the rigid bottom boundary above some reference level $z = 0$. The bottom boundary is called the *topography*. The independent variables are x, y, the horizontal coordinates, and t the time variable which has units

$$T_a = \frac{L}{U}, \tag{2.4}$$

where L is the "appropriate" length scale for horizontal motions with corresponding velocity scale U. Hence T_a is the typical time scale for a fluid particle to move a distance L. In problems involving vortices, choosing L to be the length scale for the vortex and U to be the typical swirl velocity of the vortex, T_a is the typical time for a fluid particle to rotate about the vortex centre. For this reason T_a is sometimes called the *eddy turnover time*. The remaining quantities in the shallow water equations are the *Coriolis parameter $f = 2\Omega$*, discussed later, and $-g'\mathbf{k}$, the acceleration due to the reduced gravity of the fluid. In the context of the abyssal ocean the single layer model can be though of as a layer of relatively dense fluid lying under an infinitely deep less dense upper layer (sometimes called the $1\frac{1}{2}$-layer model), where the interface between the layers is free to deform. Then the reduced gravity is $g' = g\Delta\rho/\rho$, where g is the acceleration due to gravity, ρ is the fluid density and $\Delta\rho$ is the difference in density between the lower layer and the infinite upper layer.

The vertical scales in the derivation of the shallow water equations are D, the typical layer depth and W, the typical vertical velocity. The notion of a thin layer is made precise by insisting that

$$\frac{D}{L} \ll 1, \tag{2.5}$$

i.e. the horizontal length scale is much larger than the vertical length scale. Equation (2.5) is the *definition*[1] of the shallow water model, and it implies that the vertical acceleration is $(D/L)^2$. Thus a particle with initially zero vertical velocity maintains a zero vertical velocity to within small values

---

[1] This constraint implies that the fluid pressure is $p = \rho g(h - z) + p_0$, with p_0 the pressure at the surface, i.e. the hydrostatic approximation. The hydrostatic approximation could also be taken as the definition of the shallow water model. It is this that enables the equations to be written in terms of the fluid depth H, rather than the pressure directly.

of order $(D/L)^2$ compared with the horizontal accelerations. The tendency of the motion of a thin rotating fluid to become strongly aligned with the rotation axis is a famous result, known as the Taylor-Proudman theorem. Taylor (1923) demonstrated that when an obstacle is dragged through a rotating fluid at right angles to the rotation axis, the column initially above the obstacle moves as a column with the obstacle. The "Taylor columns" are a feature of thin rotating fluids, and enable the two dimensional description of the large scale horizontal motions.

The choice of a rotating frame of reference gives rise to an apparent force in the momentum equations, $-f\mathbf{k} \wedge \mathbf{u}$, known as the *Coriolis force*. Importantly the Coriolis force acts at right angles to the direction of the fluid motion, i.e. to the right (left) looking in the direction of the motion in the northern (southern) hemisphere. On the Earth the local horizontal component of the Coriolis force is unimportant, at least in the mid latitudes (e.g. Gill (1982)), and the vertical component varies linearly with the sine of the latitude ϕ. The Coriolis parameter is

$$f = 2\Omega_E \sin\phi, \tag{2.6}$$

where $\Omega_E = 7.292 \times 10^{-5}\text{s}^{-1}$ is the angular velocity of the earth. Taking a fixed latitude ϕ is equivalent to a tangent plane approximation to the curved surface of the planet, and is called the *f-plane*. The *f*-plane describes well mid-latitude motions with only small meridional (i.e. latitudinal) variations.

The Coriolis parameter varies with latitude due to the sphericity of the Earth sphericity. Rossby (1939) developed a model in which the Coriolis parameter varies linearly with latitude in the mid latitudes. In this model, known as the β-plane, f is approximated by linearising about some mean latitude ϕ_0,

$$f = f_0 + \beta y, \tag{2.7}$$

where $f_0 = 2\Omega \sin\phi_0$ and y is the coordinate in the latitudinal direction. The parameter β measures the variation of the Coriolis parameter in the latitudinal direction and is given by

$$\beta = \frac{2\Omega}{r_0} \cos\phi_0, \tag{2.8}$$

where r_0 is the radius of the Earth. The value of β at, for example 30° N, is $1.9 \times 10^{-13}\text{cm}^{-1}\text{s}^{-1}$. The β-plane model has proved to be very useful in understanding the large scale motion of the atmosphere and oceans. The motion of vortices on the β-plane has has attracted considerable attention, and a review is given in the following chapter. It is shown below that the β-plane

13

approximation is equivalent to the f-plane approximation with linearly sloping topography, and for this reason comparison of vortex motion near sharp topographic features with vortex motion on the β-plane is made throughout this thesis.

In shallow water theory there is a physical quantity of such importance that the governing equations can be written as a single conservation law. The *potential vorticity* is

$$\Pi = \frac{\zeta + f}{H}, \tag{2.9}$$

where

$$\zeta = \frac{\partial v}{\partial y} - \frac{\partial u}{\partial x}, \tag{2.10}$$

is the relative (i.e. to an observer in the rotating frame) vorticity, which is aligned with the rotation axis. The potential vorticity is conserved on fluid columns,

$$\frac{D}{Dt}\left(\frac{\zeta + f}{H}\right) = 0, \tag{2.11}$$

where

$$\frac{D}{Dt} \equiv \frac{\partial}{\partial t} + (\mathbf{u}.\nabla) \tag{2.12}$$

is the material or *advective* derivative, which expresses the rate of change of a scalar quantity following a fluid element in its evolution. The conservation law, (2.11) states that relative vorticity is generated due to vortex column stretching (i.e. changes in H) in the planetary vorticity field f as fluid columns move over topographic or Coriolis gradients. This single expression encapsulates the essence of geophysical fluid dynamics. The ubiquitous acquisition of relative vorticity by the fluid is characteristic of the large scale motions of the atmosphere and oceans. Potential vorticity conservation is responsible, for example, for the tendency of sub-inertial frequency (*Rossby*) waves to adopt a preferential westward phase velocity, or for strong circulating cyclonic currents to follow curved northwest paths.[2]

The motion of fluid in the atmosphere and oceans is approximately in a state of so called *geostrophic* balance, i.e. the Coriolis force approximately balances the horizontal pressure gradient. Steady, linearised shallow water motion has velocity components

$$u = -\frac{g}{f}\frac{\partial \eta}{\partial y} \tag{2.13}$$

$$v = \frac{g}{f}\frac{\partial \eta}{\partial x} \tag{2.14}$$

---

[2]This latter statement holds in the northern hemisphere only.

where η is the deviation in the free-surface from its resting value. Thus η is a streamfunction for the flow. Since η is proportional to the fluid pressure, the flow is equivalently along the isobars, which is why the isobars are used as a diagnostic in evaluating the weather.

2.2 Quasigeostrophic motion

The small departures of the fluid motion from purely geostrophic flow are of most interest. To examine these departures the shallow water equations are rescaled, with the assumptions that the free surface deviations and the topographic variations are small with respect to the average layer depth. The equations are then expanded in a series in the *Rossby number*

$$Ro = \frac{U}{fL}, \tag{2.15}$$

which is a small parameter, i.e. interest is focused on motions whose time scale is much larger than the inertial period. Small Rossby number flows in dimensional terms are those that evolve over weeks and months as opposed to hours or days. In the context of vortex motion the Rossby number is the ratio of the inertial period to the eddy turnover time, and is therefore a gauge of the importance of rotation on the vortex evolution. In particular if Ro is of order unity or less then the rotation of the Earth plays an important role in the vortex motion. Typical values of, for example, an Aghulas ring at 35° S are $f = 8 \times 10^{-5}\text{s}^{-1}$, $U = 50$ cm s^{-1} and $L = 80$ km, leading to $Ro \approx 0.1$ (McDonald (1999)).

The derivation is described in detail in Pedlosky (1979), and leads to the conservation law

$$\frac{DQ}{Dt} = 0, \tag{2.16}$$

where the conserved quantity,

$$Q = \nabla^2 \psi - \left(\frac{L}{R_D}\right)^2 \psi + \beta y + Sh_B, \tag{2.17}$$

is the *quasigeostrophic* potential vorticity in the context of a single layer β-plane. Here ψ is a streamfunction for the flow and is proportional to the free-surface deviation or the fluid pressure. The leading order velocity field in this scaling is

$$u = -\frac{\partial \psi}{\partial y}, \tag{2.18}$$

$$v = \frac{\partial \psi}{\partial x}, \tag{2.19}$$

hence the name "quasigeostrophic". The potential vorticity consists of three parts. First, the term $\nabla^2\psi$ in (2.17) is the relative vorticity. The second term $\left(\frac{L}{R_D}\right)^2\psi$ is a contribution due to variations in the free surface elevation, and the parameter L/R_D is the ratio of the horizontal length scale to the *Rossby (deformation) radius*,

$$R_D = \frac{\sqrt{gD}}{f}. \tag{2.20}$$

The Rossby radius is a length scale which arises naturally in the derivation of the quasigeostrophic governing equation. It is the ratio of the gravity wave speed to the Coriolis parameter, and is the length scale on which the relative vorticity and the surface elevation make equal contributions to the potential vorticity, or alternatively, the length scale on which the tendency of the surface to become flat due to adjustment under gravity is balanced by the tendency of the Coriolis effect to deform the surface. It is of great importance in geophysical fluid dynamics, and its presence in (2.17) defines a preferential length scale for the motion. In particular, the free-surface effect of the rotating fluid tends to cause disturbances to decay on distances of the order of the Rossby radius.

These first two terms in (2.17) are due to the relative motion. The remaining terms are present independently of the motion and are therefore called the *ambient potential vorticity*. The variable part of the ambient potential vorticity, $\beta y + Sh_B$ consists of the planetary vorticity field and the topography.[3] Gradients in the ambient potential vorticity provide a restoring mechanism for wave generation. To see this consider the case of $h_B = \text{sgn}(y)$, and $\beta = 0$, so that $y = 0$ is an interface between regions of differing Q, with higher Q lying in $y > 0$. If this interface is deformed as in Figure (2.1), the priciple of conservation of potential vorticity implies that fluid which has moved from shallow water to deep water will acquire positive relative vorticity and fluid which has moved from deep to shallow water will acquire negative relative vorticity. Hence the disturbance propagates with shallow water (i.e. higher ambient potential vorticity) to the right as shown in Figure (2.1).

It should be noted that this 'stiffness' of motion in the direction perpendicular to the ambient potential vorticity gradient is not a consequence of the quasigeostrophic assumption; precisely the same conclusions can be reached by consideration of the shallow water potential vorticity in equation (2.9). In fact, the choice of topography mimics the variation of potential vorticity on the β-plane, increasing in the poleward direction. Potential vorticity waves on the β-plane are known as Rossby

---

[3]It is well known (e.g. Pedlosky (1979)) that the linear variation in the Coriolis parameter is equivalent to a linearly sloping topography on an f-plane. This is apparent even in (2.17), since setting $\beta = 0$ and $h_B = \beta'y$ is equivalent to rescaling $\beta = S\beta'$ over flat topography. This fact enables the β-plane to be modelled in a rotating, sloping bottomed tank in a laboratory. Throughout this work comparisons will be made with vortex motion on the β-plane.
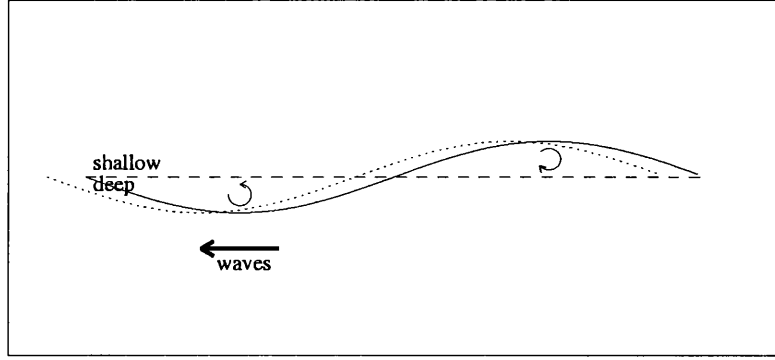
Figure 2.1: The generation of waves by redistribution of ambient potential vorticity. The waves propagate with higher ambient potential vorticity to the right.

waves. Such waves exist whenever there is a gradient in the potential vorticity. Since this occurs for background sheared currents and variable topography as well as the meridional variation of f, potential vorticity waves are ever-present in the atmosphere and oceans.

Furthermore, the swirl velocity of a vortex will cause redistribution of the background potential vorticity leading to relative vorticity production. The secondary currents associated with this process will in turn affect the motion and longevity of the vortex - indeed potential vorticity conservation lends vortices the ability to self propagate. The dimensionless parameter S in (2.17) is a measure of the strength of this interaction, and can be written as a ratio of time scales

$$S = \frac{L/U}{\delta^{-1}f^{-1}} = \frac{T_a}{T_w}. \tag{2.21}$$

Here T_a is the eddy turnover time and δ is the change in the fractional height of the topography over the horizontal length scale[4]. Relative vorticity is produced due to vortex column stretching on the time scale $T_w = \delta^{-1}f^{-1}$, the *topographic vortex stretching time* and is the time scale on which this process of wave generation proceeds. For this reason T_w is also called the *topographic wave time scale*. Note that S can also be rewritten

$$S = \frac{\delta}{Ro}. \tag{2.22}$$

In either form S describes the relative importance of advection and topographic wave generation. Both δ and Ro are small parameters in quasigeostrophic theory, but their ratio S can take on the whole range of values. In vortex-topography interactions S is a measure of vortex intensity. For

---

[4]Note that elsewhere in the text $\delta()$ refers the delta-function. The meaning should be clear from the context.

$S \ll 1$ the vortex is said to be *intense,* since relative motion due to the swirl velocity of the vortex dominates over topographic wave generation. For $S \gg 1$, wave production occurs on a much faster time scale than advection by the vortex, and the vortex is said to be *weak.* In these two cases where the time scales are well separated, leading order solutions to initial value problems are often available. If, however, $S \approx 1$, then the interaction between the vortex and the waves is nonlinear and numerical solutions must be sought.

Throughout this thesis it is assumed that $\beta = 0$ and $h_B \neq 0$, i.e. the β-effect is negligible compared to the variation in topographic gradients. Of particular interest is the interaction of vortices with sharp (discontinuous) topographic gradients. In the following section the vortex models to be considered are presented.

2.3 Quasigeostrophic vortices

There are two models of vortices used in this work. The first is a singular vortex solution to the flat bottomed f-plane equations, and the second is a circular patch of uniform relative vorticity. These two solutions are related in the sense that a singular vortex model is often touted as a good approximation to a uniform patch of relative vorticity. As will be seen this is a reasonable assumption, at least far from the vortex centre, since both types of vortex have the same velocity profile in the far-field. From here onwards the unit of length is taken to be the Rossby radius.

2.3.1 Singular vortices on the f-plane

Singular vortex solutions appear to have been first obtained by Morikawa (1960). In the absence of topography ($h_B = 0$) and for $\beta = 0$, the conservation of potential vorticity equation (2.17) implies

$$\frac{\partial}{\partial t} \left(\nabla^2 \psi - \psi \right) = 0, \tag{2.23}$$

where the horizontal length scale has been taken to be the Rossby radius, i.e. $L = R_D$. To obtain a singular vortex solution to (2.23), suppose that at time $t = 0$, the potential vorticity distribution is given by a delta function at the origin,

$$\nabla^2 \psi - \psi = -\frac{\Gamma}{2\pi r} \delta(r), \tag{2.24}$$

18

where r is the radial distance from the origin. Equation (2.24) is radially symmetric, and away from the origin is the modified Bessel equation of order zero.

$$\frac{1}{r}\frac{\partial}{\partial r}\left[\frac{1}{r}\frac{\partial \psi}{\partial r}\right] - \psi = 0. \tag{2.25}$$

The general solution is (e.g. Abramowitz and Stegun (1972))

$$\psi(r) = AK_0(r) + BI_0(r). \tag{2.26}$$

where K_0 and I_0 are the modified Bessel functions of the first and second kind, zeroth order respectively. Since I_0 grows exponentially with its argument, solutions which remain localised must have $B = 0$. The coefficient A is determined from the circulation around the origin. The azimuthal velocity is

$$v_\theta = \frac{\partial \psi}{\partial r} = -AK_1(r), \tag{2.27}$$

where K_1 is the modified Bessel function of the first kind, first order. Hence the circulation of velocity around a small circle containing the origin is

$$\Gamma = -\lim_{r \to 0}\int_0^{2\pi} v_\theta r d\theta = \lim_{r \to 0}\int_0^{2\pi} AK_1(r)r d\theta. \tag{2.28}$$

But, $\lim_{r \to 0} K_1(r) = 1/r$, so that

$$\Gamma = \int_0^{2\pi} A d\theta = 2\pi A, \tag{2.29}$$

i.e. $A = \Gamma/2\pi$. Hence the streamfunction for a singular vortex of strength Γ at the origin is

$$\psi(r) = \frac{\Gamma}{2\pi}K_0(r), \tag{2.30}$$

The sign of Γ gives the sense of the circulation. For $\Gamma > 0$ it is clockwise (anticyclonic in the northern hemisphere) and for $\Gamma < 0$ it is positive (cyclonic). The streamlines are circular, and due to the exponentially decaying nature of the modified Bessel function are bunched near the vortex centre; this simple vortex model captures the essential effect of the free surface in rotating flows, i.e. disturbances remain localised, diminishing exponentially on the scale of the Rossby radius[5].

The angular velocity of the vortex is

$$b(r) = \frac{v_\theta}{r} = \frac{\Gamma}{2\pi r}K_1(r). \tag{2.31}$$

---

[5]It should be noted that a singular vortex violates the quasigeostrophic assumption since the amplitude of the free surface deformation becomes infinite at the vortex centre. Moreover the horizontal velocities also become infinite at the vortex centre implying that the Rossby number is of the order of unity near the vortex. These violations aren't considered important outside of a small neighbourhood of the vortex.

Figure (2.2) shows a plot of the angular velocity profile of the singular vortex. For $r \ll 1$, the small argument form for the modified Bessel functions (e.g. Abramowitz and Stegun (1972)) gives

$$b(r) \approx \frac{\Gamma}{2\pi r^2}, \qquad (2.32)$$

so that near the origin the quasigeostrophic singular vortex induces the same velocity as the barotropic[6] singular vortex of the same strength. On the other hand for large values of r the asymptotic expansions for the modified Bessel functions give, to leading order,

$$b(r) \approx \frac{\Gamma}{2\pi r} \sqrt{\frac{\pi}{2r}} e^{-r}. \qquad (2.33)$$

Thus, the velocity field due to the quasigeostrophic singular vortex decreases *exponentially* with distance, on a scale of the Rossby radius, as opposed to the geometric decay in the case of the barotropic vortex. Finally, the sign of Γ is the same as the sign of ψ, so cyclones (resp. anticyclones) correspond to a depression (raising) of the free surface. This is in keeping with oceanic cold (warm) core rings which are cyclonic (anticyclonic) and have depressed (raised) profiles.

2.3.2   A circular patch of uniform relative vorticity

In the absence of topography ($h_B = 0$), a circular patch of uniform relative vorticity centred at the origin has

$$\nabla^2 \psi_0 - \psi_0 = -\alpha H(a - r), \qquad (2.34)$$

where a is the patch radius, $H(z)$ is the unit Heaviside step function and α gives the sense of the circulation. For $\alpha > 0$ it is clockwise (anticyclonic) and for $\alpha < 0$ it is anticlockwise (cyclonic). The streamfunction $\psi_0 = \psi_0(r)$ is radially symmetric. For $r < a$ equation (2.34) is an inhomogeneous modified Bessel's equation of order zero. Solutions which are bounded at the origin have the form

$$\psi_0(r) = \alpha(1 + AI_0(r)), \quad r \leq a. \qquad (2.35)$$

For $r > a$ (2.34) is the homogeneous Bessel's equation of order zero, and has solutions which vanish in the far-field (i.e. the vortex is localised),

$$\psi_0(r) = \alpha B K_0(r), \quad r > a. \qquad (2.36)$$

---

[6]The barotropic approximation is obtained by taking $R_D \to \infty$ in (2.17), and in the absence of topography $\nabla^2 \psi =$ constant is an exact solution. Alternatively by imposing a rigid lid on the fluid the same is true, except ψ is a mass transport streamfunction, $\psi \propto \log r$. For details regarding the dynamics of barotropic singular vortices see e.g. Aref et. al. (1988)
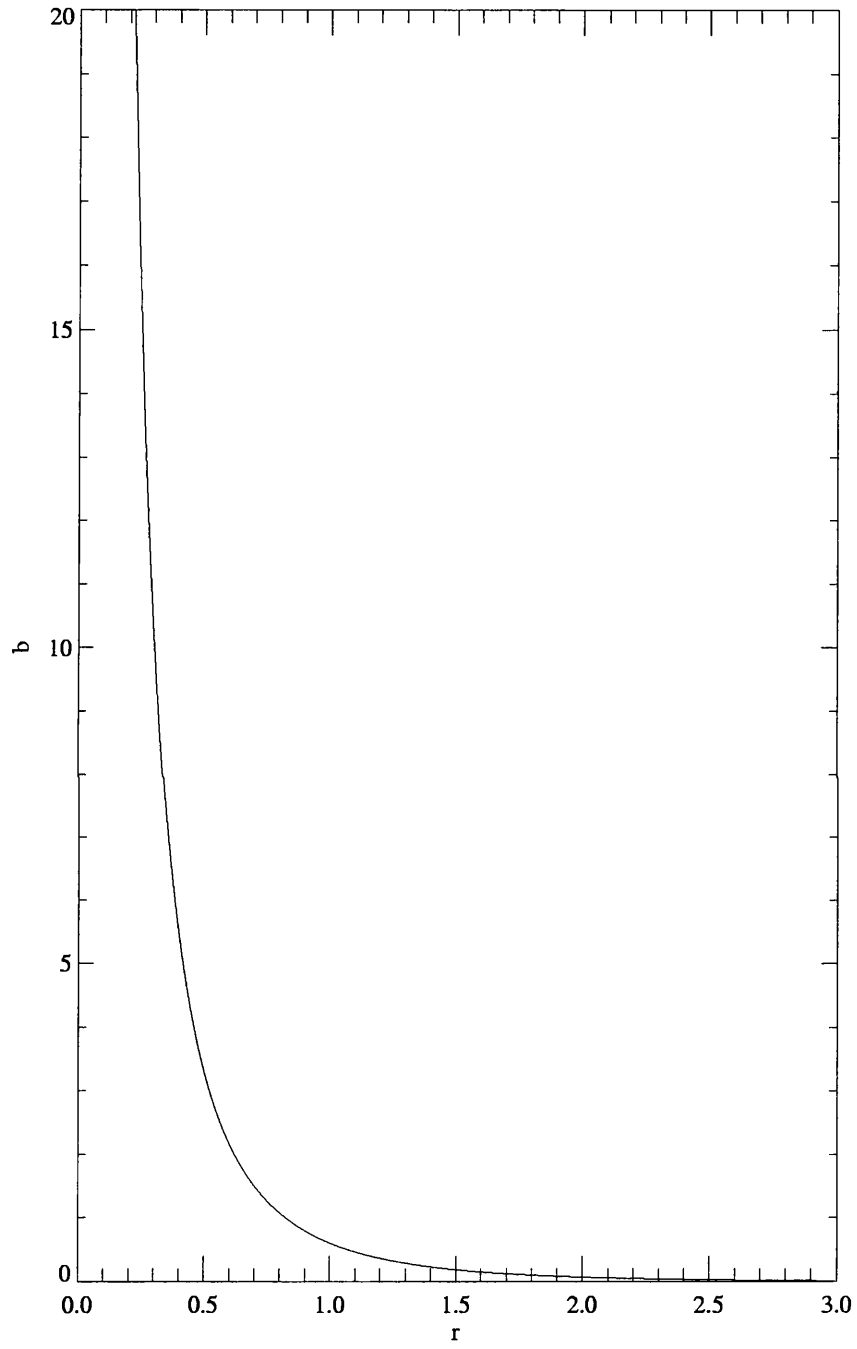
Figure 2.2: Profile of the angular velocity, $b(r)$ of a singular vortex with strength $\Gamma = 1$. Note the rapid decay with e-folding length 1, or in dimensional terms, R_D.

The constants A and B are determined by requiring that ψ_0 and its radial derivative $\partial \psi_0 / \partial r$ are continuous on the patch boundary $r = a$. Making use of the Wronskian for the modified Bessel equations (e.g. Abramowitz and Stegun (1972)),

$$I_n(z) K_{n+1}(z) + I_{n+1}(z) K_n(z) = \frac{1}{z}, \tag{2.37}$$

the solution is

$$\psi_0(r) = \begin{cases} \alpha - \alpha a K_1(a) I_0(r), & r \leq a \\ \alpha a I_1(a) K_0(r), & r > a \end{cases} \tag{2.38}$$

The angular velocity of the vortex patch, required later is

$$b(r) = \frac{1}{r} \frac{\partial \psi_0}{\partial r} = \frac{1}{r} \begin{cases} -\alpha a K_1(a) I_1(r), & r \leq a \\ -\alpha a I_1(a) K_1(r), & r > a \end{cases} \tag{2.39}$$

Figure (2.3) show plot of the profiles of the streamfunction and the angular velocity.

The singular vortex is often used as an approximation to a uniform vortex patch. There are two ways to conceive of this approximation. First, if the motion in the far field is of interest then a singular vortex with strength $\Gamma = 2\pi \alpha a I_1(a)$ has the same swirl velocity as a circular vortex patch of radius a. Alternatively,

$$\lim_{a \to 0} \alpha a I_1(a) = \alpha \frac{a^2}{2}. \tag{2.40}$$

Hence a singular vortex of strength $\Gamma = \alpha \pi a^2$ is the solution for a vanishingly small vortex patch.

2.4 Contour dynamics

For investigating flows with piecewise-constant distributions of potential-vorticity, a well-known technique is contour dynamics[7], a scheme which integrates the full nonlinear governing equation (2.17). To derive the algorithm the quasigeostrophic governing equation is recast in a different, but equivalent form. The following is an adaptation of the derivation by Dritschel (1985) in the barotropic limit. First, write $q = (\nabla^2 - 1)\psi$, so that the potential vorticity is,

$$Q = q + Sh_B. \tag{2.41}$$

Conservation of potential vorticity then leads to the inhomogeneous Helmholtz equation at any given time,

$$(\nabla^2 - 1)\psi = q. \tag{2.42}$$

[7]or perhaps more correctly "contour advection".
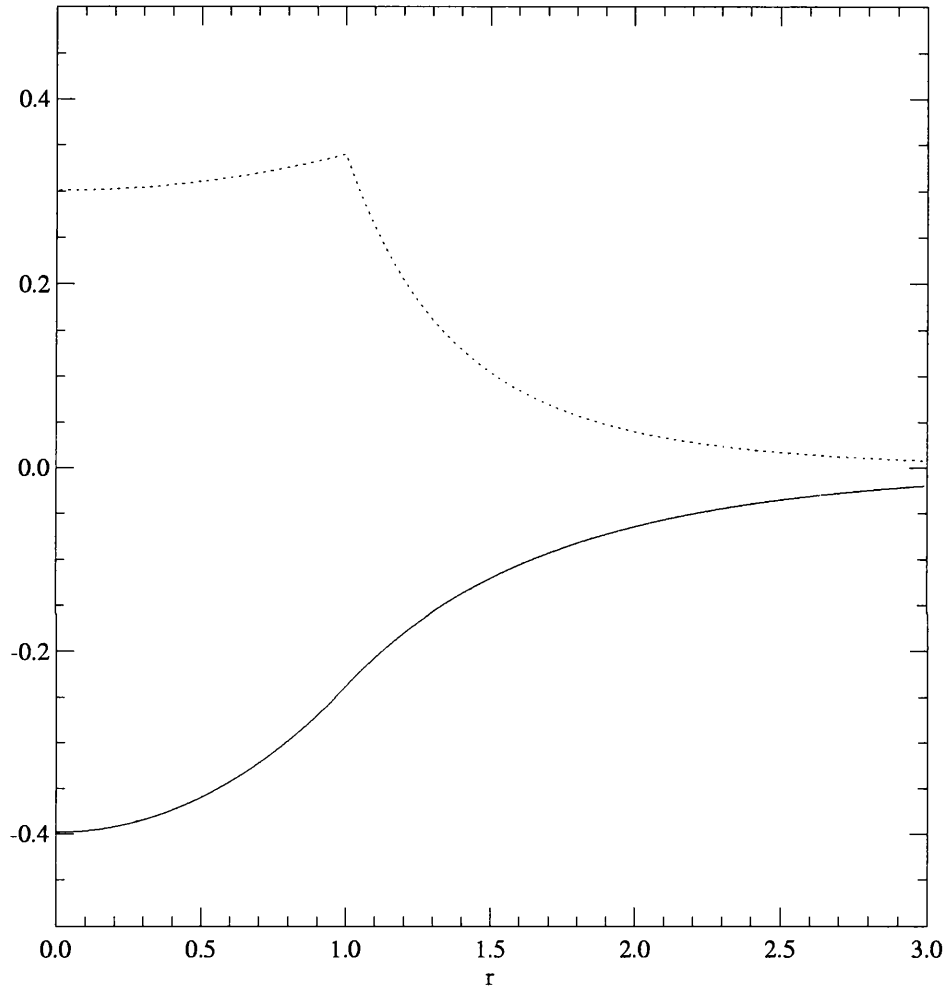
Figure 2.3: Profiles of the streamfunction, $\psi_0(r)$ (solid line) and the angular velocity, $b(r)$ (dotted line) for a circular patch of uniform relative vorticity. The particular case shown has patch radius $a = 1$ and strength $\alpha = -1$, i.e. a cyclone.

The Helmholtz operator, $(\nabla^2 - 1)$, has the Greens function $-K_0(r)/2\pi$, which leads to

$$\psi(x,y) = -\frac{1}{2\pi} \int \int q(x',y') K_0(r) dx' dy', \qquad (2.43)$$

where $r^2 = (x - x')^2 + (y - y')^2$ and the integral is taken over the entire fluid domain. The velocity field, $u = -\psi_y$, $v = \psi_x$, determined by (2.43) is

$$\mathbf{u}(x,y) = (u,v) = -\frac{1}{2\pi} \int \int q(x',y') \frac{K_1(r)}{r} (-(y - y'), (x - x')) dx' dy'. \qquad (2.44)$$

Next, suppose that the anomalous potential vorticity, q, is piecewise constant in regions R_k which cover the fluid domain, i.e. $q = q_k$ if $(x,y) \in R_k$. Then (2.44) can be written

$$\mathbf{u}(x,y) = -\frac{1}{2\pi} \sum_k \Delta q_k \int \int_{R_k} \frac{K_1(r)}{r} (-(y - y'), (x - x')) dx' dy'. \qquad (2.45)$$

Applying Stokes theorem,

$$\int \int_R \left(\frac{\partial R}{\partial x'} - \frac{\partial P}{\partial y'} \right) dx' dy' = \int_{\partial R} (P dx' + R dy'), \qquad (2.46)$$

to u, with $R = 0$ and $P = -K_0(r)$, and to v with $R = -K_0(r)$ and $P = 0$ leads to the velocity field in terms of line integrals,

$$\mathbf{u}(x,y) = \frac{1}{2\pi} \sum_k \Delta q_k \int_{C_k} K_0(r_k) d\mathbf{x}_k, \qquad (2.47)$$

where C_k is the boundary of R_k, $\mathbf{x}_k = (x_k, y_k)$ is a point on C_k, and $r_k^2 = (x - x_k)^2 + (y - y_k)^2$[8]. The C_k are "contours", enclosing fluid of constant anomalous potential vorticity, and are material curves, i.e. no fluid can cross them. It is straightforward to follow the time evolution of the contours since the velocity at each point on the contours is given by (2.47).

In the present work the topography is an infinitely long escarpment. Suppose that the escarpment is aligned along $y = 0$, so $h_B = \text{sgn}(y)$. Consider the flow regions, shown in Figure (2.4). There are two contours in the problem. The first is the topographic contour, T, which lies along $y = 0$, and the second is the advected, material contour A, initially coincident with T, but which deforms as the flow evolves. At subsequent times the advected contour moves away from its initial position, at first by advection by the vortex. The flow then consists of the three types of region depicted in Figure (2.4). Fluid in regions such as (I) originates in deep water, and has crossed the escarpment, gaining net anticyclonic circulation, and with $q = S$. Fluid in regions such as (II) originates on the shallow side of the escarpment, and has $q = -S$, due to vortex stretching. The q-field is

$$q = \begin{cases} S, & \text{in regions (I)} \\ -S, & \text{in regions (II)} \\ 0, & \text{elsewhere.} \end{cases} \qquad (2.48)$$

24

(a)

(b)
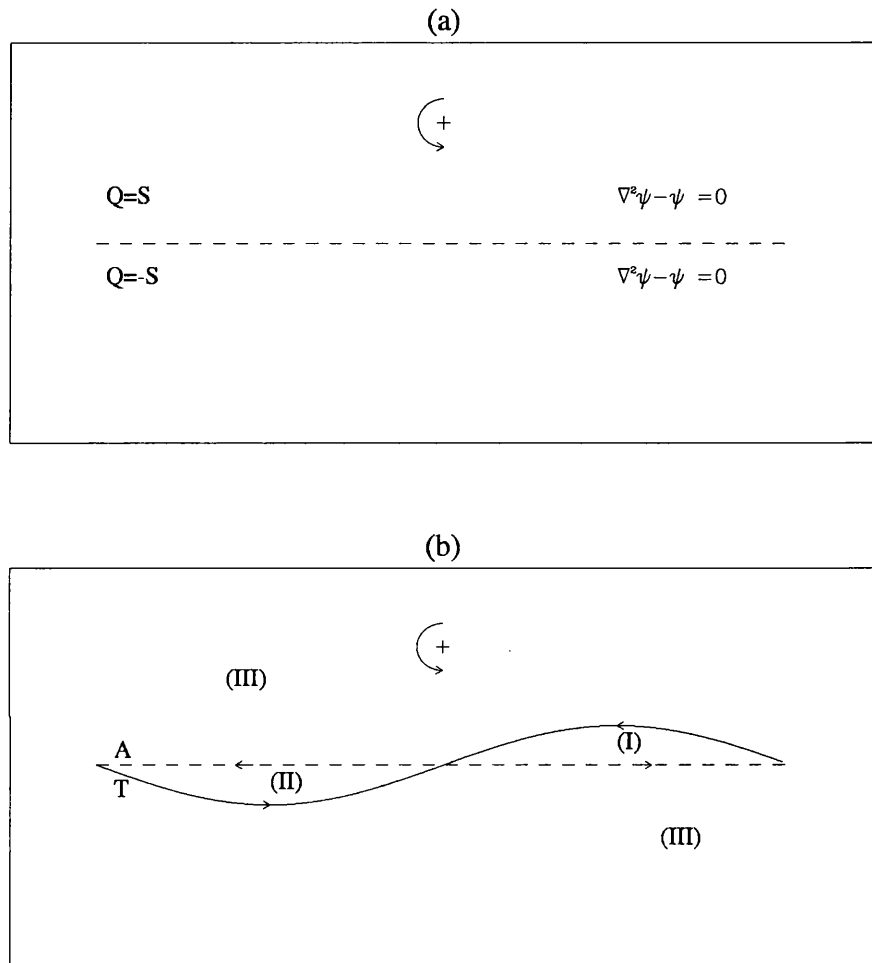
Figure 2.4: The various regions of the flow. (a) Initially the topographic contour and the advected contour coincide along $y = 0$. The dynamic potential vorticity $q = \nabla^2\psi - \psi$, is zero everywhere, fluid of high ambient potential vorticity lies in $y > 0$ and that of low ambient potential vorticity is in $y < 0$. Any initial deflection of the advected contour is solely due to the vortex. (b) At subsequent times the fluid may lie in three types of region. In (I), above the topographic contour, but below the advected contour fluid has moved from deep to shallow water and has $q = S$. Fluid in regions such as (II), below T but above A similarly have $q = -S$ and elsewhere (III) q remains zero.

Only the regions (I) and (II) contribute to the velocity of the fluid. The arrows in Figure (2.4) indicate the direction of integration around the boundary of the regions, clockwise in regions (I) and anticlockwise around regions (II). Equivalently

$$(u, v) = \frac{S}{2\pi} \int_A K_0(r) d\mathbf{x}_k - \frac{S}{2\pi} \int_T K_0(r) d\mathbf{x}_k, \tag{2.49}$$

where r is the distance from the point (x, y) to the point (x_k, y_k) on A or T respectively. There are three problems under consideration in this thesis, and the contour dynamics algorithm has to be applied in a different way in each case.

Singular vortex

In Chapter 4 the motion of a singular vortex near an escarpment is considered. Since there is no self-advection of a singular vortex, the vortex centre is treated as a passive particle, and the velocity field calculated from (2.49). The velocity at each of the contour nodes is due to the integral around the contours *and* the velocity due to the vortex centre.

Circular vortex patch

In Chapter 5 the motion of an initially circular vortex patch is considered. Now the vortex does contribute to its advection. Denote the boundary of the vortex by V. Then the velocity field at any point of either V or T is

$$(u, v) = \frac{S}{2\pi} \int_A K_0(r_A) d\mathbf{x}_k - \frac{S}{2\pi} \int_T K_0(r_A) d\mathbf{x}_k + \frac{\alpha}{2\pi} \int_V K_0(r_V) d\mathbf{x}_k, \tag{2.50}$$

where r_V is the distance from the point on V.

Coastal topography

In Chapter 6 the motion of a singular vortex near an escarpment running parallel to a plane wall is considered. To apply the contour dynamics algorithm in this case the velocity field due to the image of the vortex in the wall and the images, T' and A', of the topographic and advected contours is included. The velocity at the vortex is due to its image, and the contours T, A, T' and A'. The velocity at the contour nodes has the additional contribution due to the vortex and its image.

During the computational runs the advected contours are represented by a discrete set of nodes *and* a cubic polynomial through the nodes. The purpose of this is twofold. First, when time-stepping (by fourth order Runge-Kutta), the contribution to the integrals for the velocity field between adjacent

---

[8]Note that the sense of the potential vorticity jump is important. Specifically Δq_k is the potential vorticity to the left minus the potential vorticity to the right as the contour is traversed.

nodes is calculated to the first order in the departure from a straight line between the nodes, using the coefficients of the polynomial. Second, the nodes are redistributed at each time step, the spacing being determined by a non-local node density function, which depends on developing curvature and velocity. The nodes are then placed at appropriate positions on the cubic polynomial curve. Surgery is carried out at a predetermined cut-off scale. Full details of the algorithm are given in Dritschel (1988). Finally, unlike the case of a seamount (e.g. Davey *et. al.* (1993)), there is no analytical result for the integral along the undeflected topographic contour. The contribution to the velocity field is obtained numerically at each time step, in the same way as that of the advected contour.

There are two important considerations to make. First, the infinitely long advected contour necessarily has a finite representation during computational runs. Therefore, the contour length must be chosen such that its ends remain undisturbed during the runs. The particular contour length needed for any given parameter values depends on how localised the initial disturbance remains. Second, in the analytical considerations in the present work, and that of McDonald (1998) for the intense vortex limit, the topography is initialised near a pre-existing vortex. In the contour dynamics computations a vortex is switched on near a pre-existing contour. However, as will be seen later, contour dynamics results compare well with analytical results in both the weak and intense limits, so it is assumed that this is the case for all parameter values.

The codes were tested in several ways. First the time step was decreased until no discernible difference in the results occurred. Second, the same procedure was carried out with the spatial resolution parameter. Third, many of the runs were carried out both with and without surgery. In all cases the trajectory of the vortex centre with surgery active was identical with the trajectory obtained without surgery. The saving in the number of contour nodes needed was as much as a factor of 10 over long runs.

Chapter 3

Quasigeostrophic vortex-wave interactions

The ubiquity of vortices in quasi two-dimensional fluids and the generation of waves through potential vorticity conservation makes vortex-wave interaction a subject of importance in geophysical fluid dynamics. As pointed out in the introduction vortices are important in the general circulation of the ocean, but their effects have to be parameterised in general circulation models. Considerable attention has been paid to their study through laboratory experiments, numerical studies and theoretical investigations. In this chapter a brief review is given of some of the literature relevant to this thesis.

3.1   Vortex motion on the β-plane

The study of the motion of potentially highly destructive tropical cyclones has motivated much of the research into vortex motion in the atmosphere. These structures are intensive, long lived and have a size comparable to the Rossby radius. Planetary curvature is a leading influence on the trajectory of a tropical cyclone, and consequently the motion of intense cyclones on the β-plane has received considerable attention. The theory of Gulf stream rings has also followed this line of study. A review of some[1] of the literature is presented here. The work has followed two distinct routes: initial value problems and solitary wave models. This review focuses on the former approach, i.e. the evolution of an initially circular vortex under the β-effect. There are two reasons for this. First, the techniques employed in β-plane vortex problems are adopted in the present work. Second,

---

[1]It would take dozens of pages to simply cite all of the work!

as described previously, the β-plane is equivalent to linear sloping topography and it is of interest to compare the response of a vortex near a sharp topographic gradient with that of a vortex over smooth topography.

The evolution of a weak vortex on the β-plane is well understood. Flierl (1977) used linear quasi-geostrophic theory to show that a weak localised disturbance moves west under the influence of β and decays rapidly due to Rossby wave radiation. The decay is substantially slower for more intense vortices. Laboratory experiments by Firing and Beardsley (1976), and numerical investigations by McWilliams and Flierl (1979) and Mied and Lindeman (1979) show that a highly nonlinear (i.e. an intense) vortex decays slowly and its westward drift speed approaches the Rossby long wave speed. The effect of nonlinearity is to increase the longevity of the vortex, *and* to induce meridional motion.

These early studies revealed the first stage of the evolution of an intense vortex under the influence of β. The studies of McWilliams and Flierl (1979) and Mied and Lindeman (1979) both showed that an intense cyclone (resp. anticyclone) with an initially Gaussian vorticity distribution, follows a curved northwest (southwest) trajectory. The physical mechanism for this process is well understood. Consider the case of a cyclone. The sense of the circulation implies that fluid lying to the east of the vortex is advected north, and by virtue of potential vorticity conservation gains anticyclonic relative vorticity. To the west of the vortex, fluid advected south gains cyclonic relative vorticity. Thus initially, a dipolar secondary circulation is set up by the primary vortex sweeping fluid columns across the potential vorticity gradient. The sense of this dipole, the so-called β-gyres[2], is such as to initially induce a northward motion in the vortex. In the case of the weak vortex Rossby wave production dominates and energy is rapidly radiated away from the vortex, which in turn decays. In the case of an intense vortex the strong axisymmetric swirl of the vortex dominates the near field dynamics and the β-gyres remain in the vicinity of the vortex. In turn the axisymmetric swirl of the vortex rotates the axis of the dipolar β-gyres and consequently the vortex follows a curved northwest trajectory. The case of an anticyclone is analogous, but with the exception that the motion is southwest.

Analytical expressions have been found for the β-gyres in certain cases, and importantly the evolution of the initially symmetric dipole has been described. Sutyrin and Flierl (1994) considered the evolution of an initially axisymmetric vortex of piecewise constant potential vorticity using the

---

[2]This term was coined by Fiorino and Elsberry (1989) in a numerical study of non-divergent (aka barotropic) vortex motion on the β-plane.

quasigeostrophic β-plane model. Azimuthal mode-1 (i.e. the β-gyres) is mainly responsible for the motion of the vortex and in this case an expression for the drift of the vortex centre was obtained. The initial symmetric disturbance evolves into a uniform westward stream at large times and the vortex drift speed approaches the Rossby long wave speed. Similar expressions were obtained by Reznik and Dewar (1994) investigating the dynamics of an initially circular vortex with arbitrary distribution of relative vorticity with zero circulation using a barotropic β-plane model, and also by Reznik (1992) investigating the motion of singular vortices on the β-plane.

This early stage of the vortex evolution is well understood. However since the vortex drift velocity approaches the Rossby long wave limit the question arises as to the possible influence of wave radiation, or put another way, the effect of the higher order normal modes. Reznik and Dewar (1994) and Sutyrin *et. al.* (1994) have shown that the influence of higher order modes reduces the vortex amplitude and decelerates its westward drift velocity. Until recently all analytical attempts at describing the second stage of the vortex evolution have assumed that the vortex tends to some purely westward quasisteady state with a radiated Rossby wave train in its wake. For example, Flierl (1984), investigating the motion of an intense warm core ring in a two layer non-quasigeostrophic model, used a solvability condition on the order one field to determine the time evolution of the lowest order field. In this model the isolated vortex in the upper layer radiates Rossby waves in the lower layer. In turn this radiation gives rise to a drag on the vortex, which migrates southward in response.

Recently Reznik and Grimshaw (1998) have argued against this approach on three counts. First they claim that there is no numerical or laboratory evidence that the radiated wave field is quasi-steady. Indeed, they argue, that a non-divergent (barotropic) vortex always has a meridional drift speed of the same order as the zonal drift speed, and so the establishment of a quasisteady wave wake is not possible. Second the quasisteady wave wake has infinite energy, which is unphysical, since the system of vortex and waves conserves energy. In particular the vortex must lose energy to the radiated waves. Third, no previous theories conserve energy or enstrophy.

Reznik and Grimshaw (1998) present a new theory to remedy this charge. In it they show, through considering solution to higher order terms in a perturbation series in β, that an intense divergent (quasigeostrophic) vortex on the β-plane *does* adopt a quasisteady state, but that this is a non-radiating state. It is shown that the leading order solution (the β-gyres) tends to a uniform westward

flow matching the drift speed of the Rossby waves. This "kills" the β-effect and the vortex moves steadily westward adopting a nonradiating state. At the next order the β-gyres produce a correction consisting of an axisymmetric component and a quadrupolar component. The quadrupole spreads out from the central region containing the vortex and has little influence on the vortex motion. The axisymmetric component is opposite in sign to the primary vortex in the vortex core and opposite in sign outside of the vortex core. The anticyclonic rotation of the annulus in turn advects the planetary vorticity *in the opposite sense* to the primary vortex. Thus the correction at the third order is also dipolar and is termed the "secondary β-gyres". Since this term is opposite in sense to the primary β-gyres the vortex drift velocity is retarded at large times. The important conclusion of this paper is that the dipolar component of the secondary circulations controls the vortex drift up to times when the vortex decays. Since this is a near field effect, it is argued that far-field radiation has negligible effect on the dynamics.

A further recent study is a numerical investigation which compliments the theoretical results of Reznik and Grimshaw (1998), by Lam and Dritschel (1998), who apply the new "contour-advective semi-Lagrangian" (CASL) algorithm of Dritschel and Ambaum (1998) to the evolution of an initially circular quasigeostrophic vortex on the β-plane. In doing so the hitherto highest resolution numerical simulations to date have been produced. Moreover the dependence of the dynamics on the size and intensity of the vortex was examined. Two key features are identified. First is the existence of a region of fluid moving with the vortex, a "trapped zone". This is consistent with the results of Sutyrin and Flierl (1994), and is due to the axisymmetric component of the secondary circulation identified by Reznik and Grimshaw (1998). The trapped zone helps to shield the vortex from the effect of the radiated Rossby waves. Results confirm the rapid decay of a weak vortex and the longevity and northwest trajectory of a cyclone. Importantly it was shown that moderate intensity vortices undergo the greatest meridional displacement. The mechanism for this enhanced poleward motion is identified as a "trailing front", which is part of the radiated Rossby wave train. To describe it differently, and to reinforce one of the conclusions of this thesis, the trailing front consists of a patch of anticyclonic relative vorticity and it is the formation of a dipolar mechanism of comparable strength with the primary vortex that enhances the meridional motion of moderates vortices.

3.2 Vortex motion near sharp potential vorticity gradients

There are regions of sharp (discontinuous) potential vorticity gradients in the ocean. Currents such as the Gulf Stream are examples of such flows. Near a jet stream the shear flow forms a potential vorticity interface with the rest of the flow. Vortices are often formed by pinching off from the jet stream and the local shear flow dominates over the β-effect on these vortices. In the abyssal ocean there are sharp topographic gradients such as seamounts, escarpments and canyons. These features similarly dominate over planetary curvature in steering deep ocean eddies.

Hide (1961) showed that for Taylor columns to exist in flow over a finite height object the ratio $S = \delta/Ro$ must exceed some critical value. Here δ is the height of the obstacle expressed as a fraction of the depth of the fluid. If the obstacle is a topographic feature, then S, referred to as the *Hide parameter* in flow over finite height object problems, is the same as the S appearing in the quasigeostrophic potential vorticity (2.17). A right circular cylinder is often used to model a seamount. Johnson (1984) considered the topographic waves admissible over a seamount, and found that they cycle clockwise around the obstacle with the frequency of the lowest mode of azimuthal wavenumber-1. This work was extended by Davey *et al* (1993) to flow over a seamount in multilayer flow, using contour dynamics. Importantly when the oncoming flow is sufficiently strong or the height of the seamount sufficiently low, a vortex is created over the seamount as the flow sweeps the fluid off the seamount and downstream. Also considered was the capture of incident eddies by the seamount. McDonald and Dunn (1999) have recently made a preliminary investigation into the evolution of a vortex patch near a seamount. It was found that anticyclones tended to form dipoles with the fluid initially located on the seamount.

The limit that the seamount has infinite radius is the case of an escarpment. Longuet-Higgins (1968) derived the wave solutions to the shallow water equations over a topographic escarpment. These waves have unidirectional phase and group velocities, propagating with shallow water to the right in the northern hemisphere. The amplitude is maximum over the escarpment, and decays exponentially with distance on either side. These waves are thus dubbed *double Kelvin waves* or *seascarp waves*. Johnson and Davey (1990) studied the surface adjustment problem in f-plane quasigeostrophic motion over an escarpment, and also found that the escarpment acts as a wave guide, the waves propagating with shallow water to their right.

McDonald (1992) considered the time dependent response of fluid to a source of buoyancy near an escarpment using f-plane quasigeostrophic dynamics. It was found that a wavetube is excited and grows linearly in time at the group velocity of the long topographic waves. However it was found that the flux of fluid away from the source region is less than the flux of fluid at the source so eventually nonlinear effects must become important. Numerical studies showed that if the source is located on the shallow side of the escarpment then eddies are formed which self-propagate due to the presence of the escarpment. In two further studies the role of the escarpment in steering bottom eddies was investigated. McDonald (1996) investigated the interaction of a modon, (a dipolar distribution of potential vorticity), with an escarpment. Linear theory predicts that when the modon moves within the range of possible topographic wave phase speeds, a radiated wave train is left in the wake of the modon. As a result the modon speed and radius decay exponentially. There is also an anomalous case in which the modon moves at the long wave group velocity, so that energy cannot escape from the vicinity of the modon and the response must eventually become nonlinear. In this case the evolution of the topographic waves is governed by a forced Kortweg-de Vries equation, which leads to the same result for the rate of decay of the modon as in the linear theory.

In a further study McDonald (1998) studied the motion of an intense singular vortex near a topographic escarpment, again using quasigeostrophic f-plane dynamics. The leading order drift velocity components were found and it was shown that (if the escarpment is chosen to lie in the east-west direction) an intense cyclone follows a curved northwest trajectory and an anticyclone follows a curved southwest trajectory, qualitatively the same behaviour as a β-plane vortex. An important difference, however, is that the westward drift speed is less than the topographic long wave group speed. The westward drift speed is intimately related to the distance of the vortex from the escarpment. This indicates an important difference between the case of the continuous topographic gradient and the sharp topography considered in this thesis: on the β-plane there is no meaning in "distance from the topography", since the gradient of the topography is constant. It is anticipated that there will be new types of behaviour in vortex interactions near an escarpment. McDonald (1998) found an expression for the large time response of the vortex by equating the momentum flux of the radiated waves with the rate of change of momentum of the vortex. If the vortex is within about a Rossby radius of the escarpment then it migrates south (north) if it is an anticyclone (cyclone). Contour dynamics simulations of the full equations confirmed the analytical results.

Recent experimental results of particular relevance to the present study are due to Zavala Sanson *et. al.* (1999) who have investigated the behaviour of barotropic vortices near an escarpment, both experimentally and numerically. In that investigation the escarpment lay in the meridional direction on a β-plane. The β parameter was small in comparison to the height of the topography, and mainly served to bring the vortex near to the escarpment. The strength of the vortices was of the same order of magnitude as the relative vorticity produced by fluid crossing the escarpment, or, in the terminology of the present work, $S \approx 1$. It was found that anticyclones situated on the shallow side of the escarpment were able to "climb" the topographic gradient, whilst cyclones were "back-reflected". This behaviour is also observed in the following investigation.

There are two further works which should be mentioned. Large scale warm (cyclonic) and cold (anticyclonic) rings are formed by the meanders of the Gulf Stream. It has been observed that if the vortex is weak, compared with the shear flow, then it can drift antiparallel to the stream (this is analogous to eastward propagation on the β-plane). Stern and Flierl (1987) investigated the interaction of a singular vortex with an idealised shear flow, in which the potential vorticity is assumed piecewise constant in two regions, using both barotropic and quasigeostrophic dynamics. They noted that if an anticyclonic vortex is sufficiently distant (i.e. weak) from an interface of cyclonic vorticity then it moves antiparallel to the stream. Vortices which are close to the interface "capture" the contour and wrap it up, qualitatively the same behaviour observed by McDonald (1998). In a similar study Bell (1989) investigated the interaction of a weak singular vortex and a potential vorticity interface, using contour dynamics in quasigeostrophic theory with $R_D = \infty$. It was found that if the vortex moves within the range of possible phase speeds of the potential vorticity waves then a radiated wave train is left in the wake of the vortex (cf McDonald (1996)). The singular vortex responds by moving towards or away from the interface depending on the sense of the circulation. If the vortex moves at a speed outside of the wave phase speeds then the interface adopts a quasisteady shape, which constitutes a patch of relative vorticity of the opposite sign to the vortex. The vortex and the deformed interface move together.

This latter phenomenon is of particular importance in the rest of this work. In all cases examined below it is found that a weak vortex near an escarpment behaves as if the escarpment were a plane wall. The physical mechanism for this process is identified as a quasisteady deformation of the contour initially separating shallow and deep water. This disturbance is a patch of relative vorticity

of the opposite sign to the primary vortex. This phenomenon is expected to be a generic feature of the interaction of a weak vortex with sharp potential vorticity gradients and for this reason, in this thesis, it has been named the *pseudoimage* of the vortex.

The rest of this thesis consists of three different studies of vortex topography interaction. In Chapter 4 the work of McDonald (1998) is extended to cover the full range of values of S for the motion of a singular vortex near an escarpment. In Chapter 5 the motion of an initially patch of uniform relative vorticity near an escarpment is investigated for the full range of values of S. In Chapter 6 the motion of a vortex near coastal topography (i.e. an escarpment running parallel to a plane wall) is investigated. Analytical results for the weak vortex limit are given and some preliminary contour dynamics results are given for the intense and moderate regimes.

Chapter 4

Motion of a singular vortex near an escarpment

The investigation of McDonald (1998) into the motion of an intense, $(S \ll 1)$, singular vortex near an escarpment was described in the previous chapter. The aim of the present chapter is to extend this work to investigate the full range of values of the vortex intensity.

First the weak vortex limit, $S \gg 1$, is investigated. The leading order solution on the topographic wave time scale is found using linear theory. The large time solution is then investigated under the assumption that the response remains linear on the advective time scale. This assumption is verified through contour dynamics experiments. Second, the results of McDonald (1998), for an intense singular vortex are summarised, partially for completeness, but also to investigate the departure of the vortex dynamics from the intense regime to the moderate regime. Finally the case of a moderate intensity singular vortex, for which there is no analytical theory, is investigated through contour dynamics experiments.

4.1 Topographic waves

All of the work presented in this thesis assumes quasigeostrophic dynamics, described previously in Chapter 2. The f-plane is used, to isolate the effects of sharp topographic gradients from the β-effect. Here the explicit nondimensionalisation for the present study is given. Denote the original,

dimensional variables by superscript *, and introduce the following, nondimensional variables,

$$t = \frac{1}{T_a}t^*, \qquad x = \frac{1}{L}x^*, \qquad y = \frac{1}{L}y^*, \qquad \psi = \frac{1}{RofL^2}\psi^*. \qquad (4.1)$$

Here the horizontal length scale, L, is the Rossby radius, and the time scale T_a is the advective (or eddy turnover) time L/U or equivalently, by geostrophy, $D/f\Lambda$, where D is a typical fluid depth, $f > 0$ (i.e. the northern hemisphere) is the Coriolis parameter, Λ is a suitable scale for the vortex amplitude and U is a typical vortex velocity due to geostrophy. The Rossby number, $Ro = U/fL$, is necessarily small for the quasigeostrophic approximation. Under this scaling the governing equation is

$$\frac{\partial}{\partial t}(\nabla^2\psi - \psi) + J[\psi, \nabla^2\psi - \psi] + S\frac{\partial\psi}{\partial x}\frac{\partial h_B}{\partial y} = 0, \qquad (4.2)$$

where the conserved quantity is the quasigeostrophic potential vorticity,

$$Q = \nabla^2\psi - \psi + Sh_B(y). \qquad (4.3)$$

The nondimensional topography $h_B(y)$ is assumed to vary only in the y-direction, and the parameter S is the ratio of the eddy turnover time to the topographic vortex stretching time, or, equivalently, of the fractional height of the topography to the Rossby number:

$$S = \frac{L/U}{\delta^{-1}f^{-1}} = \frac{\delta}{Ro} = \frac{T_a}{T_w}, \qquad (4.4)$$

where $\delta = \Delta D/D$ is half the fractional height of the topography in a layer of depth D. Figure (4.1a) shows the present choice of topography, an infinitely long escarpment aligned along $y = 0$, which can be expressed as

$$h_B(y) = \text{sgn}(y). \qquad (4.5)$$

By analogy with the β-plane, shallow fluid lies in the direction of increasing y. For convenience of description, the direction of increasing y is identified as north, and increasing x as west. In reality there is no preferential direction on the f-plane, so this choice is made simply so as to align the isobaths, or potential vorticity contours, in the β-plane sense. The fluid motion is strictly *not* quasigeostrophic near $y = 0$, since there the topography has infinite gradient, so the flow must be three-dimensional near the escarpment. Given that $\delta \ll 1$ in the derivation of the quasigeostrophic governing equations, it is assumed that the three-dimensional effects near the escarpment are negligible and have no leading order effect on the dynamics. The two numbers, δ and Ro are small parameters, but their ratio S can, of course, take the whole range of values.

38
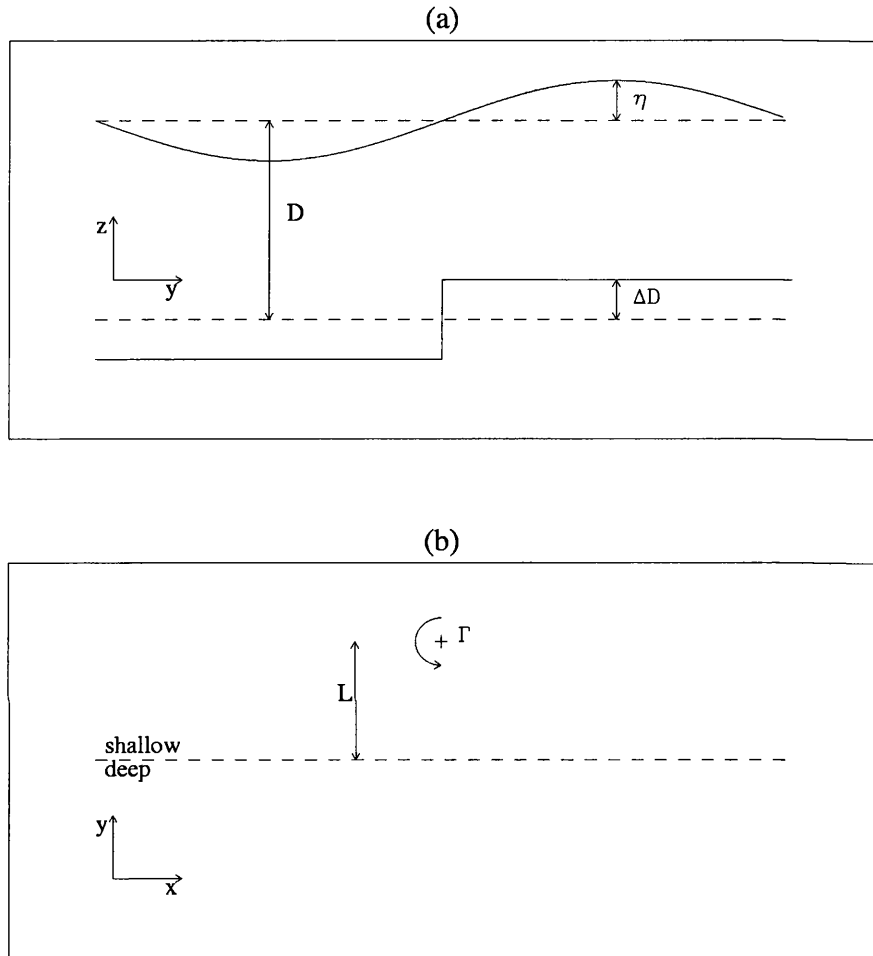
Figure 4.1: The present problem. (a) is a plot of the cross section of the fluid domain, and the dimensional variables. The free surface elevation, η is scaled on $Rof L^2$ and written ψ; D is the typical layer depth in the absence of motion, and $\delta = \Delta D/D$ is half the fractional height of the topography. (b) shows the initial condition, which is a vortex (here a cyclone), distance L from the escarpment, which is aligned along $y = 0$. Shallow water lies in the half-plane $y > 0$, and so contains fluid with high ambient potential vorticity.

Of interest in the present study is the interaction between a vortex and the topographic waves. The linear wave solutions to (4.2) can be obtained by setting $\epsilon = S^{-1}$ and introducing the rescaled time variable $\tau = \epsilon t$, so that the unit of time is T_w, the time scale for topographic wave generation. Under this rescaling the governing equation is

$$\frac{\partial}{\partial\tau}(\nabla^2\psi - \psi) + \epsilon J[\psi, \nabla^2\psi - \psi] + \frac{\partial h_B}{\partial y}\frac{\partial\psi}{\partial x} = 0. \tag{4.6}$$

For $\tau \ll \epsilon^{-1}$, the advection term is negligible, and (4.6) becomes a linear topographic wave equation,

$$\frac{\partial}{\partial\tau}(\nabla^2\psi - \psi) + \frac{\partial h_B}{\partial y}\frac{\partial\psi}{\partial x} = 0. \tag{4.7}$$

Note that this implies that $\nabla^2\psi - \psi = 0$, everywhere except $y = 0$. The boundary conditions at the escarpment are (see Johnson and Davey (1990)),

$$[\psi] = 0 \quad , \qquad y = 0 \tag{4.8a}$$

$$[\psi_{y\tau}] + 2\psi_x = 0 \quad , \qquad y = 0. \tag{4.8b}$$

where [ ] denotes the jump of the enclosed quantity across the escarpment, i.e. $[g] = g(0^+) - g(0^-)$. The first condition is continuity of ψ across the escarpment, whilst the second, obtained by integrating (4.7) across the escarpment, is continuity of pressure.

Wave solutions which vanish in the far-field have the form

$$\psi \propto e^{-\sqrt{k^2+1}|y|}e^{i(kx-\omega\tau)}, \tag{4.9}$$

and the dispersion relation, obtained by substitution into (4.8b), is

$$\omega = -\frac{k}{\sqrt{k^2+1}}. \tag{4.10}$$

The waves have maximum amplitude over the escarpment, and decay exponentially with distance from the escarpment, the same properties as the linearised shallow-water escarpment waves of Longuet-Higgins (1968). Note also that the wave amplitude decreases exponentially with the wavenumber k, so that the short waves have minimum amplitude. The phase and group velocities are

$$c_p(k) \;\; = \;\; \frac{\omega}{k} = -\frac{1}{\sqrt{k^2+1}}, \tag{4.11a}$$

$$c_g(k) \;\; = \;\; \frac{\partial\omega}{\partial k} = -\frac{1}{(k^2+1)^{3/2}} \tag{4.11b}$$

40

so both the phase and energy of the waves propagate in the direction of decreasing x, i.e. with shallow water to the right. Figure (4.2) shows a plot of the phase and group velocities. The escarpment acts as a wave guide and dictates the preferential west direction of the wave propagation. This is analogous to the Rossby wave on the β-plane, where the one dimensional topographic gradient induces west propagation of wave phase and energy. The restoring mechanism for the waves is the production of relative vorticity due to vortex stretching or contraction as fluid crosses the escarpment, as demanded by potential vorticity conservation (4.3) . Figure (4.6) below shows this mechanism schematically.

In the following section the solution for the initial value problem of a weak singular vortex near an escarpment is investigated.

4.2 A weak singular vortex

From chapter 2 isolated singular vortex solutions to (4.2) in the absence of topography, and with the Rossby Radius as the characteristic length scale of the motion, are

$$\Psi_v(x - X, y - Y) = \frac{\Gamma}{2\pi} K_0 \left(\left((x - X)^2 + (y - Y)^2 \right)^{1/2} \right), \tag{4.12}$$

where $(X(t), Y(t))$ is the position of the vortex centre, and K_0 the modified Bessel function of the first kind, order zero. Here $\Gamma = \pm 1$ gives the sense of the circulation; for $\Gamma > 0$ it is clockwise (anti-cyclonic) and $\Gamma < 0$ anti-clockwise (cyclonic). The vortex is initially O(1) distance from the escarpment. Suppose at $t = 0$ there is a vortex of the form (4.12) with location

$$(X(0), Y(0)) = (0, L). \tag{4.13}$$

See Figure (4.1b). The aim is to determine the subsequent motion of the vortex $(X(t), Y(t))$. Seeking a solution of the form,

$$\psi = \Psi_v(x - X, y - Y) + \phi, \tag{4.14}$$

the governing equation becomes

$$(\nabla^2 \phi - \phi)_t + J[\phi, \nabla^2 \phi - \phi] + S\frac{\partial \phi}{\partial x}\frac{\partial h_B}{\partial y} = -S\frac{\partial \Psi_v}{\partial x}\frac{\partial h_B}{\partial y}. \tag{4.15}$$

In the following subsection the leading order solution for the weak vortex limit is found by simple Fourier analysis.
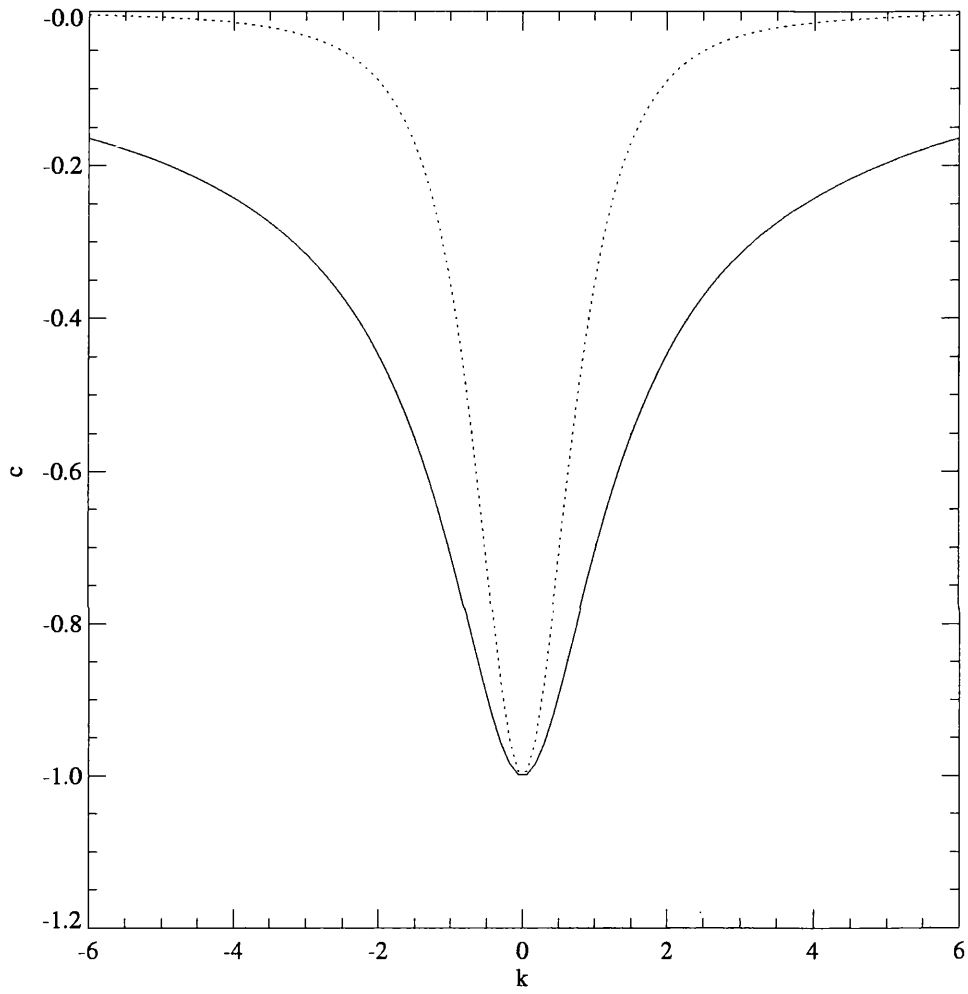
Figure 4.2: A plot of the phase velocity (solid line) and group velocity (dotted line) against the wavenumber k. Note that both $c_p, c_g < 0$, so the wave phase and energy both propagate to the west.

4.2.1 Short time solution

As in the previous section set $\epsilon = S^{-1} \ll 1$ and introduce the rescaled time variable $\tau = \epsilon t$, so that the unit of time is the short, topographic wave time scale T_w, and denote the solution on this time scale by ϕ_0. For $\tau < O(\epsilon^{-1})$ the advection term in (4.15) is negligible, so for times up to $\tau = O(\epsilon^{-1})$,

$$(\nabla^2 \phi_0 - \phi_0)_\tau + \frac{\partial \phi_0}{\partial x} \frac{\partial h_B}{\partial y} = -\frac{\partial \Psi_v}{\partial x} \frac{\partial h_B}{\partial y}, \tag{4.16}$$

which is a linear, forced topographic wave equation, the forcing being due to the vortex. On this time scale scale the vortex drift velocity components are $O(\epsilon)$, and advection of the vortex is by the regular ϕ_0-field[1], so that

$$\frac{dX}{d\tau} = -\epsilon \frac{\partial \phi_0}{\partial y}\bigg|_{x=X, y=Y}, \tag{4.17a}$$

$$\frac{dY}{d\tau} = \epsilon \frac{\partial \phi_0}{\partial x}\bigg|_{x=X, y=Y}. \tag{4.17b}$$

Hence, for times up to $\tau = O(\epsilon^{-1})$, $X = O(\epsilon)$ and $Y = L + O(\epsilon)$, and the vortex term is, to leading order

$$\Psi_v = \Psi_v(x, y - L), \tag{4.18}$$

on this time scale. Also $\partial h_B / \partial y = 2\delta(y)$ so away from $y = 0$ (4.16) is

$$\nabla^2 \phi_0 - \phi_0 = 0. \tag{4.19}$$

The topography is "switched on" near a pre-existing vortex at $\tau = 0$, i.e the initial condition is

$$\phi_0(x, y, 0) = 0. \tag{4.20a}$$

The boundary conditions are

$$\nabla \phi_0 \to 0 \quad , \qquad x^2 + y^2 \to \infty, \tag{4.20b}$$

$$[\phi_0] = 0 \quad , \qquad y = 0, \tag{4.20c}$$

$$[\phi_{0yt}] + 2\phi_{0x} = -2\Psi_{vx}(x, -L) \quad , \qquad y = 0. \tag{4.20d}$$

Condition (4.20b) is the requirement that the fluid to be at rest far from the escarpment, whilst (4.20c) and (4.20d) are the matching conditions (4.8a) and (4.8b) respectively. The solution to this problem is obtained through standard Fourier transform methods. Define the Fourier transform of ϕ_0 by

$$\hat{\phi}_0(k, y, \tau) = \int_{-\infty}^{\infty} \phi_0(x, y, \tau) e^{-ikx} \, dx. \tag{4.21}$$

---

[1] since there is no self advection by a singular vortex.

In Fourier space the problem becomes

$$\hat{\phi}_{0yy} - (k^2 + 1)\hat{\phi}_0 = 0, \quad , \qquad y \neq 0 \tag{4.22a}$$

$$\hat{\phi}_0 \to 0 \quad , \qquad y \to \pm\infty, \tag{4.22b}$$

$$\left[\hat{\phi}_0\right] = 0 \quad , \qquad y = 0. \tag{4.22c}$$

Equations (4.22a), (4.22b) and (4.22c) have solutions of the form

$$\hat{\phi}_0(k, y, \tau) = B(k, \tau)e^{-\sqrt{k^2+1}|y|}. \tag{4.23}$$

The function B is determined from boundary condition (4.20d), which transforms to the ODE

$$-\sqrt{k^2 + 1}\, B_\tau + ikB = -ik\, \hat{\Psi}_v\Big|_{y=0}, \tag{4.24}$$

with initial condition $B(k, 0) = 0$. Also Ψ_v is even in x so that

$$\hat{\Psi}_v = 2\int_0^\infty \Psi_v \cos kx\, dx = \frac{\Gamma}{2\sqrt{k^2+1}}e^{-|y-L|\sqrt{k^2+1}}. \tag{4.25}$$

The final equality in (4.25) is obtained from the following identity (Gradshteyn and Rhyzik (1980), p736);

$$\int_0^\infty K_0\left(\eta\sqrt{x^2 + \beta^2}\right)\cos\gamma x\, dx = \frac{\pi}{2\sqrt{\eta^2 + \gamma^2}}e^{-\beta\sqrt{\gamma^2+1}}, \tag{4.26}$$

for η, $\beta > 0$. Thus equation (4.24) becomes

$$B_\tau + i\omega B = -\frac{i\omega\Gamma}{2\sqrt{k^2+1}}e^{-|L|\sqrt{k^2+1}}, \tag{4.27}$$

where ω is the topographic wave frequency given by (4.10). Equation (4.27) is linear and is easily solved using the integrating factor method, giving

$$B(k, \tau) = \frac{\Gamma}{2\sqrt{k^2+1}}e^{-|L|\sqrt{k^2+1}}\left(e^{-i\omega\tau} - 1\right), \tag{4.28}$$

and hence from (4.23)

$$\hat{\phi}_0(k, y, \tau) = \frac{\Gamma}{2\sqrt{k^2+1}}e^{-(|y|+|L|)\sqrt{k^2+1}}\left(e^{-i\omega\tau} - 1\right). \tag{4.29}$$

The inverse Fourier transform is

$$\phi_0(x, y, \tau) = \frac{1}{2\pi}\int_{-\infty}^\infty \hat{\phi}_0(k, y, \tau)e^{ikx}\, dk, \tag{4.30}$$

Using the evenness of $\hat{\phi}_0$ and identity (4.26) it is straightforward to show that the solution consists of a steady term and a topographic wave term,

$$\phi_0 = \phi_0^{(s)} + \phi_0^{(w)}, \tag{4.31}$$

44

where

$$\phi_0^{(s)} = -\frac{\Gamma}{2\pi} K_0 \left(\left(x^2 + (|y| + |L|)^2 \right)^{1/2} \right), \qquad (4.32)$$

and

$$\phi_0^{(w)} = \frac{\Gamma}{2\pi} \int_0^\infty A(k,y) \cos(kx - \omega\tau) \, dk, \qquad (4.33)$$

with

$$A(k,y) = \frac{e^{-(|y|+|L|)\sqrt{k^2+1}}}{\sqrt{k^2+1}}. \qquad (4.34)$$

At $\tau = 0$ the topographic wave term $\phi_0^{(w)}$ cancels with the steady term $\phi_0^{(s)}$, i.e. the correct initial condition. Below it is shown that the wave term decays rapidly on this time scale, so after the initial adjustment the response for times of order of the topographic wave time, T_w, is steady. The two terms are now considered separately.

The steady term.

The steady term $\phi_0^{(s)}$ is reminiscent of an image of the vortex in the escarpment $y = 0$. Note however the important distinction: if $L < 0$ then $\Psi_v + \phi_0^{(s)}$ vanishes for $y > 0$ and similarly if $L > 0$ then $\Psi_v + \phi_0^{(s)}$ is zero for $y < 0$. Thus the fluid on the same side of the escarpment as the vortex feels the effect of an image vortex in the escarpment, whereas the fluid across the escarpment from the vortex is undisturbed with respect to the steady term, $\Psi_v + \phi_0^{(s)}$. For this reason the steady term, $\phi_0^{(s)}$, is dubbed the *pseudoimage* of the vortex. The streamlines of $\Psi_v + \phi_0^{(s)}$ are shown in Figure (4.3).

The importance of the pseudoimage in the following theory cannot be overstated. In the contour dynamics investigations described below, it will be seen that the behaviour of the vortex is well predicted by the pseudoimage description for many eddy turnover times. It should be emphasised that the pseudoimage has a definite physical meaning. It is *part* of the topographic wavetrain, a wavetrain which is initially excited by the circulation of the vortex pushing fluid across the escarpment. It is non-dispersive, is even in y, and *is not* singular anywhere. The relative vorticity associated with the disturbance $\phi_0^{(s)}$ is precisely enough to advect the vortex as if the escarpment were a plane wall. Importantly, it will be shown that the dispersive topographic waves rapidly propagate away from the vortex, and have no influence on it for times $\tau \to \epsilon^{-1}$, i.e. for large times the advection of the vortex is due solely to its pseudoimage. The properties of the dispersive waves are discussed next.

The topographic wave term.
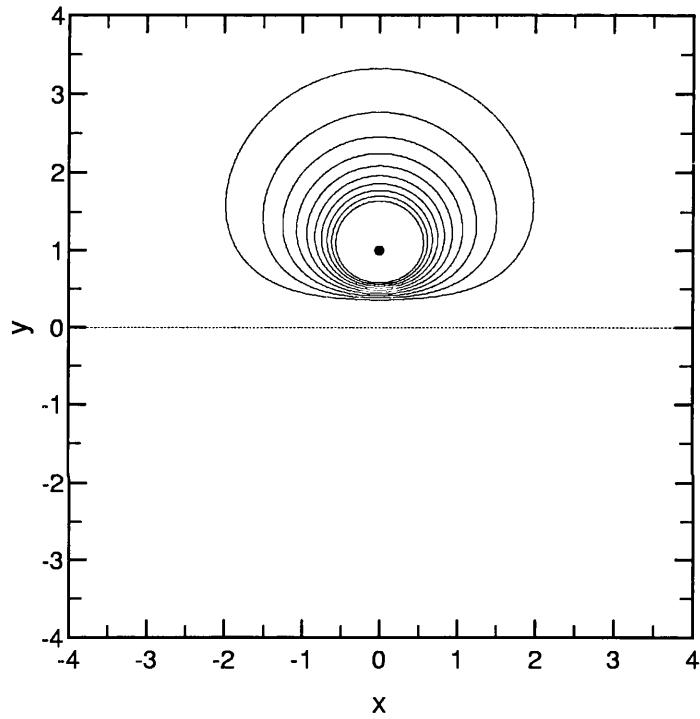
Figure 4.3: Streamlines for the steady term ψ_{stat}. The vortex has unit strength and is located at $(0,1)$. The contour interval is 0.01, and the position of the escarpment is indicated by the dashed line. Note the closed streamlines on the side of the escarpment occupied by the vortex. The fluid on the opposite side is undisturbed.

The unsteady part of the solution $\phi_0^{(w)}$ given by (4.33) is a Fourier superposition of the escarpment waves discussed in section 4.1. The amplitude is maximum over $y = 0$, i.e. over the most rapidly varying topography. The dispersion relation is given by (4.10) and the group and phase velocities are given by equations (4.11b) and (4.11b) respectively.

Standard asymptotic methods are employed to deduce the large time behaviour of $\phi_0^{(w)}$. The integrand in (4.33) is analytic, so the only contributions to the integral as $\tau \to \infty$ come from the points of stationary phase (see, for example, Bender and Orszag (1978)). Rewrite the integral (4.33) in the form

$$\phi_0^{(w)} = \frac{\Gamma}{4\pi} \int_{-\infty}^{\infty} A(k, y) e^{if\tau} \, dk, \tag{4.35}$$

where

$$f(k) = \frac{kx}{\tau} - \omega. \tag{4.36}$$

The points of stationary phase are the solutions of $f'(k_s) = 0$, and the method of stationary phase gives, for fixed $\zeta = x/\tau$ as $\tau \to \infty$,

$$\phi_0^{(w)} \approx \frac{\Gamma}{2\pi} \sum_{k_s} A(k_s, y) e^{i\tau f(k_s)} \left[\frac{2\pi}{\tau |f''(k_s)|} \right]^{1/2} e^{i\pi\mu/4}, \tag{4.37}$$

with $\mu = \mathrm{sgn}(f''(k_s))$, the sum is taken over all the points of stationary phase and the real part is understood to be taken. In the present case there is only one point of stationary phase, which occurs for $-\tau < x < 0$, and is given by

$$k_s = \left((-\zeta)^{-2/3} - 1 \right)^{1/2}. \tag{4.38}$$

Moreover

$$f''(k_s) = -3k_s(\zeta)^{5/3} < 0, \tag{4.39}$$

since $k_s > 0$ and $\zeta < 0$. Hence

$$\phi_0^{(w)} \approx -\frac{\Gamma}{\sqrt{2\pi}} e^{-(|y|+|L|)\sqrt{k_s^2+1}} \left(\frac{1}{3\tau\zeta k_s} \right)^{1/2} \cos\left(k_s x - \omega_s \tau - \frac{\pi}{4} \right), \tag{4.40}$$

where $\omega_s = -k_s(k_s+1)^{-1/2}$. Hence, for large τ, at fixed $-\tau < x < 0$ the topographic wave amplitude decays like $\tau^{-1/2}$.

The stationary phase approximation breaks down at the point $x = -\tau$, corresponding to the point of maximum group velocity $\omega''(k) = c_g'(k) = 0$, since then the denominator in (4.37) vanishes. Denote by $k = k_m$ the wavenumbers for which this occurs,

$$c_g'(k_m) = 0. \tag{4.41}$$

47

By considering a third-order expansion of the phase, $\theta = kx - \omega\tau$, about $k = k_m$, Lighthill (1974), shows that for $k \approx k_m$,

$$\phi_0^{(w)} \approx \frac{\Gamma}{2} \frac{A(k_m)}{\left|c_g''\tau/2\right|^{1/3}} \cos(k_m x - \omega(k_m)\tau) \text{ Ai}\left(-\frac{x - c_g(k_m)\tau}{\left|c_g''\tau/2\right|^{1/3}}\right), \tag{4.42}$$

as $\tau \to \infty$. Here Ai() is the Airy function, which satisfies the ODE

$$\frac{d^2}{dx^2}\text{Ai} - x\text{Ai} = 0. \tag{4.43}$$

The Airy function decays exponentially for negative argument and for positive argument oscillates like the cosine of the two-thirds power of its argument (see Abramowitz and Stegun (1972) for details). In the present case $k_m = 0$, so the waves with maximum group velocity are the long waves. Moreover, the maximum group velocity is $c_g(0) = -1$. Hence, near $x = -\tau$, as $\tau \to \infty$

$$\phi_0^{(w)} \approx -\frac{\Gamma}{2}\frac{e^{-(|y|+|L|)}}{(3\tau/2)^{1/3}}\cos\tau \text{ Ai}\left(-\frac{x - \tau}{(3\tau/2)^{1/3}}\right). \tag{4.44}$$

Thus, $\phi_0^{(w)}$ decays exponentially for $x < -\tau$ and oscillates for $x > -\tau$. The amplitude of this maximum oscillation at the wavefront decays like $\tau^{-1/3}$, and the wavefront approximation smoothly matches the topographic waves to the undisturbed fluid ahead of the train (see Lighthill (1974) for details). The wave term evaluated over $y = 0$ is illustrated in Figure (4.4a). The plot is obtained by numerical integration of (4.33). The west propagating topographic waves are evident. Note the largest amplitude oscillations near the wavefront, and the rapid decay near $x = 0$. Equation (4.44) predicts that, for the given parameters at $\tau = 60$ the value at $x = -\tau$ is

$$\phi_0^{(w)}(-\tau, 0) \approx \pi\frac{e^{-2}}{90^{1/3}}\cos 60 \text{ Ai}(0) \approx 0.0032, \tag{4.45}$$

using Ai(0) ≈ 0.355028 from Abramowitz and Stegun (1972). This compares favourably to the numerical value of 0.0028.

Of particular importance is the influence of the waves at the vortex centre. The wave amplitude decays most rapidly at the x-location of the vortex centre, and this can be seen as follows. There are no points of stationary phase for $x = 0$. Equation (4.33) evaluated at the vortex centre is

$$\phi_0^{(w)}(0, L, \tau) = \frac{\Gamma}{2\pi}\int_0^\infty \frac{e^{-2|L|\sqrt{k^2+1}}}{\sqrt{k^2+1}}\cos\frac{k\tau}{k^2+1}\,dk. \tag{4.46}$$

Writing $\xi = k/\sqrt{k^2+1}$ this may be rewritten

$$\phi_0^{(w)}(0, L, \tau) = \frac{\Gamma}{2\pi}\int_0^1 h(\xi)\cos\xi\tau\,d\xi, \tag{4.47}$$
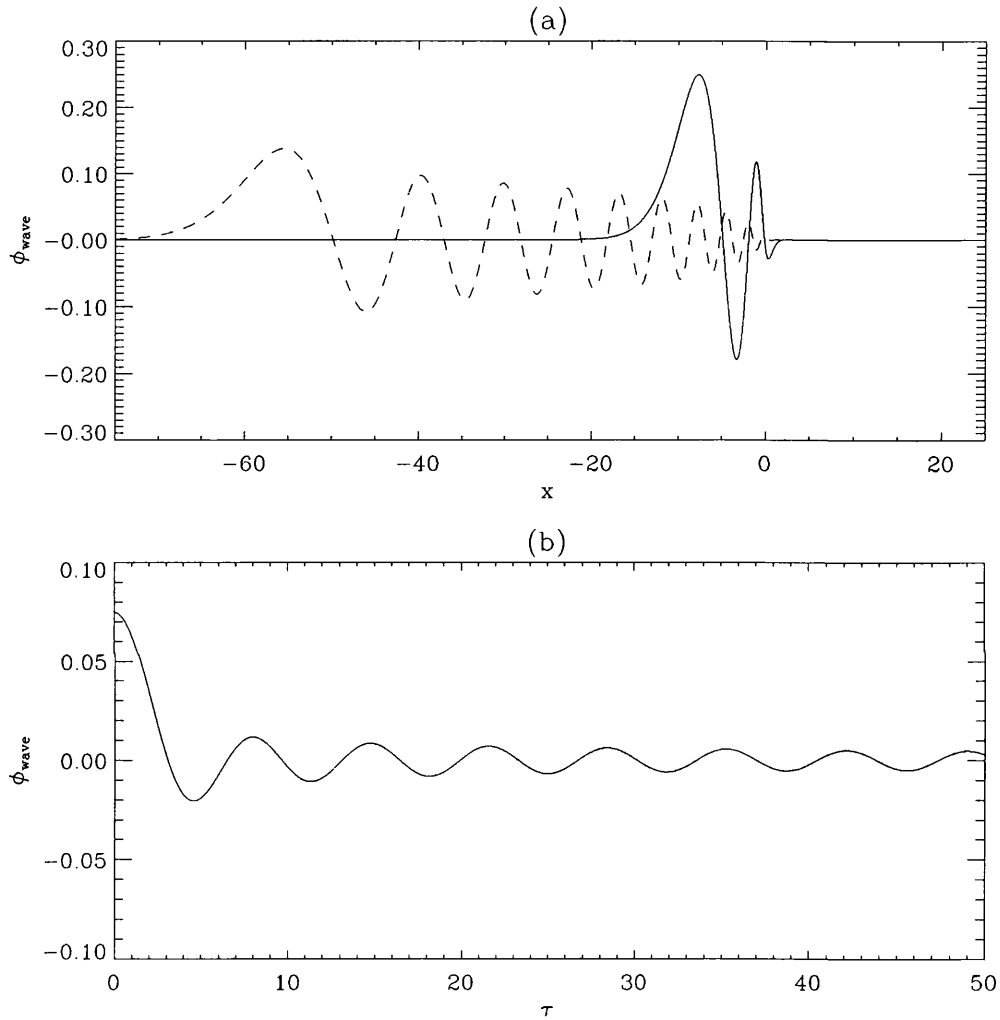
Figure 4.4: (a) Plot of $\phi_0^{(w)}$ evaluated over $y = 0$. Times are $\tau = 10$ (solid curve) and $\tau = 60$ (dashed curve). (b) The wave term evaluated at the vortex centre as a function of τ. In each case $\Gamma = 1$, i.e. an anticyclone, and the solution has been scaled by 2π. See text for further comments.

where,

$$h(\xi) = \frac{e^{-2|L|/\sqrt{1-\xi^2}}}{\sqrt{1-\xi^2}}. \tag{4.48}$$

The Riemann-Lebesgue Lemma (e.g. Bender and Orszag (1978)) states that if

$$\int_0^1 |h(\xi)| \ d\xi \tag{4.49}$$

exists then the integral in (4.47) decays like τ^{-1} as $\tau \to \infty$. This is clearly the case here, since $h(\xi)$ is bounded for all $\xi \in [0,1]$. Hence, the influence of the waves on the vortex decreases algebraically for large τ. Figure (4.4b), shows a plot of the response at the vortex centre, obtained by numerical integration of (4.46).

It has been shown that the topographic waves decay algebraically on the topographic wave time scale, T_w. Significantly their decay is most rapid at the vortex centre, and so as $\tau \to \epsilon^{-1}$ they have no influence on the vortex drift velocity. The trajectory of the vortex centre on topographic wave time scale is considered in detail in the next subsection.

4.2.2 Short-time vortex trajectory

As stated above advection of the vortex is by the regular field ϕ_0. First consider times $\tau \ll 1$. The regular term (4.31) is, to leading order in τ,

$$\phi_0 \approx \frac{\Gamma\tau}{2\pi} \int_0^\infty \omega A(k,y) \sin kx \ dk, \tag{4.50}$$

as $\tau \to 0$. The pseudoimage term cancels with the $\cos kx$ term in the expansion of the wave term, and so the pseudoimage has no leading order effect on the vortex at initial times. The vortex velocity components given by (4.17a) are then

$$\frac{dX}{d\tau} = 0, \tag{4.51a}$$

$$\frac{dY}{d\tau} = \frac{\epsilon\Gamma\tau}{2\pi} \int_0^\infty \omega A(k,L)dk. \tag{4.51b}$$

The integral in (4.51b) converges, since $|A(k,y)| < e^{-k}$, and is negative, since ω is negative for $k > 0$. Hence, for $\tau \ll 1$ the vortex moves with velocity increasing linearly in time, in the y-direction. Cyclones ($\Gamma < 0$) drift north and anticyclones ($\Gamma > 0$) move south, regardless of the sign of L.

For times $1 \ll \tau < \epsilon^{-1}$. The topographic waves have propagated away and have no influence on the vortex. Then, the advection of the vortex is due solely to the pseudoimage. From equations (4.17a)

and (4.17b)

$$\frac{dX}{d\tau} = -\epsilon u, \qquad \frac{dY}{d\tau} = 0, \tag{4.52}$$

where

$$u = -\frac{\Gamma}{2\pi} K_1(2|L|) \mathrm{sgn} L \tag{4.53}$$

Anticyclones ($\Gamma > 0$) move west (resp. east) in shallow (deep) water, whilst cyclones ($\Gamma < 0$) move east (resp. west) in shallow (deep) water. Compare this with the results of Bell (1989) and Stern and Flierl (1987), who find that a weak vortex near a potential vorticity interface and a shear flow respectively, also moves in the sense of its image in the interface.

To understand the physical mechanism responsible for the drift of the vortex, consider Figure (4.5). This plot shows the evolution of the streamlines associated with the ϕ_0-field, for $\Gamma = 1$, i.e. an anticyclone. In Figure (4.5a), the streamlines of the short time solution given by equation (4.50) are plotted. The initial response is the establishment of a secondary dipole, centred over the escarpment and with its axis aligned along the y-axis. This is the result of the anticyclone drawing fluid to its west from the deep side of the escarpment, and pushing fluid to its east away from the shallow side of the escarpment. The vortex moves south along the dipole axis[2]. These secondary circulations, induced by the circulation of the primary vortex diminish rapidly, as energy is lost to the topographic waves. This process is clear in Figures (4.5b,c), which show the rapid west propagation of the topographic waves, away from the vortex centre. The final frame, Figure (4.5d), shows that as $\tau \to \infty$ all that remains is the non-dispersive pseudoimage term. Figure (4.6) shows the same process schematically, this time for a cyclone, $\Gamma = -1$.

This behaviour is in contrast to the motion of an intense singular vortex near an escarpment. McDonald (1998) showed that intense cyclones move northwest, while intense anticyclones move southwest. Importantly, both cyclones and anticyclones approach a steady westward drift velocity that matches a possible topographic wave phase velocity, so that wave radiation must eventually become an important factor in the motion of the vortex. In the present weak limit this is not always the case as, for instance, shallow water cyclones and deep-water anticyclones move east, i.e. antiparallel to the topographic waves. The large time response of the vortex is the subject of the following section.

---

[2]This is precisely the initial response for an intense vortex near an escarpment *and* on a β-plane. In those cases however the strong circulation of the vortex rotates the dipole axis before the initial disturbance can disperse as topographic waves, causing the southwest (northwest) curved trajectories for anticyclones (cyclones).
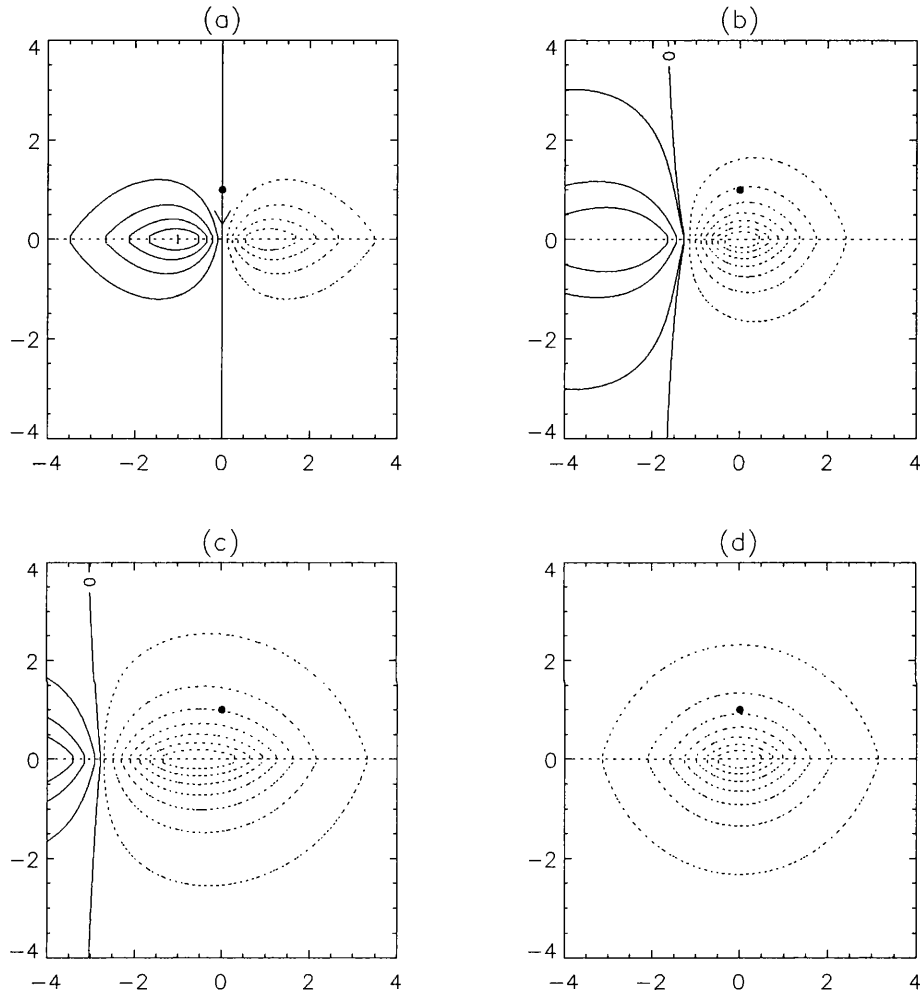
Figure 4.5: The advection of the vortex, here an anticyclone, by the regular field. (a) evaluation of ϕ at $\tau = 0^+$, by equation (4.50). The contour values have been scaled by $\tau/2\pi$. Note the initial advection is south, along the dipole axis. (b) ϕ evaluated at $\tau = 4$ and (c) evaluated at $\tau = 7$, from equation (4.31), (d) is the pseudoimage term, the regular field as $\tau \rightarrow \infty$. See text for further comments.

(a)

(b)
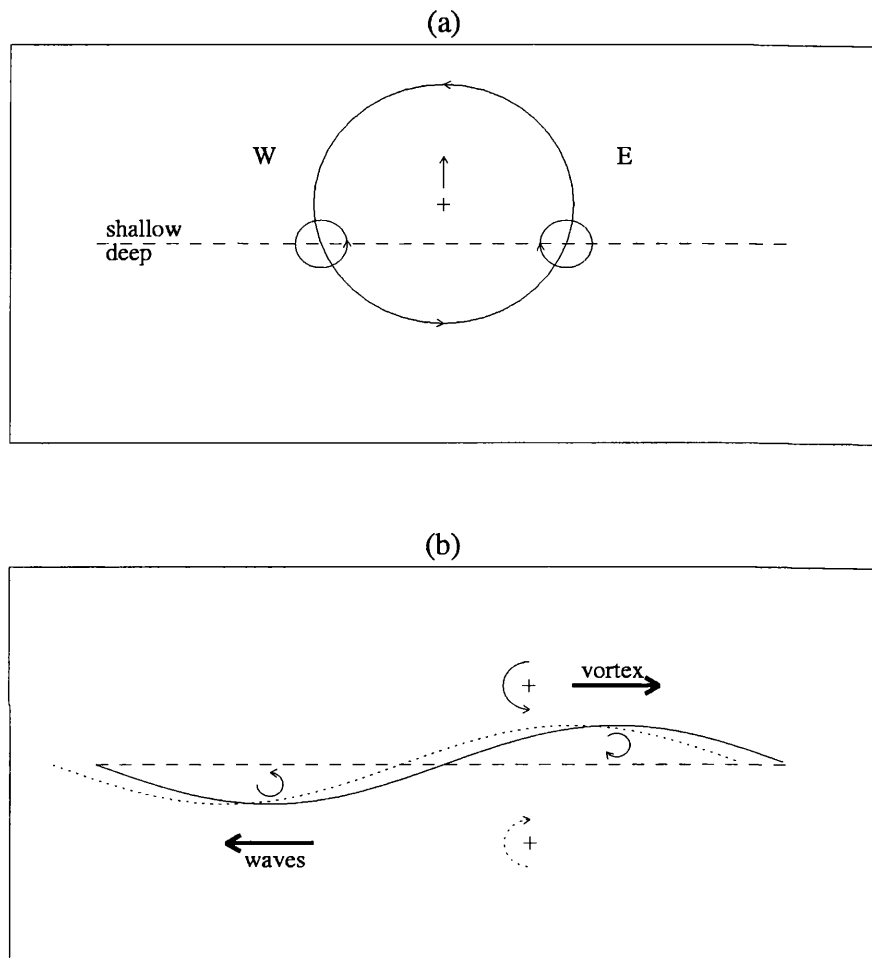
Figure 4.6: The mechanisms for the vortex and wave propagation. (a) The circulation of the vortex, here a cyclone, moves fluid to its east from deep to shallow water, and fluid to its west from shallow to deep water. The fluid gains net relative vorticity in the sense shown, and the dipolar nature of the disturbance advects the vortex northwards. (b) The preferential direction of the waves is west, and is also due to the initial relative vorticity production. The waves propagate away from the vortex, which is then advected by its pseudoimage, shown by the dotted arrow.

53

4.2.3 Large-time solution

In this section the solution on the long, advective time scale is investigated. A natural approach is to use the fact that ϵ is small, and seek a solution to equation (4.2) in the form of a perturbation series in ϵ,

$$\phi = \phi_0 + \epsilon\phi_1 + \dots \tag{4.54}$$

However, this leads to a solution which grows secularly. See Appendix A for details. Instead, the adjustment on the short, topographic wave time scale is assumed to happen instantaneously on the advective time scale. That is, the large τ asymptotic, steady solution of the previous subsection is taken as the initial condition. Denote by ϕ_1 the solution to (4.15) on the advective time scale. The two solutions are then matched by demanding that

$$\lim_{t \to 0^+} \phi_1 = \lim_{\tau \to \infty} \phi_0 = -\Psi_v(x, |y| + |L|). \tag{4.55}$$

For times $t \ll 1$, from equation (4.53) the vortex centre moves with the steady drift velocity $X(t) = ut$, suggesting a solution of the form

$$\psi(x, y, t) = \Psi_v(x - ut, y - L) + \phi_1(x, y, t). \tag{4.56}$$

Note that $J[\nabla^2 \phi_0, \phi_0] = 0$ in equation (4.2). That is, the response is linear as $t \to 0^+$. It is assumed that this remains the case for finite t. This assumption is justified *a posteriori*, by contour dynamics investigations of the full nonlinear problem.

The linear governing equation for ϕ_1 is then

$$\epsilon \left(\nabla^2 \phi_1 - \phi_1 \right)_t + \frac{\partial \phi_1}{\partial x} \frac{\partial h_B}{\partial y} = -\frac{\partial \Psi_v}{\partial x} \frac{\partial h_B}{\partial y}. \tag{4.57}$$

Away from $y = 0$ this is

$$\nabla^2 \phi_1 - \phi_1 = 0. \tag{4.58}$$

The initial condition is given by (4.55) and the boundary conditions obtained as above are

$$\nabla\phi_1 \to 0 \quad , \qquad x^2 + y^2 \to \infty \tag{4.59a}$$

$$[\phi_1] = 0 \quad , \qquad y = 0 \tag{4.59b}$$

$$\epsilon\,[\phi_{1yt}] + 2\phi_{1x} = -2\Psi_{vx}(x - ut, -L) \quad , \qquad y = 0 \tag{4.59c}$$

Denote the Fourier transform of ϕ_1 by $\hat{\phi}_1$, so (4.58) and (4.59a,b) have solutions of the form

$$\hat{\phi}_1(k, y, t) = B_1(k, t) e^{-\sqrt{k^2 + 1}\,|y|}. \tag{4.60}$$

From the properties of Fourier transforms,

$$\hat{\Psi}_v(x - ut, -L) = e^{-ikut}\hat{\Psi}_v(x, -L), \tag{4.61}$$

so the transform of (4.59c) is, using identity (4.25) and after some manipulation:

$$\frac{d}{dt}\left(B_1 e^{i\omega t}\right) = -\frac{i\omega\Gamma}{2\sqrt{k^2 + 1}}e^{-|L|\sqrt{k^2+1}}e^{i(ku-\omega)t}, \tag{4.62}$$

with solution,

$$B_1 e^{i\omega t} = C(k) + \frac{\omega\Gamma}{2\sqrt{k^2 + 1}}\frac{e^{-|L|\sqrt{k^2+1}}}{ku - \omega}e^{i(\omega-ku)t}, \tag{4.63}$$

where,

$$\omega = -\frac{k}{\epsilon\sqrt{k^2 + 1}}, \tag{4.64}$$

is the topographic wave frequency on the advective time scale. Initial condition (4.55) gives $\phi_1(x, 0, 0) = -\Psi_v(x, |L|)$ from which,

$$C(k) = -\frac{\Gamma}{2\sqrt{k^2 + 1}}\frac{ku}{ku - \omega}e^{-|L|\sqrt{k^2+1}}. \tag{4.65}$$

Thus,

$$\hat{\phi}_1(k, y, t) = -\frac{\Gamma}{2\sqrt{k^2 + 1}}e^{-(|y|+|L|)\sqrt{k^2+1}}\frac{1}{ku - \omega}\left(kue^{-i\omega t} - \omega e^{-ikut}\right). \tag{4.66}$$

Note that this may be rewritten

$$\hat{\phi}_1(k, y, t) = -\hat{\Psi}_v(x, |y| + |L|)\frac{kue^{-i\omega t} - \omega e^{-ikut}}{ku - \omega}, \tag{4.67}$$

so in particular, when $t = 0$

$$\hat{\phi}_1(k, y, 0) = -\hat{\Psi}_v(x, |y| + |L|), \tag{4.68}$$

which is the correct initial condition. The solution consists of a quasi-steady term and a topographic wave term, and can be written

$$\phi_1(x, y, t) = \phi_1^{(s)} + \phi_1^{(w)}, \tag{4.69}$$

where

$$\phi_1^{(s)} = -\frac{\Gamma}{4\pi}\int_C \frac{e^{-(|y|+|L|)\sqrt{k^2+1}}}{1 + \epsilon u\sqrt{k^2 + 1}}\frac{1}{\sqrt{k^2 + 1}}e^{ik(x-ut)}dk, \tag{4.70a}$$

$$\phi_1^{(w)} = -\frac{\Gamma\epsilon u}{4\pi}\int_C \frac{e^{(-|y|+|L|)\sqrt{k^2+1}}}{1 + \epsilon u\sqrt{k^2 + 1}}e^{i(kx-\omega t)}dk. \tag{4.70b}$$

The $\phi_1^{(s)}$ term is a non dispersive term of the form $\phi_1^{(s)} = \phi_1^{(s)}(x - ut, y)$, and so is a disturbance which propagates with the vortex. To leading order in the binomial expansion with respect to ϵ of the integrand this term is the steadily propagating pseudoimage. The second term $\phi_1^{(w)}$ is a Fourier

55

superposition of topographic waves. The dispersion relation is given by (4.64), and so the phase and group velocities are

$$c_p(k) = -\frac{1}{\epsilon\sqrt{k^2+1}}. \tag{4.72a}$$

$$c_g(k) = -\frac{1}{\epsilon(k^2+1)^{3/2}} \tag{4.72b}$$

as before. Note that the appearance of ϵ in these quantities is due to the time scale being the advective time scale.

Each of (4.70a) and (4.70b) has simple poles for $k = \pm\gamma$ where

$$\gamma = \left(\frac{1}{\epsilon^2 u^2} - 1\right)^{1/2}, \tag{4.73}$$

whenever $-1 < \epsilon u < 0$, i.e. whenever the vortex drifts west. In order that the waves radiate away from the vortex the inversion contour, C, must pass *below* these poles as in Figure (4.7). The existence of poles gives rise to the possibility of wave radiation as $t \to \infty$. There are only two cases to consider since the case $u = 0$ is of no interest because there is no vortex, and the cases $|\epsilon u| \geq 1$ are ruled out, otherwise u is an $O(1/\epsilon)$ quantity, contradicting the weak vortex assumption which constrained u to be at most $O(1)$.

(i) $0 < \epsilon u < 1$

This is the case of either a cyclone located on the shallow side of the escarpment or an anticyclone located on the deep side of the escarpment, and since $1 + \epsilon u(k^2+1)^{1/2} \neq 0$, there are no singularities. Thus the inversion contour C may be deformed back to the real k-axis. For large t the wave term is dominated by the single point of stationary phase, occurring for $-t < x < 0$,

$$k_s = \left((-\epsilon\zeta)^{-2/3} - 1\right)^{1/2}, \tag{4.74}$$

where $\zeta = x/t$. A similar calculation to that in section 4.1 yields

$$\phi_1^{(w)} \approx \frac{\Gamma u\epsilon}{\sqrt{2\pi}} \frac{e^{-(|y|+|L|)\sqrt{k_s^2+1}}}{1+\epsilon u\sqrt{k_s^2+1}} \left(\frac{1}{3tk_s\zeta^{5/3}}\right)^{1/2} \cos\left(k_s x - \omega_s t - \frac{\pi}{4}\right), \tag{4.75}$$

for ζ constant as $t \to \infty$. The waves are transient, decaying like $t^{-1/2}$, leaving only the steadily propagating vortex and pseudoimage as $t \to \infty$. The vortex is moving at a velocity outside the range of topographic wave phase velocities, and in particular, since $u > 0$, is moving in the opposite direction to the waves. The vortex propagates away from the wave bundle, which consequently

56
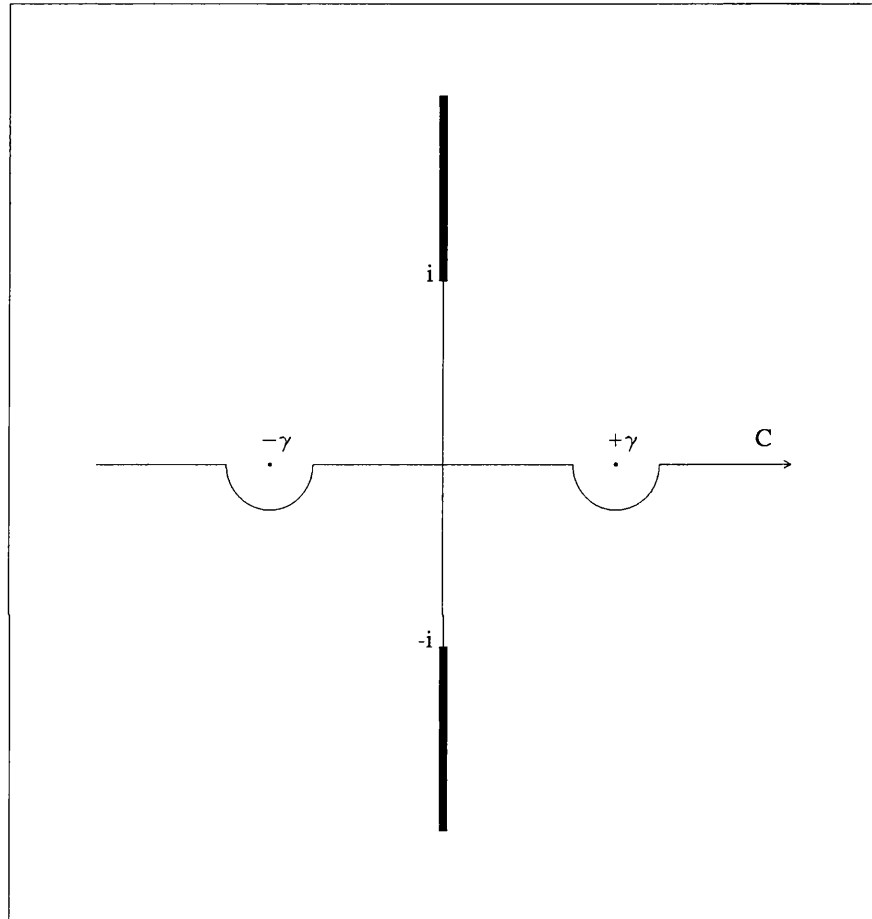
Figure 4.7: The inversion contour, C, in the complex k-plane. The radiation condition dictates that the contour should pass below the singularities at $k = \pm\gamma$. Branch cuts made from $\pm i$ to $\pm i\infty$, are shown by the heavy lines.

decays, leaving only the quasi-steady term. The transient nature of the disturbance is illustrated by Fast Fourier Transform of the regular field ϕ_1 over the escarpment in Figure (4.8). The large, localised disturbance near the vortex centre is the nondispersive part of the topographic wave train (i.e the pseudoimage), whilst the topographic waves propagate away to the west, with amplitudes decaying with time.

(ii) $-1 < \epsilon u < 0$

This is the case of west travelling anticyclones located on the shallow side of the escarpment or cyclones located on the deep side of the escarpment. There are simple poles in the integrals (4.70a) and (4.70b) at $k = \pm\gamma$, given by (4.73). At large times the the solution is dominated by the behaviour near the poles, for which

$$k \approx \frac{1}{\epsilon u} \gg 1, \tag{4.76}$$

corresponding to *short* waves. Also, a simple rearrangement of (4.73) reveals

$$u = -\frac{1}{\epsilon\sqrt{\gamma^2 + 1}} = c_p(\pm\gamma), \tag{4.77}$$

since $u < 0$. The asymptotic behaviour is dominated by the short waves with phase velocities close to the velocity of the vortex.

Consider first the non-dispersive term $\phi_1^{(s)}$. The contribution to the integral from the semi-circular arcs is exponentially small as $x - ut \to -\infty$. However the same is not true for $x - ut \to \infty$. In this case the inversion contour, C, must be closed in the upper half-plane and the integral evaluated by the method of residues. In doing so it is necessary to introduce a branch cut from $k = i$ to $k = \infty i$, since $\sqrt{k^2 + 1}$ is double valued. The inversion contour must then be deformed round the branch cut. As $x - ut \to \infty$ the contribution due to the branch cut is exponentially small and may be ignored. To make the poles explicit write

$$\frac{1}{1 + \epsilon u\sqrt{k^2 + 1}} = \frac{1}{(\epsilon u)^2} \frac{\epsilon u\sqrt{k^2 + 1} - 1}{k^2 - \gamma^2}, \tag{4.78}$$

so that,

$$\phi_1^{(s)} = -\frac{\Gamma}{4\pi(\epsilon u)^2} \int_C \frac{e^{-(|y|+|L|)\sqrt{k^2+1}}}{k^2 + \gamma^2} \frac{\epsilon u\sqrt{k^2 + 1} - 1}{\sqrt{k^2 + 1}} e^{ik(x-ut)} dk. \tag{4.79}$$

The residue of the integrand at the pole $k = \gamma$ is

$$\frac{\epsilon u}{\gamma} \exp\left(-\frac{|y| + |L|)}{|\epsilon u|}\right) e^{i\gamma(x-ut)}. \tag{4.80}$$

58
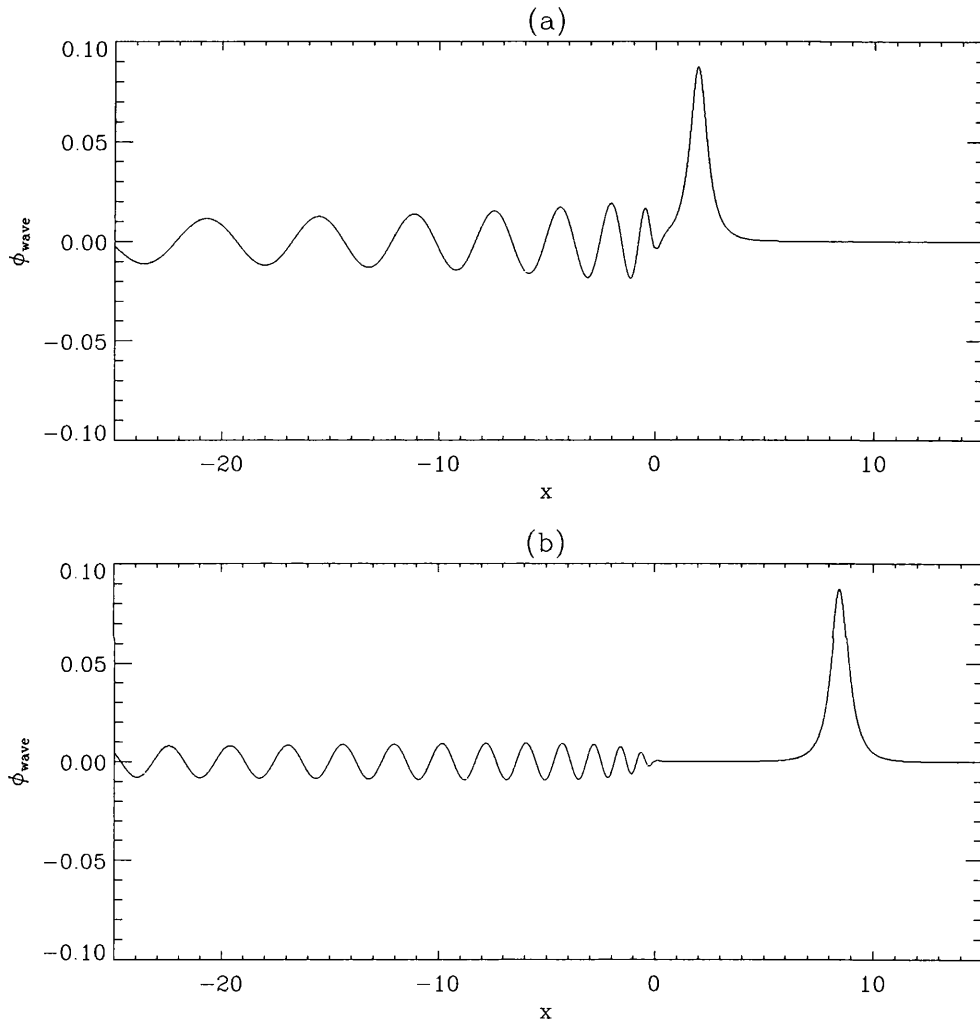
Figure 4.8: FFT evaluation of the regular solution over $y = 0$, for a nonradiating weak vortex. The parameter values used are $\Gamma = -1$, $\epsilon = 0.1$ and $L = 0.5$. The times are (a) $t = 7$ and (b) $t = 30$.

Similarly the residue at $k = -\gamma$ is

$$-\frac{\epsilon u}{\gamma} \exp\left(-\frac{|y| + |L|)}{|\epsilon u|}\right) e^{-i\gamma(x-ut)}. \tag{4.81}$$

The large time behaviour of $\phi_1^{(s)}$ is then given by $2\pi i$ times the sum of the residues, i.e. for large t,

$$\phi_1^{(s)} \approx \frac{\Gamma}{\epsilon u \gamma} \exp\left(-\frac{|y| + |L|)}{|\epsilon u|}\right) \sin\gamma(x - ut)H(x - ut), \tag{4.82}$$

where $H(x)$ is the unit Heaviside step function, which arises due to the fact that there is no contribution for $x - ut < 0$. Next consider the wave term $\phi_1^{(w)}$. Near the poles $k = \pm\gamma$ a Taylor expansion gives,

$$\omega(k) + ku \approx \omega(\pm\gamma) \pm \gamma + (\omega'(\gamma) + u)(k \mp \gamma)$$

$$= (c_g(\gamma) + u)(k \mp \gamma), \tag{4.83}$$

since $w'(k) = c_g$. Hence near the poles,

$$\phi_1^{(w)} \approx -\frac{\Gamma u \epsilon}{4\pi} \int_C \frac{e^{-(|y|+|L|)\sqrt{k^2+1}}}{1 + \epsilon u\sqrt{k^2 + 1}} e^{ik(x - c_g(\gamma)t)} e^{\mp i\gamma(-c_g + u)t} \, dk. \tag{4.84}$$

There is no contribution due to the poles as $x - c_g(\gamma)t \to -\infty$. A residue calculation for $x - c_g(\gamma)t \to \infty$ then yields

$$\phi_1^{(w)} \approx -\frac{\Gamma}{\epsilon u \gamma} \exp\left(-\frac{|y| + |L|)}{|\epsilon u|}\right) \sin\gamma(x - ut)H(x - c_g t), \tag{4.85}$$

where $\omega(\gamma) = -\gamma u$ has been used. Note that for $k = \pm\gamma$ the inequality $u < c_g < 0$ holds. Thus the large time response for the radiated case is

$$\phi_1 \approx g(y) \, \sin\gamma(x - ut) \, [H(x - ut) - H(x - c_g t)], \tag{4.86}$$

where

$$g(y) = \frac{\Gamma}{\epsilon u \gamma} \exp\left(-\frac{|y| + |L|}{|\epsilon u|}\right) \tag{4.87}$$

This is a wave tube existing for $ut < x < c_g(\gamma)t$, and whose width, say D, grows like the difference of the phase and group velocities of the radiated waves:

$$|D| \approx \epsilon^{-1}t\left((\epsilon u) - (\epsilon u)^3\right), \tag{4.88}$$

since $\epsilon c_g = \epsilon c_p^3$ at $k = \pm\gamma$. Since ϵ^3 is negligible, the rate of growth of the wave tube is approximately u, the phase velocity of the radiated waves. Figure (4.9) illustrates the process of the wavetube formation. Here, the solution ϕ_1 has been evaluated over the escarpment by Fast Fourier Transforms. The waves ahead of the vortex decay. Note also the pseudoimage, i.e the non-dispersive part of the
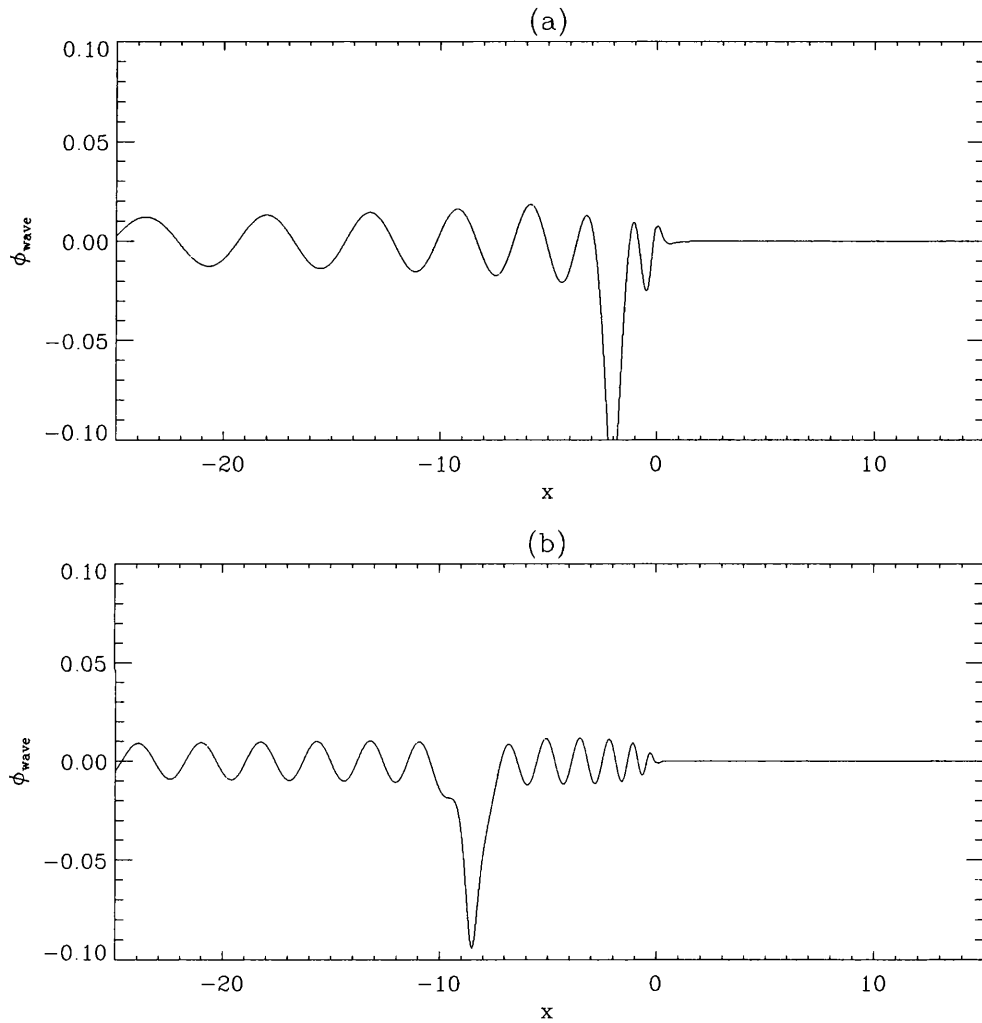
Figure 4.9: FFT evaluation of the regular solution over $y = 0$, for a radiating weak vortex. The parameter values used are $\Gamma = +1$, $\epsilon = 0.1$ and $L = 0.5$. The times are (a) $t = 7$ and (b) $t = 30$. The non-dispersive pseudoimage is evident, and the waves ahead of it are the dispersive wave. The waves in the wake of the vortex are the steadily propagating radiated waves.

wavetrain which propagates with the vortex. The waves are radiated from the pseudoimage, which must decrease in size, and which in turn must affect the vortex drift velocity.

In summary, in the radiating cases (anticyclone located on the shallow side or cyclone located on the deep side of the escarpment) the topographic waves decay like $t^{-1/2}$ except for the particular short waves with wavenumber $k = \pm\gamma$, which have phase velocity equal to the vortex zonal drift velocity. A wave train of finite length forms in the wake of the vortex. The trailing edge of this wave train moves at the group velocity of the radiated waves. Thus there is no disturbance for $x > c_g t$, and in particular the fluid is at rest at the initial position of the vortex.

Since the radiating waves have non-zero energy flux, they must exert a drag on the vortex, which in turn must respond to this loss of energy. Bell (1989) argued that a weak singular barotropic vortex moves perpendicular to a potential vorticity interface due to wave radiation. In the following section global momentum arguments are used to calculate the effect of wave radiation upon the vortex drift velocity.

4.2.4   Large time vortex trajectory

For the case of an intense singular vortex, McDonald (1998) calculates the response of the vortex to the radiating waves by equating the energy flux of the wave tube to that of the vortex to derive an ODE for L, the distance of the vortex centre from the escarpment. In the present case an analogous equation is obtained by equating the *momentum* flux of the vortex to the pseudomomentum (see McIntyre (1981), Lam and Dritschel (1998)) of the wave tube. This has the advantage that the calculations are simpler; however the momentum and energy flux arguments are equivalent and yield the same result. The energy density in the wave tube (4.86) is

$$
\begin{aligned}
\rho &= \frac{1}{2}\left(\bar{\phi}_{1x}^2 + \bar{\phi}_{1y}^2 + \bar{\phi}_1^2\right), \\
&= \frac{\Gamma^2}{\gamma^2(\epsilon u)^4}\exp\left(-2\frac{|y|+|L|}{|\epsilon u|}\right),
\end{aligned}
\tag{4.89}
$$

where the overbar denotes the average over one wave period. Note that by ϕ_1 in this equation is meant the large time asymptotic solution given in (4.86). The wave power (i.e. the total energy flux), F, of the radiated waves is found by integrating ρ over all y and multiplying the result by the group velocity. The "appropriate" group velocity is the rate of growth of the wave tube given by(4.88). This gives the wave power,

$$F = \Gamma^2 e^{-|2L/\epsilon u|}. \tag{4.90}$$

The rate of change of the wave pseudomomentum is then the wave power divided by the phase velocity,

$$\frac{F}{\epsilon u} = \frac{\Gamma^2}{\epsilon u} e^{-|2L/\epsilon u|}. \tag{4.91}$$

This quantity is also the drag on the vortex, which must respond by losing momentum. See e.g McIntyre (1981). The leading order x-momentum of the vortex is, by a generalisation of the result for barotropic vortices in Batchelor (1967),

$$M_x = -\int\int y(\nabla^2 \psi - \psi) dA = \Gamma L, \tag{4.92}$$

the integral being taken over all space. Note that $d\Gamma/dt = 0$, (i.e. conservation of circulation), so any change in the vortex momentum is manifested only by a change in L. Taking the time derivative of (4.92) and equating it with the wave momentum flux (4.91) yields the differential equation for L

$$\frac{dL}{dt} = \frac{\Gamma}{2\epsilon u} e^{-|2L/\epsilon u|}. \tag{4.93}$$

Note that $u < 0$, so both shallow water anticyclones and deep water cyclones drift towards the escarpment in response to topographic wave radiation. The drift is very slow,

$$\frac{dL}{dt} = O(e^{-1/\epsilon}). \tag{4.94}$$

This might be expected for two reasons. First, the energy density of the radiating waves is localised near the escarpment. This is evident in the expression (4.89). Second, the wave energy is concentrated in the long topographic waves, and which propagate rapidly away from the vortex centre. Thus, the west traveling vortices radiate only the less energetic, short topographic waves. This in turn is a consequence of the weak vortex assumption, which constrains the vortex velocity to be $O(\epsilon)$ on the topographic wave time scale. The topographic waves whose phase speed matches the vortex drift speed are the short waves.

It has been shown in this subsection that the pseudoimage description of the vortex motion is valid on the long advective time scale, for so long as linear theory is valid on that time scale. In the following subsection the validity of the linear theory is tested numerically by contour dynamics experiments.

4.2.5 Contour dynamics results

The numerical algorithm, which integrates the full nonlinear equation (4.15), has been described in Chapter 2. Before proceeding to describe and discuss the results two points should be made. First, the infinitely long topographic contour necessarily has a finite representation during computational runs. The contour length must be chosen so that its ends remain undisturbed during the computations. Given that the time scale employed for the contour dynamics algorithm is the advective time scale, this is hampered by the fact that the waves travel rapidly away from the vortex centre and introduce end effects during the numerical runs. For small values of ϵ runs up to $t = 10$ are possible before end-effects become important.

The time step used in all the runs presented here is $\Delta t = 0.1$. Several of the runs have been repeated with a time step of $\Delta t = 0.05$, which resulted in no difference in the vortex trajectories. Also, surgery is carried out at a spatial cut-off scale of $\mu = 0.15$. Several of the runs were repeated with a spatial resolution of $\mu = 0.1$, and also with no surgery. In each case there was no difference in the computed vortex trajectories.

In the preceding sections linear theory was used to predict the evolution of a weak vortex on the advective time scale. The main focus of the numerical investigation is to test the hypothesis that the evolution of the vortex is well described by the linear theory, for times beyond that for which that theory is formally applicable. In particular, for what range of values of ϵ is the linear theory applicable? Indeed, what is the appropriate time scale for the applicability of the linear theory? Of further interest is the effect of wave radiation on the path of the west travelling vortices.

Attention is restricted to the case $L > 0$, i.e. to vortices (of both signs) located on the shallow side of the escarpment. There is no loss of generality here, since the governing equation (4.15) is invariant under the transformation

$$\psi(x, y) \to -\psi(x, -y). \tag{4.95}$$

Analogous results for vortices located on the deep side of the escarpment may be deduced by symmetry. The behaviour of anticyclones differs from that of cyclones, and each case is treated separately.

Anticyclones

Experiments were carried out for values $\epsilon = 0.1$, 0.2 and 0.4, with $L = 0.5$ in each case. Figure

(4.10a) shows a plot of the vortex zonal drift velocity compared with the linear theory prediction given in equation (4.53). It is apparent that the prediction agrees well with the numerical results, even up to $\epsilon = 0.4$.

Figure (4.10b) shows a plot of the vortex trajectory, again compared with the linear theory prediction. Note the initial southward movement in all cases presented. This observation is consistent with the linear theory, which stated that anticyclones initially move south as the result of the establishment of a secondary dipole (see the earlier discussion).

Figure (4.11) shows a plot of the evolution of the advected contour for $\epsilon = 0.1$. The west travelling dispersive waves are evident. Note also the disturbance which propagates with the vortex. The steadily propagating disturbance consists of fluid originally located on the shallow side of the escarpment, and which has crossed the escarpment to the deep side gaining net cyclonic relative vorticity of magnitude $2\epsilon^{-1}$. In the limit of small ϵ the circulation of this patch has precisely the correct magnitude to advect the primary vortex in the sense of its pseudoimage in the escarpment. Put another way, the steadily propagating cyclonic relative vorticity *is* the pseudoimage, and as noted in the analytical discussions above forms a non-dispersive part of the topographic wave train. There is no visible evidence of topographic wave radiation in this plot, and this observation is reinforced by the vortex drift, which, after the initial southward movement is predominantly zonal.

However, consider Figure (4.12), which shows the evolution of the contour for $\epsilon = 0.4$. Here, the topographic waves and the pseudoimage are also apparent. Note the radiating waves, of larger amplitude than for the weaker vortex, in the wake of the pseudoimage. This behaviour is qualitatively the same as that shown in the FFT plot of the analytical solution shown in Figure (4.9). Enhanced meridional drift is the response of the vortex to topographic wave radiation. Given that the vortex is singular, and so cannot change its shape, escarpment-ward meridional drift is the *only* response that the vortex can have to wave radiation.

Cyclones

Again experiments were carried out for values $\epsilon = 0.1$, 0.2 and 0.4, with $L = 0.5$ in each case. Figure (4.13a) shows a plot of the vortex zonal drift velocity compared with the linear theory prediction given in equation (4.53). The prediction is in good agreement with the numerical results for small values of ϵ, but it is evident that the linear theory predicts the vortex motion for a smaller range of
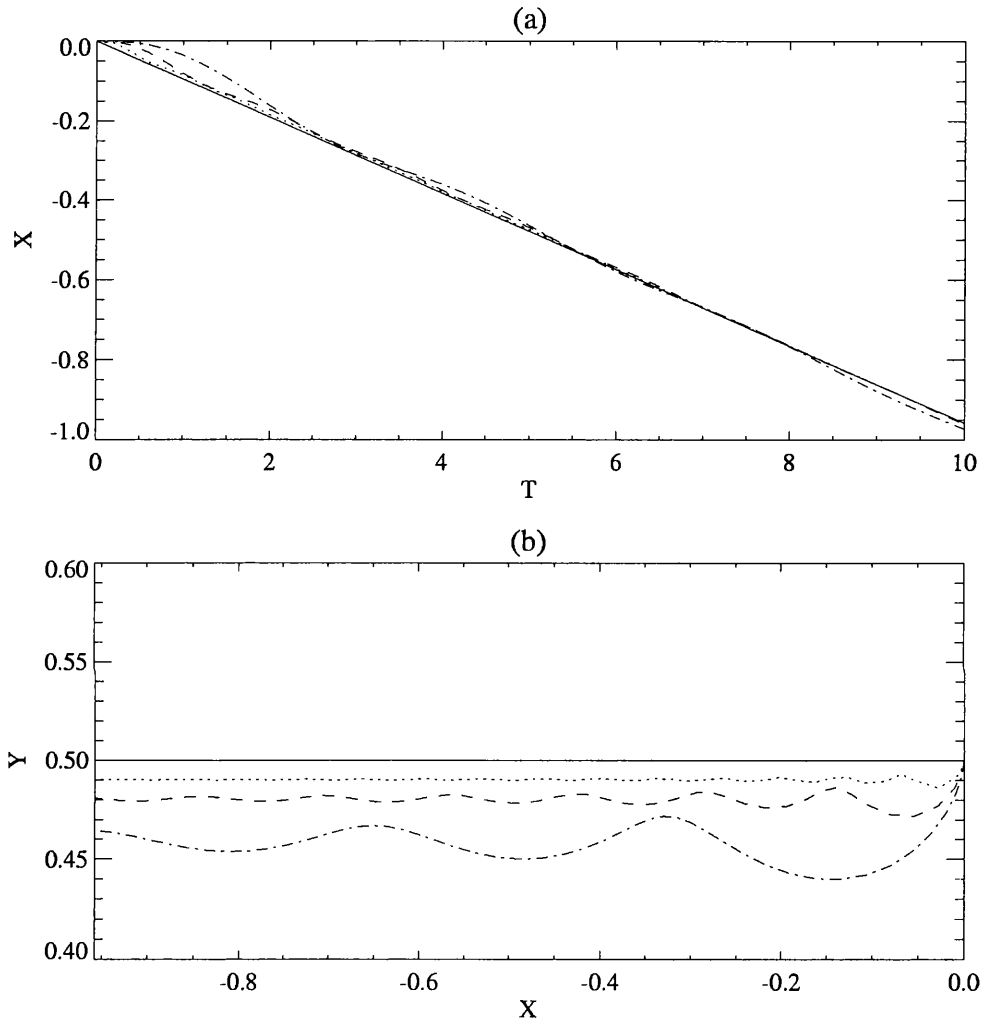
Figure 4.10: The drift of anticyclonic singular vortices, for $0 < t < 10$. The parameter values used are $L = 0.5$, $\epsilon = 0.1$ (dotted line), $\epsilon = 0.2$ (dashed line) and $\epsilon = 0.4$ (dot-dashed line). The x-displacement of the vortex centre is shown in (a) and the path of the vortex centre in (b). The solid line shows the analytic prediction, calculated from (4.53).
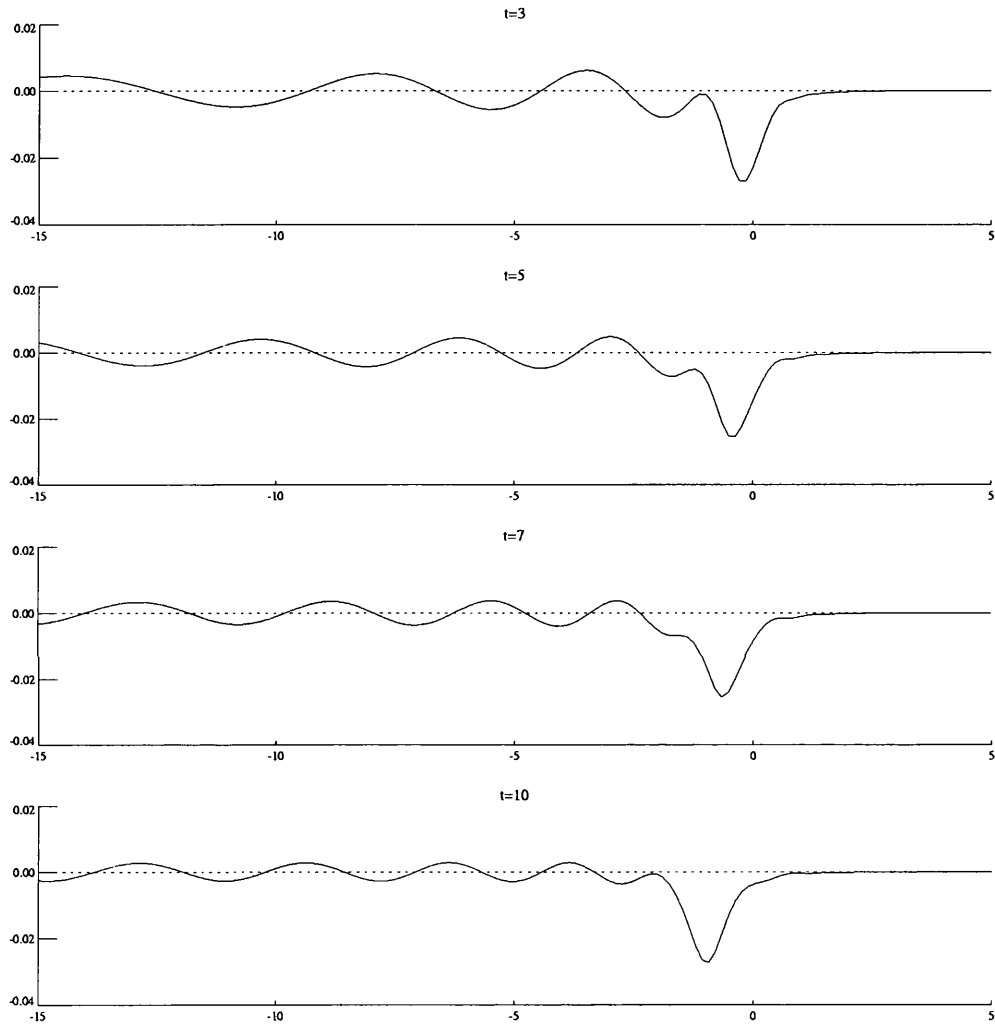
Figure 4.11: The evolution of the contour for a weak anticyclone. The parameter values used are $L = 0.5$, $S = 10$ (i.e. $\epsilon = 0.1$). Note the small amplitude disturbance, and the non-dispersive pseudoimage.
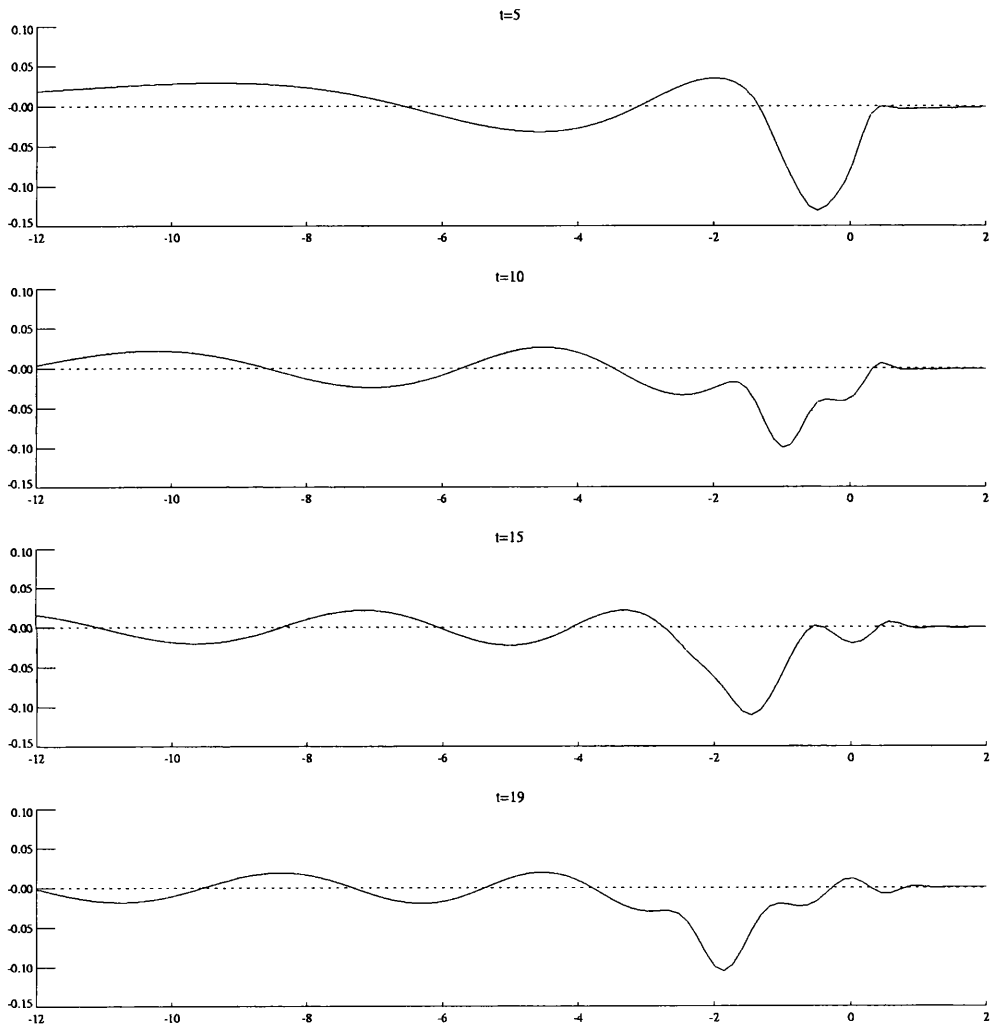
Figure 4.12: as Figure (4.11), except $\epsilon = 0.4$.

values of ϵ for cyclones than it does for anticyclones. This statement is reinforced in Figure (4.13b), which shows the trajectory of the vortex centre. For $\epsilon = 0.4$ the cyclone has undergone substantial meridional drift. This *cannot* be the result of wave radiation, since the cyclone propagates in the opposite direction to the topographic waves. Therefore, the meridional drift must be the result of nonlinear effects.

To understand why nonlinear effects are more pronounced for cyclones than anticyclones consider Figure (4.14), a plot of the evolution of the contour for $\epsilon = 0.1$. As for the anticyclones the dispersive topographic waves are evident. The pseudoimage is also evident, this time consisting of a patch of fluid which had crossed the escarpment from deep to shallow water, gaining net anticyclonic vorticity, and which, in the limit $\epsilon \to \infty$, has precisely the right circulation to advect the cyclone as if the escarpment were a plane wall.

Next consider Figure (4.15), which shows the contour evolution for a cyclone with $\epsilon = 0.4$, and illustrates a fundamental difference between a near weak cyclone and a near weak anticyclone. The initial disturbance "wants" to move west, dispersing as topographic waves. However, in this case the sense of the vortex circulation is such as to counter this tendency and is sufficiently strong to prevent the initial disturbance from moving away from the vicinity of the vortex. In contrast an anticyclone reinforces the westward propagation of the initial disturbance. For a cyclone a dipole consisting of the primary vortex together with the newly formed anticyclonic relative vorticity is formed, and by $t \approx 6$ this dipole propagates northeast, away from the escarpment. It will be shown below that for moderate intensity cyclones located on the shallow side of the escarpment, the formation of dipoles is a generic feature.

4.2.6 Discussion

It has been shown that, in the limit $\epsilon \to 0$, linear theory predicts that a weak singular vortex near an escarpment drifts in the sense of its image in the escarpment. Whilst an explicit definition of a pseudoimage is new, the phenomenon has been noted in two previous works. Bell (1989) and Stern and Flierl (1987) investigated the motion of a singular barotropic vortex near a potential vorticity interface and a shear flow respectively, and found that weak vortices move parallel to the interface in the image sense.
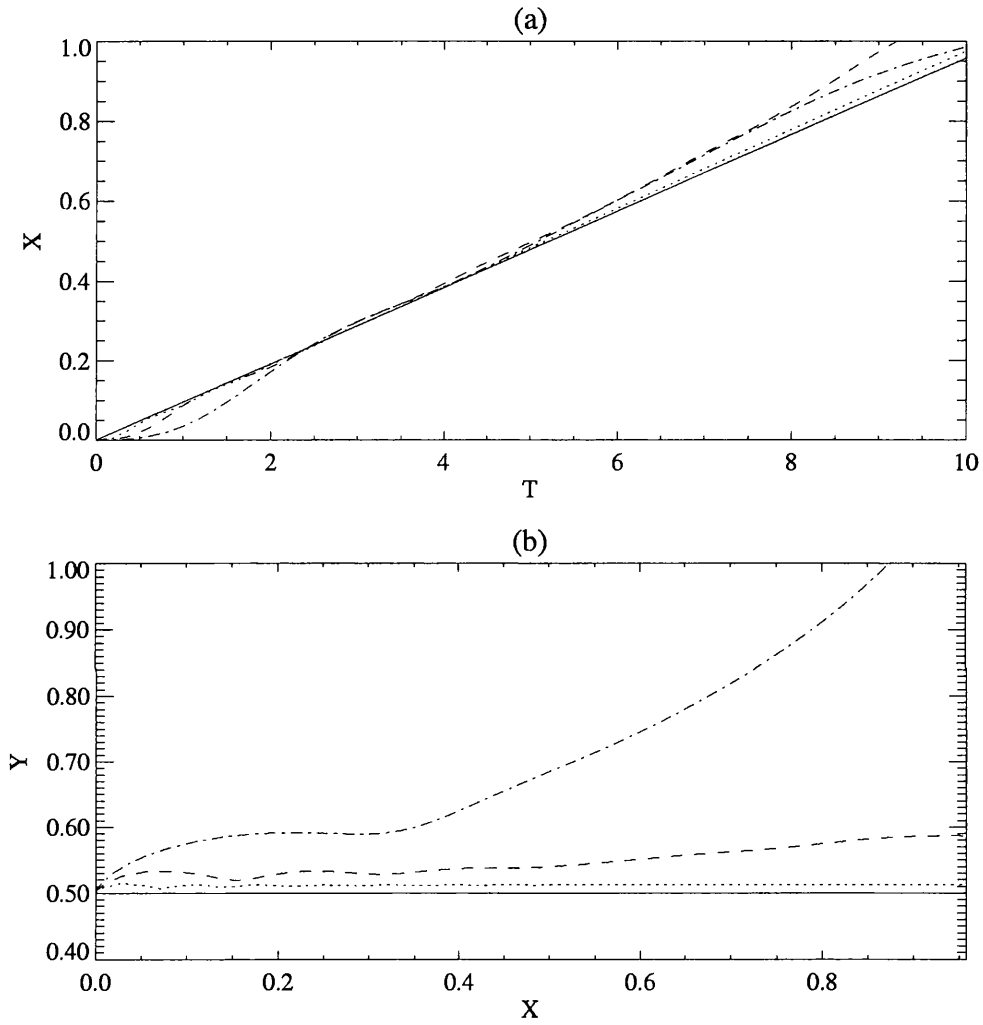
Figure 4.13: The drift of cyclonic singular vortices. The parameter values used are $L = 1$, $\epsilon = 0.1$ (dotted line), $\epsilon = 0.2$ (dashed line) and $\epsilon = 0.4$ (dot-dashed line). The x-displacement of the vortex centre is shown in (a) and the path of the vortex centre in (b). The solid line shows the analytic prediction, calculated from (4.53).
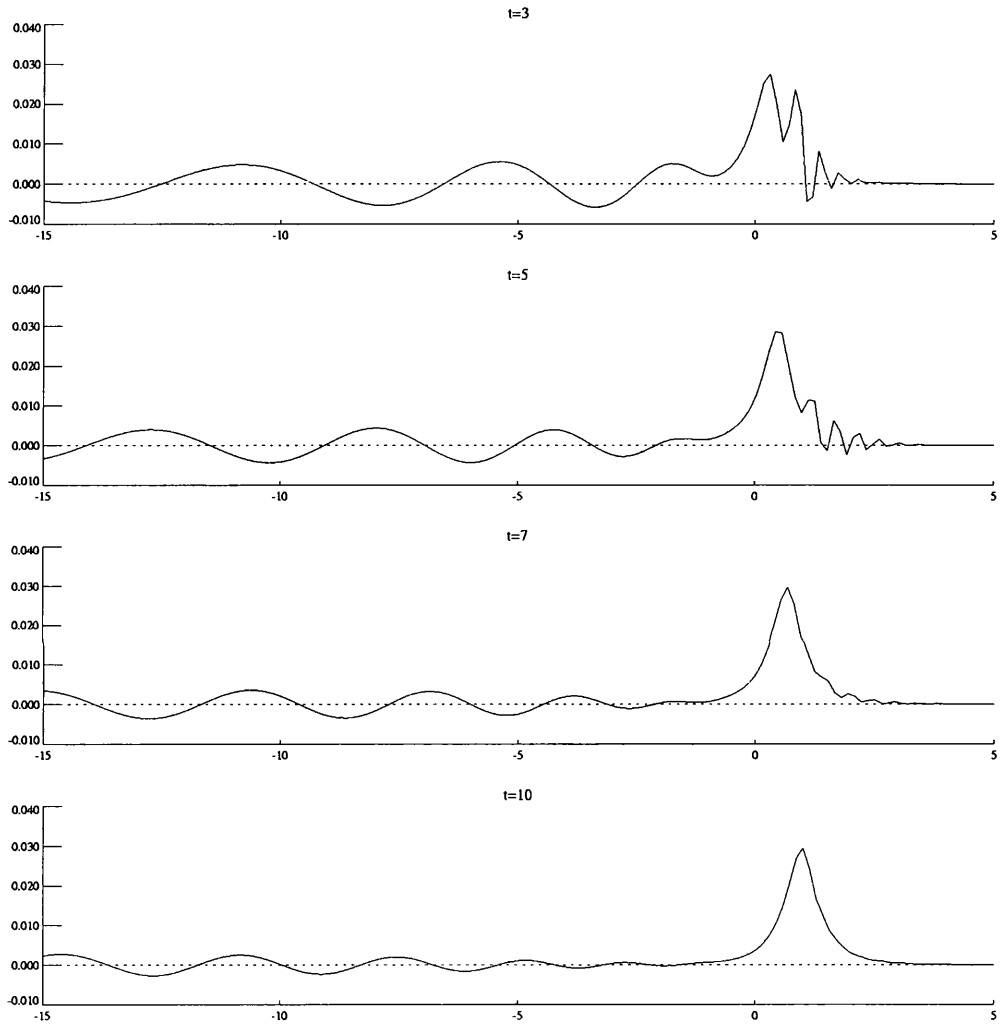
Figure 4.14: The evolution of the contour for a weak cyclone. The parameter values used are $L = 0.5$, $S = 10$ (i.e. $\epsilon = 0.1$).
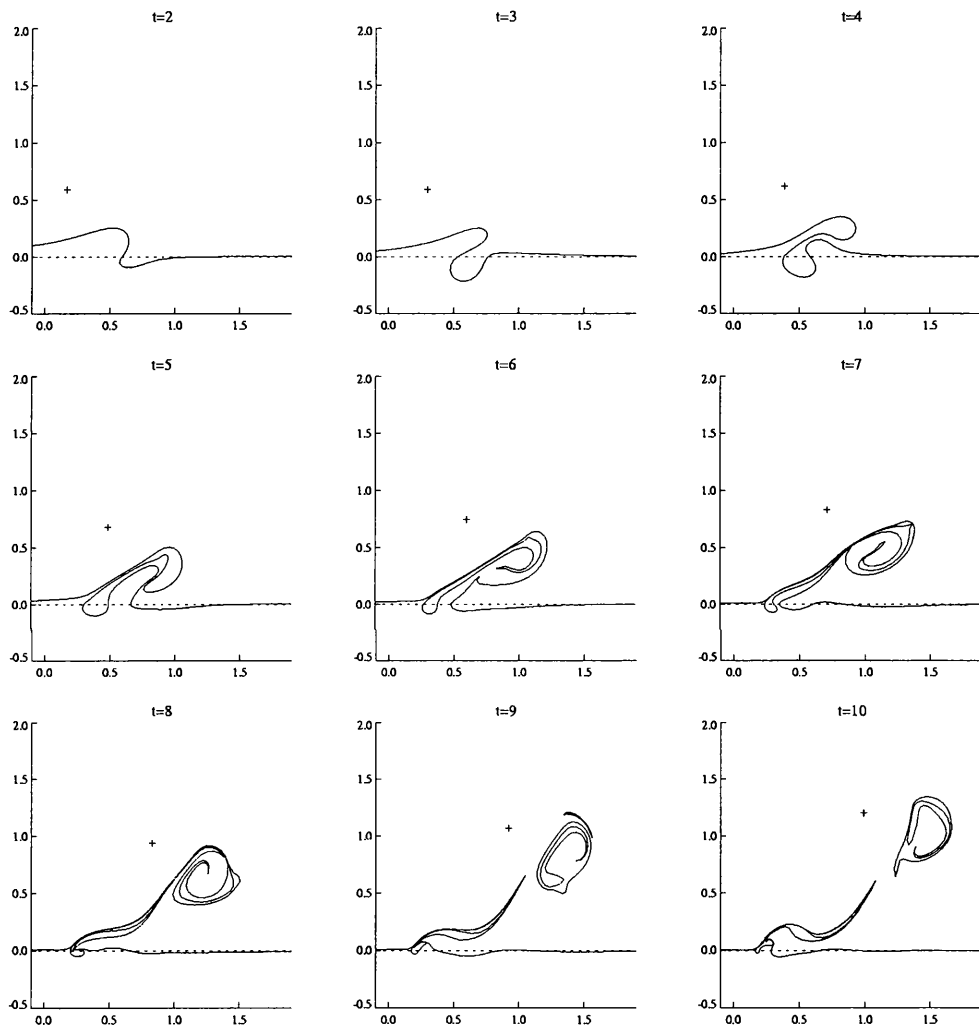
Figure 4.15: As Figure (4.14), except $\epsilon = 0.4$. The vortex centre is indicated by the cross.

West travelling anticyclones (resp. cyclones) located on the shallow (deep) side of the escarpment radiate short topographic waves as $t \to \infty$. Global momentum arguments were used to estimate the meridional drift of the vortex centre due to the wave radiation. This drift is exponentially slow since the energy flux associated with the short waves is small. It should be emphasised that meridional drift is the *only* possible response of a singular vortex to wave radiation, since its' shape is fixed. Thus "vortex breakdown" has no meaning in the present context. It is anticipated that a patch of vorticity may change its shape in response to wave radiation, and decay at large times. The problem of a vortex patch near an escarpment is the subject of the following chapter. McDonald (1996) investigated the motion of a modon near an escarpment. The modon moves parallel to the escarpment by self advection, and the west travelling modons decrease in radius in response to wave radiation. It is worth highlighting that there is no β-plane analogy for a weak singular vortex, since the Bessel function structure of the singular vortex dictates that the circulation is necessarily strong near the vortex centre. That is, near the vortex centre the β contours will be strongly wrapped up, even for a "weak" vortex. The present results are a consequence of there being some distance between the vortex and the topographic gradient.

Contour dynamics experiments have shown that for small ϵ linear theory does indeed describe the drift of the vortex centre for many eddy turnover times. Both anticyclones and cyclone drift parallel to the escarpment at the velocity due to the pseudoimage. The physical meaning of the pseudoimage was identified as a non-dispersive path of relative vorticity in the deflected topographic contour.

For anticyclones located on the shallow side of the escarpment, linear theory is accurate up to $\epsilon = 0.4$ and beyond. The wave induced meridional drift of the vortex centre increase with increasing ϵ, and the amplitude of the radiated waves also increases with ϵ.

On the other hand it has been shown that nonlinear effects are important for cyclones at smaller values of ϵ. The primary mechanism for the breakdown of the linear theory for cyclones is the accumulation of anticyclonic relative vorticity near the vortex centre. This is a result of the circulation of the primary vortex driving fluid against the preferred direction of the topographic waves. This anticyclonic relative vorticity is then able, through a dipole mechanism, to advect the primary vortex northeast. At large times the cyclone leaves the vicinity of the escarpment, a process which Zaval Sanson *et. el.* (1999) refer to as "back-reflection". A more thorough discussion of this phenomenon is given below, in the investigation of the behavior of moderate intensity vortices.

4.3 An intense singular vortex: a review

In this section a review of the results of McDonald (1998) is presented, for completeness of description, and more importantly to understand how the asymptotic analysis for the intense singular vortex limit breaks down. In solving the full nonlinear equation (4.15), in the limit $S \ll 1$, McDonald (1998) showed that the leading order vortex drift velocity components are (Su, Sv) where, u and v are given by the integral expressions

$$u = \frac{2}{\pi} \int_{|L|}^{\infty} (\cos b(r)t - 1)K_1(r)\sqrt{r^2 - L^2} \, dr \qquad (4.96a)$$

$$v = \frac{2}{\pi} \int_{|L|}^{\infty} \sin b(r)t \, K_1(r)\sqrt{r^2 - L^2} \, dr. \qquad (4.96b)$$

where $b(r) = -\Gamma K_1(r)/2\pi r$ is the angular velocity of the vortex. This solution is formally valid for $t < O(S^{-1})$. Asymptotic results show that anticyclones follow a curved southwest trajectory, whilst cyclones follow a curved northwest trajectory. As $t \to S^{-1}$, the vortex drift is purely zonal, with

$$u = -\exp(-|L|), \qquad (4.97)$$

for both anticyclones and cyclones. As $t \to \infty$ global momentum arguments show that the intense vortices have a wave radiation induced meridional drift, and have "rest-latitudes" about a Rossby radius from the escarpment. It is interesting to consider how the analytical results for $S \ll 1$ breakdown as S is increased.

First consider the case of intense anticyclones. Figure (4.16) shows a comparison of contour dynamics trajectories with the analytic prediction for $S = 0.01, 0.1$ and 0.2. The analytical trajectory has been calculated by fourth order Runge-Kutta, with the vortex drift velocity components given by (4.96a,b). The prediction is exceptionally good for small S. However, for $S = 0.2$ the vortex centre initially drifts further west, and less far south. Significantly at later times the westward drift velocity begins to retard, whilst the southwards drift velocity increases.

Consider Figure (4.17), which shows the evolution of the contour for $S = 0.01$. Note the initial dipolar structure of the front as the vortex circulation deflects the contour. The flow is later characterised by strong axisymmetrisation near the vortex centre. The vortex winds up the contour and build a shield of weak anticyclonic relative vorticity around itself. At later times the dipole axis has tilted, and the vortex trajectory curves to the west.
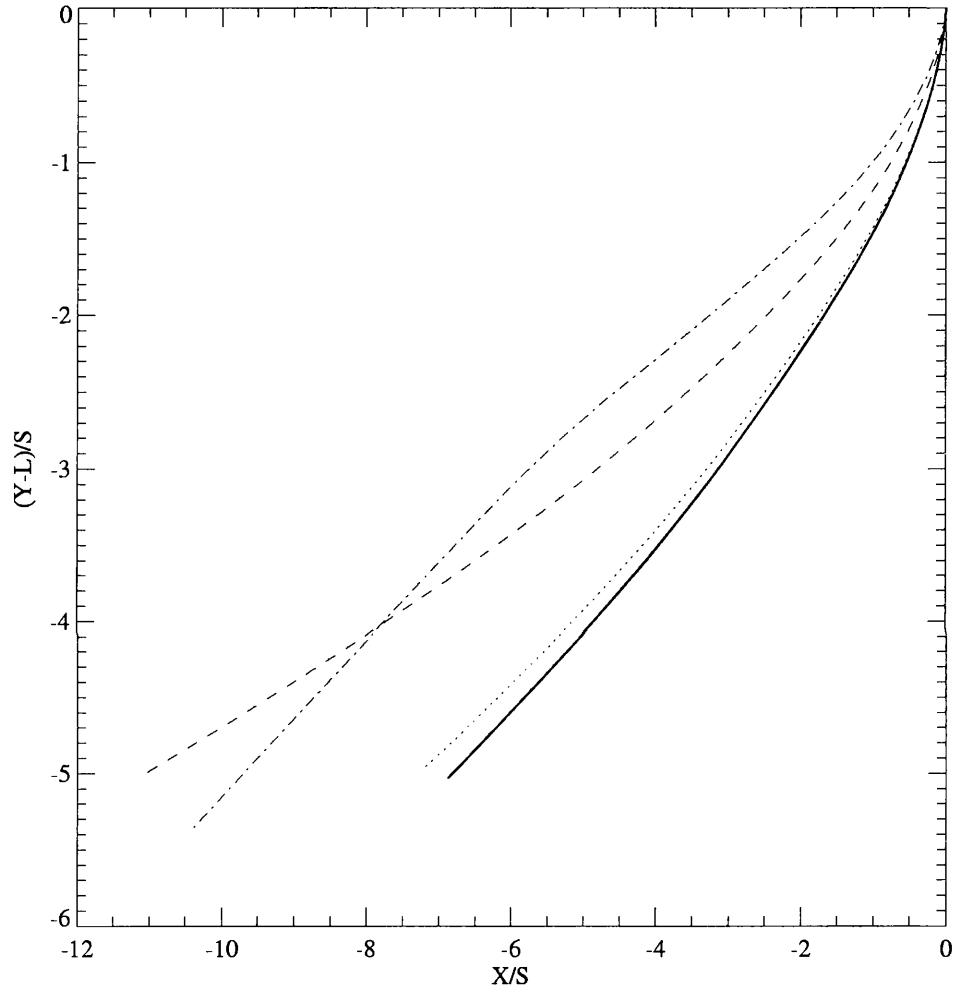
Figure 4.16: Comparison of the contour dynamics results with the analytical prediction for intense anticyclones for $0 < t < 30$. The parameter values used are $L = 0.5$ and $S = 0.01$ (dotted line), $S = 0.1$ (dashed line) and $S = 0.2$ (dot-dashed line). the analytical trajectory is shown by the solid line.
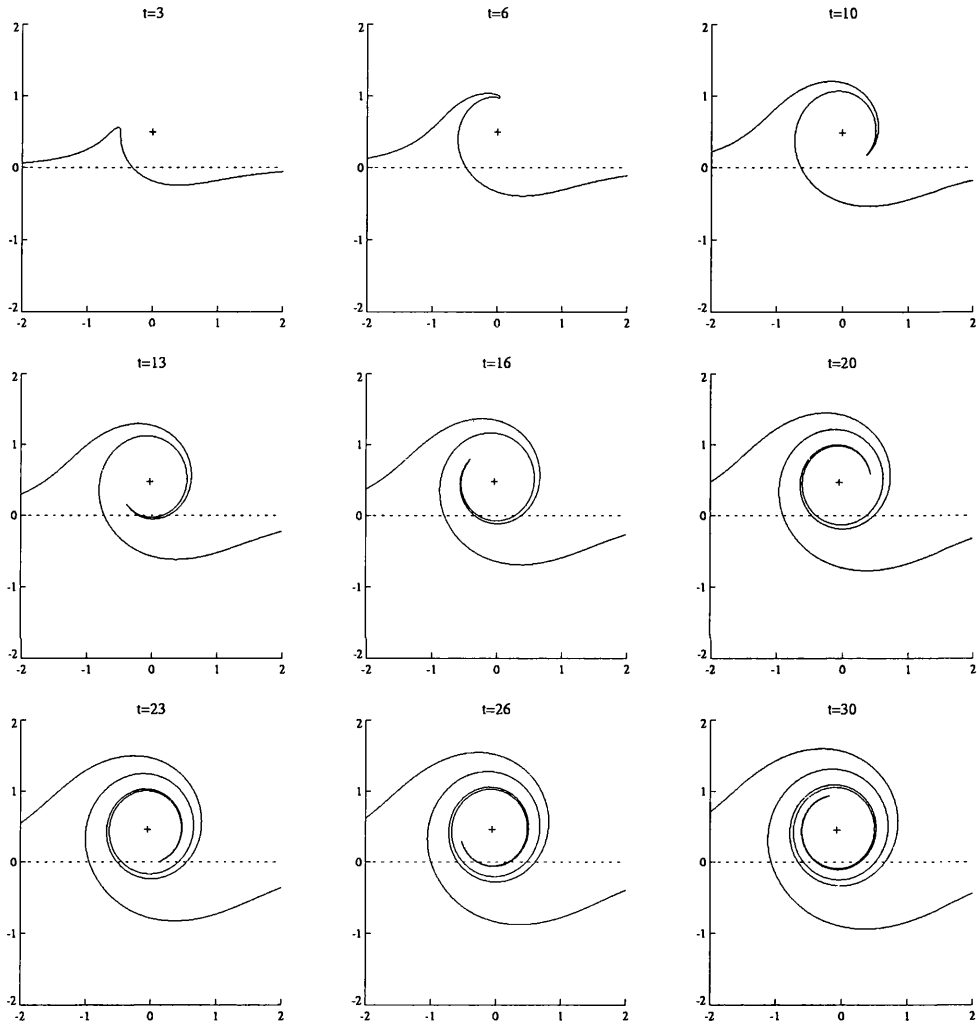
Figure 4.17: The evolution of the contour for an intense anticyclone. The parameter values used are $L = 0.5$ and $S = 0.01$.

Compare this with Figure (4.18), which shows the contour evolution for $S = 0.2$. The initial front is stronger than that formed for smaller S, accounting for the initial increase in both the meridional and zonal drift speeds. The weaker vortex is less able to wind the contour. As the dipole crosses the escarpment the cyclonic part of the dipole increases in size and has more influence on the vortex centre than the anticyclonic relative vorticity. It is the vortex centre and the cyclonic relative vorticity forming a dipole that retards the westward drift velocity and increases the southward drift velocity.

Next consider the case of intense cyclones. Figure (4.19) shows a comparison of the vortex drift produced by the contour dynamics experiments compared with the analytical prediction. Once again the analytical prediction is good for small S. Note with increasing S the theory underpredicts the westward drift speed, and at later times, for $S = 0.2$ the vortex centre begins to drift *east*.

Figure (4.20) shows the evolution of the contour for $S = 0.01$. Again, note the initial dipolar structure of the front as the cyclones deflects the contour, and later the strong winding of the contour near the vortex centre. Next consider Figure (4.21), a plot of the evolution of the contour for $S = 0.2$. In this case the initial dipole is still evident, but the vortex, being weaker than it is for small S is less able to wrap up the contour. A patch of anticyclonic relative vorticity forms to the east of the vortex centre. The dipole consisting of the primary vortex and this anticyclonic patch the begins to move north and east.

The formation of dipoles seen here becomes much more pronounced for moderate intensity vortices. This issue is covered in more depth in the following section.

4.4 A moderate singular vortex: contour dynamics results

To complete the study of the motion of a singular vortex near an escarpment contour dynamics results are presented in this section for moderate vortices. There is no theory available for the $S \approx 1$ regime, since the magnitude of the circulation of the relative vorticity produced due to deflection of the topographic contour is of the same order as the circulation of the primary vortex.

Attention is restricted to the cases $S = 2$ (moderately weak vortex), $S = 1$ (moderate vortex) and $S = 0.5$ (moderately intense vortex). Once again only vortices located on the shallow side of the
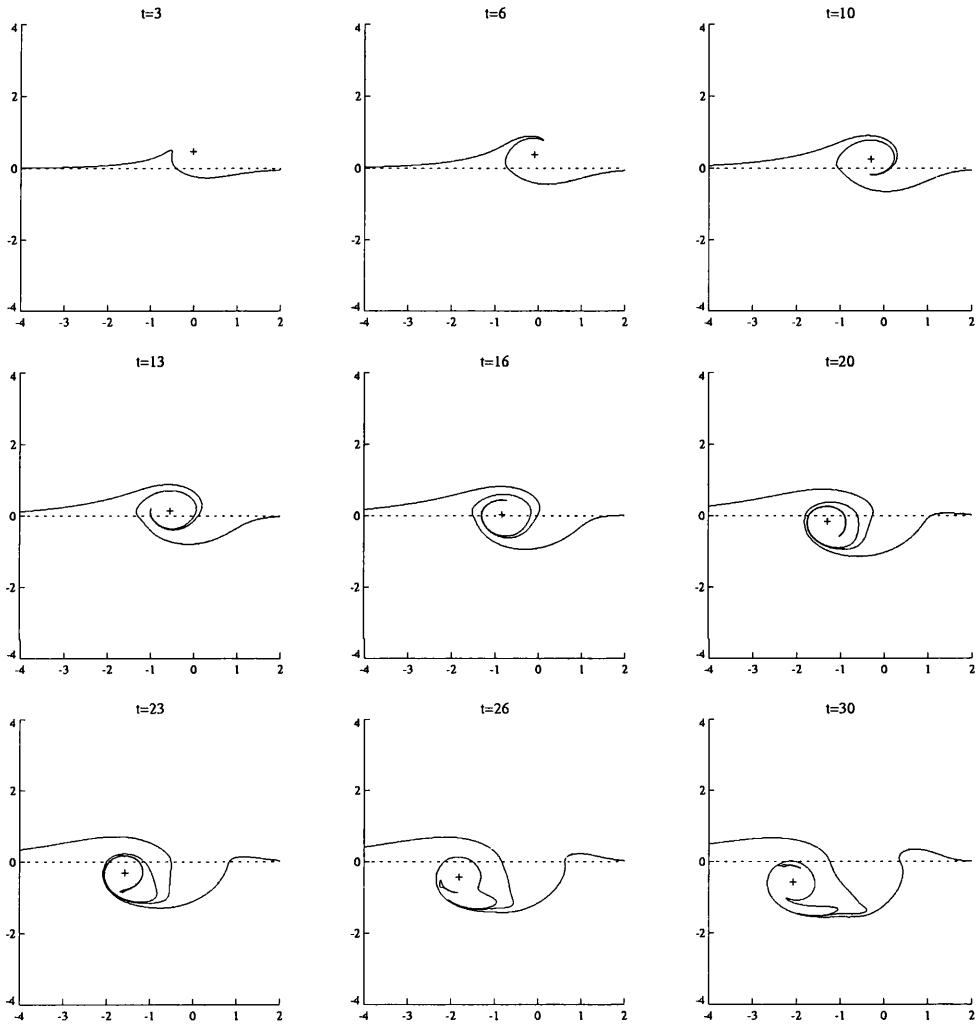
Figure 4.18: The evolution of the contour for a near intense anticyclone. The parameter values used are $L = 0.5$ and $S = 0.2$.
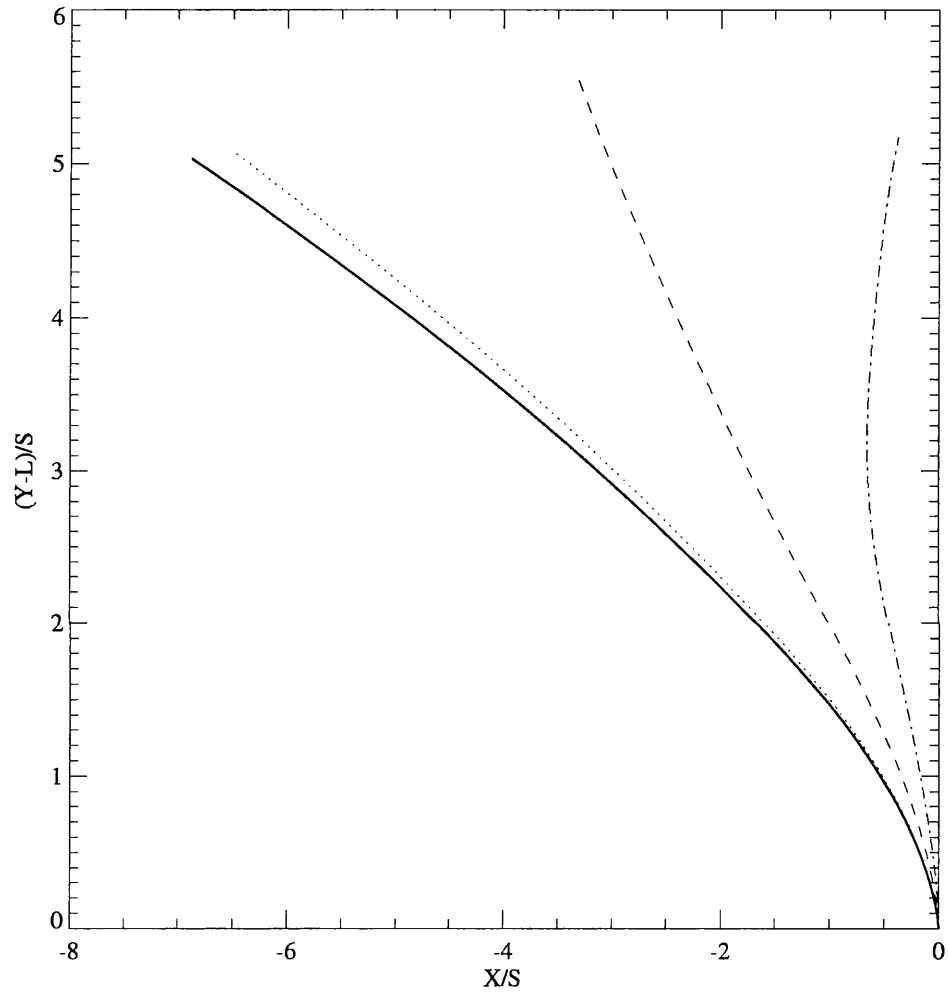
Figure 4.19: Comparison of the contour dynamics results with the analytical prediction for intense cyclones for $0 < t < 30$. The parameter values used are $L = 0.5$ and $S = 0.01$ (dotted line), $S = 0.1$ (dashed line) and $S = 0.2$ (dot-dashed line). the analytical trajectory is shown by the solid line.
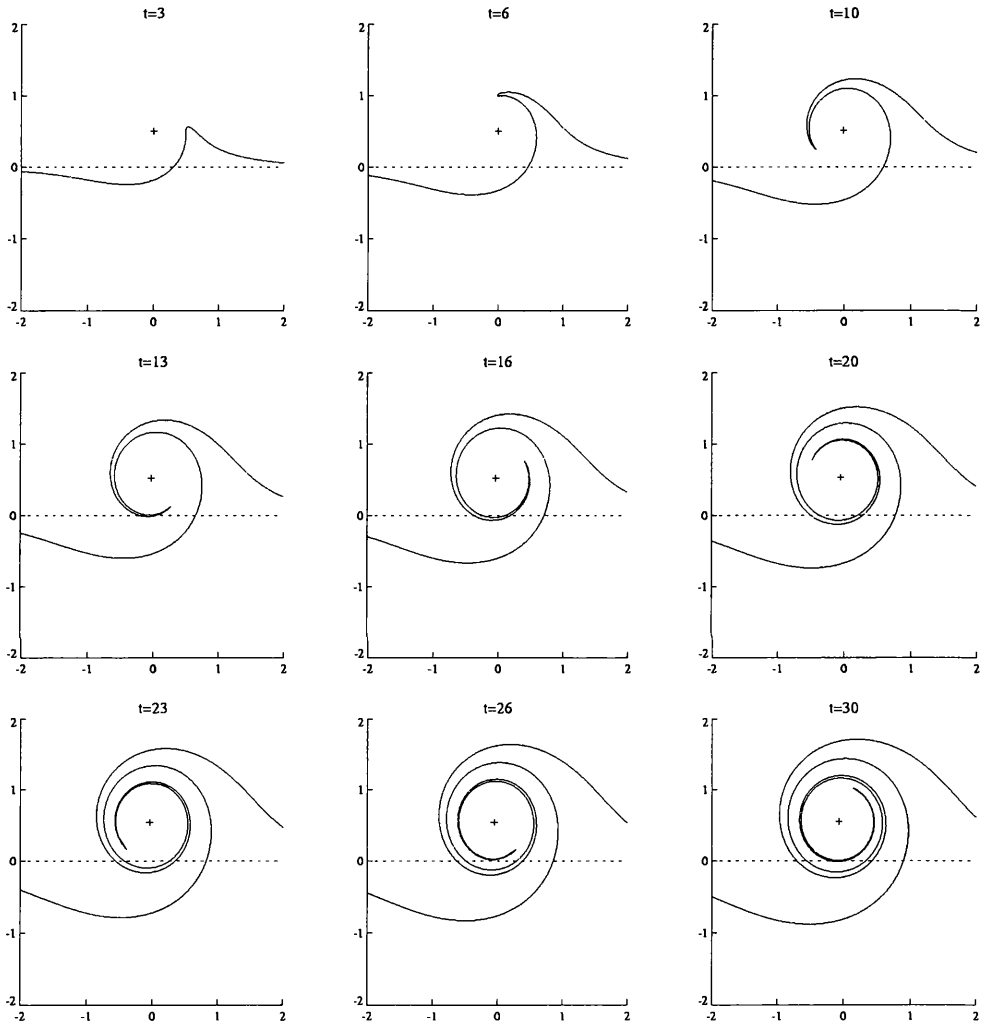
Figure 4.20: The evolution of the contour for an intense cyclone. The parameter values used are $L = 0.5$ and $S = 0.01$.
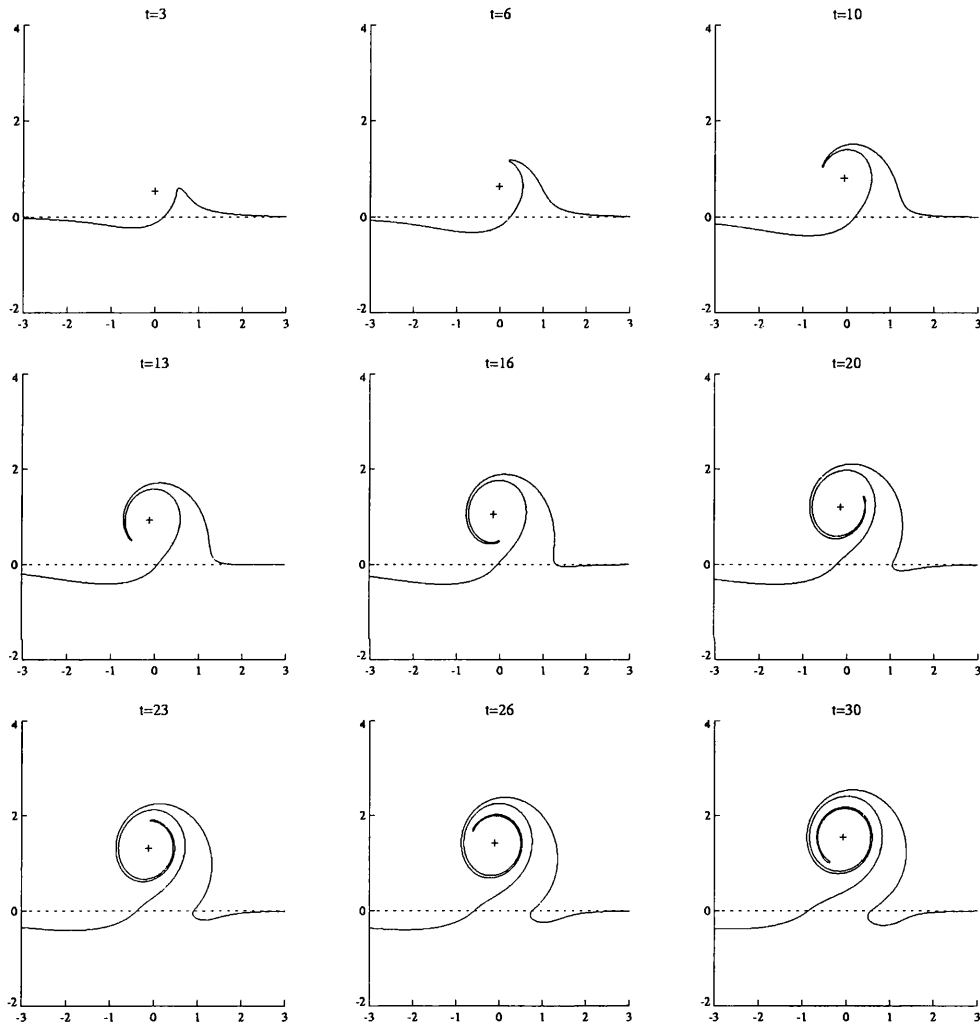
Figure 4.21: The evolution of the contour for a near intense cyclone. The parameter values used are $L = 0.5$ and $S = 0.2$.

81

escarpment are considered and the cases of anticyclones and cyclones are considered separately.

4.4.1 Anticyclones

Figure (4.22) shows a plot of the trajectories of the moderate anticyclones. For $S = 2$, the moderately weak anticyclone appears to still be well modelled by the linear theory. At large times the drift is purely zonal. For the moderate anticyclone ($S = 1$), the initial response also appears to be linear. However the vortex centre later turns south and crosses the escarpment, traversing a large arc before finally turning east. The moderately intense anticyclone ($S = 0.5$) also moves sharply south, crosses the escarpment and turns east at later times, with the exception that the initial westward displacement is much reduced.

Figure (4.23) show the contour evolution for $S = 2$. The response does indeed appear linear. The pseudoimage and radiated waves are apparent. It must be concluded that linear theory predicts the motion of anticyclones even for $S = 2$ (i.e. $\epsilon = 0.5$), for at least forty eddy turnover times.

Next consider Figure (4.24). At short times the topographic waves are linear and the vortex centre is advected by the pseudoimage. The wave radiation appears strong enough to cause the vortex to reach and cross the escarpment. At this stage the vortex begins to wrap the topographic contour, and has a small but significant patch of cyclonic relative vorticity nearby. The dipole mechanism then turns the vortex from its westward drift and the vortex centre moves east at large times.

Figure (4.25) show the evolution of the contour for $S = 0.5$. At short times the vortex wraps the contour up, and then crosses the escarpment. As for the previous case a patch of cyclonic relative vorticity accompanies the vortex in its evolution and the dipole mechanism turns the vortex east at later times.

4.4.2 Cyclones

Figure (4.26) shows a plot of the trajectories of the moderate cyclones. For $S = 2$, the moderately weak cyclone follows a generally north east path. For the moderate anticyclone ($S = 1$), the initial motion is also northeast, but path of the vortex centre then "loops". However the net migration of the vortex centre is north and east. The moderately intense ($S = 0.5$) cyclone exhibits the same
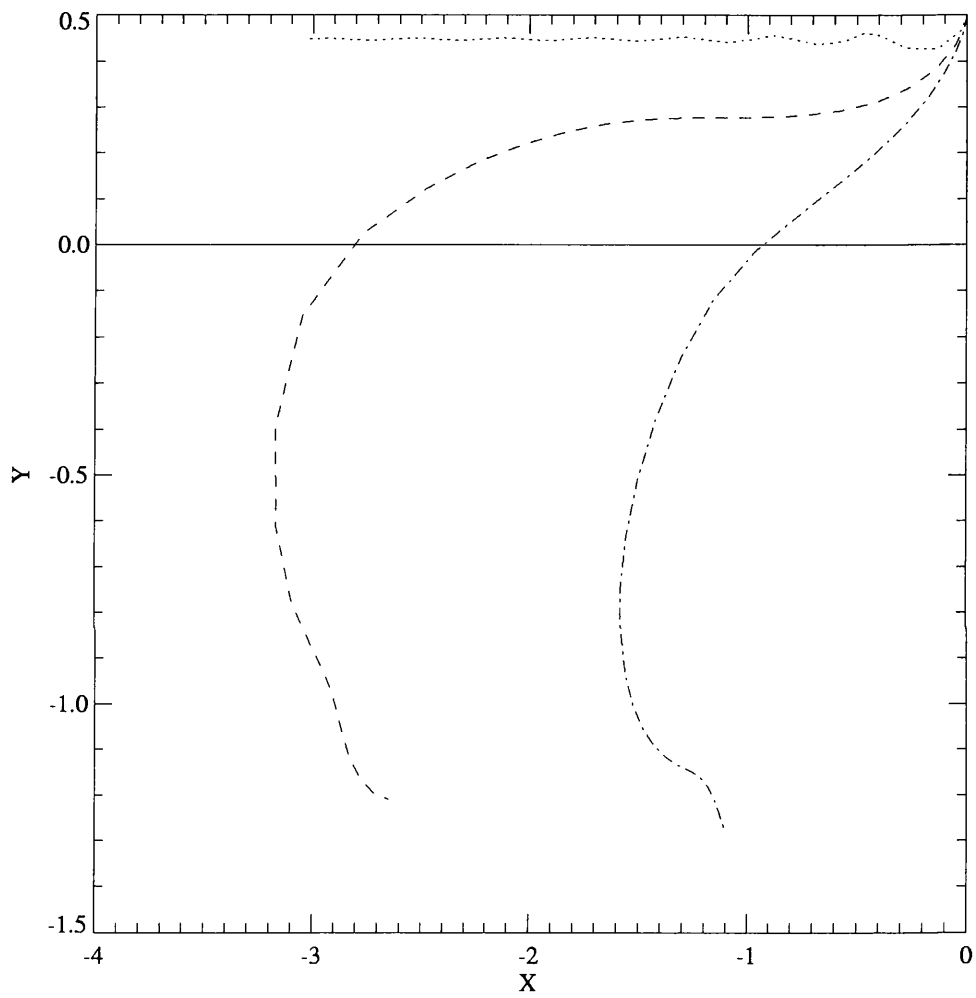
Figure 4.22: A plot of the trajectories for the moderate intensity anticyclones for $0 < t < 40$. The parameter values used are $L = 0.5$, $S = 2$ (dotted line), $S = 1$ (dashed line) and $S = 0.5$ (dot-dashed line).
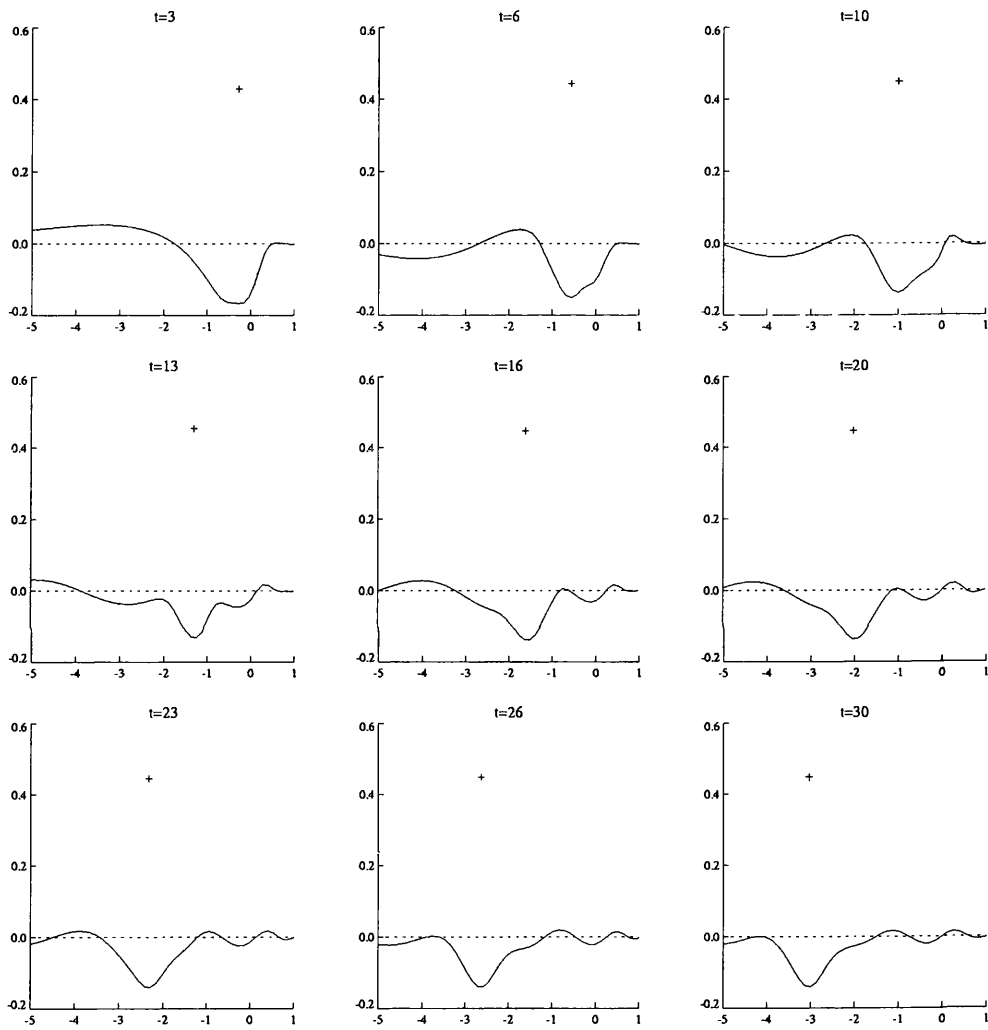
Figure 4.23: Evolution of the contour for an anticyclone with $L = 0.5$ and $S = 2$.
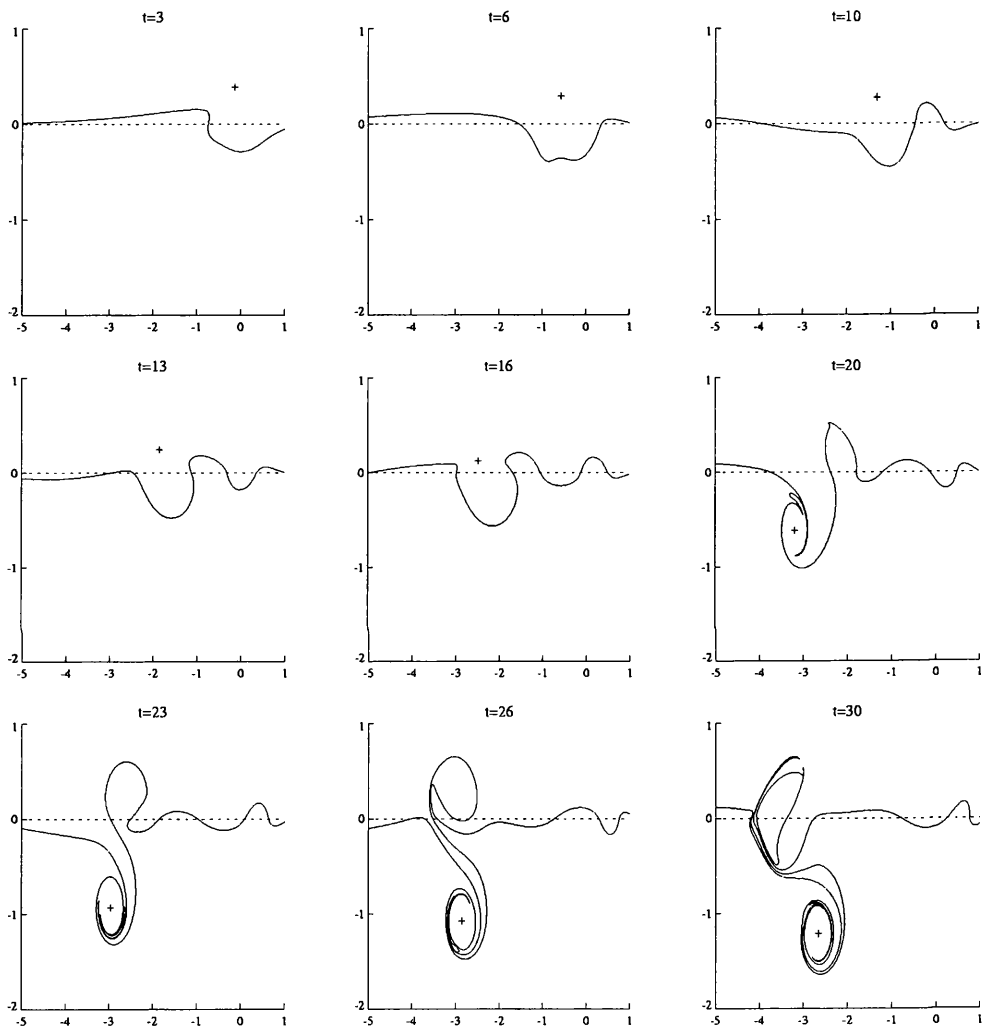
Figure 4.24: As Figure (4.23) except $S = 1$.
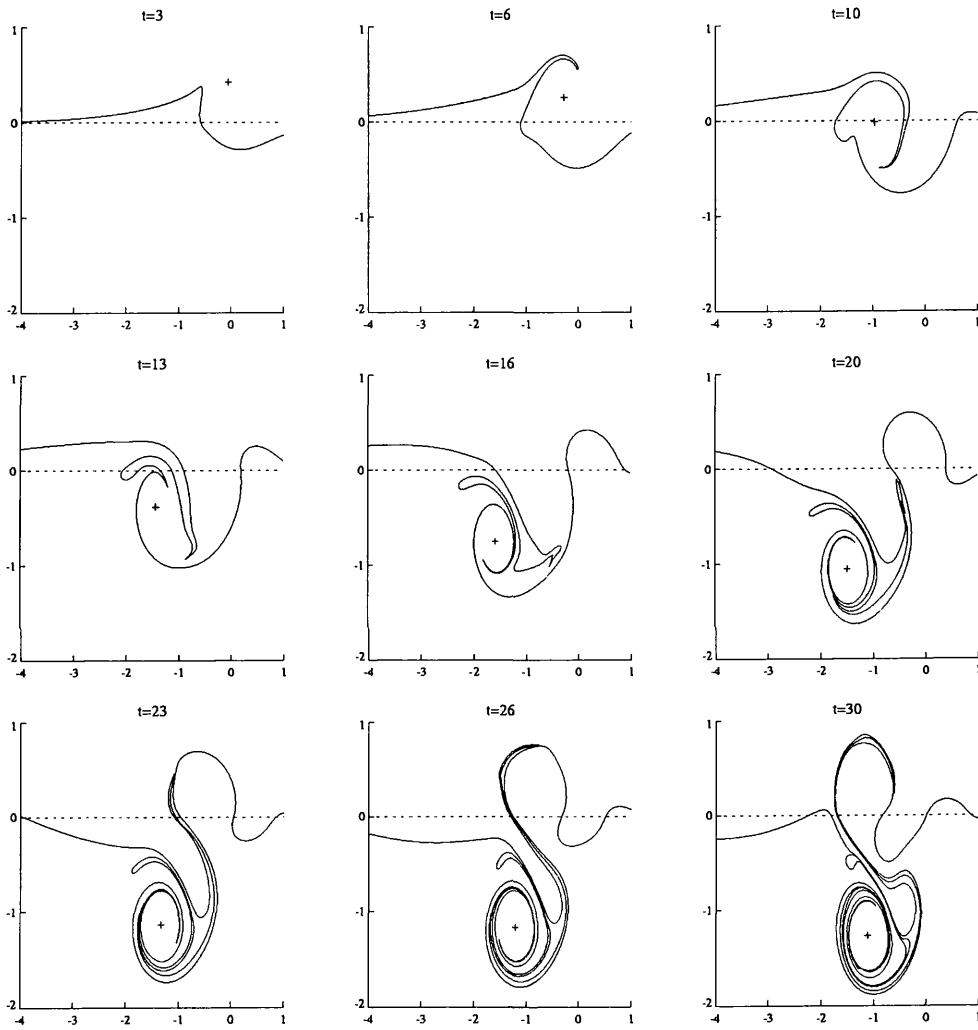
Figure 4.25: As Figure (4.23) except $S = 0.5$.

behaviour except that the drift is more east and less north.

Figures (4.27) -(4.29) show the contour evolution for the moderate anticyclones. The behaviour is qualitatively the same in all cases. The cyclone pinches off some of the topographic contour. This anticyclonic relative vorticity together with the primary cyclonic vortex form a dipole, and the general migration of the dipole is northeast. In particular the vortex propagates away from the escarpment, and is only affected by the anticyclonic path at later times. The looping motion is characteristic of a dipole with differing magnitude poles.

4.4.3   Discussion

It has been shown that for moderate singular vortices the characteristic of the motion is the formation of dipoles, and curiously, both cyclones and anticyclones drift east at large times. The process by which this happens differs slightly for anticyclones compared with cyclones.

The anticyclone crosses the escarpment. A large patch of fluid initially located on the shallow side of the escarpment accompanies the vortex as is crosses the escarpment. This fluid gains cyclonic relative vorticity, and forms a dipole with the primary vortex. The dipole mechanism curves the path of the vortex to the east at large times.

On the other hand the cyclones draw fluid from the deep side of the escarpment. This fluid has anticyclonic relative vorticity, and the dipole formation proceeds more quickly than the case of anticyclones. The cyclones move northeast from the outset, and at large times move away from the escarpment. The process of dipole formation occurs for cyclones over a larger range of parameter values than for anticyclones. This was indicated in the discussion of the weak cyclones, where, even for relatively large values of S the circulation of the vortex competes with the topographic wave mechanism, causing a build up of anticyclonic relative vorticity near the vortex centre.

It is worth highlighting that the results of this subsection are entirely in keeping with the experimental results of Zavala Sanson *et. al.* (1999) who have recently investigated the behaviour of barotropic vortices near an escarpment, both experimentally and numerically. In that investigation the escarpment lay in the meridional direction on a β-plane. The β effect was small in comparison to the topography, and mainly served to bring a vortex near to the escarpment. The strength of the
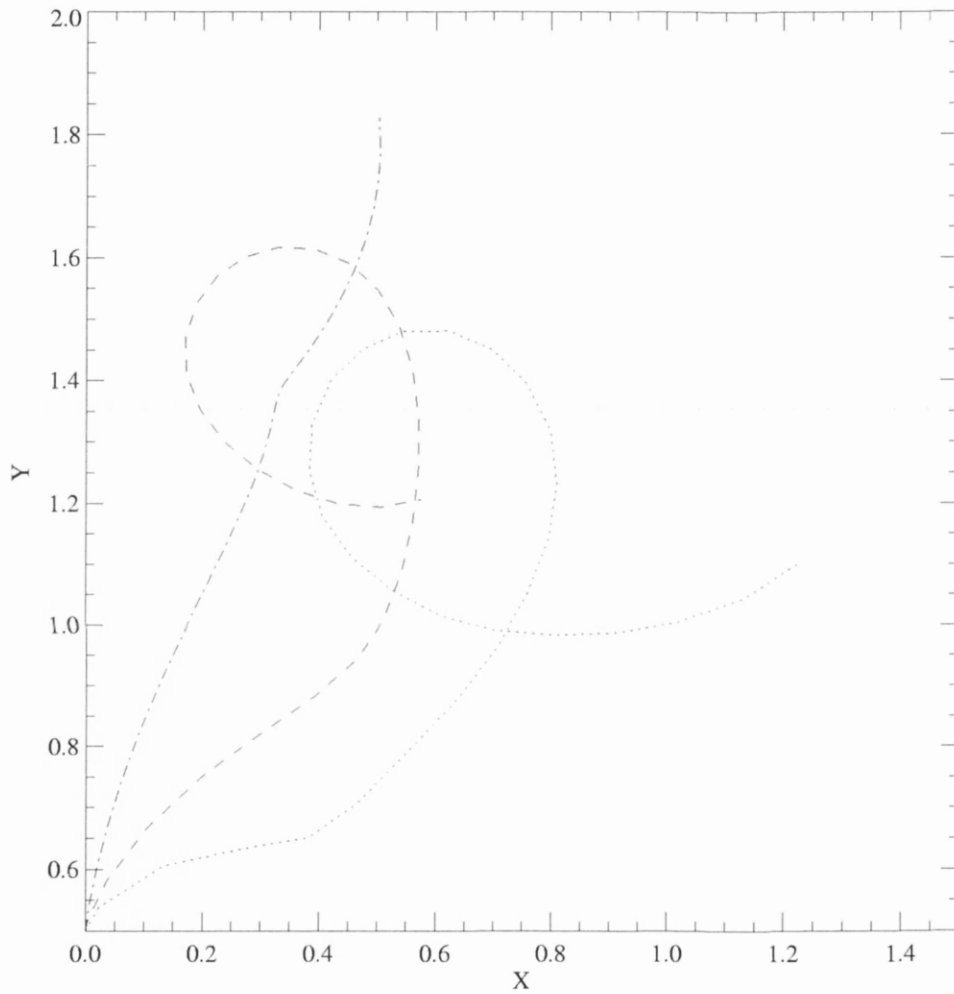
Figure 4.26: A plot of the trajectories for the moderate intensity cyclones for $0 < t < 30$. The parameter values used are $L = 0.5$, $S = 2$ (dotted line), $S = 1$ (dashed line) and $S = 0.5$ (dot-dashed line).
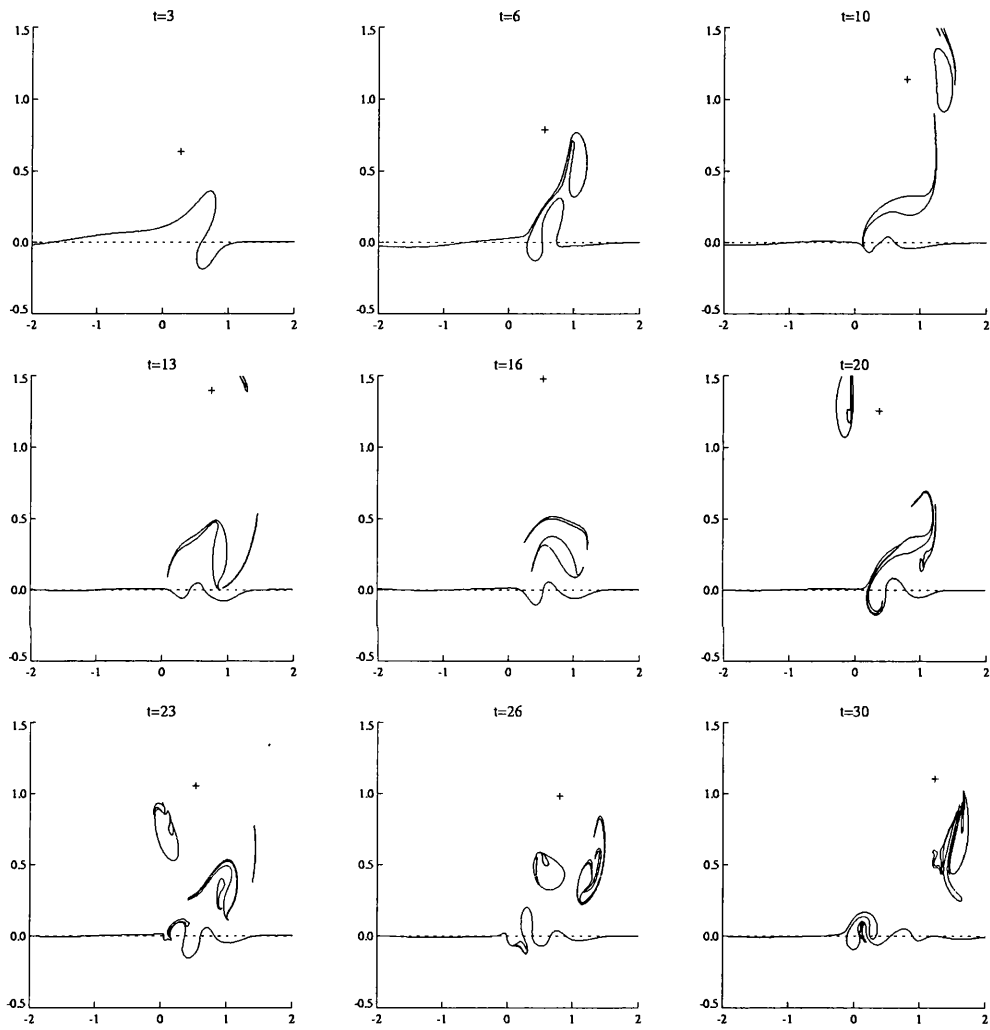
Figure 4.27: Evolution of the contour for a cyclone with $L = 0.5$ and $S = 2$.
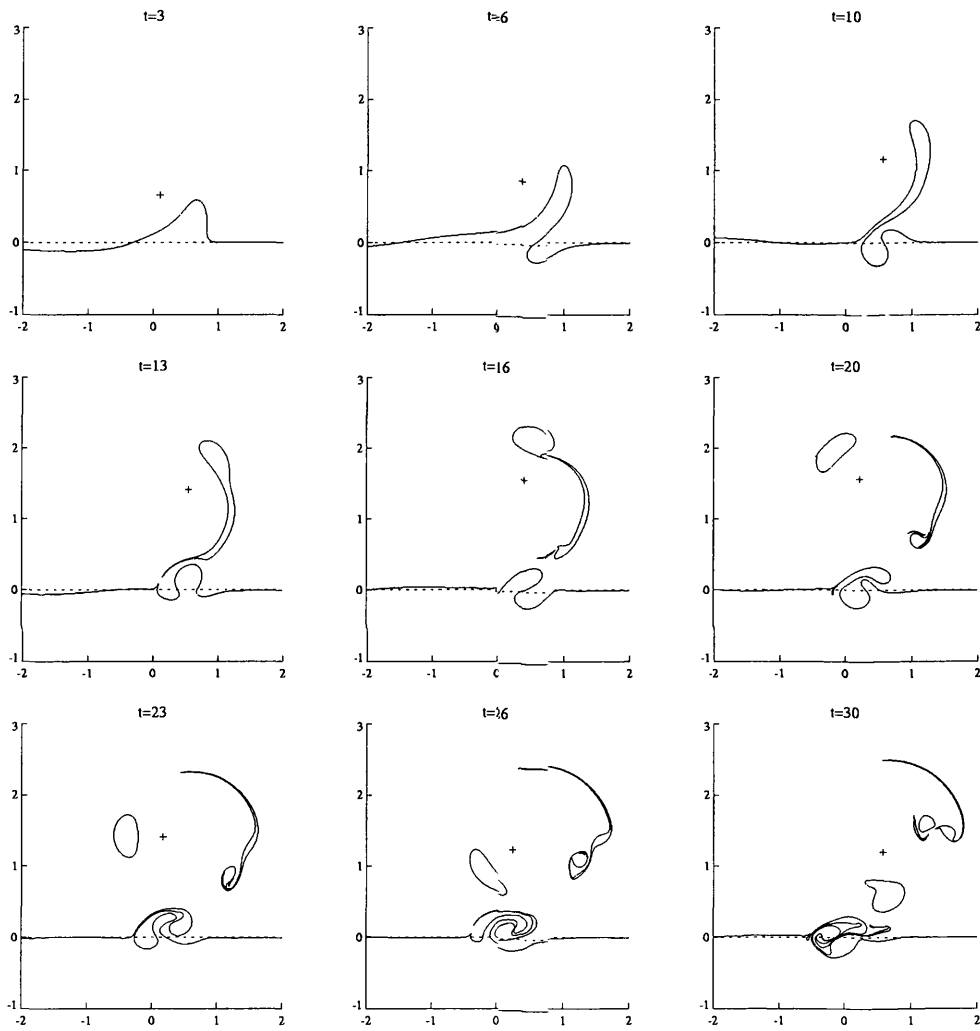
Figure 4.28: As Figure (4.27) except $S = 1$.
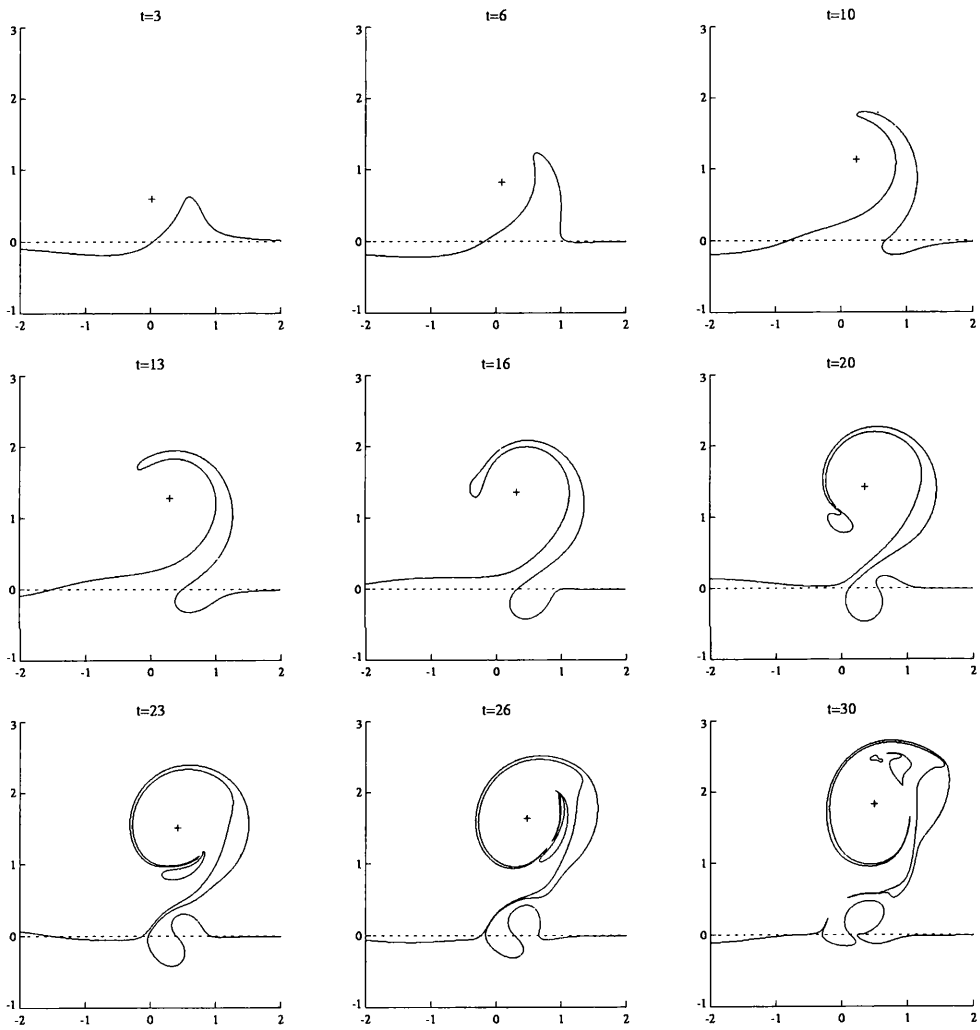
Figure 4.29: As Figure (4.27) except $S = 0.5$.

vortices was of the same order of magnitude as the relative vorticity produced by fluid crossing the escarpment, or, in the terminology of the present work, $S \approx 1$. It was found that anticyclones situated on the shallow side of the escarpment were able to "climb" the topographic gradient, whilst cyclones were "back-reflected", precisely the behaviour observed in these contour dynamics experiments.

Lam and Dritschel (1998) find that maximum meridional displacement of a circular vortex on a β-plane occurs for moderate intensity vortices. They describe the mechanism for this process in terms of a "trailing eddy", i.e. a part of the radiated Rossby wave train that has circulation in the opposite sense to the primary vortex. Put another way, for the moderate intensity β-plane vortex, a dipole forms between the primary vortex and the shed vorticity. This is precisely the same mechanism that has been observed in the present case. It might be expected that dipole formation in more general moderate intensity vortex-wave interactions is common. For example dipole formation maybe extremely important in cross-frontal mixing, something which needs to be understood and parameterised in General Circulation Models.

4.5 Conclusions

In this chapter a study of the motion of an intense singular vortex near an escarpment has been carried out for the full range of values of vortex intensity. Several important conclusions may be drawn.

First, analytic results for a weak vortex have predicted that the escarpment act like a plane wall. This phenomenon was dubbed the "pseudoimage of the vortex", since there is no true image vortex. In the case where the vortex travels in the same direction as the topographic waves, expressions for vortex drift induced by wave radiation and based on pseudomomentum arguments, were found. This drift is purely meridional and negligible for times of order unity. Contour dynamics confirmed the analytical predictions and revealed that the pseudoimage is a steadily propagating, non-dispersive, patch of relative vorticity in the deflected topographic contour. It might be anticipated that more realistic models of weak vortices near an escarpment, or indeed any sharp topographic gradient such as a seamount, might evolve in the sense of its image in the potential vorticity interface.

Second, contour dynamics show that dipole formation is generic for moderate intensity vortices.

This is fully in keeping with experimental results, and directly analogous to numerically observed dynamics of a vortex on the β-plane.

Third, the model doesn't account for changes in vortex shape. For a more realistic model vortex shape changes may be of great import, and as a first step in understanding the evolution of a continuously distributed vortex near an escarpment, an initially circular patch of uniform relative vorticity is considered in the following Chapter.

Appendix A: Secular growth in singular perturbation solution

In this appendix it is shown that a perturbation series solution for the weak singular vortex problem contains secular terms. Seek a solution to equation (4.2) in the form,

$$\phi = \phi_0 + \epsilon\phi_1 + \dots \tag{4.A1}$$

As noted above the vortex velocity is $O(\epsilon)$, so expanding Ψ_v about $(X, Y) = (0, L)$ gives

$$\Psi_v(x - X, y - Y) = \Psi_v(x, y - L) - \epsilon u t \Psi_{vx}(x, y - L) + O(\epsilon^2), \tag{4.A2}$$

anticipating that $\dot{X} = \epsilon u$. Substituting (4.A1) into (4.2) and equating the $O(1)$ terms yields the problem for ϕ_0

$$\left(\nabla^2\phi_0 - \phi_0\right)_t + \phi_{0x}d_y = -\Psi_{vx}d_y, \tag{4.A3}$$

with initial and boundary conditions identical to (4.20a)-(4.20d). The first order solution is then the same as the short time solution above:

$$\phi_0 = -\frac{\Gamma}{2\pi}K_0\left[\left(x^2 + (|y| + |L|)^2\right)^{1/2}\right] + \phi_{wave}. \tag{4.A4}$$

Since ϕ_{wave} decays rapidly near the vortex take

$$\phi_0 = -\frac{\Gamma}{2\pi}K_0\left[\left(x^2 + (|y| + |L|)^2\right)^{1/2}\right], \tag{4.A5}$$

so $X = \epsilon u t$. Noting that ϕ_0 solves the nonlinear terms, the $O(\epsilon)$ equation is

$$\left(\nabla^2\phi_1 - \phi_1\right)_t + \phi_{1x}d_y = ut\Psi_{vxx}d_y, \tag{4.A6}$$

with initial condition (4.20a) and boundary conditions (4.20b) and (4.20c). The solution is of the form

$$\hat{\phi}_1(k, y, t) = A_1(k, t)e^{-\sqrt{k^2+1}|y|}. \tag{4.A7}$$

The remaining boundary condition is

$$[\phi_{1yt}] + 2\phi_{1x} = 2ut\Phi_{vxx}(x, -L), \quad y = 0 \tag{4.A8}$$

giving the differential equation

$$-\sqrt{k^2+1}A_{1t} + ikA_1 = -utk^2\hat{\Psi}_v(x, y-L),$$ (4.A9)

with solution

$$A_1(k, t) = \frac{\Gamma u}{2}e^{-|L|\sqrt{k^2+1}}\left[it\omega + (1 - e^{i\omega t})\right],$$ (4.A10)

where $\omega = k/\sqrt{k^2+1}$, as before. After some manipulation this gives the $O(\epsilon)$ solution,

$$\phi_1 = \frac{\Gamma u}{2\pi}\int_0^\infty e^{-(|v|+|L|)\sqrt{k^2+1}}\left(\cos kx - \cos(kx + \omega t)\right)\ dk\quad - \frac{\Gamma ut}{2\pi}\int_0^\infty \omega e^{-(|v|+|L|)\sqrt{k^2+1}}\sin kx\ dk.$$ (4.A11)

This has terms of $O(t)$, and so grows secularly; i.e. $\phi_1 \to \infty$ as $t \to \infty$. This suggests the need to rescale the time variable, *a la* Herman *et. al.* (1989). This is done above in subsection 4.2.3.

94

Chapter 5

Evolution of an initially circular vortex patch near an escarpment

A limitation of the singular vortex model of Chapter 4 is the inability of the singular vortex to change its shape as it evolves. The Bessel function structure of the singular vortex is preserved for all time, and so the velocity field associated with the vortex is always radially symmetric. Consequently the process of vortex deformation is absent in the singular vortex model, and this, in turn, has two implications regarding the ability of that model to describe the physical mechanisms of a more realistic vortex-topography model. First, the contribution of vortex deformation to the velocity field are excluded, so that a description of both the vortex drift and the advection of the ambient potential vorticity by the vortex is incomplete. Second, the possibility that the vortex responds to wave radiation by deforming is excluded. A more realistic model of vortex motion near an escarpment should examine the effects of vortex deformation on the evolving flow. This chapter investigates the motion of an initially circular patch of uniform potential vorticity near an escarpment. Of particular interest is a comparison of the motion with the singular vortex model, i.e. how well does the singular vortex model describe the motion of the vortex patch centroid, and what features of the motion of the vortex patch model are absent in the singular vortex model?

The evolution of a vortex patch on the β-plane has received considerable attention, and a literature review was presented in Chapter 3. The approach to the present problem is adapted from the now standard formulation of Sutyrin and Flierl (1994), where the equation for the production of relative vorticity by advection of the ambient potential vorticity (the so-called "regular" field) is written in a form independent of vortex deformation. This latter effect (the so-called "singular field") is then

described by an equation forced by the leading order regular field. The particular formulation given below is adapted from the formulation of Reznik and Grimshaw (1998), which explicitly includes an equation for the drift of the vortex centroid. A further work which has influenced the present study is that of Lam and Dritschel (1998), in which the evolution of an initially circular vortex patch on the β-plane is investigated using a contour advective semi-Lagrangian (CASL) algorithm. The high resolution results obtained by Lam and Dritschel (1998) are discussed below in comparison to the results for the motion of a vortex patch near an escarpment.

The effect of the topography on the vortex is of primary interest, so the question of how the vortex came to be near the escarpment is ignored. It could have, for example, been carried by a background mean flow, or arrived due to the drift induced by the β-effect. In the following, it is assumed that no part of the vortex straddles the escarpment at the initial time, i.e. the vortex radius is less than the distance of the vortex centre from the escarpment. This assumption greatly simplifies the analysis.

The chapter is organised as follows. First the leading order solution on the topographic wave time scale for a weak vortex patch is obtained by Fourier analysis. The large time behaviour for a weak vortex is investigated by contour dynamics. Second, the leading order solution for an intense vortex patch is obtained by the Green's function method. The large time behaviour for the intense vortex is also investigated by contour dynamics. Finally the case of a moderate intensity vortex patch, for which no analytical theory is available, is investigated by contour dynamics.

5.1   Problem formulation

The f-plane quasigeostrophic governing equation, with the same scalings (4.1) as in Chapter 4 is, for convenience, rewritten as,

$$Q_t + J[\psi, Q] = 0, \tag{5.1}$$

where

$$Q = \nabla^2 \psi - \psi + S h_B(y). \tag{5.2}$$

Here S is the ratio of the eddy turnover time to the topographic vortex stretching time,

$$S = \frac{L/U}{\delta^{-1} f^{-1}} = \frac{\delta}{Ro} = \frac{T_a}{T_w}. \tag{5.3}$$

and the topography

$$h_B(y) = \frac{1}{2}\text{sgn}(y),\tag{5.4}$$

i.e. an infinite escarpment aligned along $y = 0$, is also the same as the previous chapter, except for the factor of a half. This factor has been included so that when $S = 1$ the the ambient potential vorticity jump across the escarpment has the same magnitude as the relative vorticity of the primary vortex.

The initial condition is a circular patch of uniform relative vorticity, which with the Rossby radius as the characteristic length scale, can be written,

$$\nabla^2\psi_0 - \psi_0 = -\alpha H(a - r),\tag{5.5}$$

where a is the patch radius, r is the radial distance from the vortex centre and $\alpha = \pm1$ gives the sense of the circulation. For $\alpha > 0$ it is clockwise (anticyclonic) and for $\alpha < 0$ it is anticlockwise (cyclonic). The solution, derived in Chapter 2 (see equation (2.34)), is

$$\psi_0(r) = \begin{cases} \alpha - \alpha a K_1(a) I_0(r), & r \le a \\ \alpha a I_1(a) K_0(r), & r > a \end{cases}\tag{5.6}$$

and the angular velocity of the vortex is

$$b(r) = \frac{1}{r}\frac{\partial\psi_0}{\partial r} = \frac{1}{r}\begin{cases} -\alpha a K_1(a) I_1(r), & r \le a \\ -\alpha a I_1(a) K_1(r), & r > a \end{cases}\tag{5.7}$$

Figure (2.3) shows a plot of the profiles of the streamfunction and the angular velocity.

The present problem considers the evolution of an initially circular vortex patch near an escarpment. The topography is "switched on" near a pre-existing vortex at time $t = 0$. In a frame of reference with the origin attached to the vortex centroid (to be defined), the governing equation is

$$\frac{\partial}{\partial t}(\nabla^2\psi - \psi) + J[\tilde{\psi}, \nabla^2\psi - \psi] + S\frac{\partial h_B}{\partial y}\frac{\partial\psi}{\partial x} = 0\tag{5.8}$$

where $\tilde{\psi} = \psi - uy + vx$ and $\mathbf{u} = (u, v)$ is the drift velocity of the vortex centroid $(x_c(t), y_c(t))$. The initial relative vorticity is

$$\Omega_0 = \nabla^2\psi_0 - \psi_0 = -\alpha H(a - r),\tag{5.9}$$

and the initial potential vorticity is

$$Q_0 = \Omega_0 + \frac{S}{2}\text{sgn}(y + L),\tag{5.10}$$

for a vortex of radius a with centroid initially located at $(0, L)$. Figure (5.1) shows the initial condition.

The boundary between the two different values of Ω_0 represented in (5.9) by the Heaviside function is a material line and is advected with the flow, so subsequently the relative vorticity must have the form

$$\Omega = \nabla^2 \psi - \psi = -\alpha H(r_0 - r) + q(x, y, t).$$ (5.11)

Here q is the correction to the relative vorticity, and $r_0 = r_0(\theta, t)$ is the equation of the evolving patch boundary, so initially $r_0(\theta, t) = a$. Substituting (5.11) into (5.8) and equating to zero the regular and singular parts in the resulting expression[1] leads to

$$\frac{\partial q}{\partial t} + J[\tilde{\psi}, q] + S\frac{\partial h_B}{\partial y}\frac{\partial \psi}{\partial x} = 0$$ (5.12a)

$$\alpha\frac{\partial r_0}{\partial t} + J[\tilde{\psi}, r_0 - r]\bigg|_{r=r_0} = 0.$$ (5.12b)

These equations describe the two processes which contribute to the motion. The first equation (5.12a) describes relative vorticity production due to advection of the ambient potential vorticity. It does not contain advection of the relative vorticity $H(r_0 - r)$ of the vortex patch, which is instead described by the second equation (5.12b), which states that deformation of the vortex shape is due to advection of the vortex boundary. To leading order then, advection is due to relative vorticity production. It is the appearance of the vortex shape in the problem which was missing from the singular vortex model, and which complicates the solution.

To close the problem a definition of the vortex centroid is required. It is now standard (e.g. Reznik and Grimshaw (1998) or Lam and Dritschel (1998)) to choose the geometric centroid of the evolving patch, i.e. the centre of vorticity for a patch with uniform vorticity. This choice is not necessary since obtaining the solution in any coordinate frame yields all of the information about any characteristic point associated with the vortex. The centroid location $(x_c(t), y_c(t))$ is

$$x_c = \frac{\int\int_V x\,dx\,dy}{\int\int_V dx\,dy}, \qquad y_c = \frac{\int\int_V y\,dx\,dy}{\int\int_V dx\,dy},$$ (5.13)

where V is the vortex patch bounded by the curve $r_0(\theta, t)$. Using Green's theorem these are, in polar coordinates,

$$x_c(t) = \frac{1}{3\pi a^2}\int_0^{2\pi} r_0^3(\theta, t)\cos\theta\,d\theta,$$ (5.14a)

$$y_c(t) = \frac{1}{3\pi a^2}\int_0^{2\pi} r_0^3(\theta, t)\sin\theta\,d\theta.$$ (5.14b)

---

[1]By which is meant the following. The Heaviside function leads to terms $\delta(r_0 - r)$ upon substitution into the governing equation. The terms that are multiplied by the delta function are equated to zero and all remaining terms are similarly equated to zero. Hence the names "regular" and "singular", despite the fact that the equations are in fact both regular. This is standard practice for vortex patch analysis.

Here the fact that the area πa^2 of the initial patch is conserved has been used. In the moving frame $x_c(t) = y_c(t) = 0$ so the problem is closed by the condition

$$\int_0^{2\pi} r_0^3 e^{i\theta} d\theta = 0. \tag{5.15}$$

Equations (5.12a), (5.12b) and (5.15) together with the initial conditions

$$\psi(r,\theta,0) = \psi_0(r), \tag{5.16a}$$

$$q(x,y,0) = 0, \tag{5.16b}$$

$$r_0(\theta,0) = a, \tag{5.16c}$$

$$(x_c(0), y_c(0)) = (0,L), \tag{5.16d}$$

describe the evolution of the vortex patch. A complete study of the problem requires consideration of the three parameters S, a and L. The leading order solutions for $S \gg 1$ (a weak vortex) and for $S \ll 1$ (an intense vortex) are obtained analytically. The case of a moderate intensity vortex ($S \approx 1$) is investigated numerically by contour dynamics. The investigation of the dependence of the motion on the vortex radius, a, and its distance from the escarpment, L, is limited to the question of whether the motion of the vortex patch is well approximated by a singular vortex as $a/L \to 0$. Also $L \approx 1$, so that the vortex is close enough to the escarpment to interact with it.

5.2 A weak vortex patch

For a weak vortex, $S \gg 1$, set $\epsilon = S^{-1}$ and rescale the time variable $\tau = \epsilon t$, so that the unit of time is T_w, the topographic wave time scale. Under this rescaling the equations (5.12a) and (5.12b) become

$$\frac{\partial q}{\partial \tau} + \epsilon J[\tilde{\psi}, q] + \frac{\partial h_B}{\partial y}\frac{\partial \psi}{\partial x} = 0, \tag{5.17a}$$

$$\alpha \frac{\partial r_0}{\partial \tau} + \epsilon \left. J[\tilde{\psi}, r_0 - r]\right|_{r=r_0} = 0, \tag{5.17b}$$

which express the fact that advection is $O(\epsilon)$ on this time scale. In particular, for times $\tau \ll \epsilon^{-1}$, deformation of the patch boundary, which is due to advection, is $O(\epsilon)$. Thus, the parameter r_0 can be taken to be constant, at least on the topographic wave time scale T_w. In the following subsection the leading order solution to this problem is obtained by Fourier analysis.

99

5.2.1 Leading order solution

For times $\tau \ll \epsilon^{-1}$, ignoring the advection terms in (5.17a) and (5.17b) yields

$$\frac{\partial q}{\partial \tau} + \frac{\partial h_B}{\partial y}\frac{\partial \psi}{\partial x} = 0, \tag{5.18a}$$

$$r_0 = a. \tag{5.18b}$$

This implies that for times $\tau \ll \epsilon^{-1}$ the singular part of the flow (i.e. the flow due to the vortex) is steady at its initial value ψ_0. The regular field (i.e. the secondary circulations) can be obtained by writing

$$\psi = \psi_0 + \phi. \tag{5.19}$$

The magnitude of the regular field ϕ can be O(1) or greater since $S \gg 1$ is the magnitude of the relative vorticity, q, acquired by a fluid particle crossing the escarpment. Substituting this into (5.11), with $r_0(\theta, \tau) = a$ for all τ, leads to

$$q = \nabla^2 \phi - \phi. \tag{5.20}$$

Equation (5.18a) is then a forced topographic wave equation,

$$\frac{\partial}{\partial \tau}(\nabla^2 \phi - \phi) + \frac{\partial h_B}{\partial y}\frac{\partial \phi}{\partial x} = -\frac{\partial h_B}{\partial y}\frac{\partial \psi_0}{\partial x}, \tag{5.21}$$

where for convenience the frame of reference is the inertial frame with the escarpment aligned along $y = 0$, i.e. $h_B(y) = \text{sgn}(y)/2$. This problem is very similar to the weak singular vortex problem of Chapter 4, and may be solved in precisely the same fashion. Matching the solution across the escarpment, as in section (4.1), the problem for ϕ is

$$\nabla^2 \phi - \phi = 0 \quad , \qquad y \neq 0 \tag{5.22a}$$

$$\phi(x, y, 0) = 0 \quad , \qquad \tau = 0 \tag{5.22b}$$

$$\nabla \phi \to 0 \quad , \qquad x^2 + y^2 \to \infty \tag{5.22c}$$

$$[\phi] = 0 \quad , \qquad y = 0 \tag{5.22d}$$

$$[\phi_{y\tau}] + \phi_x = -\psi_{0x} \quad , \qquad y = 0. \tag{5.22e}$$

Apart from the additional factor of a half in the equation for the topography, this differs from the weak singular vortex problem only in the form of the forcing term ψ_{0x} in the right hand side of (5.22e). Since a circular vortex doesn't contribute to its own drift, the advection of the vortex centre

(x_c, y_c) is due to the regular field, i.e. the vortex drift velocity components are

$$\frac{dx_c}{d\tau} = -\epsilon\phi_y|_{x=x_c, y=y_c} \tag{5.23a}$$

$$\frac{dy_c}{d\tau} = \epsilon\phi_x|_{x=x_c, y=y_c} \tag{5.23b}$$

Hence, for times up to $\tau = O(\epsilon^{-1})$, $x_c = O(\epsilon)$ and $y_c = L + O(\epsilon)$, and the vortex term is, to leading order

$$\psi_0 = \psi_0(x, y - L), \tag{5.24}$$

on this time scale.

The leading order solution is obtained by standard Fourier analysis. Denote the Fourier transform of ϕ by

$$\hat{\phi}(k) = \int_{-\infty}^{\infty} \phi e^{-ikx} dx. \tag{5.25}$$

In Fourier space (5.22a), (5.22c) and (5.22d) are

$$\hat{\phi}_{yy} - (k^2 + 1)\hat{\phi} = 0 \quad , \qquad y \neq 0, \tag{5.26a}$$

$$\hat{\phi} \to 0 \quad , \qquad y \to \pm\infty, \tag{5.26b}$$

$$\left[\hat{\phi}\right] = 0 \quad , \qquad y = 0, \tag{5.26c}$$

with solutions of the form

$$\hat{\phi} = B(k, \tau)e^{-\sqrt{k^2+1}|y|}. \tag{5.27}$$

The matching condition (5.22e) together with the initial condition (5.22b) give the initial value problem for B,

$$2\sqrt{k^2+1}B_\tau - ikB = -ik\hat{\psi}_0|_{y=0} \tag{5.28a}$$

$$B(k, 0) = 0. \tag{5.28b}$$

For $L > a$, so that no part of vortex patch crosses the escarpment[2], the forcing term evaluated at the escarpment is,

$$\psi_0(x, 0) = \alpha a I_1(a) K_0((x^2 + L^2)^{1/2}). \tag{5.29}$$

Making use of identity (4.30) the Fourier transform of this is

$$\hat{\psi}_0|_{y=0} = \frac{\alpha a I_1(a)\pi}{\sqrt{k^2+1}}e^{-|L|\sqrt{k^2+1}}. \tag{5.30}$$

---

[2]This is consistent with the idea described in the introduction that the vortex has approached the escarpment from elsewhere. Without this assumption the Fourier transform of the forcing is more difficult.

Substitution of this expression in (5.28a) gives

$$B_\tau + i\omega B = -\frac{\alpha a I_1(a)\omega\pi}{\sqrt{k^2+1}}e^{-|L|\sqrt{k^2+1}},\qquad(5.31)$$

with solution

$$B(k,\tau) = \frac{\alpha a I_1(a)\pi}{\sqrt{k^2+1}}e^{-|L|\sqrt{k^2+1}}\left(e^{-i\omega\tau}-1\right),\qquad(5.32)$$

where

$$\omega = -\frac{1}{2\sqrt{k^2+1}},\qquad(5.33)$$

is the frequency of the topographic waves. Note the appearance of the factor of two in the denominator of ω, which is due to the chosen form for the escarpment topography (5.4). The solution for the regular field consists of a steady term and a topographic wave term,

$$\phi = \phi^{(s)} + \phi^{(w)},\qquad(5.34)$$

where

$$\phi^{(s)} = -\alpha a I_1(a)K_0\left((x^2+(|y|+|L|)^2)^{1/2}\right),\qquad(5.35\text{a})$$

$$\phi^{(w)} = \alpha a I_1(a)\int_0^\infty A(k,y)\cos(kx-\omega\tau)dk,\qquad(5.35\text{b})$$

with

$$A(k,y) = \frac{e^{-(|y|+|L|)\sqrt{k^2+1}}}{\sqrt{k^2+1}}.\qquad(5.36)$$

The topographic wave term is identical with the topographic wave term for the weak singular vortex (4.38), with the exception of the factor before the integral. Immediately then it is apparent that the waves decay like $\tau^{-1/3}$ at the wavefront, like $\tau^{-1/2}$ in the wavetrain and importantly like τ^{-1} at the x-location of the vortex centre (see Chapter 4 for details). Figure (5.2) illustrates the decaying nature of the dispersive topographic waves.

The steady part of the solution, $\psi_0 + \phi^{(s)}$, is analogous to the pseudoimage of the weak singular vortex. For $\text{sgn}(y) = -\text{sgn}(L)$, (i.e. across the escarpment from the vortex) the fluid is at rest. On the other hand for $\text{sgn}(y) = \text{sgn}(L)$, (on the same side of the escarpment as the vortex), the fluid behaves as if there were an equal and opposite circular patch of relative vorticity centred at $(0, -L)$. On the fast topographic wave time scale, this pseudoimage remains circular to within values of $O(\epsilon)$.

The fact that both the wave term and the steady term in this solution are identical to the leading order solution for a singular vortex is to be expected, since the flow exterior to a circular vortex

102
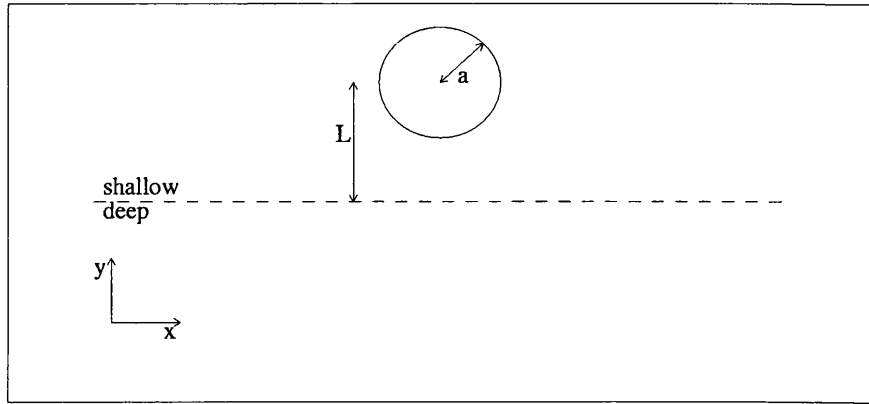
Figure 5.1: The initial condition for the present problem. A circular patch of uniform relative vorticity of radius a is initially located with its centre distance L from the escarpment.
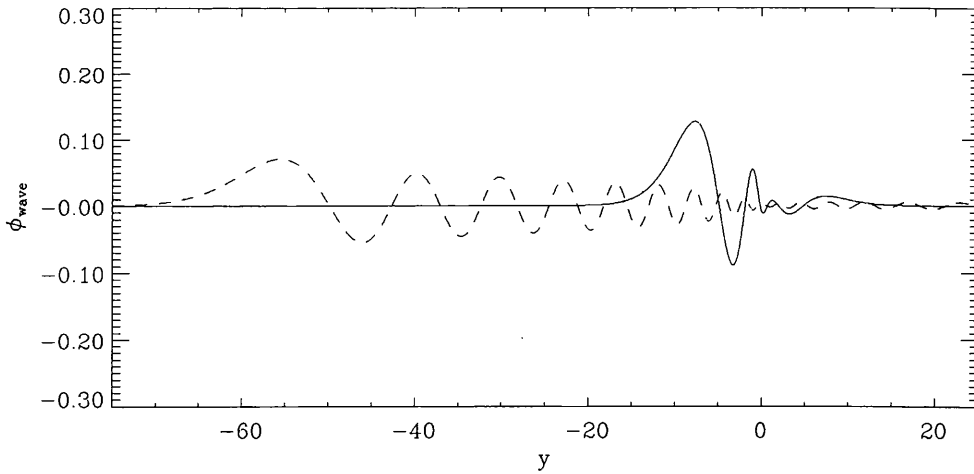
Figure 5.2: The topographic wave term $\phi^{(w)}$ evaluated over $y = 0$ at times $\tau = 10$ (solid line) and $\tau = 60$ (dotted line). The parameter values used are $\alpha = 1$, $a = 1$ and $L = 1.2$.

103

patch is identical to that of a singular vortex. However, the vortex may deform for longer times and so the question as to whether the pseudoimage description is meaningful on the slow advective time scale is discussed below in the contour dynamics investigation.

The vortex drift velocity components as $\tau \to 0$, obtained from equations (5.23a) and (5.23b), via a leading order expansion of the solution (5.35a) and (5.35b) are

$$u = 0, \qquad v = \epsilon \alpha a I_1(a) \tau \int_0^\infty \omega A(k, L) dk, \tag{5.37}$$

whilst as $\tau \to \infty$, the advection of the vortex centre is solely due to the pseudoimage, giving

$$v = 0, \qquad u = \epsilon \alpha a I_1(a) K_1(2|L|) \text{sgn} L. \tag{5.38}$$

The integral in (5.37) converges, since $|A(k, y)| < e^{-k}$, and is negative. Hence, for $\tau \ll 1$ the vortex moves linearly in the y-direction. Cyclones ($\alpha < 0$) drift north and anticyclones ($\alpha > 0$) drift south, the same short-time behaviour as a weak singular vortex and the mechanism is precisely the same. Figure (5.3) shows the evolution of the regular solution, $\psi = \phi^{(s)} + \phi^{(w)}$ for a weak vortex patch. The initial response to the advection of fluid across the escarpment by the swirl velocity of the vortex is the establishment of a secondary dipole, seen in Figure (5.3a) which advects cyclones (resp. anticyclones) north (south). The dispersive topographic waves rapidly propagate away from the vortex, as in Figure (5.3b,c), and as $\tau \to \infty$ only the solitary non-propagating disturbance (the pseudoimage) remains. The relative vorticity of the pseudoimage is $O(\epsilon^{-1})$, and is precisely strong enough to advect the weak primary vortex as if the escarpment were a wall. Thus, the weak cyclones move east when located on the shallow (deep) side of the escarpment and anticyclones drift west (east) when located on the shallow (deep) side of the escarpment.

The results of this subsection could have been obtained by replacing the vortex patch by a singular vortex of strength

$$\Gamma = \frac{\alpha a I_1(a)}{2\pi}, \tag{5.39}$$

initially located at $(0, L)$. That is, for as long as the linear theory is valid, the motion of a weak vortex patch is adequately modelled by the linear theory for a weak singular vortex. Formally, the linear theory is only valid on the topographic wave time scale, i.e. $t = O(\epsilon)$. Further analysis is possible if the vortex patch is assumed to remain circular for times $t = O(1)$. Such an approach is reasonable for $a \ll L$, but amounts to little more than modelling the vortex patch by a singular vortex. Since the effect of vortex shape changes is of particular interest in the present study, the
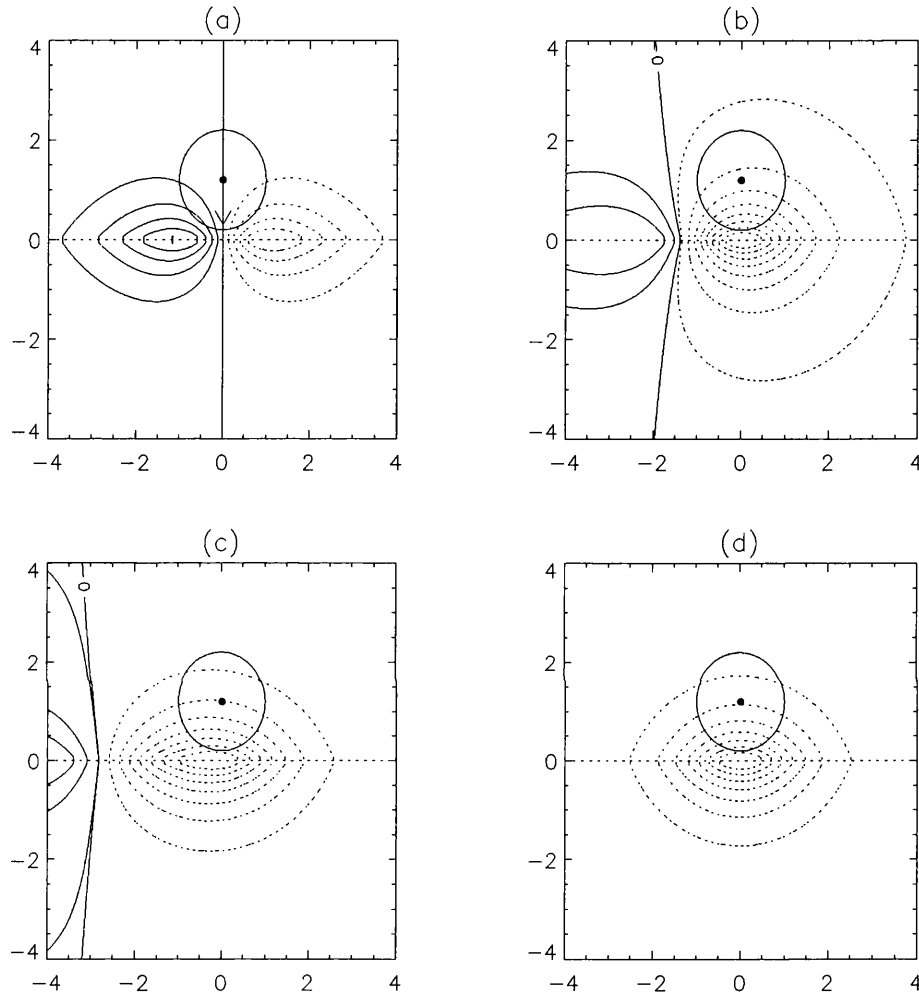
Figure 5.3: The advection of the vortex, here an anticyclone, by the regular field. (a) evaluation of ϕ at $\tau = 0^+$. Note the initial advection is south, along the dipole axis. (b) ϕ evaluated at $\tau = 4$ and (c) evaluated at $\tau = 7$, from equation (5.34), (d) is the pseudoimage term, the regular field as $\tau \to \infty$. The vortex is shown by the circle and its centre by the dot. The parameter values used are $a = 1$, $\alpha = -1$ and $L = 1.2$.

large time behaviour is examined numerically by contour dynamics in the following subsection.

5.2.2 Contour dynamics results

In Chapter 4 it was shown that linear theory described the evolution of a weak singular vortex for many eddy turnover times, far beyond the formal time of the applicability of the theory. This leads to the main question of this section: does the pseudoimage of the linear theory describe the evolution of the weak vortex patch for times $t \geq O(1)$? That is, does the weak vortex patch near an escarpment evolve as if the escarpment were a wall? The problem of the motion of a vortex patch near a wall is itself difficult; the changing vortex shape due to interaction with its image has to be tackled numerically[3]. The plots of the evolution of a vortex patch near a wall presented below were obtained by contour dynamics, and are used for comparison with the vortex shape changes for a vortex patch near an escarpment. The vortex drift is compared with the velocity predicted by the singular vortex linear theory, i.e. with the drift predicted by (5.38). Two further issues are considered in detail. First, the effect of topographic wave radiation on the shape of a west travelling vortex patch is discussed. Second, the hypothesis that the singular vortex linear theory is more accurate for smaller vortex patches is considered.

Following the observation in Chapter 4 that the governing equation (5.1) is invariant under the transformation

$$\psi(x,y) \rightarrow -\psi(x,-y), \tag{5.40}$$

attention is restricted to the case $L > 0$, i.e. the vortex is initially located on the shallow side of the escarpment. The evolution of a vortex on the deep side can then be deduced by symmetry. The cases of an anticyclone and a cyclone are treated separately.

Anticyclones

Figures (5.4), (5.5) and (5.6) show comparisons between the evolution of an anticyclonic vortex patch near an escarpment with that of an equivalent anticyclonic vortex patch near a wall, for $\epsilon = 0.1$, 0.2 and 0.4 repectively. In each case $\alpha = 1$, $a = 1$ and $L = 1.2$. The patch near the escarpment is shown in the solid line, and its centroid by a cross. The evolving patch near a wall, also computed by contour dynamics, is shown by the dashed line and its centroid by a dot.

---

[3]There are a class of steadily propagating solutions, the so-called *V-states*, of Pierrehumbert (1980). In the terminology of the present work these are circular for $a \ll L$ and approach the singular vortex solution in the limit $a/L \rightarrow 0$.
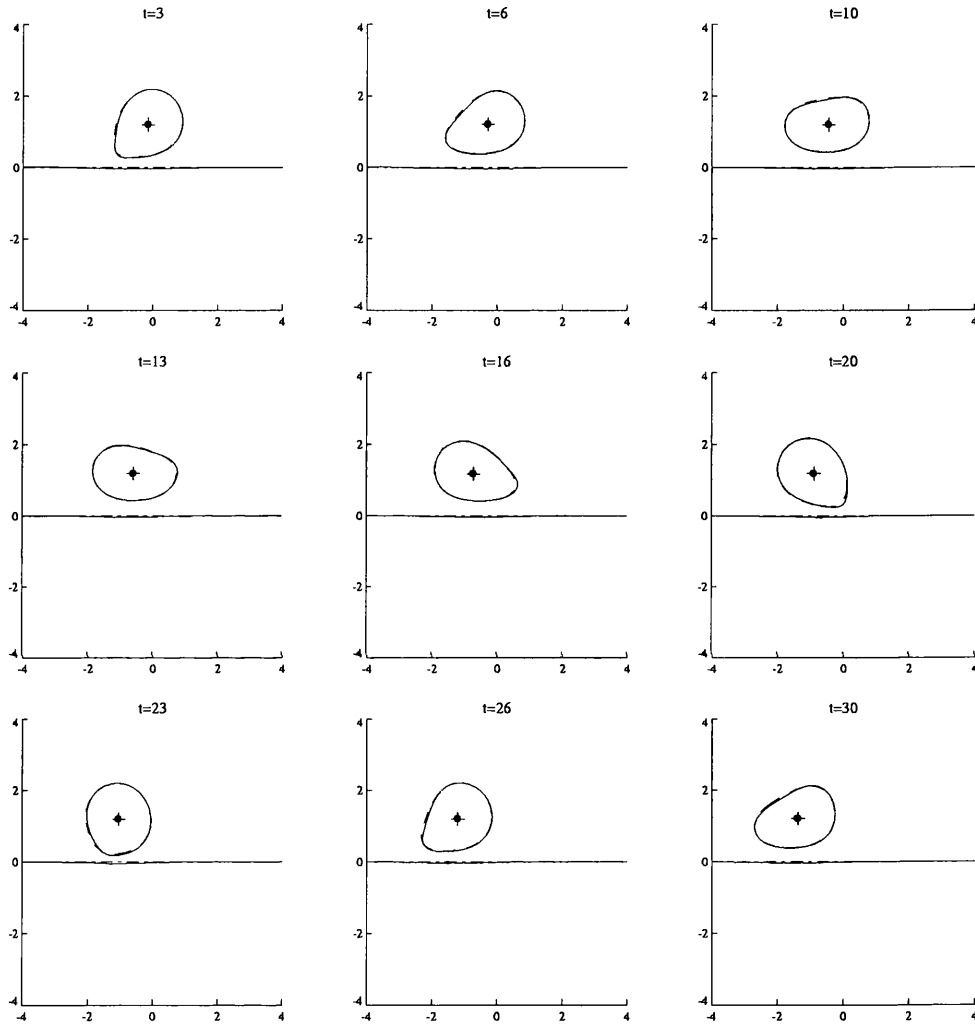
Figure 5.4: Comparison of the evolution of a vortex patch near an escarpment (solid line) with that of a vortex patch near a wall (dashed line). The centroid locations are shown by a cross (escarpment) and a dot (wall), and the parameter values used are $\alpha = 1$ (anticyclone), $a = 1$, $L = 1.2$ and $\epsilon = 0.1$.
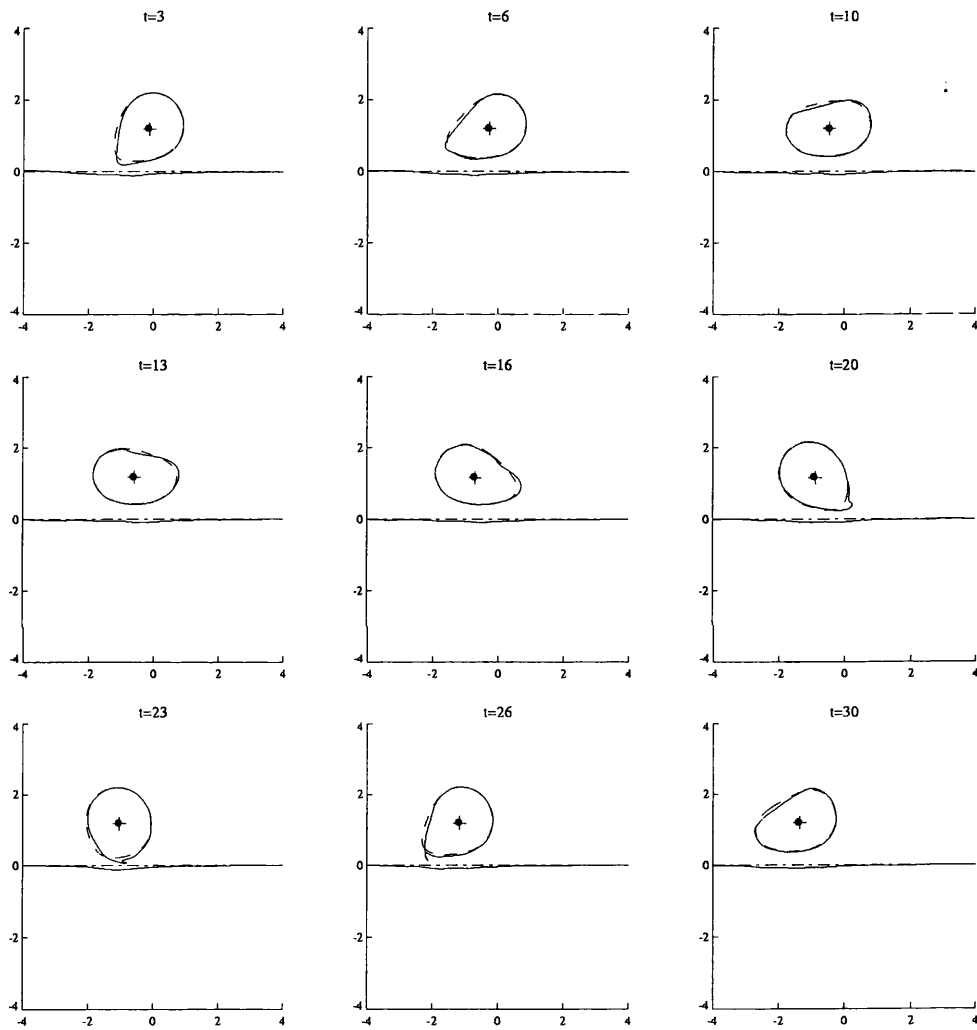
Figure 5.5: As Figure (5.4) except $\epsilon = 0.2$.
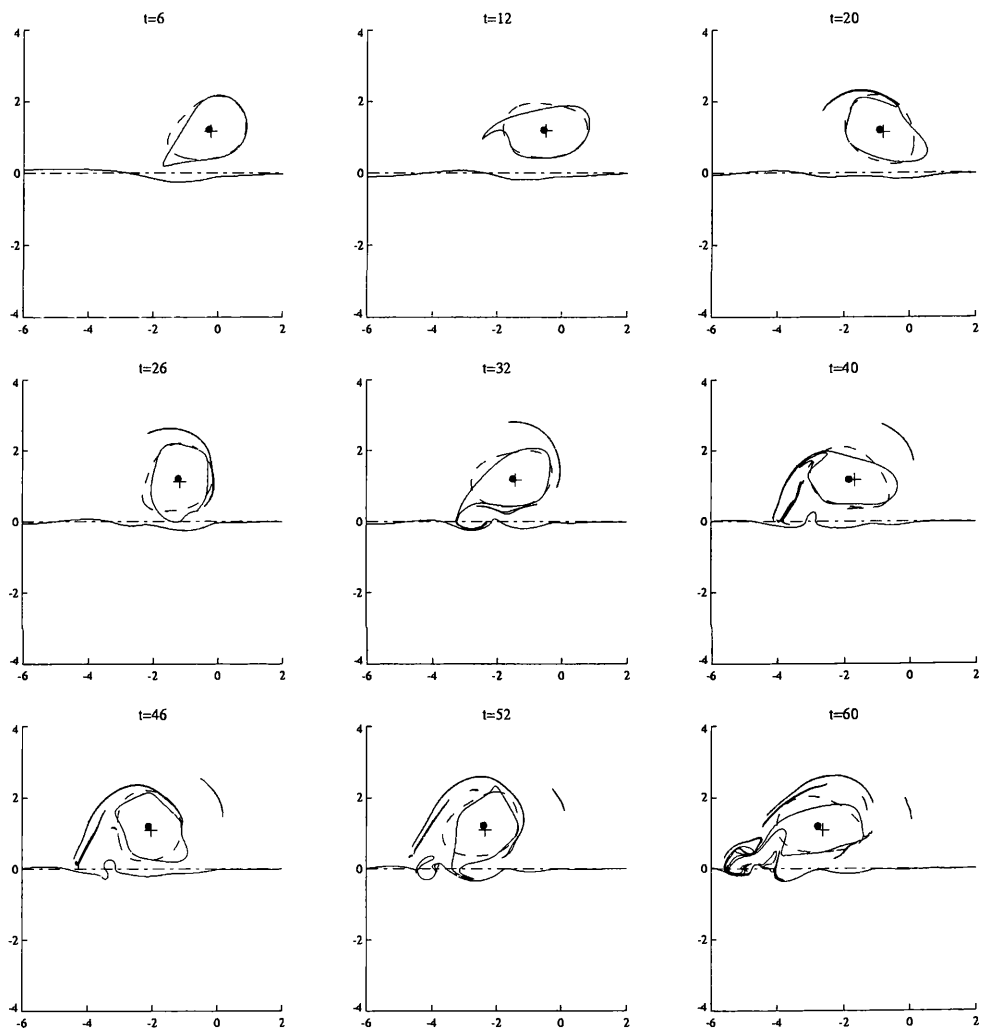
Figure 5.6: As Figure (5.4) except $\epsilon = 0.4$.

In Figure (5.4) it is clear that the weak vortex patch evolves almost precisely in the sense if its pseudoimage as $\epsilon \rightarrow 0$. Both the patch boundary and the centroid are practically coincident with those of the patch evolving near a wall. For $\epsilon = 0.05$ (not shown) the two patches are coincident at the resolution of the plot. This feature is robust, the calculation proceeding to 30 eddy turnover times without any significant deviation. The computation was stopped at $t = 30$ due to large distortions near the left end of the topographic contour, here located at $x = -15$.

Figure (5.5) shows the evolution of the contours for $\epsilon = 0.2$. There are some small deviations in the vortex boundary, compared with the pseudoimage prediction, and the beginning of some filamentation. This process is more clear in Figure (5.6), which shows the contour evolution for $\epsilon = 0.4$. Whilst, the centroid location is still well predicted by the pseudoimage theory, the filamentation of the patch boundary, and its deformation from the shape predicted by the pseudoimage theory is clear. At later times the vortex patch is ripped apart. To understand this process it is useful to consider the evolution of the topographic contour.

Figure (5.7) shows a close up of the contour which initially lay over the escarpment, for $\epsilon = 0.1$. The west travelling dispersive waves are clearly evident, as is the nondispersive disturbance (the pseudoimage), which travels with the vortex in its evolution. As for the singular vortex, this non-dispersive part of the topographic wave train consists of cyclonic relative vorticity, and in the limit $\epsilon \rightarrow 0$ its circulation has precisely the correct magnitude to advect the vortex in the sense of its image in the escarpment.

Next, consider Figure (5.8), which shows the topographic waves for $\epsilon = 0.4$. Initially, the pseu-doimage dominates the motion, and the vortex evolves according to the pseudoimage description. However, at later times topographic waves are radiated in the wake of the pseudoimage. The plot shows clearly that the circulation associated with the relative vorticity of the radiated waves is strong enough to attract the vortex boundary into the wave train. Consequently the relatively weak anticyclone is eroded as a result of wave radiation.

To compare the drift of the anticyclonic patches with the singular vortex model, consider Figure(5.9), which shows the drift of an anticyclone for values of $\epsilon = 0.1, 0.2$, and 0.4. The linear singular vortex prediction (5.38) is in good agreement with the contour dynamics results for the x-velocity, and the agreement improves as $\epsilon \rightarrow 0$, as is shown in Figure(5.9a). The net drift in the y-direction is
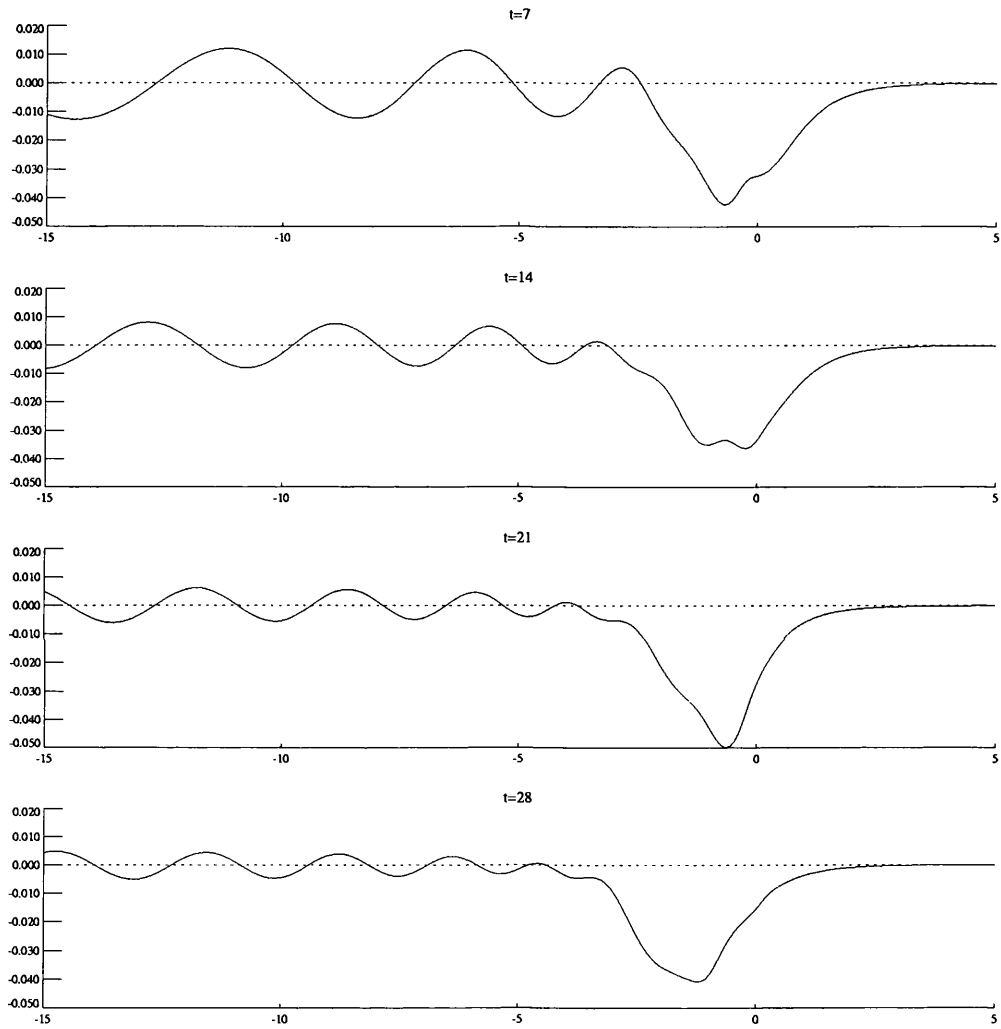
Figure 5.7: A close-up of the evolution of the topographic contour, for an anticyclone. The parameter values used are $a = 1$, $L = 1.2$ and $\epsilon = 0.1$.
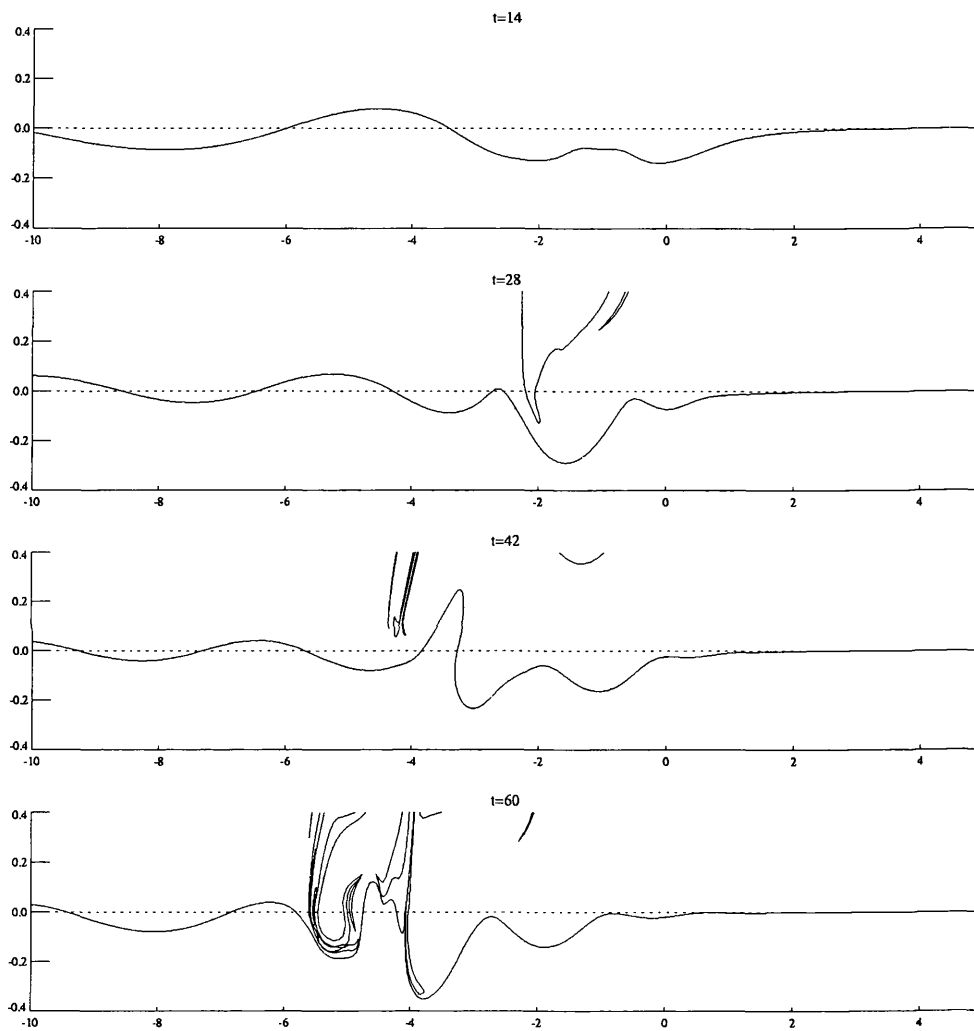
Figure 5.8: As Figure (5.7) except $\epsilon = 0.4$.

small, as can be seen from the scale of the y ordinate in Figure(5.9b) but nonetheless increases with ϵ as topographic wave radiation induces escarpment-ward meridional drift, in addition to vortex filamentation. The singular vortex prediction improves with smaller a, at fixed L, as can be seen in Figure(5.10), which is identical with Figure(5.9), except that $a = 0.25$, i.e. the vortex is small compared with the Rossby radius. The contour plots (not shown) indicate that for the small vortices the vortex shape remains approximately circular.
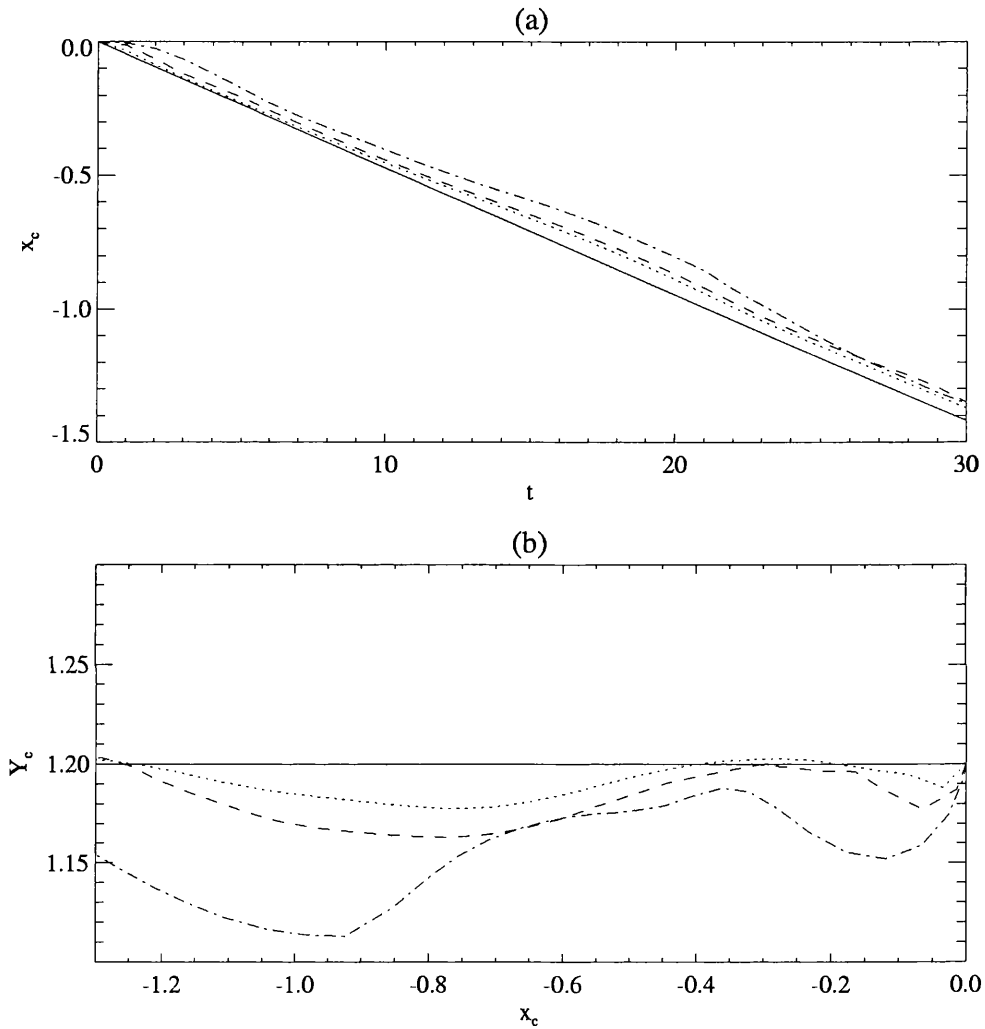
Figure 5.9: Comparison of the drift of the weak anticyclones with the singular vortex prediction. The analytic prediction given in equation (5.38) is shown by the solid line. The parameter values used are $a = 1$, $L = 1.2$ and $\epsilon = 0.1$ (dotted line), $\epsilon = 0.2$ (dashed line) and $\epsilon = 0.4$ (dot-dashed line). The x-velocity is shown in (a) and the centroid trajectories in (b).
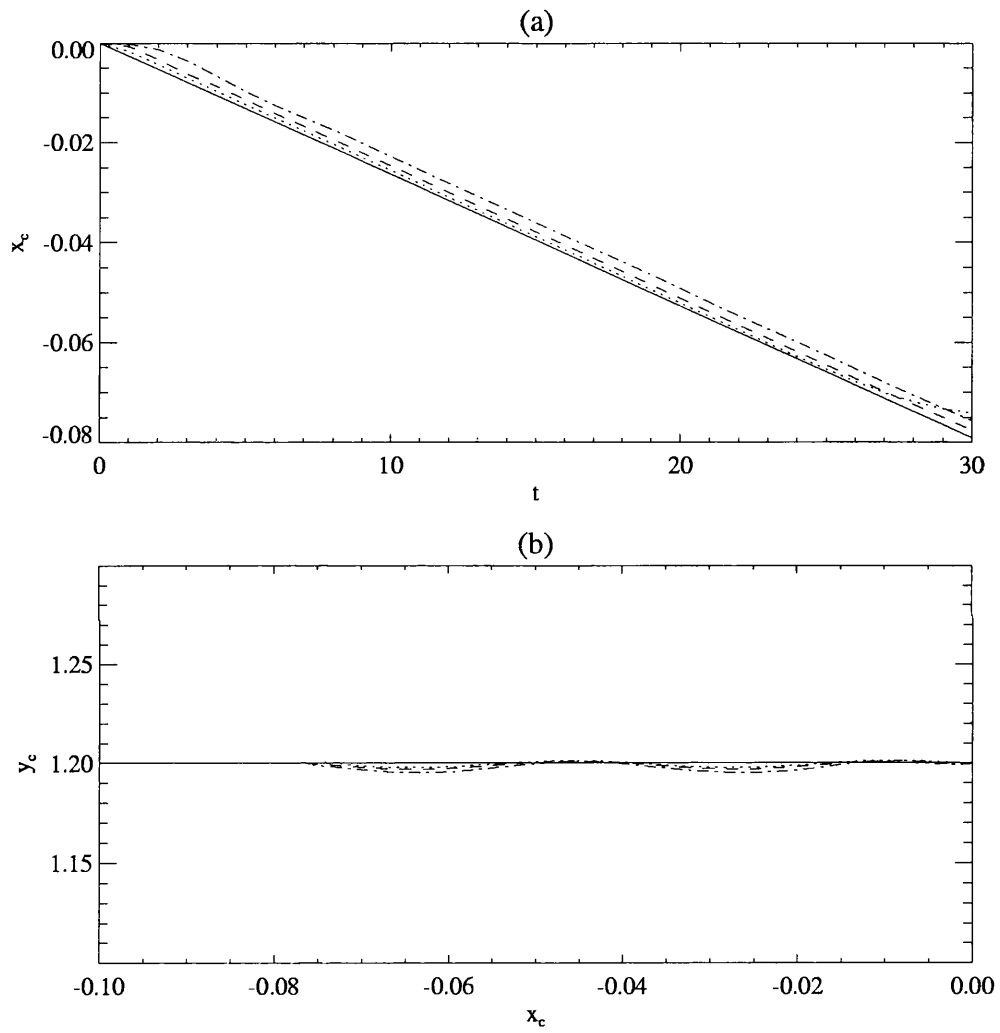
Figure 5.10: As Figure (5.9), except $a = 0.25$, i.e. a small vortex.

115

Cyclones

Figures (5.11)-(5.13) show comparisons between the evolution of a cyclonic vortex patch near an escarpment with that of an equivalent vortex patch near a wall. The parameter values are $\epsilon = 0.1$, 0.2 and 0.4 as in the case of an anticyclone presented previously. Once again in each case $\alpha = 1$, $a = 1$ and $L = 1.2$. The patch near the escarpment is shown in the solid line, and its centroid by a cross. The evolving patch near a wall, is shown by the dashed line and its centroid by a dot.

For $\epsilon = 0.1$, shown in Figure (5.11) it it can be seen that the linear pseudoimage description of the vortex evolution is in excellent agreement with the contour dynamics results. For $\epsilon = 0.05$ (not shown) the boundary of the vortex patch near an escarpment is coincident with the boundary of a vortex patch near a wall to within the resolution of the plot.

However, for $\epsilon = 0.2$, shown in Figure (5.12) it can be seen that the pseudoimage description is good for about 20 eddy turnover times, but then begins to breakdown. By $t = 30$ neither the vortex patch boundary, or its centroid are accurately predicted by the pseudoimage theory. This is in contrast to the anticyclone for the same parameter values, where the linear theory still describes the vortex evolution well. The failure of the linear theory becomes even more pronounced for $\epsilon = 0.4$, shown in Figure (5.13), where it can be seen that the contour evolution differs significantly from the pseudoimage prediction. The linear description of the vortex patch evolution is less robust for cyclones than anticyclones.

To understand the difference between the cases of anticyclones and cyclones, consider the close ups of the topographic contour evolution for $\epsilon = 0.1$ and 0.4, shown in Figures (5.14) and (5.15) respectively. In the case $\epsilon = 0.1$, the dispersive topographic waves propagate away from the vortex. Also note the nondispersive disturbance (the pseudoimage), travelling with the vortex. This patch consists of fluid which has crossed the escarpment from the deep side to the shallow side, thus gaining cyclonic relative vorticity. In the limit $\epsilon \rightarrow 0$ the circulation of the pseudoimage is of precisely the correct magnitude to act as an image of the vortex in the escarpment. The weak circulation of the vortex is dominated by the strong cyclonic pseudoimage.

For the case $\epsilon = 0.4$, the initial displacement of the topographic contour is greater, as the circulation of the vortex patch is stronger. The pseudoimage is closer to the vortex that in the case of an anticyclone. The initial disturbance of the contour "wants" to disperse to the west, in the form of
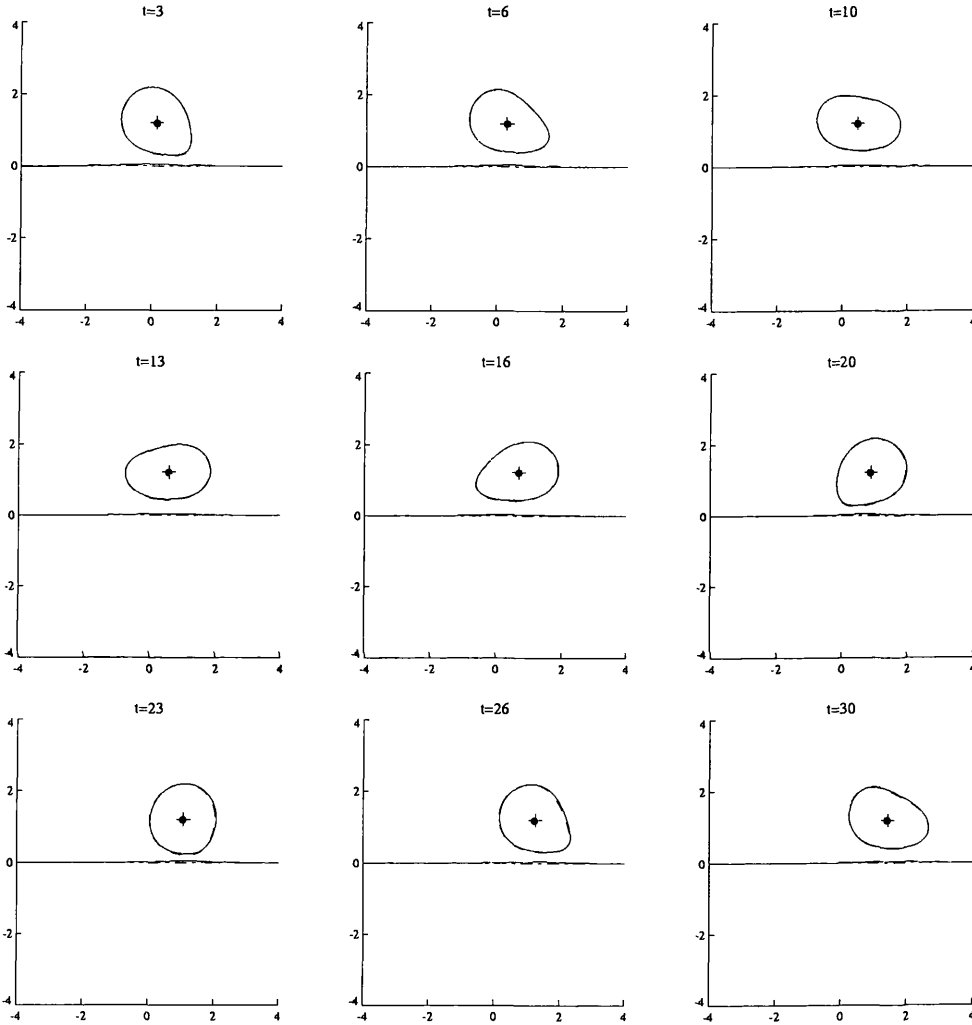
Figure 5.11: Comparison of the evolution of a vortex patch near an escarpment (solid line) with that of a vortex patch near a wall (dashed line). The centroid locations are shown by a cross (escarpment) and a dot (wall), and the parameter values used are $\alpha = 1$ (cyclone), $a = 1$, $L = 1.2$ and $\epsilon = 0.1$.
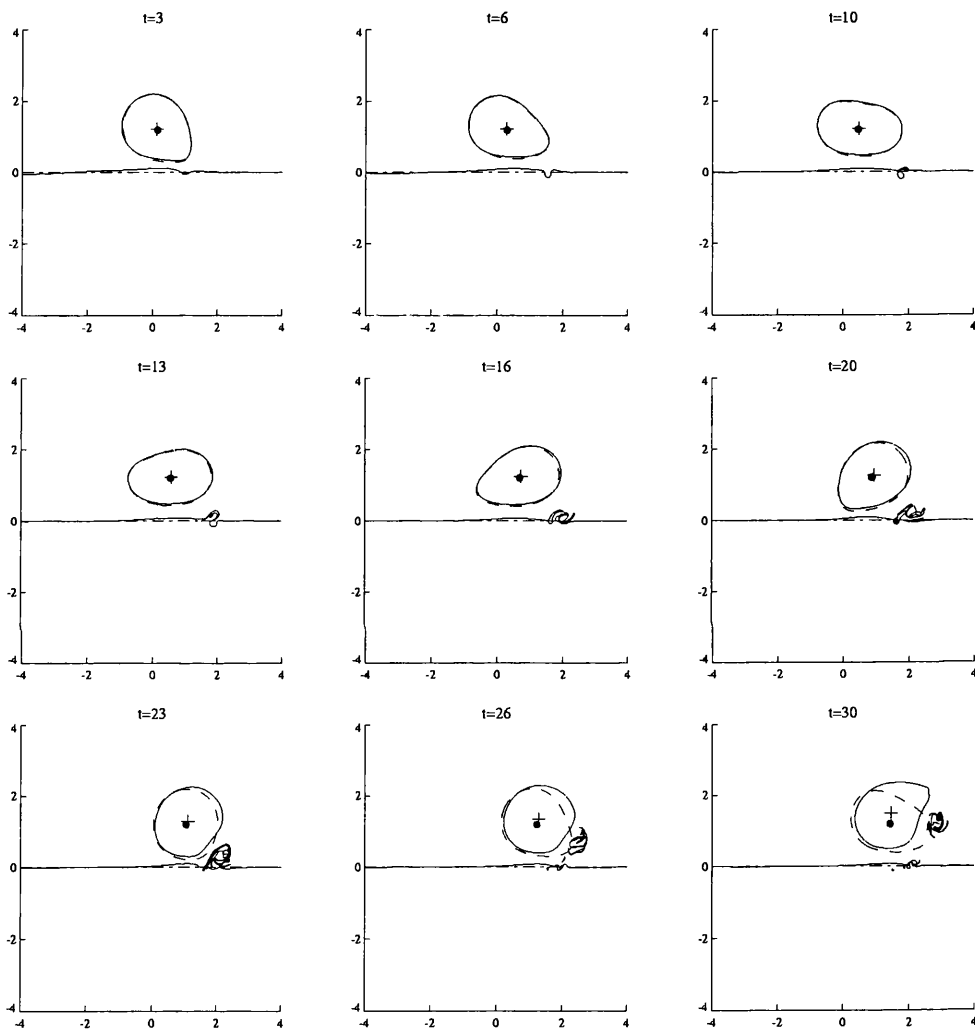
Figure 5.12: As Figure(5.11), except $\epsilon = 0.2$.

118
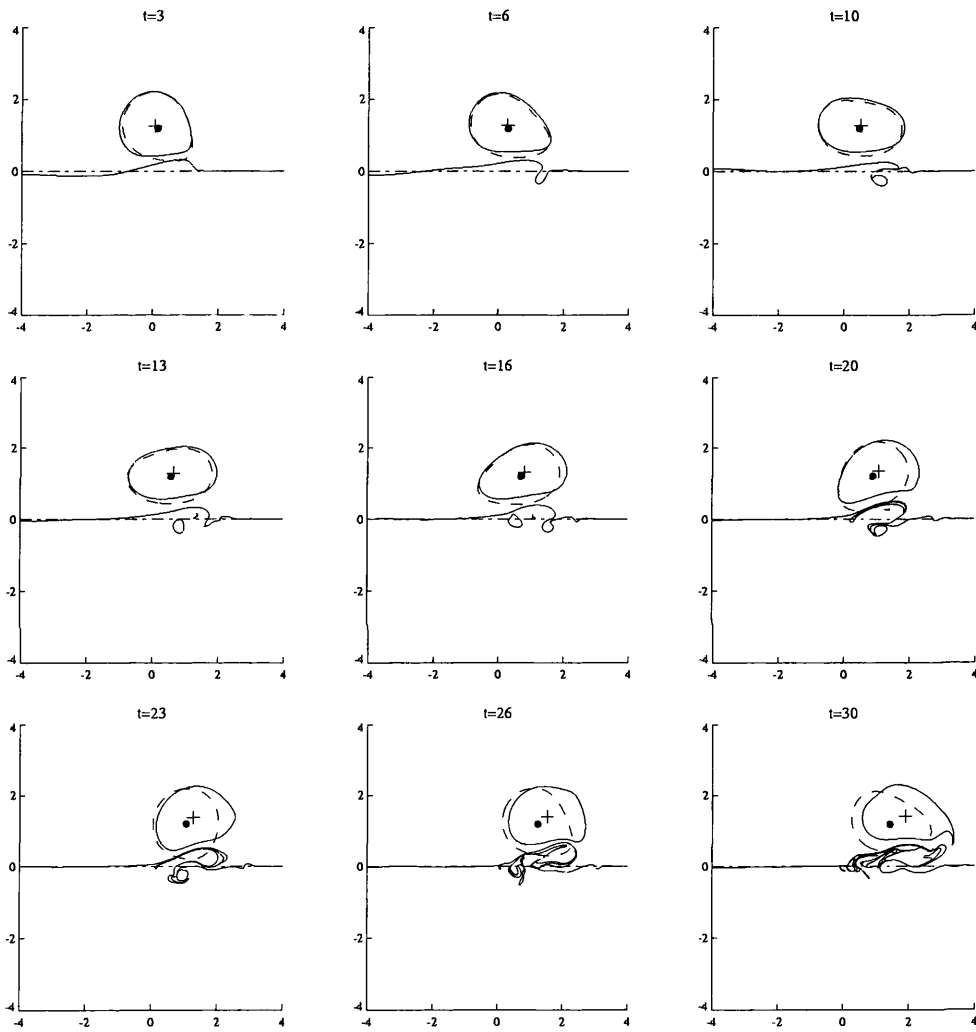
Figure 5.13: As Figure(5.11), except $\epsilon = 0.4$.

topographic waves. This tendency is counteracted by the increased swirl velocity of the primary vortex, which acts to advect the disturbance to the east. The result of these competing tendencies is a build up of anticyclonic vorticity near the primary vortex, and this accumulation has a significant effect on both the deformation of the vortex shape and its drift velocity. This doesn't happen for an anticyclone, since in that case the swirl velocity associated with the vortex pushes fluid in the same direction as the topographic waves, and so there is no local build up of relative vorticity near the vortex.

Figure (5.16) shows a comparison of the vortex drift with the linear singular vortex prediction given in (5.38). Note the initial northward motion, consistent with the initial dipole formed by advection of fluid across the escarpment. The eastward drift is well described by the analytical prediction for 30 eddy turnover times and beyond for $\epsilon \leq 0.2$. However, for $\epsilon = 0.4$, the zonal drift speed exceeds that predicted by the linear theory. Moreover the meridional drift is significant for $\epsilon = 0.4$.

Finally, consider Figure (5.17), which shows the drift of a small ($a = 0.25$) cyclone, compared to the linear singular vortex prediction, for various values of ϵ. As for the case of anticyclones the singular vortex approximation is more accurate for smaller vortices. However, note that for $\epsilon = 0.4$ both the zonal and meridional drift differs significantly from the theory.

5.2.3 Discussion

It has been shown that as $\epsilon \to 0$ the vortex patch evolution is described by the pseudoimage for many eddy turnover times. This statement holds for both cyclones and anticyclones. It has been shown that the vortex patch boundary deformation is accurately predicted by the pseudoimage theory by comparison with an equivalent vortex near a wall. Moreover, the vortex patch drift velocity is equally well described by the linear singular vortex approximation given in equation (5.38), and this agreement improves for $a/L \to 0$.

Wave radiation for the west propagating anticyclones appears insignificant for small ϵ. This is be expected, given the singular vortex results in the previous Chapter. It was shown that wave induced drift is $O(e^{-1/\epsilon})$, (see equation (4.93)), for a weak singular vortex, which is a result of the vortex travelling at the topographic *short* wave velocity. The same is true in the present case, and since the short waves are least energetic it is reasonable that the effects of wave radiation are not evident for
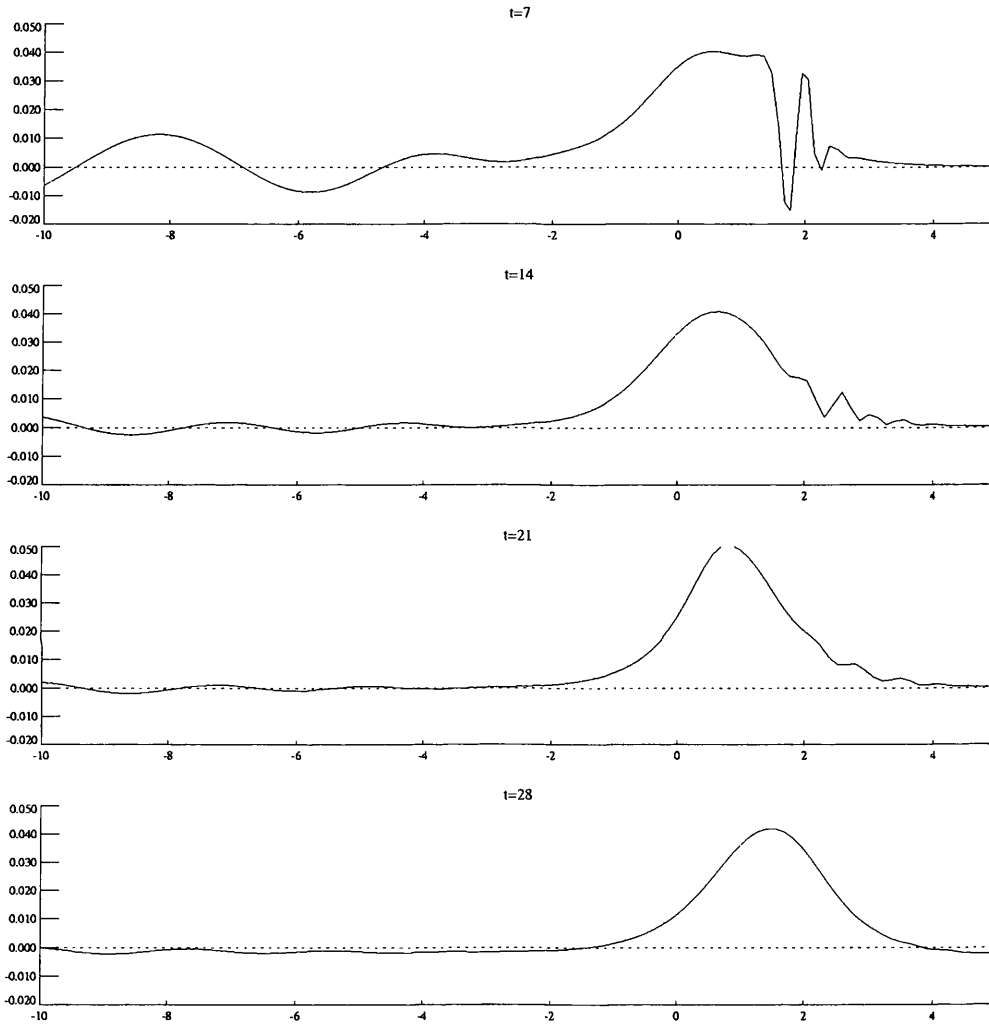
Figure 5.14: A close-up of the topographic waves, for a cyclone. The parameter values used are $a = 1$, $L = 1.2$ and $\epsilon = 0.1$.
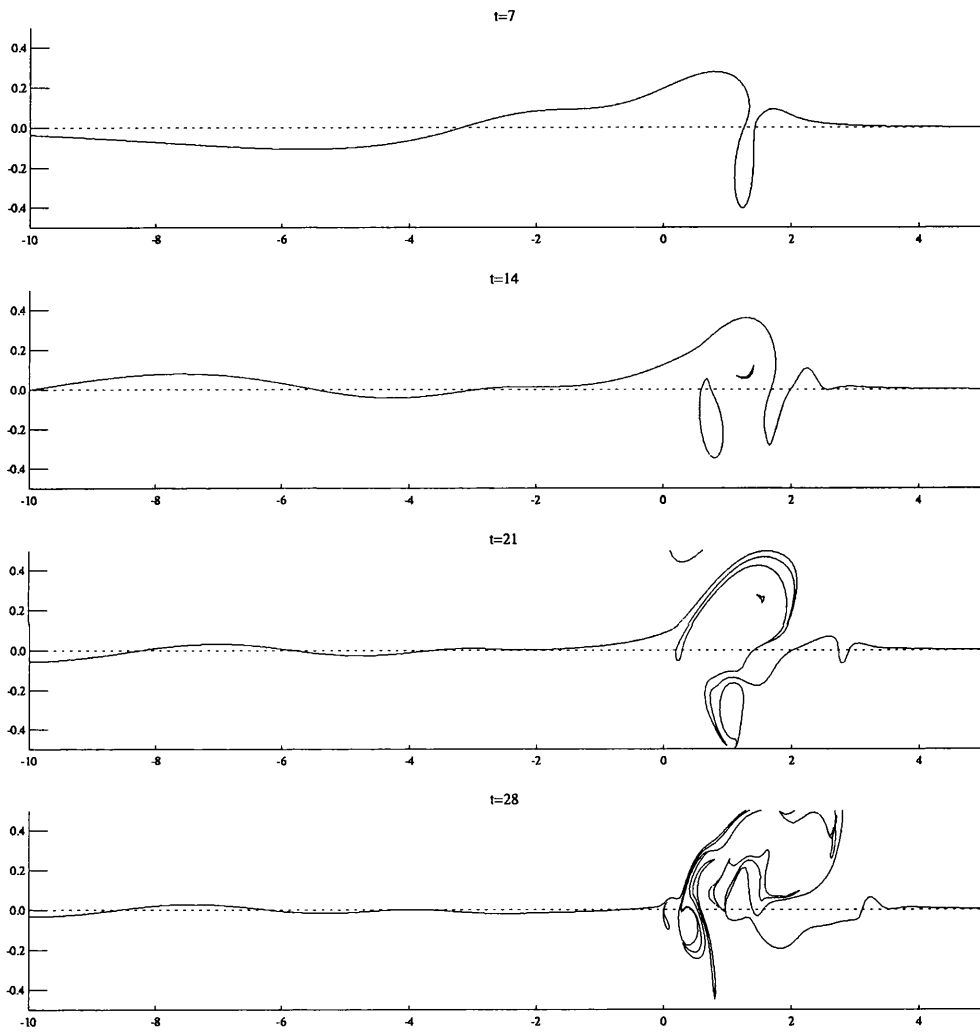
Figure 5.15: As Figure (5.14) except $\epsilon = 0.4$.
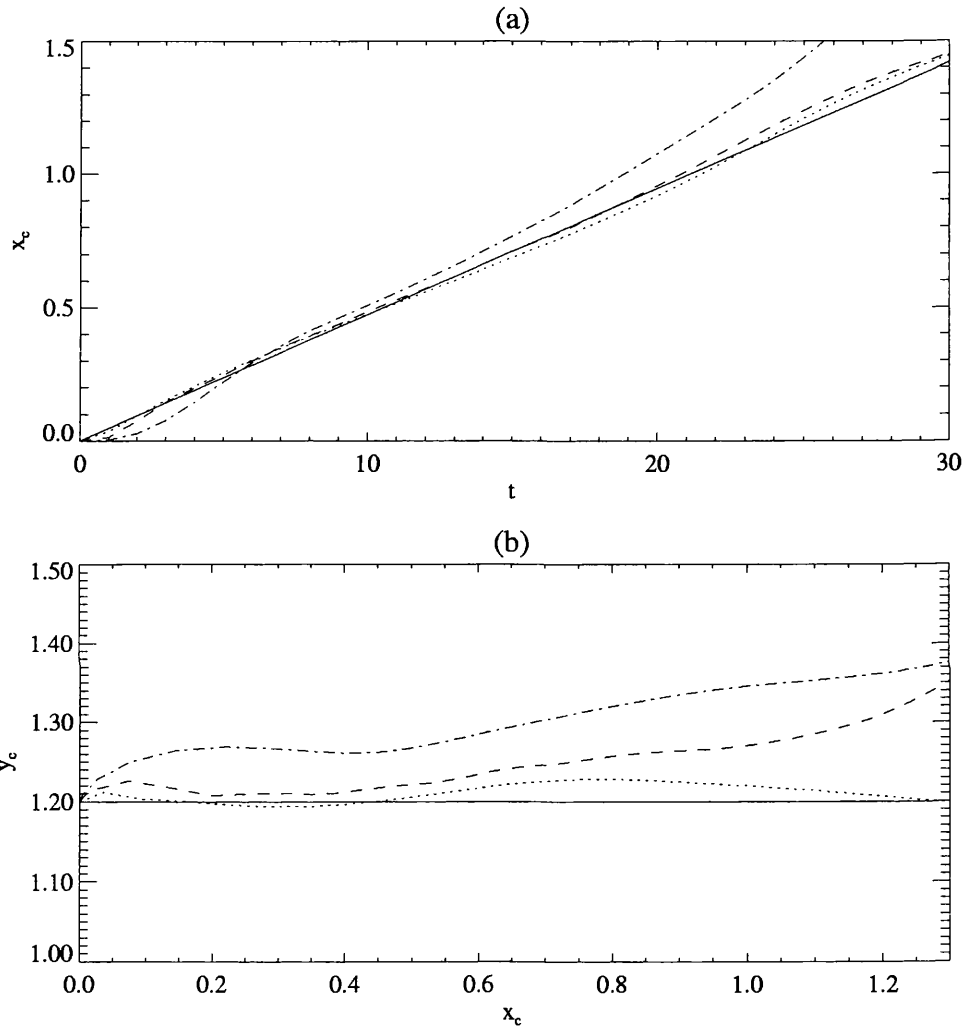
Figure 5.16: Comparison of the drift of the weak cyclones with the singular vortex prediction. The analytic prediction given in equation (5.38) is shown by the solid line. The parameter values used are $a = 1$, $L = 1.2$ and $\epsilon = 0.1$ (dotted line), $\epsilon = 0.2$ (dashed line) and $\epsilon = 0.4$ (dot-dashed line). The x-velocity is shown in (a) and the paths in (b).
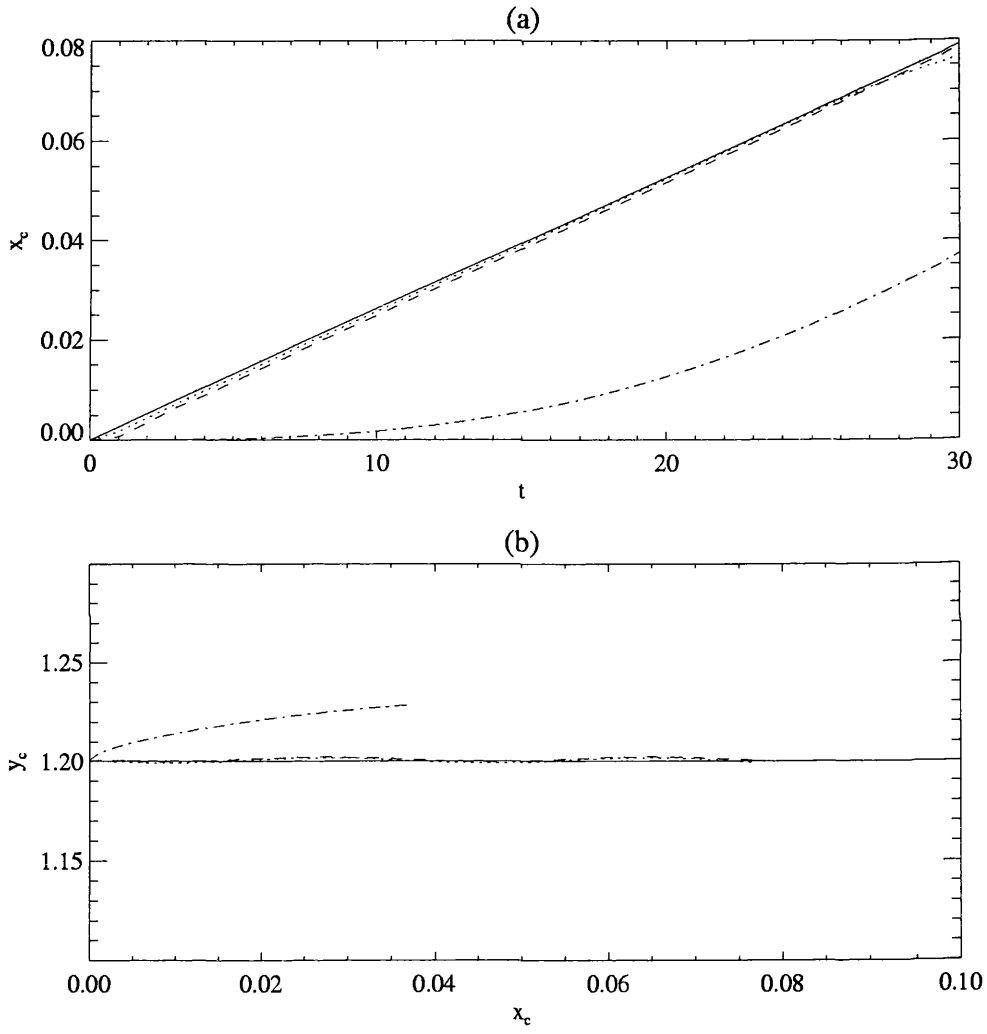
Figure 5.17: As Figure (5.9), except $a = 0.25$

124

the times of the runs given. For larger values of ϵ it has been shown that wave radiation is significant and causes enhanced escarpment-ward. It is worth highlighting that the singular weak anticyclone is *unable* to change its shape, and for values of ϵ comparable to those discussed here, the weak singular anticyclone responds to wave radiation through meridional drift only. The anticyclonic vortex patch, on the other hand, decays via stripping. This stripping is due in part to wave radiation, but this type of vortex filamentation is associated with the local shear in the flow.

The linear theory is less robust for cyclonic vortex patches, and breaks down for $\epsilon \approx 0.2$. Nonlinear effects are far more significant for cyclones than anticyclones, and is due to the circulation of the vortex competing with the preferential direction of propagation of the topographic waves. The circulation of the vortex patch induces a secondary anticyclonic circulation in its vicinity, and the dipolar nature of this structure causes a northeastward drift of the primary vortex. It is shown later that for moderate cyclones the dipole formation is characteristic of the motion and dominates the drift of the primary vortex.

Linear theory, and in particular the linear singular vortex approximation to the vortex patch evolution, describes well the drift of the vortex centroid for $\epsilon \to 0$, for both anticyclones and cyclones. The linear singular vortex approximation improves with decreasing vortex patch size.

Finally, note that there is *no* β-plane analogy for the evolution of a weak vortex patch near an escarpment; the pseudoimage description is an artefact of the discontinuous topographic gradient, and weak vortices near an escarpment are long lived, by comparison with weak vortices on the β-plane, which drift west, regardless of the sense of the circulation, and which decay rapidly as the result of Rossby wave radiation. The figures of Lam and Dritschel (1998) illustrate this process well.

5.3   An intense vortex patch

In the case of an intense vortex, $S \ll 1$ is a small parameter. To reformulate the problem note that the secondary circulations scale like S, and seek a solution to (5.12a) and (5.12b) in the form

$$\psi(r,\theta,t) \;\; = \;\; \psi_0(r) + S\phi_1 + ..., \qquad (5.41a)$$

$$q \;\; = \;\; Sq_1 + S^2 q_2 + ..., \qquad (5.41b)$$

$$r_0 = a + Sr_1 + ..., \tag{5.41c}$$

$$(u,v) = S(u_1, v_1) + ..., \tag{5.41d}$$

The initial conditions (5.16a)-(5.16d) become, for the leading order quantities,

$$\phi_1 = q_1 = r_1 = u_1 = v_1 = 0, \quad t = 0 \tag{5.42}$$

The leading order solution, obtained below is valid for $t < O(S^{-1})$.

5.3.1 Leading order solution

Substitution of (5.41b) into (5.12a) gives the initial-value problem for the leading order vorticity correction,

$$\frac{\partial q_1}{\partial t} + b(r)\frac{\partial q_1}{\partial \theta} = -b(r)\frac{\partial h_B}{\partial \theta}, \tag{5.43a}$$

$$q_1(r,\theta,t) = 0. \tag{5.43b}$$

Hence changes in the leading order vorticity correction, q_1 are due to the advection of the ambient potential vorticity and q_1 itself by the axisymmetric circulation of the primary vortex. Equation (5.43a) is easily solved by the method of characteristics. The complimentary function is

$$\tilde{q}_1 = \tilde{q}_1(\theta - b(r)t, r), \tag{5.44}$$

and the particular integral is

$$p(r,\theta) = -\frac{1}{2}\mathrm{sgn}(r\sin\theta + y_c), \tag{5.45}$$

since $h_B = \mathrm{sgn}(r\sin\theta + y_c)/2$ in the moving polar coordinate frame. The initial condition (5.43b) leads to

$$\tilde{q}_1(r,\theta) = \frac{1}{2}\mathrm{sgn}(r\sin(\theta - b(r)t) + L), \tag{5.46}$$

so that the solution for the leading order vorticity correction is

$$q_1 = \frac{1}{2}\left[\mathrm{sgn}(r\sin(\theta - bt) + L) - \mathrm{sgn}(r\sin\theta + y_c)\right]. \tag{5.47}$$

Apart from the additional factor of 1/2 (due to the particular choice of representation for the escarpment topography), this is formally the same as the leading order vorticity correction obtained by McDonald (1998) in the case of an intense singular vortex near an escarpment, differing only in the form of the angular velocity $b(r)$. The reason that this is the case is discussed below.

126

The equations governing the next order quantities are

$$\nabla^2 \phi_1 - \phi_1 = q_1(r, \theta, t) \tag{5.48a}$$

$$\frac{\partial r_1}{\partial t} + b(a)\frac{\partial r_1}{\partial \theta} + \frac{\partial \phi_1}{\partial \theta}(a, \theta, t) + u_1 a \cos\theta + v_1 a \sin\theta = 0 \tag{5.48b}$$

$$\int_0^{2\pi} r_1(\theta, t) e^{i\theta} d\theta = 0 \tag{5.48c}$$

$$\frac{\partial q_2}{\partial t} + b(r)\frac{\partial q_2}{\partial \theta} = -J[\phi_1 + u_1 y - v_1 x, q_1] - J[\phi_1, h_B]. \tag{5.48d}$$

The piecewise continuous form of the vorticity correction, q_1, appearing as a forcing term in the equation for the streamfunction correction ϕ_1 in (5.48a), inhibits progress. To proceed, it is assumed that the response for short times is dominated by azimuthal mode-1, since, according to equation (5.48b), the leading order vortex drift velocity components (u_1, v_1) are controlled by this dipolar mode. This is analogous to the motion of an intense vortex on the β-plane where the mode-1 component is termed the β-gyres. See Chapter 3 for a review of results for vortex motion on the β-plane.

First, writing

$$r_1(\theta, t) = r_1^{(s)}(t)\sin\theta + r_1^{(c)}(t)\cos\theta, \tag{5.49}$$

and substituting into (5.48c), leads to

$$r_1 = 0, \tag{5.50}$$

i.e. the patch boundary remains circular to this order of approximation.

It is straightforward to obtain the azimuthal mode-1 Fourier coefficients for q_1. The derivation is given in Appendix A, and the result is quoted here,

$$q_1 = q_1^{(s)}(r, t)\sin\theta + q_1^{(c)}(r, t)\cos\theta, \tag{5.51}$$

where

$$q_1^{(s)} = \frac{2}{\pi r}\sqrt{r^2 - L^2}(\cos bt - 1), \quad r > |L| \tag{5.52a}$$

$$q_1^{(c)} = -\frac{2}{\pi r}\sqrt{r^2 - L^2}\sin bt, \quad r > |L| \tag{5.52b}$$

and, importantly

$$q_1^{(c)} = q_1^{(s)} = 0, \quad r < |L|. \tag{5.53}$$

In obtaining this approximation it has been assumed that $y_c = L + O(S)$. Details can be found in Appendix A. This cut-off at $r = |L|$ implies that there is no secondary relative vorticity production

near the vortex, at least for short time, and will become apparent later in the contour dynamics investigation. The deflected topographic contour remains isolated from the vortex boundary, due to the dominance of the strong azimuthal circulation of the intense vortex. Note however, that q_1 is continuous at $r = |L|$.

Next, seeking a solution to (5.48a) in the form

$$\phi_1(r, \theta, t) = \phi_1^{(s)}(r, t)\sin\theta + \phi_1^{(c)}(r, t)\cos\theta, \tag{5.54}$$

leads to

$$\left(\frac{\partial^2}{\partial r^2} + \frac{1}{r}\frac{\partial}{\partial r} - \left(\frac{1}{r^2} + 1\right)\right)\phi_1^{(\nu)} = q_1^{(\nu)}, \tag{5.55}$$

where the superscript (ν) can be either (s) or (c) for the sin or cos components respectively. The Greens function for the operator in the right hand side of (5.55), which is regular at the origin is well known (see e.g. Sutyrin and Flierl (1994) or Lam and Dritschel (1998)) and is

$$G(r|\rho) = \begin{cases} -\rho I_1(r)K_1(\rho), & r < \rho \\ -\rho K_1(r)I_1(\rho), & r > \rho \end{cases} \tag{5.56}$$

so that

$$\phi_1^{(\nu)} = \int_0^\infty G(r|\rho)q_1^{(\nu)}d\rho, \tag{5.57}$$

or, rather less appealing,

$$\phi_1^{(\nu)} = \begin{cases} -I_1(r)\int_{|L|}^\infty \rho q_1^{(\nu)}(\rho, t)K_1(\rho)d\rho, & r < |L| \\ \\ -I_1(r)\int_r^\infty \rho q_1^{(\nu)}(\rho, t)K_1(\rho)d\rho - K_1(r)\int_{|L|}^r \rho q_1^{(\nu)}(\rho, t)I_1(\rho)d\rho, & r > |L| \end{cases} \tag{5.58}$$

Note that the solution is continuous on $r = |L|$. Now, according to (5.50), equation (5.48b) becomes

$$\frac{\partial \phi_1}{\partial \theta}(a, \theta, t) + u_1 a\cos\theta + v_1 a\sin\theta = 0. \tag{5.59}$$

But,

$$\frac{\partial \phi_1}{\partial \theta} = \phi_1^{(s)}\cos\theta - \phi_1^{(c)}\sin\theta, \tag{5.60}$$

in turn implying that

$$u_1 a = -\phi_1^{(s)}(a, t) \tag{5.61a}$$

$$v_1 a = \phi_1^{(c)}(a, t). \tag{5.61b}$$

As for the weak vortex patch the constraint $a < |L|$ is adopted, for which the vortex drift velocity components are

$$u_1 = \frac{2}{\pi a}I_1(a)\int_{|L|}^\infty (\cos bt - 1)K_1(r)\sqrt{r^2 - L^2}dr, \tag{5.62a}$$

128

$$v_1 \;=\; \frac{2}{\pi a} I_1(a) \int_{|L|}^{\infty} \sin bt K_1(r)\sqrt{r^2 - L^2}\, dr. \tag{5.62b}$$

These are the *same* expressions obtained by McDonald (1998) for an intense singular vortex near an escarpment (cf equations (4.96a,b)), except for the constant multiplying the integrals, and the particular form for the vortex angular velocity $b(r)$. Moreover, as $a \to 0$, $I_1(a)/a \to 1/2$, so the singular vortex drift velocity components are recovered from (5.62a) and (5.62b) in this limit.

The asymptotic behaviour of the integrals is derived in Appendix B and is quoted here. As $t \to 0$,

$$u_1 \;\approx\; -\frac{A\alpha^2 t^2}{4\pi^2}, \tag{5.63a}$$

$$v_1 \;\approx\; -\frac{B\alpha t}{2\pi}, \tag{5.63b}$$

where A and B are positive constants which depend on L. For $t \gg 1$ but less than $\mathrm{O}(S^{-1})$

$$u_1 \;\approx\; -\frac{2I_1(a)}{a}\exp(-|L|) + \mathrm{O}\left(\frac{\log^2 t}{t}\right) \tag{5.64a}$$

$$v_1 \;\approx\; \mathrm{O}\left(\frac{\log^2 t}{t}\right) \tag{5.64b}$$

Since $\mathrm{sgn}\, v = -\mathrm{sgn}\,\alpha$ and $\mathrm{sgn}\, u = -1$ in (5.63a,b), it is apparent that for small times anticyclones ($\alpha > 0$) move south and west, whilst cyclones ($\alpha < 0$) move north and west. Equations (5.64a,b) indicate that after the initial meridional acceleration there is a slow decay in the meridional velocity. The zonal drift approaches the steady westward speed of $2SI_1(a)\exp(-|L|)/2a$. These features are clear in Figure (5.18), which shows plots of the drift velocity components, and the centroid trajectory for a cyclone with $a = 1$ (solid line) and $a = 0.5$ (dotted line). Note that the smaller vortex experiences increased meridional drift and decreased zonal drift.

This behaviour is qualitatively that of an intense vortex on the β-plane[4]. The mechanism for this behaviour is illustrated in Figure (5.19), which shows the evolution of the streamlines calculated from (5.58). Initially the vortex (here a cyclone) pushes fluid columns lying to its west (resp. east) from the shallow (deep) side of the escarpment to the deep (shallow) side. Potential vorticity conservation demands that these fluid columns acquire net cyclonic (anticyclonic) relative vorticity. This secondary dipole is initially symmetric about $x = 0$, as can be seen in Figure (5.19a), and results in an initial northwards drift of the cyclone. At later times, Figures (5.19b,c) the strong cyclonic circulation of the vortex rotates the secondary dipole anticlockwise, which results in the vortex following the curved northwest trajectory. At large times, Figure (5.19d), the flow in the vicinity of the vortex approaches a uniform westward stream.

[4]And indeed of an intense singular vortex near an escarpment.
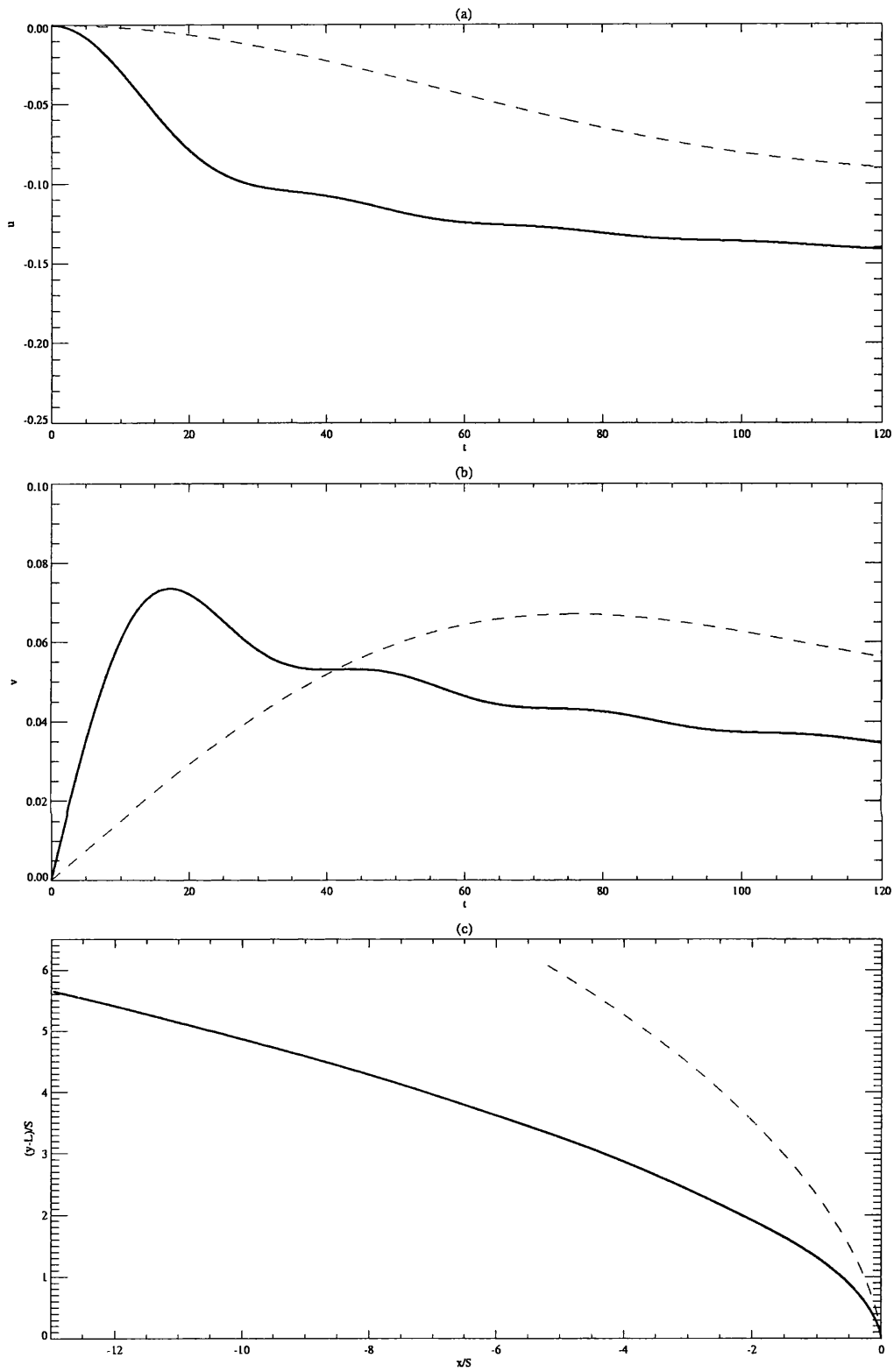
Figure 5.18: The drift of an intense vortex patch near an escarpment. (a) is a plot of the zonal drift velocity, (b) is a plot of the meridional drift velocity and (c) is a plot of the trajectory of the vortex centroid. The parameter values use are $L = 1.2$, $\alpha = -1$ (i.e. a cyclone), and $a = 1$ (solid line) and $a = 0.5$ (dashed line). See text for further comments
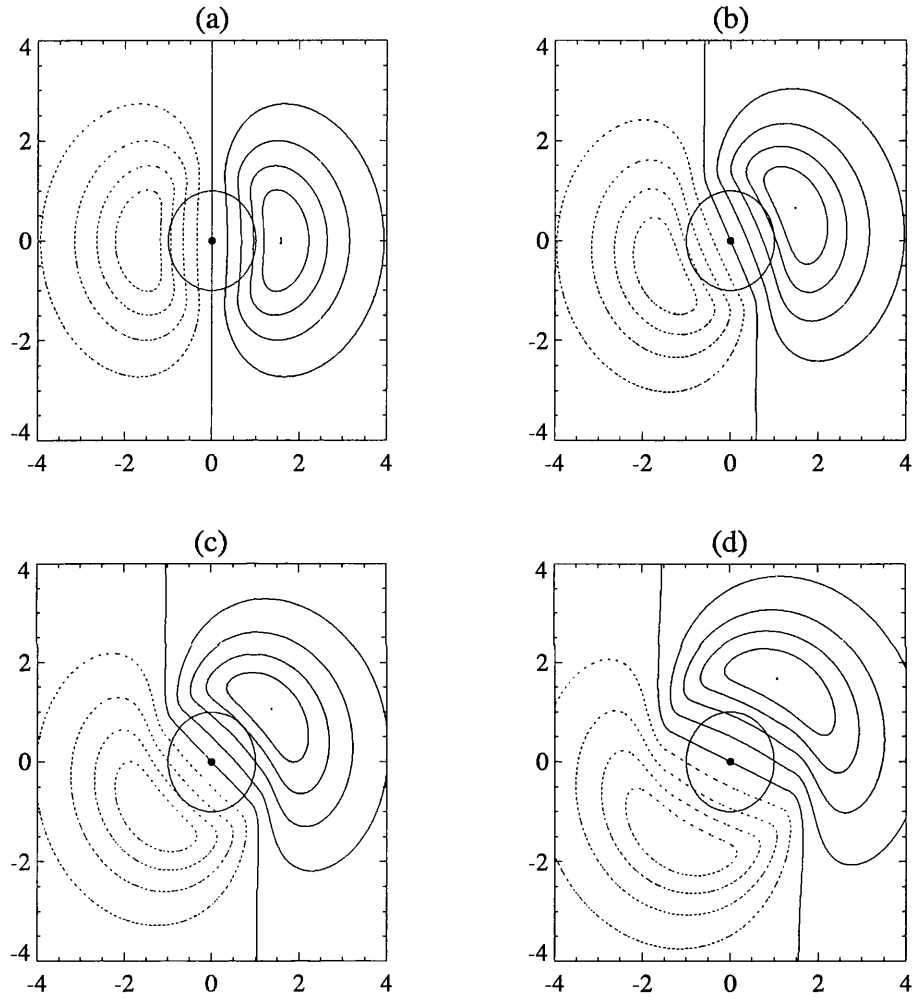
Figure 5.19: Plots of the streamlines for the leading order solution, evaluated numerically by equations (5.58). The parameter values used are $a = 1$, $L = 1.2$ and $\alpha = -1$, i.e. a cyclone. The times are (a) $t = 0^+$, (b) $t = 10$, (c) $t = 20$ and (d) $t = 50$. See text for further comments.

The flow near the dipole axis is approximately uniform, and this can be seen from the large time asymptotics for ϕ_1 (see Appendix B for details). The residual flow ϕ_{res} is

$$
\begin{aligned}
\phi_{res} &= \phi_1 + u_1 r \sin\theta - v_1 r \cos\theta \\
&= \left[\phi_1^{(s)}(r,t) - \frac{r}{a}\phi_1^{(s)}(a,t)\right]\sin\theta + \left[\phi_1^{(c)}(r,t) - \frac{r}{a}\phi_1^{(c)}(a,t)\right]\cos\theta.
\end{aligned}
\tag{5.65}
$$

The coefficients of $\sin\theta$ and $\cos\theta$ are plotted in Figure (5.20) at times $t = 20$ and $t = 100$. Note that in some region near the vortex the residual flow practically vanishes. This can also be seen from the asymptotics of ϕ_{res}. As $t \to \infty$ and for $r < |L|$ the results of Appendix B imply that near the vortex,

$$
\phi_{res} \approx \left[2I_1(r) - 2\frac{rI_1(a)}{a}\right]\exp(-|L|)\sin\theta + O\left(\frac{\log^2 t}{t}\right).
\tag{5.66}
$$

The coefficient of $\sin\theta$ is small in practice. For example, for $a = 1$ and $L = 1.2$, the maximum modulus of ϕ_{res} in the interval $0 < r < |L|$ is approximately 0.021. Apart from explaining the leading order behaviour these asymptotic results reveal some of the features of the long time evolution of the vortex.

First, consider equation (5.48d) describing the evolution of the second order vorticity correction q_2. According to equations (5.52a,b) the spatial derivatives of q_1 grow with time (the first Jacobian term in the left hand side). However, the exponentially decreasing nature of the angular velocity $b(r)$ implies that the region of most rapid growth of q_1 occurs near the vortex centre. The smallness of the residual flow ϕ_{res} compensates for this growth and the first Jacobian term in the right hand side of (5.48d) grows slowly. Similarly the spatial derivatives of ϕ_1 are slow to grow, implying in turn that the second Jacobian term in the right hand side of (5.48d) also grows slowly. The right hand side of (5.48d) multiplied by S^2 is the remainder obtained when substituting the leading order solution $\phi_0 + S\phi_1$ into the governing equation (5.8). This fact, together with slow growth of the second order vorticity correction q_2 means that the leading order solution $\phi_0 + S\phi_1$ may describe the vortex evolution beyond $t = O(S^{-1})$.

Near the vortex centre, the solution $\phi_0 + S\phi_1$ tends to

$$
\psi_\infty = \psi_0\left(((x + Su_1 t)^2 + y^2)^{1/2}\right) + Su_1 y.
\tag{5.67}
$$

In obtaining this solution the approximation $I_1(r) \approx r/2$ for sufficiently small r has been used[5]. Reznik and Grimshaw (1998) obtained a similar result for the leading order solution for an intense

---

[5]In practice $I_1(r) \approx r/2$ even for $r = 2$.
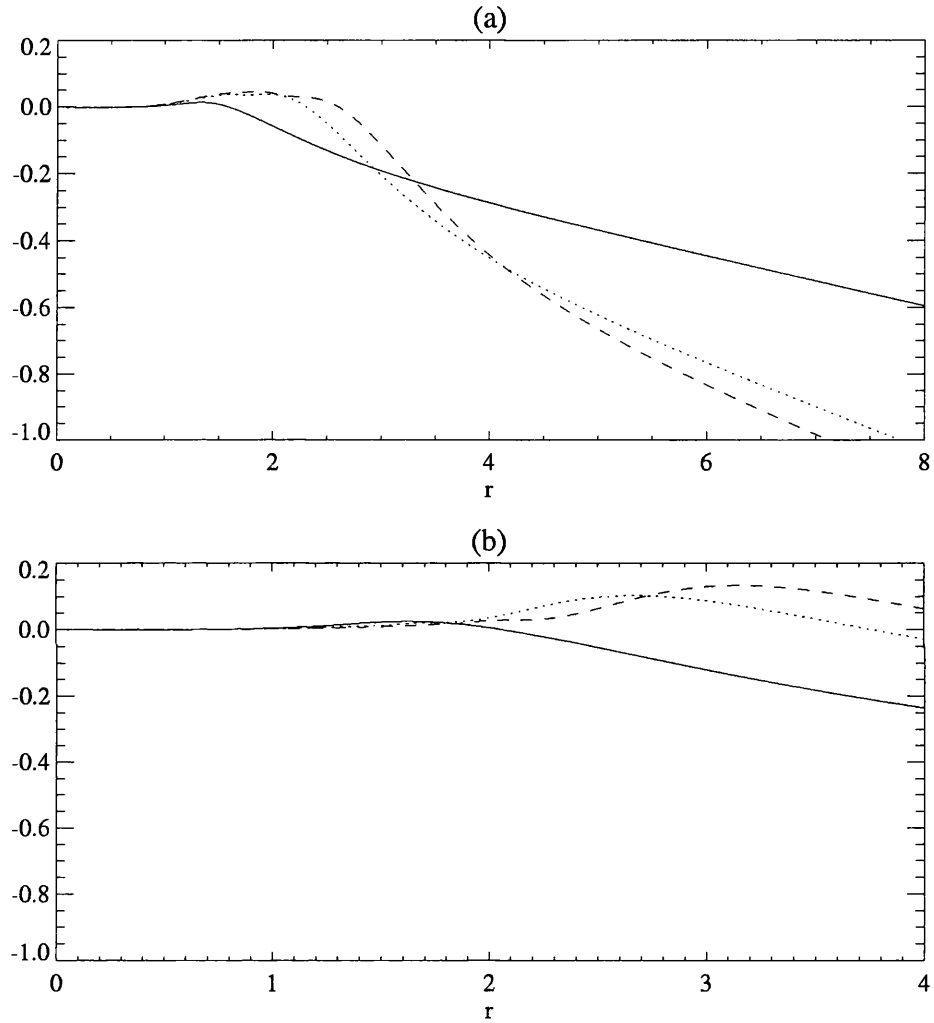
Figure 5.20: The coefficients of $\sin\theta$ and $\cos\theta$ in equation (5.65) : (a) the coefficient of $\sin\theta$ and (b) the coefficient of $\cos\theta$. The parameters used are $L = 1.2$, $a = 1$ and $\alpha = -1$ at times $t = 20$ (solid line), $t = 100$ (dotted line) and $t = 200$ (dashed line).

β-plane vortex. There is however a crucial difference with the present case. The steadily propagating vortex on the β-plane has westward drift velocity that precisely matches the Rossby long wave phase speed. The solution analogous to ψ_∞ is then an *exact* solution of the governing equation, and the authors are justified in saying that the nonlinearity "kills the β-effect", and the vortex adopts a non-radiating state. In the present case (5.67) is not a solution of (5.12a). Moreover the vortex always travels with westward drift velocity of magnitude less than unity, i.e. at a velocity matching a possible phase speed of the topographic waves. Wave radiation must become important at large times. The large time behaviour is investigated by contour dynamics in the following subsection.

5.3.2 Contour dynamics results

There are two considerations made in the contour dynamics investigations for the intense vortex patch. First, the accuracy of the leading order solution in describing the vortex trajectory is considered. Second, changes in the vortex shape due to topographic wave radiation is of interest.

Figure (5.21) shows the trajectory of an anticyclone, with $a = 1$, $L = 1.2$ and for $S = 0.05$, 0.1 and 0.2. The displacement of the vortex centroid divided by S is plotted to enable comparison with the analytic prediction. The analytic prediction, shown by the solid line is calculated by fourth order Runge-Kutta and numerical integration of (5.62a,b). As S is decreased it is evident that the centroid trajectories obtained by contour dynamics approach the theoretical prediction. Note that the contour dynamics trajectories are displaced further to the west than the theory predict, and this feature is enhanced as S is increased. This is to be expected, since an anticyclone moves southward, i.e. towards the escarpment, and, since the westward drift increases exponentially as $|L|$ decreases. This feature is not captured by the theory, where $|L|$ is assumed to be constant for $t < O(S^{-1})$. Figure (5.22) shows a similar plot for the trajectory of a cyclone produced by contour dynamics simulations. In this case the numerical calculations produce centroid trajectories which are less displaced in the y-direction than the theory predicts. Again, this is expected since cyclones move away from the escarpment, in turn implying that the magnitude of the along-escarpment velocity decreases. Finally, note in both the cases of an anticyclone and a cyclone, the trajectory for $S = 0.05$ has a slight 'bump' in comparison with the analytic trajectory. This is likely to be due to the assumption that the vortex remains circular.

The evolution of the contours for $S = 0.1$ are shown in Figures (5.23) and (5.24) for the case of an
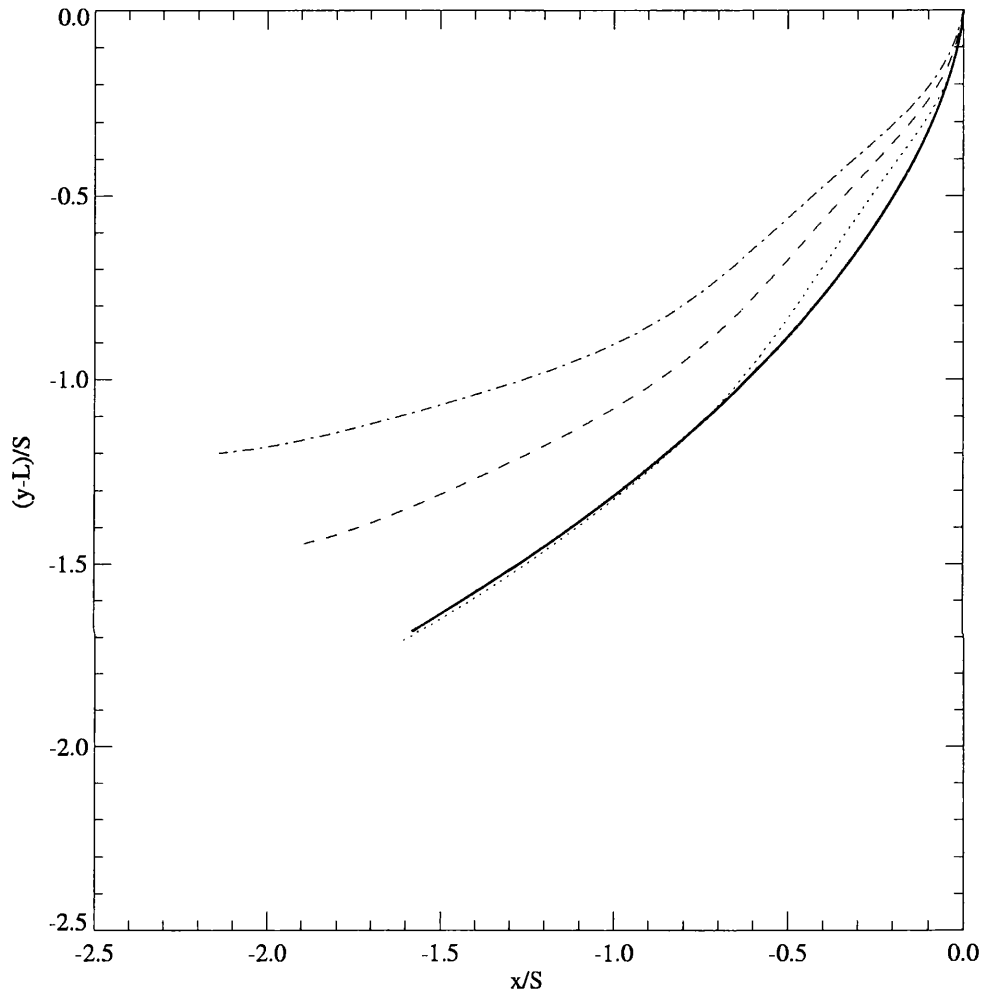
Figure 5.21: The trajectory of the vortex centroid for various values of S, for $0 < t < 30$. The parameter values used are $a = 1$, $L = 1.2$ and $\alpha = 1$, i.e. anticyclones. The analytical prediction (5.62a,b) is shown by the solid line and the contour dynamics results by the dotted line ($S = 0.01$), dashed line ($S = 0.1$) and dot-dashed line ($S = 0.2$).
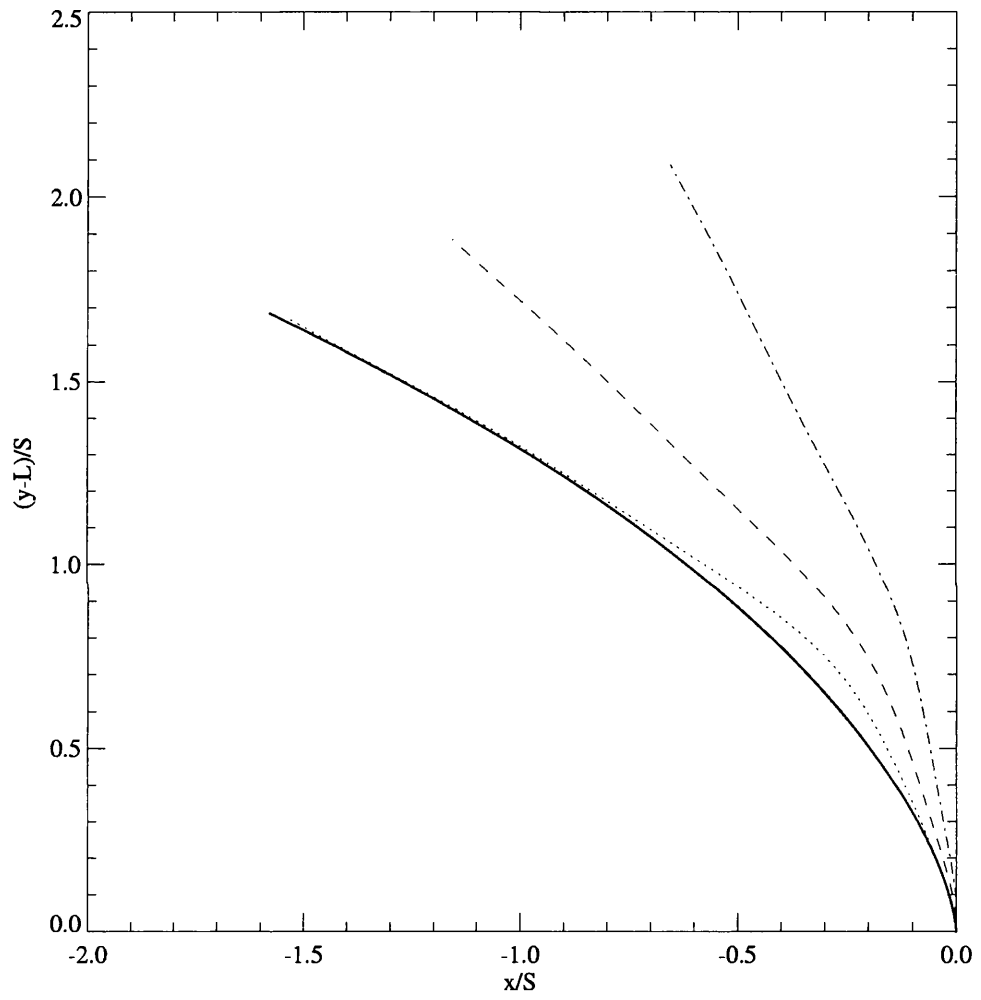
Figure 5.22: As Figure (5.21) except here $\alpha = -1$, i.e. cyclones.

anticyclone and a cyclone respectively. Note that the vortex shape remains approximately circular, even up to time $t = 180$. The slight deviation of the patch from circular accounts for the error in the prediction of the vortex trajectory. Importantly the vortex remains an isolated coherent structure, and there is little evidence that wave radiation distorts the vortex even on long time scales.

The flow for the intense vortex patch is characterised by a strong axisymmetrisation of the flow near the vortex. In the language of Lam and Dritschel (1998) this tendency defines a "trapped region", which accompanies the vortex in its evolution. Also note, at large times there is a "trailing eddy" in the wake of the vortex. For the cyclone this eddy consists of fluid which has crossed the escarpment from the deep to the shallow side, and thus consists of anticyclonic relative vorticity. Similarly, the trailing eddy in the case of the anticyclone consists of fluid with cyclonic relative vorticity.

Figure (5.25) shows the trajectories of a cyclone and an anticyclone with equal magnitudes, for $S = 0.1$ (solid lines), 0.2 (dotted lines), and for $0 < t < 180$. First note that the anticyclones experience further zonal drift than the cyclones. This is simply a consequence of them being closer to the topography and thus more susceptible to the effects of relative vorticity generation as fluid columns cross the escarpment. Second, both cyclones and anticyclones experience enhanced meridional drift as S increases.

Figures (5.26) and (5.27) show the contour evolution for $S = 0.2$ for an anticyclone and a cyclone respectively. At this parameter value, there is a marked difference between the behaviour of vortices of different signs. In the case of an anticyclone there is still strong wrapping of the topographic contour. The vortex drifts toward the escarpment, and at large times dipole formations is evident. In contrast, the cyclone doesn't wrap the topographic contour so strongly, and the dipole formation is apparent at earlier times. The vortex drifts away from the escarpment, accounting for the weaker interaction of the vortex with the topographic contour.

5.3.3 Discussion

It has been shown that for times up to $t = 30$ the analytic results for the drift of an intense vortex patch near an escarpment predict very well the drift produced by contour dynamics experiments. This agreement improves as $S \to 0$. The large time results produced by contour dynamics simulations reveal two important facts. The first is that the intense vortex patch remains approximately circular
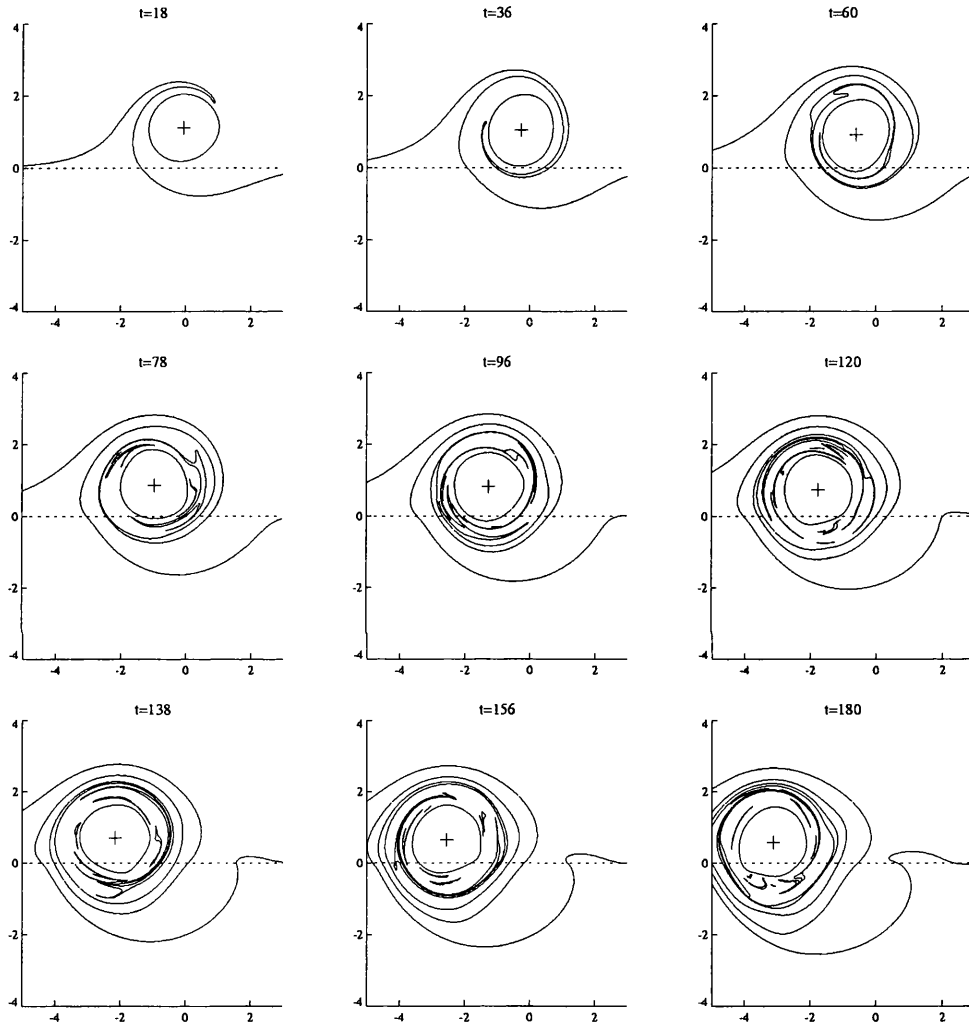
Figure 5.23: The contour evolution for an intense anticyclone ($\alpha = 1$). The parameter values used are $a = 1$, $L = 1.2$ and $S = 0.1$.
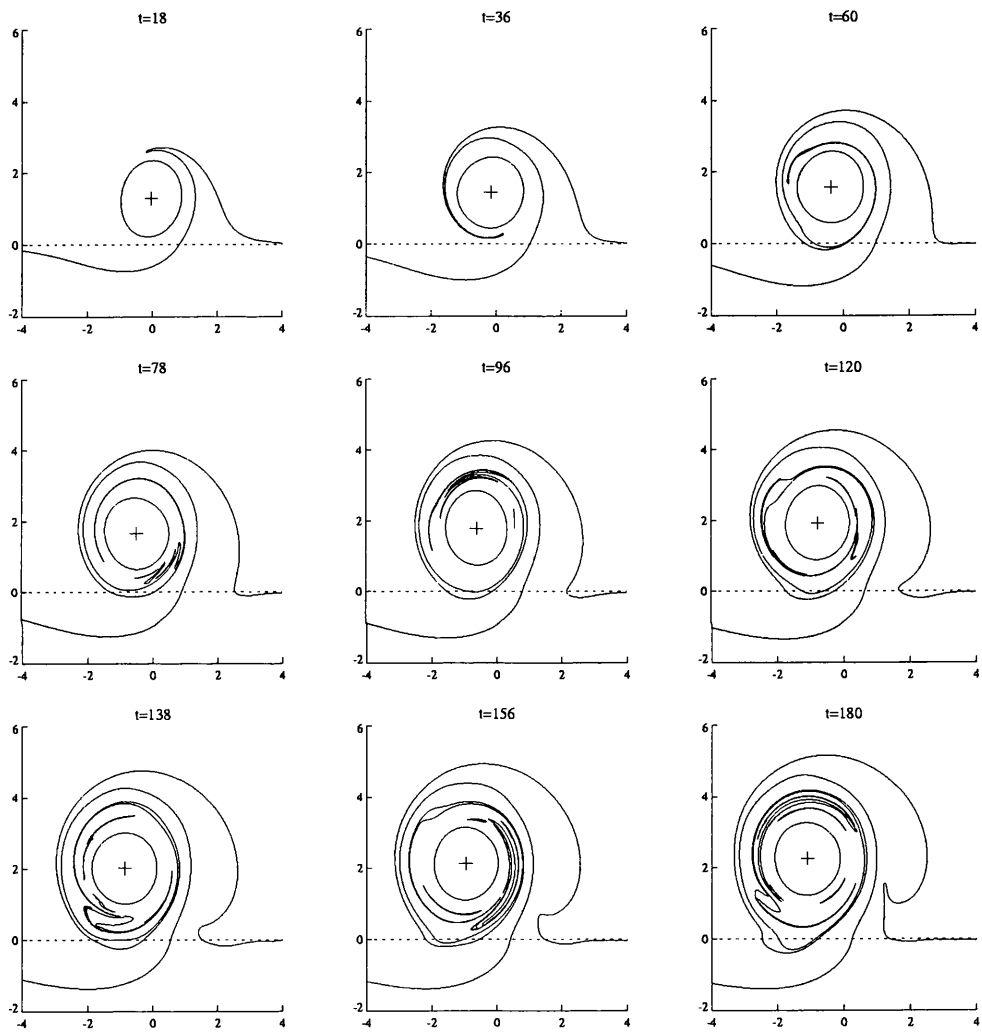
Figure 5.24: As Figure (5.23), except $\alpha = -1$, i.e. a cyclone.
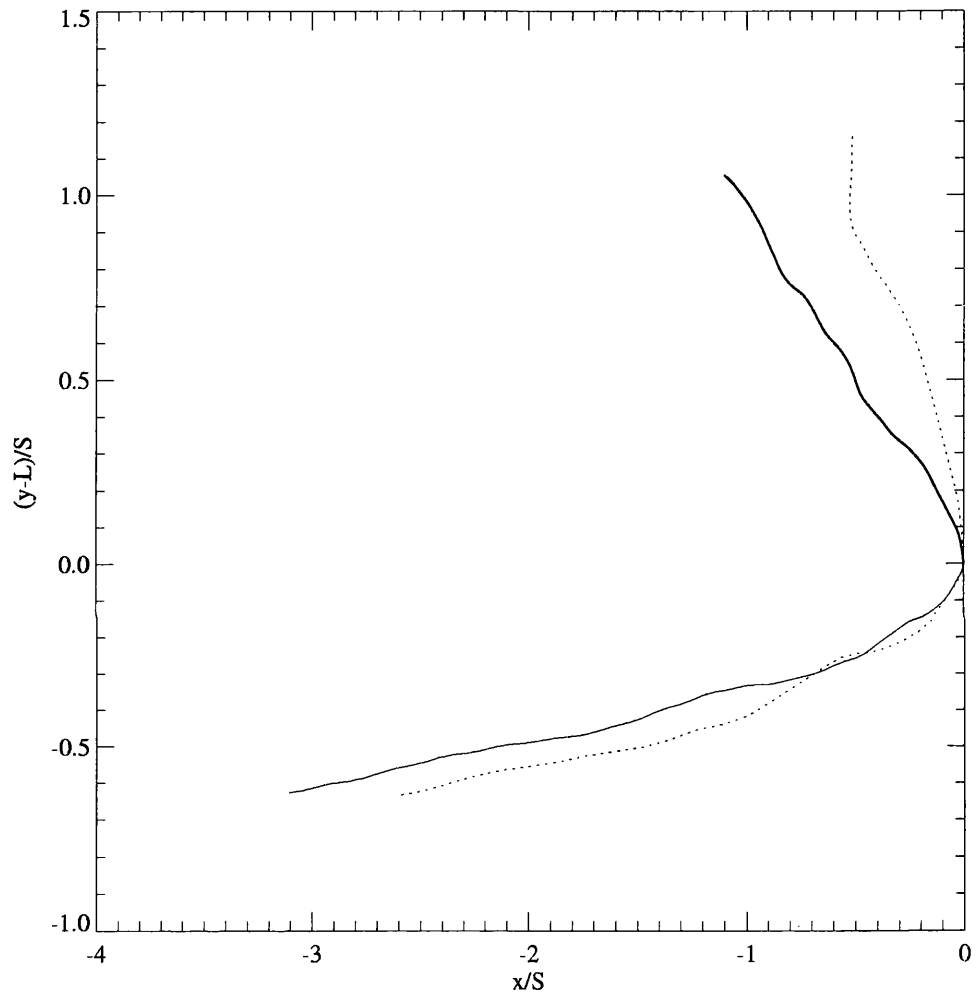
Figure 5.25: Contour dynamics trajectories for $0 < t < 180$. The parameter values used are $a = 1$, $L = 1.2$ and 0.2 (dotted line) and $S = 0.1$ (solid line). The cyclones are northwest moving and the anticyclones are southwest moving.
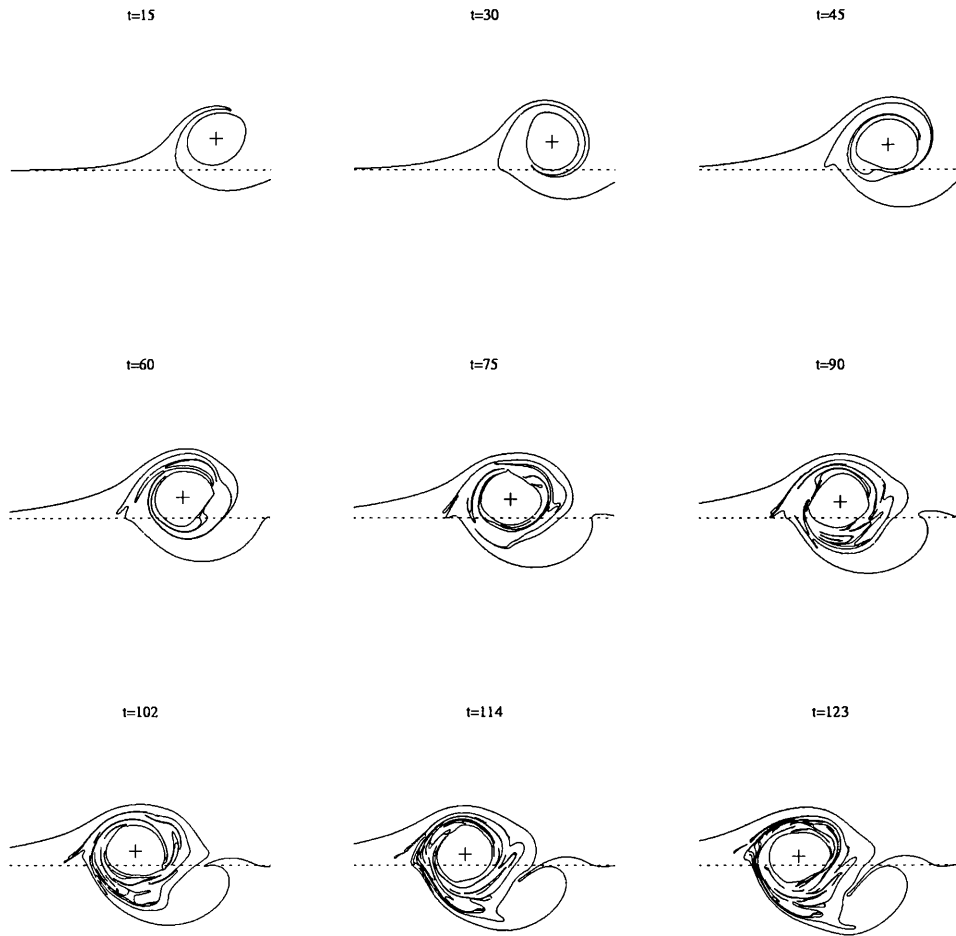
Figure 5.26: The contour evolution for a near-intense anticyclone ($\alpha = 1$). The parameter values used are $a = 1$, $L = 1.2$ and $S = 0.2$. The plots shown axis scaling $-8 < x < 2$ and $-5 < y < 5$.
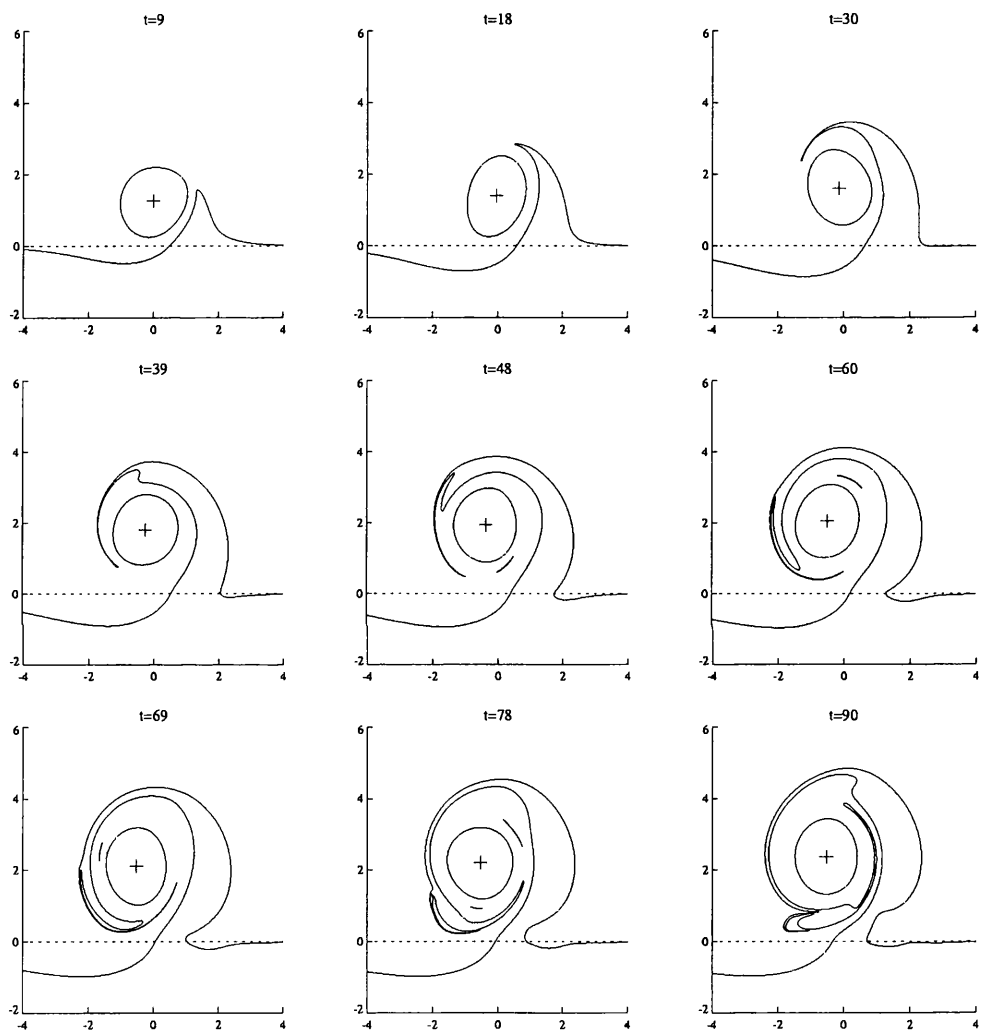
Figure 5.27: As Figure (5.26), except $\alpha = -1$, i.e. a cyclone.

for many eddy turnover times. The second is that the meridional drift of the intense vortices increases with S. These two statements hold for both intense cyclones and intense anticyclones.

Why does the vortex remain circular for the large times in the contour dynamics runs presented here? For short times azimuthal mode-1 dominates the flow, and it was shown in the theory that this mode has no leading order effect on the vortex shape. However, it is expected that, at large times, the distortion of the vortex might be significant due to the interaction of higher order normal modes and/or topographic wave radiation. The reason that this does not occur is the existence of the "trapped zone" around the vortex periphery. In the present case a small trapped zone exists from the outset of the motion, and is described by the theory. Specifically, equation (5.53) indicates that, to leading order, there is no production of relative vorticity in the annulus of radius $|L|$ around the periphery of the vortex. This feature is apparent in the contour dynamics plots for the intense vortex patches, where the topographic contour is isolated from the vortex periphery. In the region $r < |L|$ the strong axisymmetric swirl of the vortex dominates the motion.

However, it is evident from Figures (5.23) and (5.24) that the trapped zone is *larger* than $|L|$ at large times. This feature can also be predicted from the theory. Consider equation (5.48d), which can be rewritten as

$$\frac{\partial q_2}{\partial t} + b(r)\frac{\partial q_2}{\partial \theta} = F(r, t) + G^{(s)}(r, t)\sin 2\theta + G^{(c)}(r, t)\cos 2\theta, \tag{5.68}$$

where F and $G^{(\nu)}$ depend on $\phi_1^{(\nu)}$, u_1 and v_1, and contain δ-functions from the second Jacobian term in (5.23). Specifically, the second order vorticity correction consists of an axisymmetric component and a quadrupole component. In the study of Reznik and Grimshaw (1998), it was found that the axisymmetric part of the second order vorticity correction for an intense vortex patch on the β-plane fills a growing region near the vortex centre, whilst the quadrupole component decays with time. This results in a region of axisymmetric flow, the size of which grows in time near the vortex centre, and the differential rotation, due to relative vorticity production, in the growing annulus around the vortex, serves to preserve the circular shape of the vortex. The trapped region for the β-plane vortices has been well-described by Lam and Dritschel (1998). In the present case the contour dynamics simulations indicate that a trapped zone develops in the region $r < r_{div}$ say, where $r_{div} > |L|$. Figure (5.20) offers evidence that the trapped zone grows with time, with the further effect of shielding the primary vortex from radiated topographic waves.

In addition to the trapped zone, the contour dynamics simulations show the existence of a "trailing

eddy", which is of opposite sign to the primary vortex. The trailing eddy is in fact a part of the radiated topographic wave train. The strength of the trailing eddy increases with S, and enhances meridional motion in the primary vortex. For small values of S the trailing eddy is very weak, and is shielded from the vortex by the trapped zone. As S increases, the strength of the trailing eddy increases, and the size of the trapped zone appears to decrease. Hence weaker vortices experience greater meridional displacements. Distortion of the vortex shape is also greater for larger S, since the trapped zone is less able to shield the primary vortex from the trailing eddy.

The final point to make in this discussion regards the ability of the singular vortex to describe well the trajectory of the vortex centre. This is a simple consequence of the Bessel function structure of the vortex patch, and the assumption made throughout that $a < |L|$. The swirl velocity of the vortex patch at the escarpment is then proportional to $K_1(r)/r$, i.e. is the same as for a singular vortex. Moreover there is no relative vorticity production inside the annulus $r < |L|$, and the circular structure of the vortex swirl velocity is preserved inside this annulus. In short, in the region $r > |L|$, the flow "sees" the vortex patch as a singular vortex. Although it was not made explicit in McDonald (1998), it is the case that for the intense singular vortex there is also no relative vorticty production inside $r < |L|$. Hence, as far as the topographic contour is concerned, the vortex patch, so long as it remains circular, may as well be a singular vortex.

5.4 Contour dynamics investigations for $S \approx 1$

To complete the investigation of the evolution of a vortex patch near an escarpment, this section considers contour dynamics results for the case $S \approx 1$, i.e. a moderate intensity vortex. For brevity results are presented for three particular parameter values: $S = 2$ (a moderately weak vortex), $S = 1$ (a moderate vortex) and $S = 0.5$ (a moderately intense vortex). As for the weak and intense limits described above the discussion is further limited to vortices located on the shallow side of the escarpment; the analogous results for vortices situated on the deep side of the escarpment may be obtained via the transformation (5.40).

There are three main questions under consideration. First, are there any qualitative general statements that can be made regarding the vortex evolution? In particular, the long time drift of the vortex is investigated. Second, what physical mechanisms govern the processes of the vortex evolu-

tion? Third, under what conditions does a singular vortex representation describe the evolution of the vortex patch?

5.4.1 Anticyclones

Figure (5.28) shows the trajectories of the centroid for the moderate anticyclones. The moderately weak ($S = 2$) anticyclone undergoes predominantly zonal motion, but the escarpment-ward drift is greater than that seen for the weak anticyclones. The moderate ($S = 1$) anticyclone undergoes the greatest meridional drift, crosses the escarpment and begins to turn east at later times. The moderately strong ($S = 0.5$) anticyclone follows a generally southwestward trajectory, similar to an intense anticyclone.

Figures (5.29), (5.30) and (5.31) show the contour evolution for the cases $S = 2$, 1 and 0.5 respectively. At early times the moderately weak anticyclone appears to move in the sense of its pseudoimage. However, the radiated topographic waves begin to cause the patch to filament. By $t = 36$ a substantial part of the vortex has been entrained into the topographic waves, and patch distortion is significant. The vortex also drifts towards the escarpment, and at later times it is destroyed by topographic wave radiation.

This behaviour is also demonstrated by the moderate ($S = 1$) anticyclone, but happens from the outset of the motion. The vortex is rapidly distorted and the trailing cyclonic relative voticity induces significant meridional drift of the vortex. By $t = 54$ the vortex has ceased to exist as a coherent structure, and has merged with the topographic contour.

The moderately strong anticyclone is less susceptible to wave radiation. The trailing cyclonic eddy causes escarpment-ward drift of the vortex, but the vortex remains a relatively coherent structure. At later times a dipole has formed, and this dipole continues the general southwest migration.

5.4.2 Cyclones

Figure (5.32) shows the trajectories of the centroid for the moderate cyclones. In all cases a northeast drift is observed. For the moderately strong cyclone ($S = 0.5$) the trajectory of the centroid begins to loop. As in the case of a moderately intense singular cyclonic vortex this looping motion is
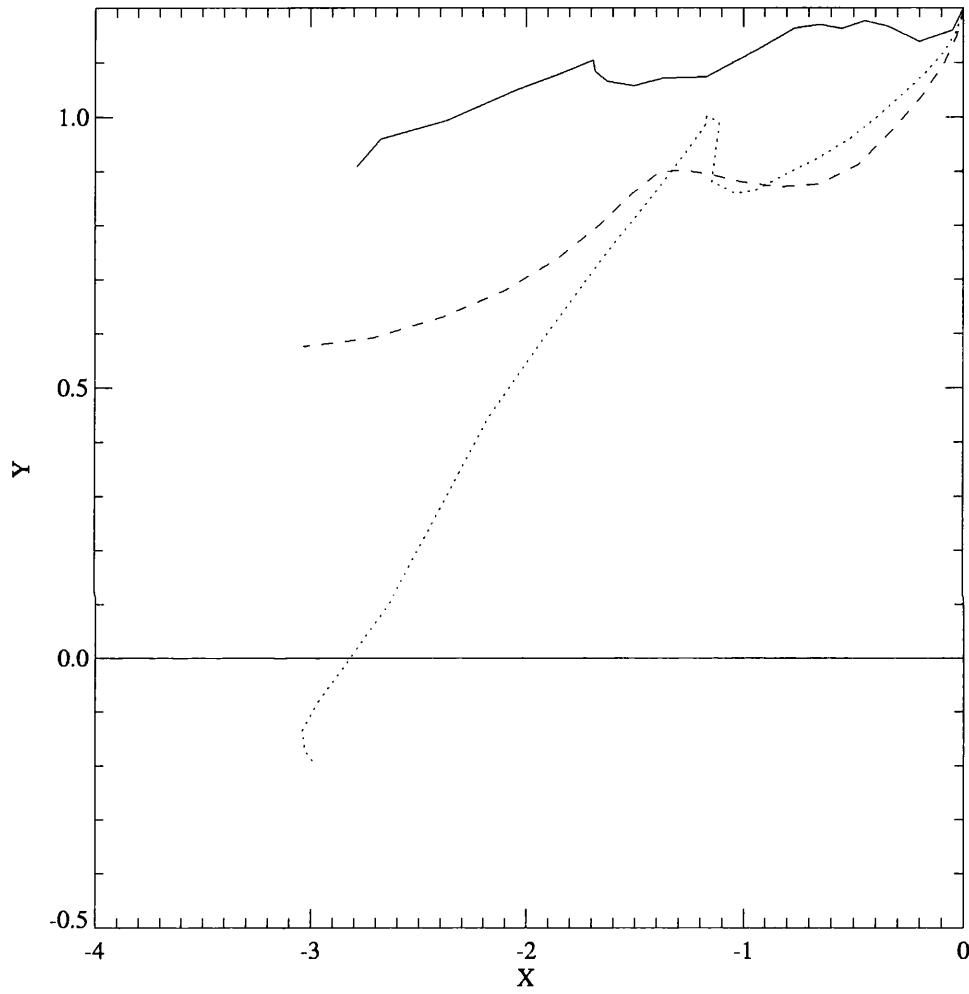
Figure 5.28: The trajectories of the moderate anticyclones for $0 < t < 60$. the parameter values used are $a = 1$, $L = 1.2$ and $S = 2$ (solid line), $S = 1$ (dotted line) and $S = 0.5$ (dashed line).
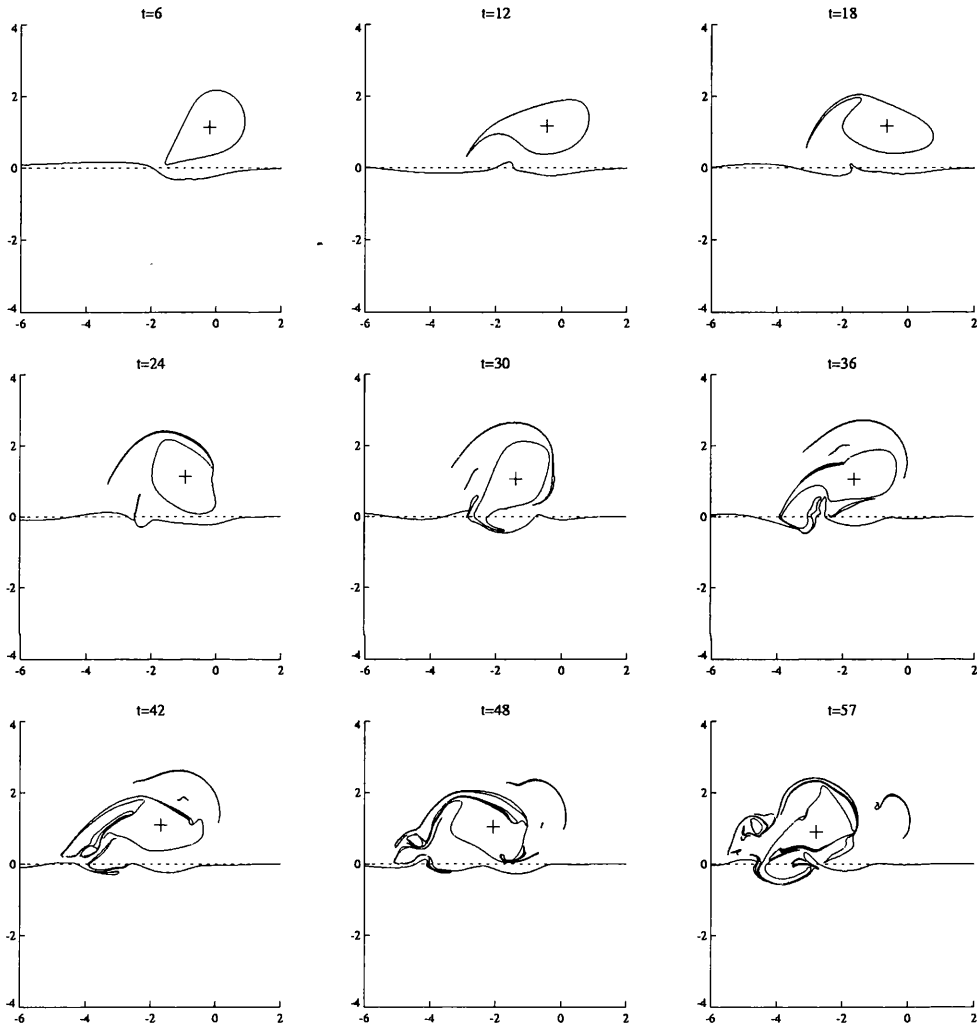
Figure 5.29: The contour evolution for a moderately weak anticyclone ($\alpha = 1$). The parameter values used are $a = 1$, $L = 1.2$ and $S = 2$.
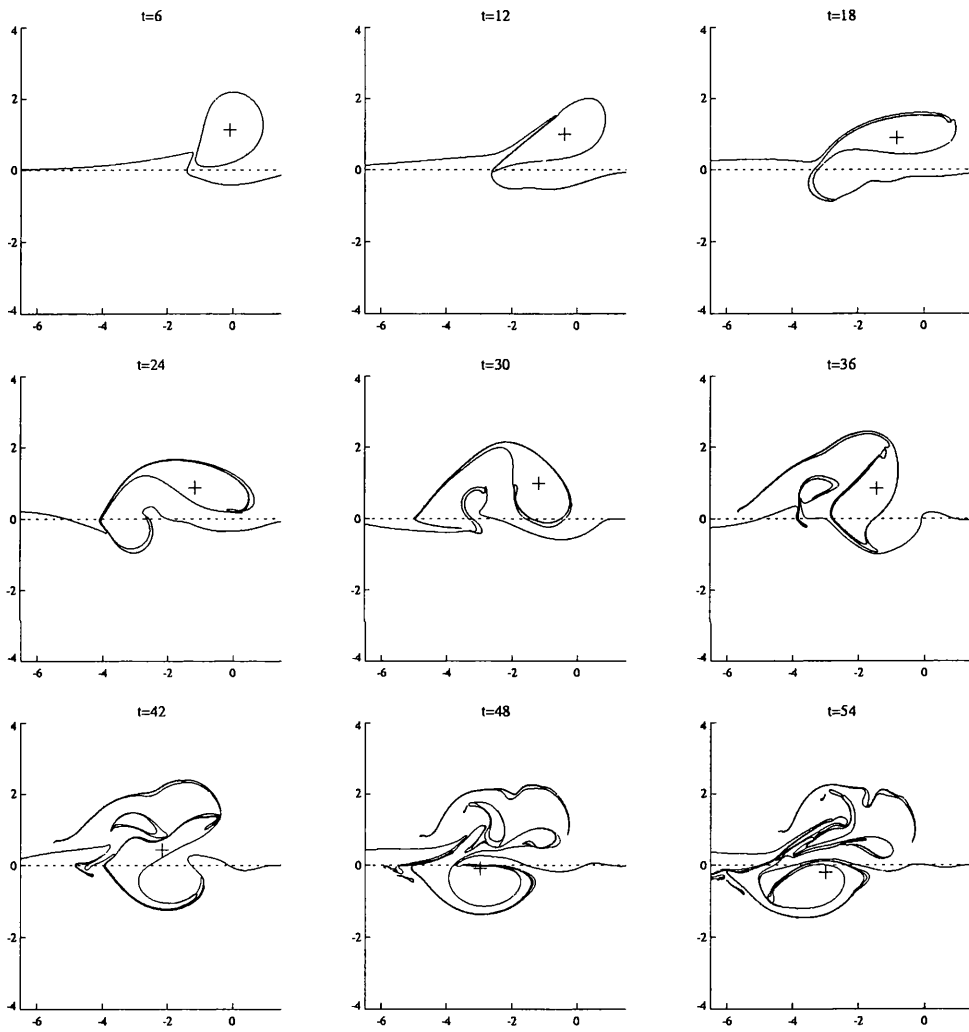
Figure 5.30: As Figure (5.29) except $S = 1$, a moderate anticyclone.

148
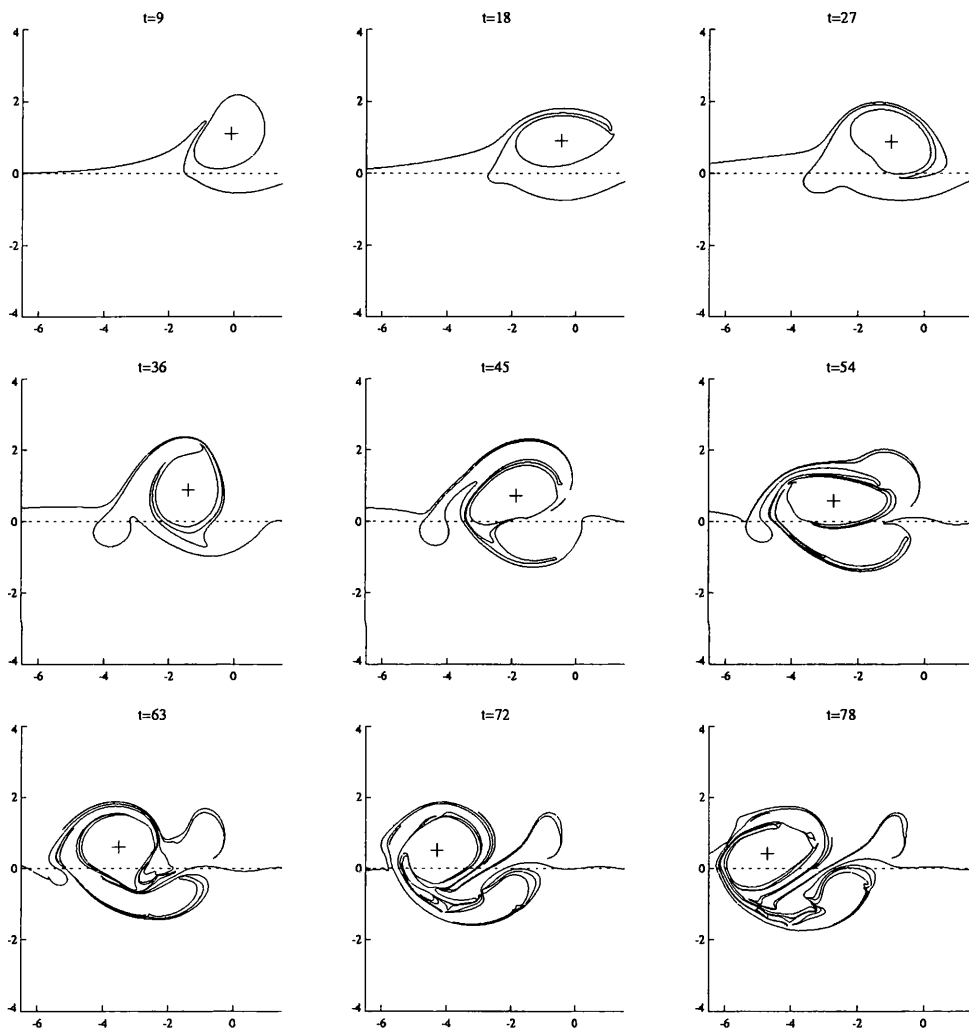
Figure 5.31: As Figure (5.29) except $S = 0.5$, a moderately intense anticyclone.

characteristic of a dipole with different magnitude circulations in its constituent cells.

Figures (5.33), (5.34) and (5.35) show the contour evolution for the cases $S = 2$, 1 and 0.5 respectively. In all cases the motion is characterised by the formation of a dipole as the primary cyclonic vortex becomes associated with the patches of anticyclonic relative vorticity, produced due to fluid columns crossing the escarpment from the deep to the shallow side.

Finally, consider Figure (5.36) which shows a comparison of the trajectories of the vortex patch centre with that of a singular vortex. The singular vortex plots were obtained using a singular vortex of strength $\Gamma = 2\pi\alpha a I_1(a)$ initially located at $(0, L)$. In each case shown $a = 1$, $L = 1.2$ and $S = 1$. Note that for both (a) anticyclones and (b) cyclones the singular vortex trajectory only predicts the vortex patch trajectory for very short times. At large times the singular vortex approximation fails to predict the vortex patch motion. The distortion of the vortex patch boundary contributes to the drift velocity of the vortex, and it is this essential feature which the singular vortex approximation fails to capture.

5.4.3 Discussion

In the case of the anticyclones wave radiation is important. The moderate and moderately weak anticyclones decay as a result of being torn apart by the radiated topographic waves. This feature is, of course, not captured by the singular vortex model of Chapter 4. For the moderately strong anticyclone however, the dipole formation that was characteristic of the moderate intensity singular anticyclones is observed. The moderately strong anticyclone moves southwest, and at large times crosses to the deep side of the escarpment.

In contrast, the moderate cyclones exhibit precisely the same features as the moderate singular cyclones. The primary vortex remains a coherent structure, and is steered away from the escarpment as a result of dipole formation. The dipole formation seems more robust for cyclones and is a result of the motion away from the escarpment, and hence away from the influence of the topography.

The moderate vortex patch undergoes greater meridional drift than either the weak or intense vortices. A similar conclusion for moderate intensity β-plane vortices was reached by Lam and Dritschel (1998). There is however an important exception. The moderate vortex near an escarpment
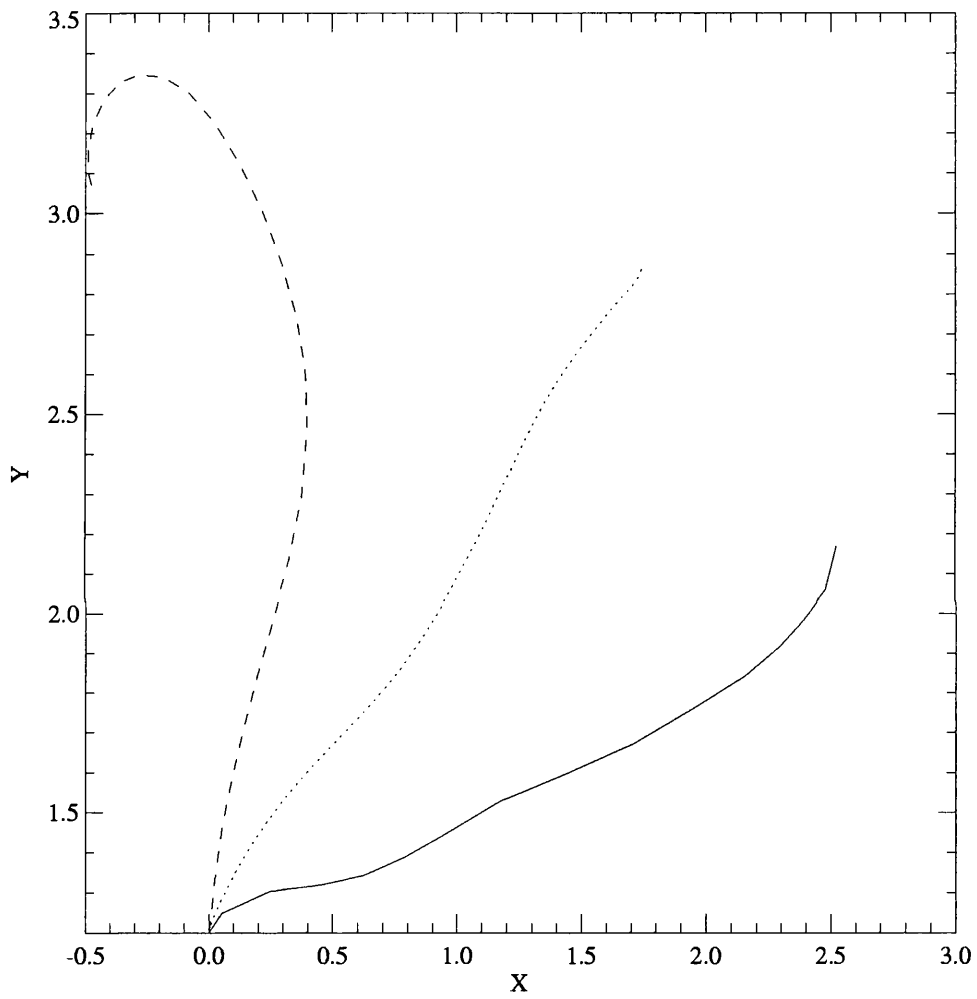
Figure 5.32: The trajectories of the moderate cyclones for $0 < t < 60$. the parameter values used are $a = 1$, $L = 1.2$ and $S = 2$ (solid line), $S = 1$ (dotted line) and $S = 0.5$ (dashed line).
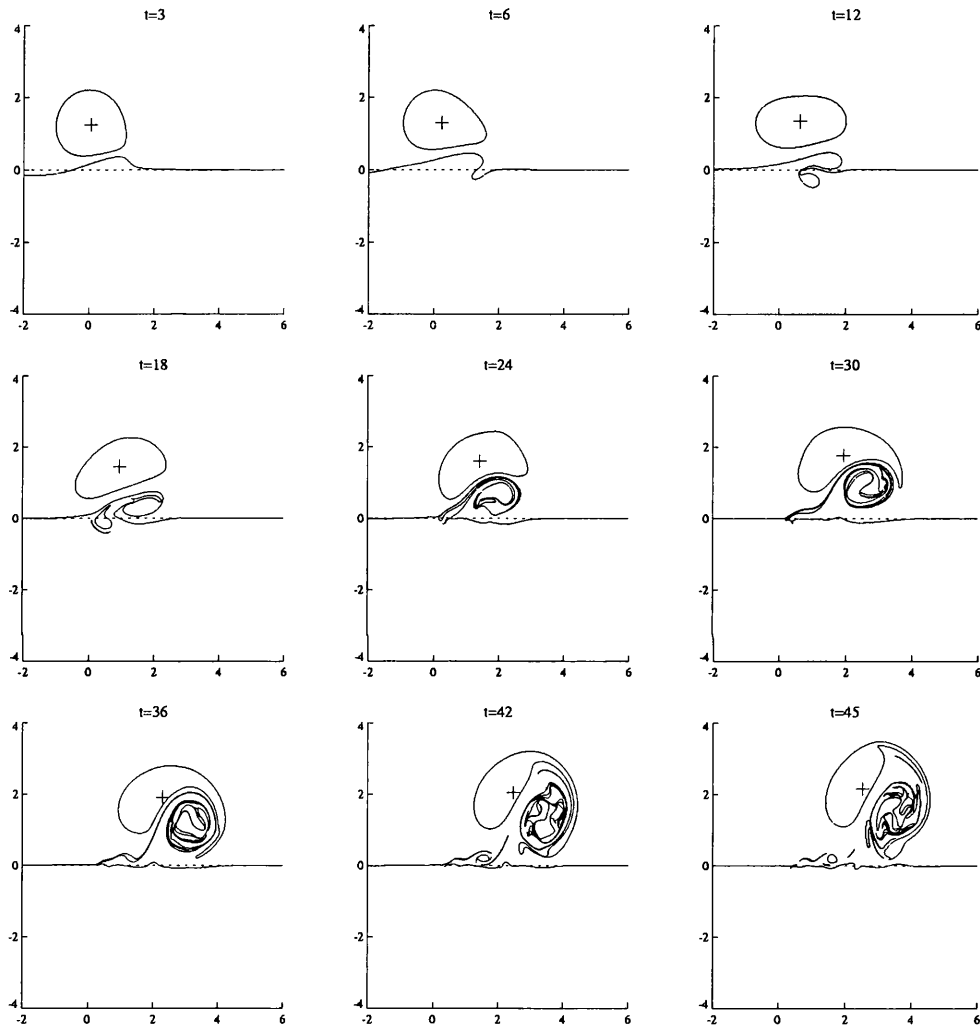
Figure 5.33: The contour evolution for a moderately weak cyclone ($\alpha = 1$). The parameter values used are $a = 1$, $L = 1.2$ and $S = 2$.
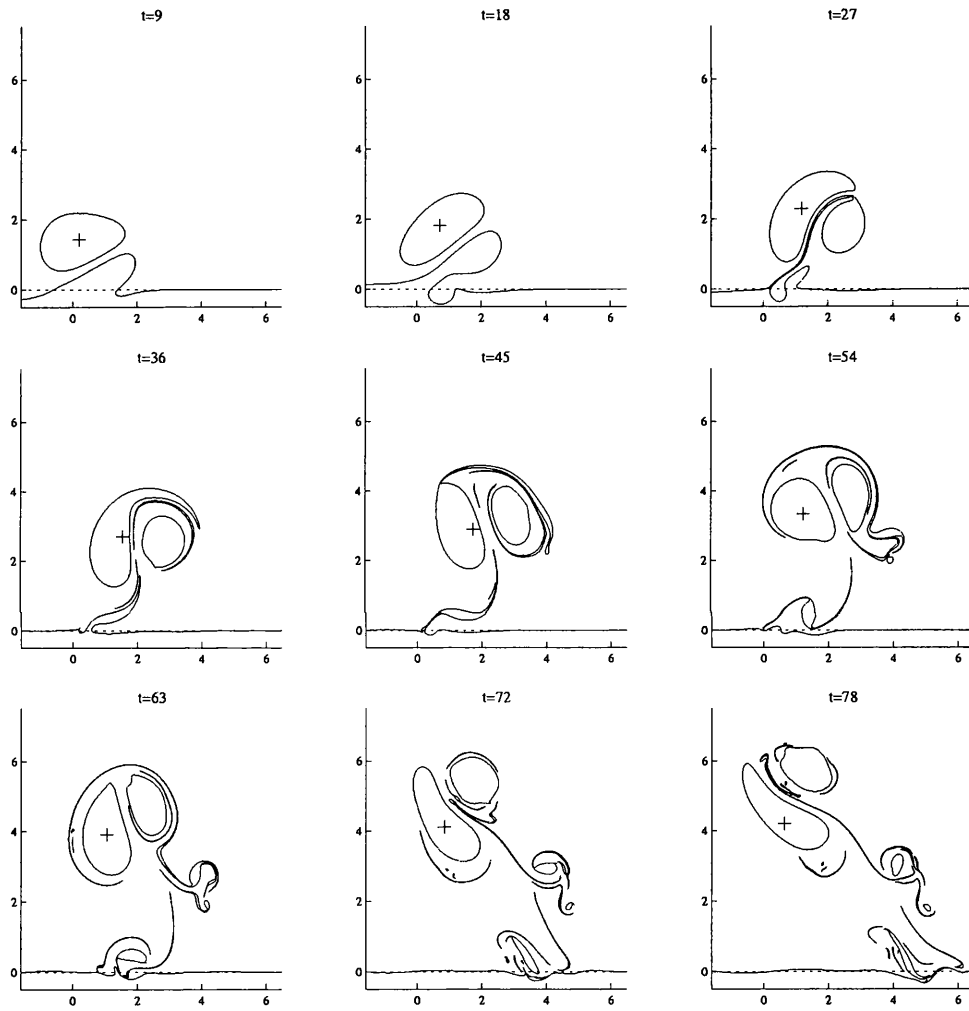
Figure 5.34: As Figure (5.33) except $S = 1$, i.e. a moderate cyclone.

153
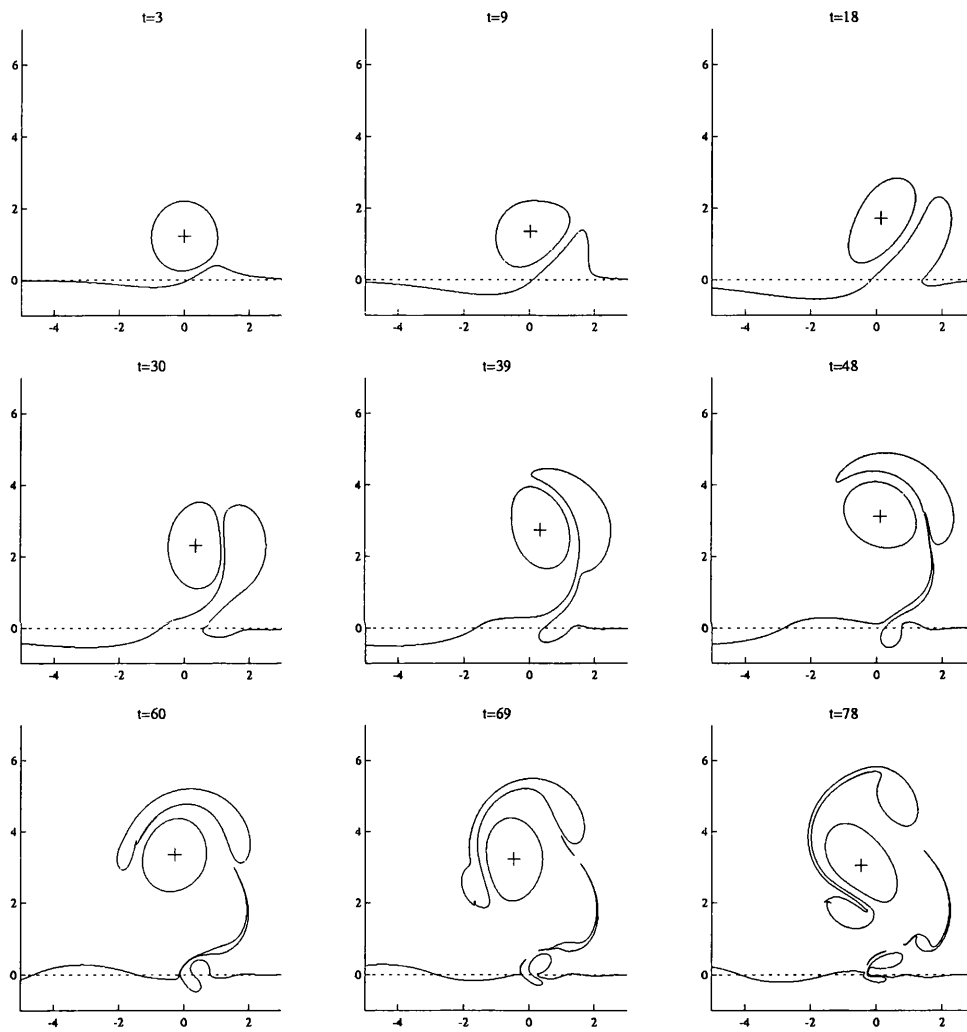
Figure 5.35: As Figure (5.33) except $S = 0.5$, i.e. a moderately strong cyclone.

154
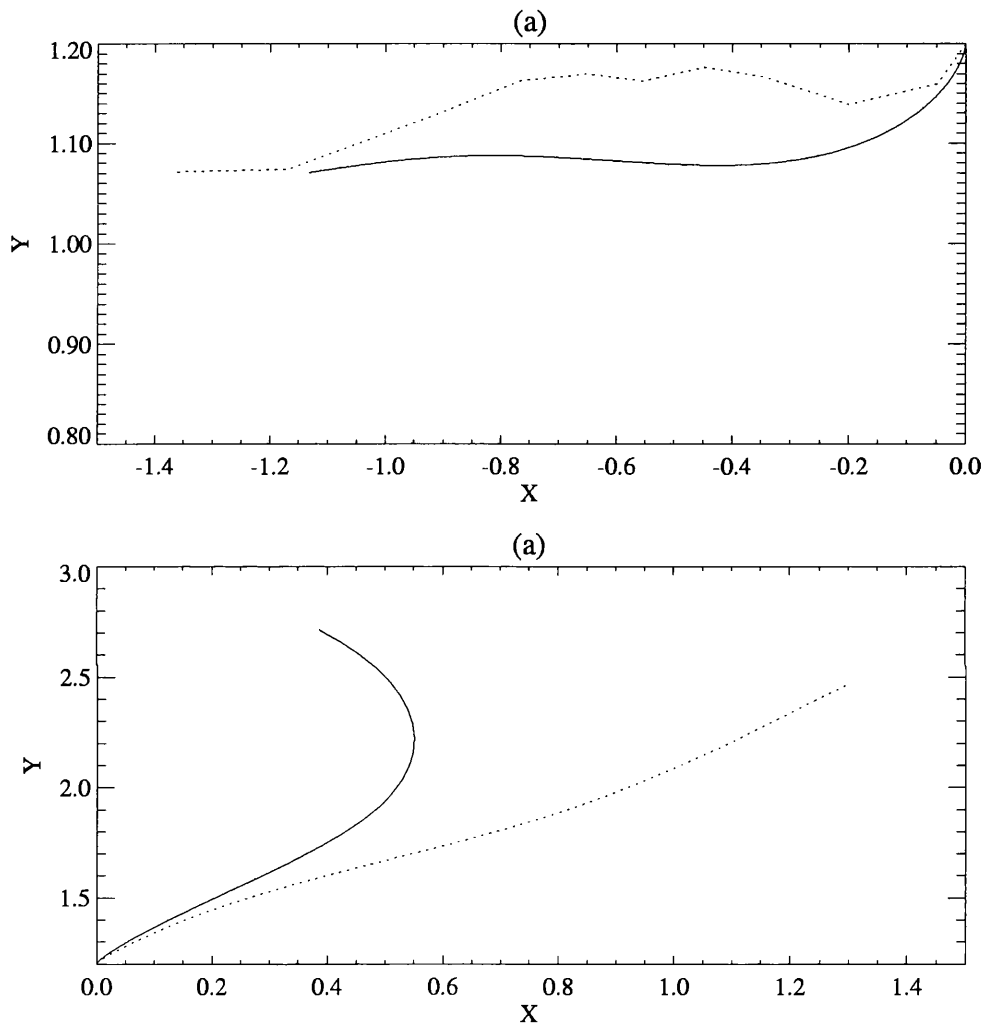
Figure 5.36: Comparison of the trajectory of a vortex patch with that of an equivalent singular vortex. In each case the vortex patch has $a = 1$, $L = 1.2$ and $S = 1$. (a) shows the drift of an anticyclone and (b) shows the drift of a cyclone. The singular vortex approximation was made using a singular vortex of strength $\Gamma = 2\pi a I_1(a)$ initially located at $(0, L)$.

155

doesn't have an associated trapped zone, except for, arguably, the moderately strong cyclone. This is due to the vortex being a finite distance from the topography, and thus being unable to wrap up the contour efficiently. Instead the trailing eddy dominates the motion and causes the enhanced meridional motion.

5.5 Conclusions

A study of the motion of a vortex patch near an escarpment has been studied for the full range of values of the vortex intensity, S. The leading order solution for the weak and intense limits was obtained. In both cases the singular vortex model accurately predicts the trajectory of the vortex centre.

The weak vortex solution was found on the topographic wave timescale. For $S \gg 1$ the vortex remains circular to leading order for times $t < O(S^{-1})$, and it is for this reason that the singular vortex model accurately predicts the drift. For longer times contour dynamics results indicate that the escarpment acts like a wall, i.e. the pseudoimage description of Chapter 4 generalises to a uniform vortex patch. It is anticipated that a distributed weak vortex near an escarpment may also be well described by the pseudoimage. At large times east travelling vortices (i.e. anticylones located on the shallow side of the escarpment or cyclones located on the deep side) are stripped as a result of topographic wave radiation. This feature was lacking in the singular vortex model.

The leading order solution on the advective time scale was found for the intense vortex. It was suggested by the theory that the singular vortex model would predict the trajectory of the vortex centre, a result arising from the fact that the vortex remains circular to leading order. Contour dynamics results confirmed this to be the case, and it was found that cyclones (resp. anticyclones) drift northwest (southwest) as a result of the formation of a secondary dipole. The westward drift speed is within the range of possible phase speeds of the topographic waves. However, for small values of S wave radiation appeared to have a negligible effect on either the vortex shape or the meridional velocity.

In contrast the singular vortex approximation fails when $S \approx 1$, since for moderate intensity vortex patches distortion of the patch boundary is important. The motion of the moderate vortices is

characterised by the formation of dipoles. Anticyclones (cyclones) located on the shallow side of the escarpment drift toward (away from) the escarpment as a result of the dipole formation. This is qualitatively the same behaviour observed previously for singular vortices, and reinforces the conclusion reached in Chapter 4. In particular these results are in agreement with those of Zavala Sanson *et al* (1999), who, recall, showed in laboratory and numerical experiments that an anticyclone approaching an escarpment from the shallow side proceeded to cross the escarpment, and a cyclone approaching an escarpment from the shallow side is "back-reflected" as a result of dipole formation. Moreover, the trailing eddy of the β-plane vortex of Lam and Dritschel (1998) is a further example of dipole formation in a vortex-topography interaction. One may speculate that dipole formation as a result of vortex interaction with potential vorticity gradients is a generic feature of geophysical fluid dynamics.

Appendix A: Derivation of the Fourier series coefficients for q_1

In this appendix the $m = 1$ Fourier series coefficients for q_1 in subsection 5.3.1 are derived. First, for times $t < O(S^{-1})$, the meridional drift velocity $v_1 = O(S)$, so that

$$y_c = L + O(S). \tag{5.A1}$$

Hence for $t < O(S^{-1})$, equation (5.47) can be written

$$q_1 = \frac{1}{2} \left[\text{sgn}(\sin(\theta - b(r)t) + L/r) - \text{sgn}(\sin\theta + L/r) \right]. \tag{5.A2}$$

Next note that if $r < |L|$ then $q_1 = 0$. For $r > |L|$ the Fourier series for q_1 is

$$q_1 = a_0 + \sum_{m=1}^{\infty} a_m \cos m\theta + b_m \sin m\theta, \tag{5.A3}$$

The constant term is

$$
\begin{aligned}
a_0 &= \frac{1}{2\pi} \int_{-\pi}^{\pi} q_1(r, \theta, t) d\theta \\
&= \frac{1}{\pi} \int_{-\pi}^{\pi} \text{sgn}(\sin(\theta - bt) + L/r) d\theta - \frac{1}{\pi} \int_{-\pi}^{\pi} \text{sgn}(\sin\theta + L/r) d\theta \\
&= \frac{1}{\pi} \int_{-\pi-bt}^{\pi-bt} \text{sgn}(\sin\theta + L/r) d\theta - \frac{1}{\pi} \int_{-\pi}^{\pi} \text{sgn}(\sin\theta + L/r) d\theta \\
&= 0,
\end{aligned}
\tag{5.A4}
$$

since the two integrands are periodic with period 2π, and the integrals are each over an interval of length 2π.

Writing $a_1 = q_1^{(c)}$ and $b_1 = q_1^{(s)}$, the $m = 1$ terms are

$$
\begin{aligned}
q_1^{(s)}(r,t) &= \frac{1}{\pi} \int_{-\pi}^{\pi} q_1 \sin\theta d\theta \\
&= \frac{1}{2\pi} \int_{-\pi}^{\pi} \mathrm{sgn}(\sin(\theta - bt) + L/r) \sin\theta d\theta - \frac{1}{2\pi} \int_{-\pi}^{\pi} \mathrm{sgn}(\sin\theta + L/r) \sin\theta d\theta \\
&= \frac{1}{2\pi} \int_{-\pi-bt}^{\pi-bt} \mathrm{sgn}(\sin\theta + L/r) \sin(\theta + bt) d\theta - \frac{1}{2\pi} \int_{-\pi}^{\pi} \mathrm{sgn}(\sin\theta + L/r) \sin\theta d\theta \\
&= \frac{\cos bt - 1}{2\pi} \int_I \mathrm{sgn}(\sin\theta + L/r) \sin\theta d\theta + \frac{\sin bt}{2\pi} \int_I \mathrm{sgn}(\sin\theta + L/r) \cos\theta d\theta,
\end{aligned}
$$

and similarly

$$
\begin{aligned}
q_1^{(c)}(r,t) &= \frac{1}{\pi} \int_{-\pi}^{\pi} q_1 \cos\theta d\theta \\
&= \frac{\cos bt - 1}{2\pi} \int_I \mathrm{sgn}(\sin\theta + L/r) \cos\theta d\theta - \frac{\sin bt}{2\pi} \int_I \mathrm{sgn}(\sin\theta + L/r) \sin\theta d\theta.
\end{aligned}
$$

where I is an interval of length 2π. To calculate the integrals in these two expressions denote by θ_c the (two) values of θ in the interval I where the sgn function changes sign, i.e. $\sin\theta_c = -L/r$. By dividing the integrals into three intervals according to whether the sgn function is positive or negative it is straightforward to show, for $r > |L|$

$$
\int_I \mathrm{sgn}(\sin\theta + L/r) \sin\theta d\theta = |\cos\theta_c| = \frac{4}{r}\sqrt{r^2 - L^2}, \tag{5.A5}
$$

$$
\int_I \mathrm{sgn}(\sin\theta + L/r) \cos\theta d\theta = 0. \tag{5.A6}
$$

Hence, the leading order behaviour of q_1 is

$$
q_1 = q_1^{(s)} \sin\theta + q_1^{(c)} \cos\theta, \tag{5.A7}
$$

where

$$
q_1^{(s)} = \frac{2}{\pi r}\sqrt{r^2 - L^2}(\cos bt - 1), \tag{5.A8}
$$

$$
q_1^{(c)} = -\frac{2}{\pi r}\sqrt{r^2 - L^2}\sin bt, \tag{5.A9}
$$

for $r > |L|$ and $q_1^{(s)} = q_1^{(c)} = 0$ otherwise.

Appendix B: Asymptotic results for drift velocity components for intense vortex.

(a) Behaviour as $t \to 0$.

For $t \ll 1$ approximate

$$
1 - \cos(bt) \approx -\frac{(bt)^2}{2} = -\frac{\alpha^2 a^2 I_1^2(a)t^2}{2r^2}K_1(r), \tag{5.B1}
$$

so that

$$u \approx -\frac{\alpha^2 a I_1^3(a) t^2}{2\pi} \int_L^\infty \frac{K_1^3(r)}{r^2} \sqrt{r^2 - L^2} dr. \qquad (5.\text{B}2)$$

The integral converges and the integrand is positive definite for $L \le r < \infty$. Hence the integral is a positive constant, say A, which depends on L, i.e.

$$u \approx -\frac{A\alpha^2 a I_1^3(a)}{2\pi} t^2 \qquad (5.\text{B}3)$$

as $t \to 0$. Similarly, approximating

$$\sin(bt) \approx bt = -\frac{\alpha a I_1(a) t}{r} K_1(r), \qquad (5.\text{B}4)$$

for $t \ll 1$, leads to

$$v \approx -\frac{B\alpha I_1^2(a)}{\pi} t, \qquad (5.\text{B}5)$$

as $t \to 0$, where B is a positive constant which depends on L.

(b) Behaviour as $t \to \infty$.

It is useful to approximate the large time behaviour of ϕ_1 in the near field of the vortex, from which the asymptotic drift velocity components can be deduced. Consider $\phi_1^{(s)}$, for $r < |L|$. From (5.58) this may be written

$$\phi_1^{(s)} = -\frac{2}{\pi} I_1(r)[P_1 + P_2 + P_3], \qquad (5.\text{B}6)$$

where

$$P_1 = -\int_L^\infty \sqrt{\rho^2 - L^2} K_1(\rho) d\rho, \qquad (5.\text{B}7)$$

$$P_2 = \int_L^{r_1} \cos bt \sqrt{\rho^2 - L^2} K_1(\rho) d\rho, \qquad (5.\text{B}8)$$

$$P_3 = \int_{r_1}^\infty \cos bt \sqrt{\rho^2 - L^2} K_1(\rho) d\rho \qquad (5.\text{B}9)$$

Here r_1 is large but fixed. First note that

$$P_1 = -\pi \exp(-|L|). \qquad (5.\text{B}10)$$

See e.g. McDonald (1998). Next consider P_2. Write the angular velocity of the vortex

$$b(r) = -\Gamma \frac{K_1(r)}{r}, \qquad (5.\text{B}11)$$

where $\Gamma = \alpha a I_1(a)$. From Abramowitz and Stegun (1972) the derivative of $K_1(r)$ is

$$K_1'(r) = -K_2(r) + \frac{1}{r} K_1(r), \qquad (5.\text{B}12)$$

159

so that

$$b'(r) = \Gamma \frac{K_2(r)}{r}.$$
(5.B13)

Hence $b'(\rho) \neq 0$ on the interval $L < \rho < r_1$. Moreover, $\sqrt{\rho^2 - L^2} K_1(\rho)$ is integrable on this interval. The Riemann-Lebesgue Lemma then implies that

$$P_2 = O(t^{-1}),$$
(5.B14)

as $t \to \infty$. For $r_1 \gg L$ approximate $\sqrt{\rho^2 - L^2} \approx \rho$ and $K_n(\rho) \approx e^{-\rho}/\sqrt{\rho}$ for $n = 1, 2$. Then

$$
\begin{aligned}
P_3 &\approx \int_{r_1}^{\infty} \cos bt\rho K_1(\rho) d\rho \\
&= \frac{1}{\Gamma} \int_{\xi_1}^{0} \cos \xi t \rho^2 \frac{K_1(\rho)}{K_2(\rho)} d\rho \\
&\approx \frac{1}{\Gamma} \int_0^{\xi_1} \cos \xi t \log^2 \xi d\xi,
\end{aligned}
$$

since for large ρ, $\xi \approx e^{-\rho}$. Here $\xi_1 = |\Gamma| K_1(r_1)/r_1$. Making a further change of variable leads to

$$P_3 \approx \frac{1}{\Gamma t} \int_0^{\xi_1 t} \sin z \log^2 \left(\frac{z}{t}\right) dz.$$
(5.B15)

Integration by parts implies that the leading order behaviour of the integral is $O(\log^2 t)$ as $t \to \infty$. That is, for large t

$$P_3 = O\left(\frac{\log^2 t}{t}\right).$$
(5.B16)

Hence it follows that

$$\phi_1^{(s)} = 2I_1(r) \exp(-|L|) + O\left(\frac{\log^2 t}{t}\right),$$
(5.B17)

as $t \to \infty$. A similar treatment for the component $\phi_1^{(c)}$ leads to

$$\phi_1^{(c)} = O\left(\frac{\log^2 t}{t}\right),$$
(5.B18)

as $t \to \infty$. Finally the vortex drift velocity components may be obtained from (5.62a), (5.62b), (5.B17) and (5.B18) and are

$$u_1 \approx -\frac{2I_1(a)}{a} \exp(-|L|) + O\left(\frac{\log^2 t}{t}\right),$$
(5.B19)

$$v_1 \approx O\left(\frac{\log^2 t}{t}\right).$$
(5.B20)

Chapter 6

The motion of a vortex near coastal topography

In this chapter the motion of a singular vortex near coastal topography is investigated. The choice of topography is an infinite escarpment running parallel to a plane wall. The interaction of the vortex with the topography is of primary interest, and the means by which the vortex came to be near the escarpment is ignored. An off shelf vortex could, for example, have been advected towards a western boundary under the β-effect, and a vortex on the shelf could have been formed near a river outlet.

The f-plane quasigeostrophic governing equation, with the same scalings (4.1) as in Chapter 4 is

$$\frac{\partial}{\partial t}(\nabla^2\psi - \psi) + J[\psi, \nabla^2\psi - \psi] + S\frac{\partial\psi}{\partial x}\frac{\partial h_B}{\partial y} = 0. \tag{6.1}$$

Here S is the ratio of the eddy turnover time to the topographic vortex stretching time,

$$S = \frac{L/U}{\delta^{-1}f^{-1}} = \frac{\delta}{Ro} = \frac{T_a}{T_w}. \tag{6.2}$$

The choice of topography is

$$h_B(y) = \text{sgn}(W - y), \tag{6.3}$$

i.e. an infinitely long escarpment aligned along $y = W$. The wall is parallel to the escarpment, and is aligned along $y = 0$, so the shallow side of the escarpment is in the region $0 < y < W$ and the deep side of the escarpment is $y > W$. Figure (6.1) shows the fluid domain, which is an attempt to model the shoaling topography which occurs near continental margins. In the following section the properties of the topographic waves are discussed.

161
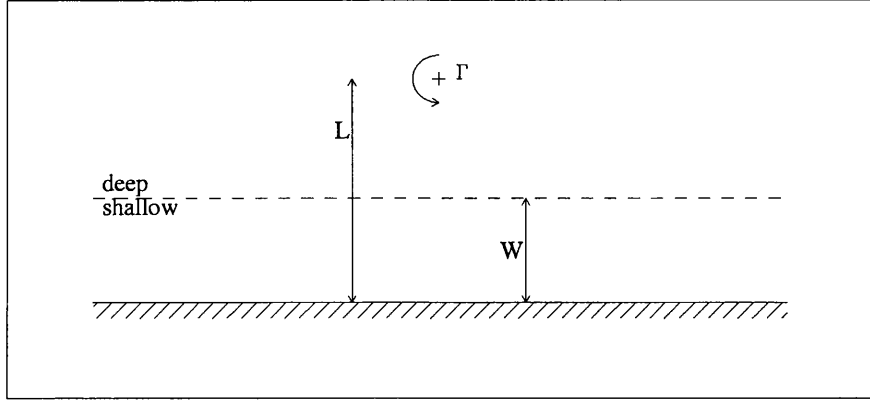
Figure 6.1: The geometry of the domain under consideration. There is an escarpment at $y = W$ parallel to a plane wall aligned along $y = 0$. The vortex is initially located at $(0, L)$.

6.1 Linear waves

For $S \gg 1$, set $\epsilon = S^{-1}$ and introduce the new time variable $\tau = \epsilon t$, so that the unit of time is T_w, the topographic wave time. For $\tau \ll \epsilon^{-1}$, the linearised governing equation is

$$\frac{\partial}{\partial \tau}(\nabla^2 \psi - \psi) + \frac{\partial \psi}{\partial x}\frac{\partial h_B}{\partial y} = 0. \tag{6.4}$$

The boundary conditions are

$$\frac{\partial \psi}{\partial x} = 0 \quad , \quad y = 0 \tag{6.5a}$$

$$\nabla \psi \to 0 \quad , \quad y \to \infty \tag{6.5b}$$

$$[\psi] = 0 \quad , \quad y = W \tag{6.5c}$$

$$[\psi_{yt}] - 2\psi_x = 0 \quad , \quad y = W \tag{6.5d}$$

Condition (6.5a) is the requirement of no normal flow at the wall, (6.5b) is the condition that the fluid is at rest in the far-field, (6.5c) is continuity of ψ across the escarpment and the final condition, (6.5d) is the matching condition found by integrating (6.1) across the escarpment as in the previous chapters. Linear waves have the form

$$\psi(x, y, \tau) = A(y)e^{i(kx - \omega \tau)}, \tag{6.6}$$

Denote the solution in the two parts of the flow by

$$\psi = \begin{cases} \psi_1 = A_1(y)e^{i(kx - \omega t)} & 0 < y < W \\ \\ \psi_2 = A_2(y)e^{i(kx - \omega t)} & y > W, \end{cases} \tag{6.7}$$

162

On the shelf

$$\psi_1 = B \sinh y \sqrt{k^2 + 1} \; e^{i(kx - \omega \tau)}, \tag{6.8}$$

satisfies boundary condition (6.5a), whilst off the shelf,

$$\psi_2 = C e^{-y\sqrt{k^2+1}} \; e^{i(kx - \omega \tau)}, \tag{6.9}$$

satisfies boundary condition (6.5b). Matching condition (6.5c) is satisfied for $\psi_1 = \psi_2$ at $y = W$, i.e. whenever

$$C = \frac{B}{2} \left(e^{2W\sqrt{k^2+1}} - 1 \right). \tag{6.10}$$

The solution is then, ignoring the constant factor,

$$\psi = \begin{cases} \sinh y \sqrt{k^2 + 1} \;\; \cos(kx - \omega \tau) & 0 < y < W \\ \frac{1}{2} \left(e^{2W\sqrt{k^2+1}} - 1 \right) e^{-y\sqrt{k^2+1}} \;\; \cos(kx - \omega \tau) & y > W \end{cases} \tag{6.11}$$

Hence the waves have maximum amplitude over the escarpment. The dispersion relation is obtained from (6.5d) which, after a little work leads to

$$\omega = \frac{k}{\sqrt{k^2 + 1}} \left(1 - e^{-2W\sqrt{k^2+1}} \right) \tag{6.12}$$

Note that

$$\lim_{W \to \infty} \omega = \frac{k}{\sqrt{k^2 + 1}}, \tag{6.13}$$

so that in the limit of the wall being infinitely far from the escarpment the dispersion relation for topographic waves in the absence of the wall is recovered. A further interesting limit is the case $W \ll 1$, for which the leading order frequency of the waves is given by

$$\omega \approx 2kW. \tag{6.14}$$

That is, for the escarpment very close to the wall the waves are, to leading order, non-dispersive. This has some interesting consequences in the weak vortex interaction described below. Plots of dispersion curves for various values of W are shown in Figure (6.2a). If W is greater than about 1, so that the escarpment is more than a Rossby radius from the wall, the dispersion curve is indistinguishable from the limiting case (6.13).

The phase and group velocities are

$$c_p(k) = \frac{\omega}{k} \;\; = \;\; \frac{1}{\sqrt{k^2 + 1}} \left(1 - e^{-2W\sqrt{k^2+1}} \right) \tag{6.15}$$

$$c_g(k) = \frac{\partial w}{\partial k} \;\; = \;\; \frac{1}{(k^2 + 1)^{3/2}} + \frac{e^{-2W\sqrt{k^2+1}}}{(k^2 + 1)^{3/2}} \left(2Wk^2 \sqrt{k^2 + 1} - 1 \right) \tag{6.16}$$
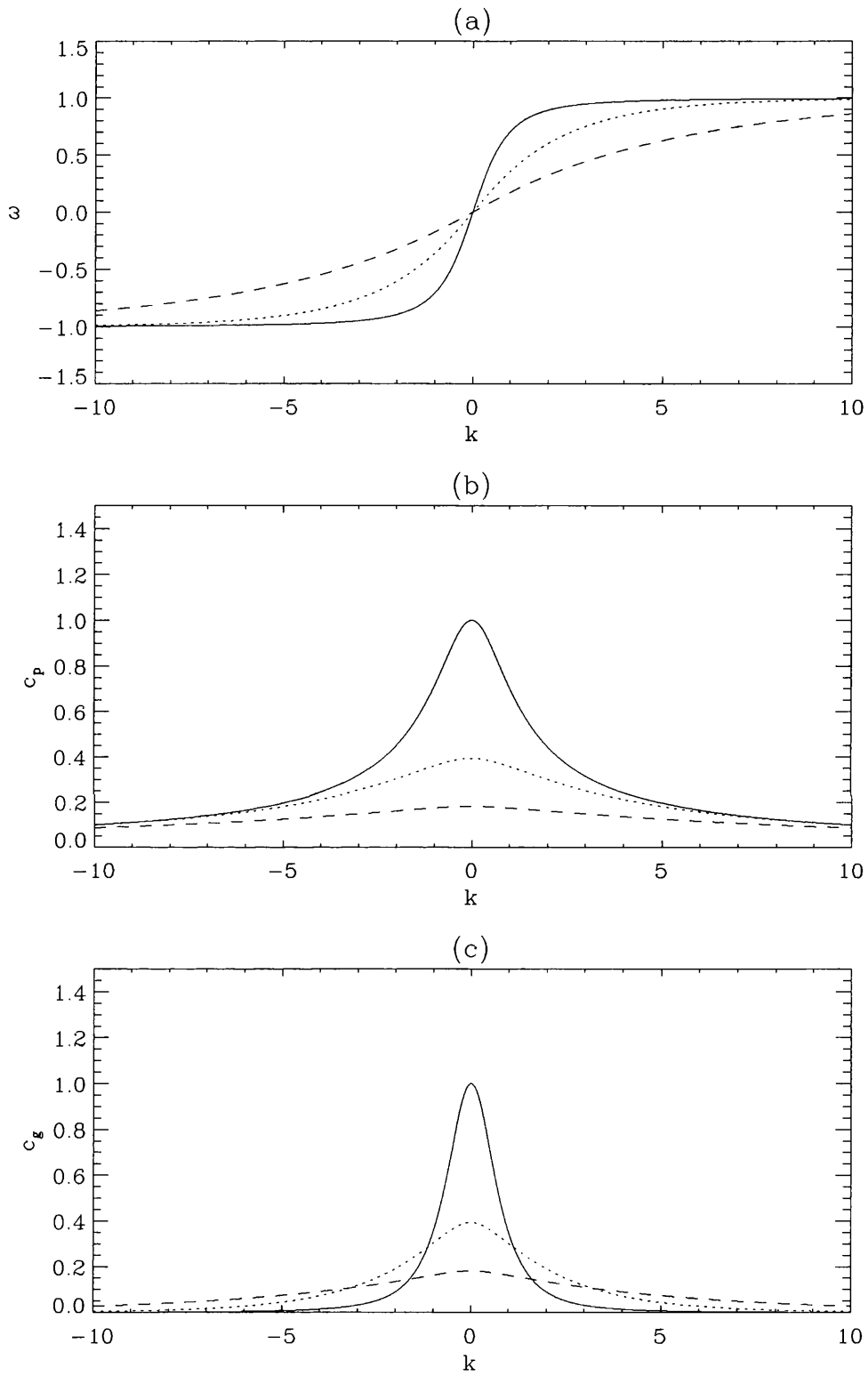
Figure 6.2: The (a) dispersion curve, (b) phase velocity and (c) group velocity for $W = 1/4$ (dotted line), $W = 1/10$ (dashed line) and for $W \to \infty$ (solid line).

The wave phase and energy both propagate toward positive y, i.e. with shallow water to the right. Figures (6.2a,b) show plots of the phase and group velocities. The maximum value of each occurs for $k = 0$, whilst the maximum value itself decreases with W. Moreover,

$$c_p(0) = c_g(0) = 1 - e^{-2W}, \tag{6.17}$$

so in particular the maximum phase and group velocities are near unity for $W \to \infty$, whilst the maximum value is approximately $2W$ for $W \ll 1$.

The presence of the wall modifies the frequency of the topographic waves. For fixed k the frequency ω is a decreasing function of W. In the limit $W \to 0$ the frequency is linear, and $c_p \to c_g$, i.e. the waves are non-dispersive and the wave phase and energy propagate at the same velocity.

6.2 A weak singular vortex

In the absence of topography, the streamfunction for a singular vortex located at a distance L from a wall aligned along $y = 0$ is the sum of the streamfunctions for the vortex and its image in the wall,

$$\Psi = \frac{\Gamma}{2\pi} \left(K_0 \left(((x - X)^2 + (y - Y)^2)^{1/2} \right) - K_0 \left(((x - X)^2 + (y + Y)^2)^{1/2} \right) \right). \tag{6.18}$$

Here $(X(t), Y(t))$ is the position of the vortex centre, and $\Gamma = \pm 1$ gives the sense of the circulation. For $\Gamma < 0$ it is anticlockwise (cyclonic) and for $\Gamma > 0$ it is clockwise (anticyclonic). Suppose at $t = 0$ there is a vortex of the form (6.18) with initial location $(0, L)$. The aim is to determine the subsequent drift of the vortex centre $(X(t), Y(t))$. Seek a solution of the form

$$\psi = \Psi + \phi, \tag{6.19}$$

so that the governing equation is

$$\frac{\partial}{\partial t}(\nabla^2 \phi - \phi) + J[\phi, \nabla^2 \phi] + S \frac{\partial \phi}{\partial x} \frac{\partial h_B}{\partial y} = -S \frac{\partial \Psi}{\partial x} \frac{\partial h_B}{\partial y}. \tag{6.20}$$

In the following subsection the solution on the fast topographic wave time scale is obtained by Fourier analysis.

6.2.1 Leading order solution

The solution on the topographic wave time scale can be found by Fourier transform methods. For a weak vortex, $S \gg 1$, set $\epsilon = S^{-1}$ and rescale the time variable $\tau = \epsilon t$. The governing equation

165

(6.20) is then

$$\frac{\partial}{\partial \tau}(\nabla^2 \phi - \phi) + \epsilon J[\phi, \nabla^2 \phi - \phi] + \frac{\partial \phi}{\partial x}\frac{\partial h_B}{\partial y} = -\frac{\partial \Psi}{\partial x}\frac{\partial h_B}{\partial y}. \tag{6.21}$$

For times $\tau \ll \epsilon^{-1}$ the advection term in (6.21) is negligible, so that, on this time scale, the governing equation is a linear forced topographic wave equation,

$$\frac{\partial}{\partial \tau}(\nabla^2 \phi - \phi) + \frac{\partial \phi}{\partial x}\frac{\partial h_B}{\partial y} = -\frac{\partial \Psi}{\partial x}\frac{\partial h_B}{\partial y}, \tag{6.22}$$

where the fact that $\nabla^2 \Psi - \Psi = 0$ has been used. It will be justified *a posteriori* that the vortex drift in the y-direction is $O(\epsilon^2)$ on this time scale. Denote by u and v the components of the vortex drift velocity in the x and y directions respectively, on the long advective time scale, so that

$$\frac{dX}{d\tau} = \epsilon u, \tag{6.23a}$$

$$\frac{dY}{d\tau} = O(\epsilon^2), \tag{6.23b}$$

The vortex is advected by its image and the ϕ-field, i.e.

$$u = \frac{\Gamma}{2\pi}K_1(2|L|) - \frac{\partial \phi}{\partial y}(X, L, t). \tag{6.24}$$

Note that u can take the full range of values since L is free to vary over the range of values. In particular if $L = O(\epsilon)$ then $u = O(\epsilon^{-1})$, and the vortex drift is order unity on the topographic wave time scale. This has interesting consequences, outlined later, because the possibility arises that the vortex can travel at the velocity of the topographic long waves. Assume further that u is constant[1], so for times $\tau \ll \epsilon^{-1}$

$$X = \epsilon u \tau, \tag{6.25a}$$

$$Y = L. \tag{6.25b}$$

Under the above assumptions the streamfunction for the vortex and image on this time scale is

$$\Psi = -\frac{\Gamma}{2\pi}\left[K_0\left(((x - \epsilon u \tau)^2 + (y - L)^2)^{1/2}\right) - K_0\left(((x - \epsilon u \tau)^2 + (y + L)^2)^{1/2}\right)\right]. \tag{6.26}$$

The topography, given by (6.3) is "switched on" near a pre-existing vortex at $\tau = 0$, so the initial-boundary value problem for $\tau \ll \epsilon^{-1}$ is

$$\nabla^2 \phi - \phi = 0 \quad , \qquad y \neq W, \tag{6.27a}$$

$$\frac{\partial \phi}{\partial x} = 0 \quad , \qquad y = 0, \tag{6.27b}$$

$$\nabla \phi \to 0 \quad , \qquad y \to \infty, \tag{6.27c}$$

---

[1]This is also justified *a posteriori*, since it is found that the leading order prediction of u is constant.

$$[\phi] = 0 \quad , \qquad y = W, \tag{6.27d}$$

$$[\phi_{y\tau}] - 2\phi_x = 2\Psi_x \quad , \qquad y = W, \tag{6.27e}$$

$$\phi(x, y, 0) = 0 \quad , \qquad \tau = 0. \tag{6.27f}$$

Note that in (6.27e) $\partial h_B/\partial y = -2\delta(W - y)$ has been used. The solution is found by Fourier transforms. Denote the Fourier transform by $\hat{\phi}$ as in (4.21). The solution satisfying (6.27a-c) is

$$\hat{\phi} = \begin{cases} A(k, \tau) \sinh y\sqrt{k^2 + 1}, & 0 < y < W, \\ \\ B(k, \tau)e^{y\sqrt{k^2+1}}, & y > W. \end{cases} \tag{6.28}$$

Condition (6.27d) implies $[\hat{\phi}] = 0$ at $y = W$, which in turn gives

$$B = \frac{1}{2}A \left(e^{2W\sqrt{k^2+1}} - 1 \right). \tag{6.29}$$

Condition (6.27e) transforms to the ordinary differential equation for A,

$$A_\tau + i\omega A = -\frac{2ik}{\sqrt{k^2 + 1}}e^{-W\sqrt{k^2+1}}\left.\hat{\Psi}\right|_{y=W}, \tag{6.30}$$

where ω is the topographic wave frequency given by (6.12). Now

$$\left.\hat{\Psi}\right|_{y=W} = \frac{\Gamma}{2\sqrt{k^2 + 1}}\tilde{\Psi}e^{-ik\epsilon u\tau}, \tag{6.31}$$

where,

$$\tilde{\Psi} = \left(e^{-|W-L|\sqrt{k^2+1}} - e^{-|W+L|\sqrt{k^2+1}} \right) \tag{6.32}$$

is obtained from identity (4.26). Note that if the vortex lies off the shelf $(L > W)$ then (6.32) can be rewritten

$$\tilde{\Psi} = 2e^{-L\sqrt{k^2+1}}\sinh W\sqrt{k^2 + 1}, \tag{6.33}$$

and if the vortex lies on the shelf $(L < W)$, then (6.32) can be rewritten

$$\tilde{\Psi} = 2e^{-W\sqrt{k^2+1}}\sinh L\sqrt{k^2 + 1}. \tag{6.34}$$

Using the integrating factor method, together with the initial condition (6.27f), which implies that $A(k, 0) = 0$, leads to

$$A(k, \tau) = \left(e^{-i\omega\tau} - e^{-ik\epsilon u\tau} \right) \frac{\Gamma k}{(k^2 + 1)} \frac{1}{\omega - \epsilon uk}e^{-W\sqrt{k^2+1}}\tilde{\Psi}. \tag{6.35}$$

The solution consists of a steadily propagating term and a topographic wave term,

$$\phi = \phi^{(s)} + \phi^{(w)}, \tag{6.36}$$

167

where

$$\phi^{(s)} = \begin{cases} -\dfrac{\Gamma}{2\pi} \displaystyle\int_C A_1(k,y), e^{ik(x-\epsilon u\tau)}, & 0 < y < W \\[2ex] -\dfrac{\Gamma}{2\pi} \displaystyle\int_C A_2(k,y), e^{ik(x-\epsilon u\tau)}, & y > W \end{cases} \tag{6.37}$$

and

$$\phi^{(w)} = \begin{cases} \dfrac{\Gamma}{2\pi} \displaystyle\int_C A_1(k,y) e^{i(kx-\omega\tau)}, & 0 < y < W, \\[2ex] \dfrac{\Gamma}{2\pi} \displaystyle\int_C A_2(k,y) e^{i(kx-\omega\tau)}, & y > W, \end{cases} \tag{6.38}$$

with

$$A_1(k,y) = \frac{k}{(k^2+1)} \frac{e^{-W\sqrt{k^2+1}}}{\omega - \epsilon u k} \tilde{\Psi} \sinh y\sqrt{k^2+1}, \tag{6.39a}$$

$$A_2(k,y) = \frac{k}{(k^2+1)} \frac{\sinh W\sqrt{k^2+1}}{\omega - \epsilon u k} \tilde{\Psi} e^{-y\sqrt{k^2+1}}. \tag{6.39b}$$

Note that the integrands in (6.37) and (6.38) have singularities when $\omega/k = \epsilon u$, i.e. whenever the vortex velocity matches a topographic wave phase speed. In these cases the inversion contour, C, must be indented to pass below the singularities.

6.2.2   Behaviour as $\tau \to 0$

Below it is shown that the quasisteady term can be interpreted as a pseudoimage of the vortex in the escarpment, i.e. the escarpment acts like a plane wall. This is true for both the vortex and its true image in the wall, and is discussed below. There is a short spin-up time associated with the establishment of the pseudoimage, and this can be seen as follows. For $0 < y < W$, $\phi_1 = \phi_1^{(s)} + \phi_1^{(w)}$ can be written

$$\phi_1 = -\frac{\Gamma}{2\pi} \int_C A_1(k,y) \left(e^{-ik\epsilon u\tau} - e^{-i\omega\tau} \right) e^{ikx} \, dk$$

$$\approx -\frac{\Gamma}{2\pi} \int_C A_1(k,y) \left(-ik\epsilon u\tau + i\omega\tau \right) e^{ikx} \, dk, \tag{6.40}$$

where the integrand has been written to leading order in the Taylor series about $\tau = 0$ for $\tau \ll 1$. This in turn can be written

$$\phi_1 = -\frac{\Gamma i\tau}{2\pi} \int_C A_1(k,y)(\omega - \epsilon u k) e^{ikx} \, dk$$

$$= \frac{\Gamma\tau}{4\pi} \int_0^\infty A_1(k,y)(\omega - \epsilon u k) \sin kx \, dk. \tag{6.41}$$

168

The second equality follows by noting that $A_1(\omega - \epsilon u k)$ is analytic (cf equation (6.39a)) and odd. Precisely the same argument leads to the approximation

$$\phi_2 \approx \frac{\Gamma \tau}{4\pi} \int_0^\infty A_2(k, y)(\omega - \epsilon u k) \sin kx \, dk. \tag{6.42}$$

The velocity components of the vortex due to the ϕ-field are then

$$u = -\left.\frac{\partial \phi}{\partial y}\right|_{(0,L)} = 0, \tag{6.43a}$$

$$v = \left.\frac{\partial \phi}{\partial x}\right|_{(0,L)} = \frac{\Gamma \tau}{2\pi} \int_0^\infty A(k, L)(\omega - \epsilon u k) \, dk, \tag{6.43b}$$

where $A = A_1$ or A_2 according to whether $0 < L < W$ or $L > W$ respectively. For $\tau \ll 1$ the ϕ-field induces a drift in the y-direction. Anticyclones ($\Gamma > 0$) move toward deep water and cyclones ($\Gamma < 0$) move toward shallow-water. The mechanism for this process is the initial advection of fluid across the isobaths, and the consequent generation of secondary circulations, which in turn advect the vortex. See Chapter 4, and in particular subsection 4.2.2 and Figure (4.3).

6.2.3   The quasisteady term

The quasisteady term of the solution is $\psi^{(s)} = \Psi + \phi^{(s)}$, and represents a disturbance that propagates with the vortex at velocity ϵu in the x-direction. To interpret this term consider the expansion

$$\frac{2k}{\sqrt{k^2+1}} \frac{e^{-W\sqrt{k^2+1}}}{\omega - \epsilon u k} = \frac{\omega}{\sinh W\sqrt{k^2+1}} \frac{1}{\omega - \epsilon u k} = \frac{1}{\sinh W\sqrt{k^2+1}} + O\left(\frac{\epsilon u k}{\omega}\right). \tag{6.44}$$

This approximation is valid for $\tau = O(1)$, but still less than ϵ^{-1}. To this order of approximation the amplitudes (6.39a,b) may be rewritten

$$A_1(k, y) = \frac{1}{2} \frac{1}{\sqrt{k^2+1}} \tilde{\Psi} \sinh y\sqrt{k^2+1}, \tag{6.45a}$$

$$A_2(k, y) = \frac{1}{2} e^{W\sqrt{k^2+1}} \tilde{\Psi} e^{-y\sqrt{k^2+1}}, \tag{6.45b}$$

both of which are analytic and even functions of k, so

$$\phi^{(s)} = \begin{cases} -\dfrac{\Gamma}{2\pi} \displaystyle\int_0^\infty \dfrac{1}{\sqrt{k^2+1}} \, \tilde{\Psi} \, \dfrac{\sinh y\sqrt{k^2+1}}{\sinh W\sqrt{k^2+1}} \cos k(x - \epsilon u\tau) \, dk, & 0 < y < W, \\[3ex] -\dfrac{\Gamma}{2\pi} \displaystyle\int_0^\infty \dfrac{e^{W\sqrt{k^2+1}}}{\sqrt{k^2+1}} \, \tilde{\Psi} \, e^{-y\sqrt{k^2+1}} \cos k(x - \epsilon u\tau) \, dk & y > W. \end{cases} \tag{6.46}$$

There are two cases to consider, according to whether the vortex lies on the shelf, i.e. in the region $0 < L < W$, or off of it.

Case 1: Vortex off the shelf

If the vortex lies off the shelf, then $L > W$ and use of (6.33) implies that (6.46) can be rewritten as

$$\phi^{(s)} = \begin{cases} -\dfrac{\Gamma}{2\pi} \displaystyle\int_0^\infty \dfrac{1}{\sqrt{k^2+1}} \left(e^{-(L-y)\sqrt{k^2+1}} - e^{-(y+L)\sqrt{k^2+1}} \right) \cos k(x - \epsilon u\tau)\, dk, & 0 < y < W, \\[4mm] -\dfrac{\Gamma}{2\pi} \displaystyle\int_0^\infty \dfrac{1}{\sqrt{k^2+1}} \left(e^{-(y-(2W-L))\sqrt{k^2+1}} - e^{-(y+L)\sqrt{k^2+1}} \right) \cos k(x - \epsilon u\tau)\, dk, & y > W. \end{cases}$$

$$(6.47)$$

Use of identity (4.26) shows that on the shelf $0 < y < W$ (6.47) is $-\Psi$, i.e. (6.47) cancels with the vortex and image terms on the shelf. In the region $y > W$, off the shelf, the second term of (6.47) cancels with the image term of Ψ. Hence the quasisteady term, $\psi^{(s)} = \Psi + \phi^{(s)}$ for a vortex lying off the shelf is,

$$\psi^{(s)} = \begin{cases} 0, & 0 < y < W, \\[3mm] \dfrac{\Gamma}{2\pi} \left[K_0(r_1) - K_0(r_2) \right], & y > W, \end{cases}$$

$$(6.48)$$

where

$$r_1^2 = (x - \epsilon u\tau)^2 + (y - L)^2, \tag{6.49a}$$

$$r_2^2 = (x - \epsilon u\tau)^2 + (y - (2W - L))^2. \tag{6.49b}$$

Expression (6.48) thus represents the vortex and its pseudoimage in the *escarpment*. After the initial spin up of the pseudoimage the true image of the vortex in the wall no longer contributes, i.e. the vortex "forgets" about the presence of the wall, which is "blocked" by the escarpment. The velocity of the vortex due to this term is

$$u = -\dfrac{\Gamma}{2\pi} K_1(2(L - W)) \tag{6.50a}$$

$$v = 0. \tag{6.50b}$$

After the initial small onshore drift of the vortex, the motion becomes purely longshore, and the magnitude increases from its initial value, $u_0 = -\Gamma/2\pi K_1(2L)$.

Case 2: Vortex on the shelf

In this case $L < W$ and substitution of (6.34) in (6.46) leads to

$$\phi^{(s)} = \begin{cases} -\dfrac{\Gamma}{2\pi} \displaystyle\int_0^\infty \dfrac{e^{-W\sqrt{k^2+1}}}{\sqrt{k^2+1}} \dfrac{\sinh L\sqrt{k^2+1}}{\sinh W\sqrt{k^2+1}} \sinh y\sqrt{k^2+1} \cos k(x - \epsilon u\tau)\, dk, & 0 < y < W, \\[4mm] -\dfrac{\Gamma}{2\pi} \displaystyle\int_0^\infty \dfrac{1}{\sqrt{k^2+1}} \left(e^{-(y-L)\sqrt{k^2+1}} - e^{-(y+L)\sqrt{k^2+1}} \right) \cos k(x - \epsilon ut)\, dk, & y > W. \end{cases}$$

$$(6.51)$$

Off the shelf, $y > W$, and in this region (6.51) cancels with the vortex and image term Ψ. In the appendix to this chapter a vortex pair in the middle of a channel of width $2W$ is considered. By

comparing the first term of (6.51) with (6.A18) it can be seen that this term is in fact the infinite set of images of a vortex pair in a channel of width $2W$. Writing the quasisteady part of the full solution $\psi^{(s)} = \Psi + \phi^{(s)}$ leads to

$$\psi^{(s)} = \begin{cases} \dfrac{\Gamma}{2\pi} \displaystyle\sum_{n=-\infty}^{\infty} \left(K_0(r_{n+}) - K_0(r_{n-}) \right), & 0 < y < W \\[2ex] 0, & y > W, \end{cases} \tag{6.52}$$

where

$$r_{n+}^2 = (x - X)^2 + (y - (2nW + L))^2, \tag{6.53a}$$

$$r_{n-}^2 = (x - X)^2 + (y - (2nW - L))^2. \tag{6.53b}$$

In this case, then, the escarpment acts as a plane wall, leading to an infinite set of pseudoimages. The velocity at the vortex centre is then due to the true image of the vortex and the pseudoimages,

$$u = -\frac{\Gamma}{2\pi} K_1(2L) - \frac{\Gamma}{2\pi} \sum_{n=1}^{\infty} \left(K_1(2nW) - K_1(2(nW - L)) \right), \tag{6.54a}$$

$$v = 0, \tag{6.54b}$$

so the vortex drift velocity decreases from its' initial value.

It has been show that, to leading order, the quasisteady term represents a pseudoimage of the vortex in the escarpment. The large time behaviour is deduced in the following section.

6.2.4   Large time behaviour

Each of the inversion integrals (6.37) and (6.38) have singularities whenever $0 < \epsilon u \leq c_p(0)$, i.e. when

$$0 < \epsilon u \leq 1 - e^{-2W}, \tag{6.55}$$

Note that *only* cyclones move in the direction of positive x, so unlike the case of a singular vortex near an escarpment with no wall nearby, wave radiation can only occur when the vortex is a cyclone. There are three cases to consider.

Case 1 $\epsilon u < 0$ or $\epsilon u > 1 - e^{-2W}$

In this case the integrands are analytic and the inversion contour C can be deformed back to the real line. The points of stationary phase are given by the solution, k_s, of

$$\frac{x}{\tau} = c_g(k). \tag{6.56}$$

By considering Figure (6.2), it is evident that there are two solutions to (6.56) whenever $0 < x/\tau < 1 - e^{-2W}$. However the solution having $k_s < 0$ must be ruled out since $\tau > 0$. Hence there is a single point of stationary phase, and by the argument given in Chapter 4 the topographic waves decay like $\tau^{-1/2}$, and so have no influence on the vortex for large times. In this case the vortex is moving at a velocity outside of the range of possible phase speeds, and the behaviour for $\tau = O(\epsilon^{-1})$ is dominated by the pseudoimage term $\phi^{(s)}$.

Figures (6.3) and (6.4) show plots of the solution evaluated over $y = W$ by Fast Fourier Transforms, for two different cases where the vortex is an anticyclone. The plots were obtained by FFT of equations (6.18), (6.37) and (6.38). In Figure (6.3) the parameter values used are $W = 0.5$ and $L = 1$, and the times shown are $\tau = 20$ and $\tau = 160$. The pseudoimage term which moves with the vortex is evident, and the topographic waves which propagate in the opposite direction to the vortex decay with time. In Figure (6.4) the parameter values used are $W = 0.03$ and $L = 0.6$ and the times shown are $\tau = 60$ and $\tau = 160$. The pseudoimage is again evident, but note that the waves, whilst smaller in amplitude than the previous case, are slow to decay and appear to be only slowly dispersive. This is in agreement with the behaviour of the topographic waves in the limit $W \to 0$, discussed previously in section 6.1, where it was shown that in this limit the waves are non dispersive to leading order. In both cases the vortex drift velocity in the x-direction was calculated using equation (6.50a).

Case 2 $0 < \epsilon u < 1 - e^{-2W}$

In this case there are singularities on the real axis whenever,

$$\frac{\omega}{k} = \epsilon u \tag{6.57}$$

i.e. whenever the vortex drift velocity matches a possible topographic wave phase speed. From the graph in Figure (6.2) it is clear that there are two poles on the real axis at $k = \pm\gamma$ where γ satisfies

$$\epsilon u = \frac{1}{\sqrt{\gamma^2 + 1}}\left(1 - e^{-2W\sqrt{\gamma^2+1}}\right). \tag{6.58}$$

The large time behaviour is dominated by the behaviour near the poles. To proceed with the residue calculations write

$$A_1(k,y) = \frac{e^{-W\sqrt{k^2+1}}}{\sqrt{k^2+1}}\frac{P(k)}{k^2 - \gamma^2}\,\tilde{\Psi}(k)\sinh y\sqrt{k^2+1}, \tag{6.59}$$

$$A_2(k,y) = \frac{\sinh W\sqrt{k^2+1}}{\sqrt{k^2+1}}\frac{P(k)}{k^2 - \gamma^2}\,\tilde{\Psi}(k)e^{-y\sqrt{k^2+1}}, \tag{6.60}$$
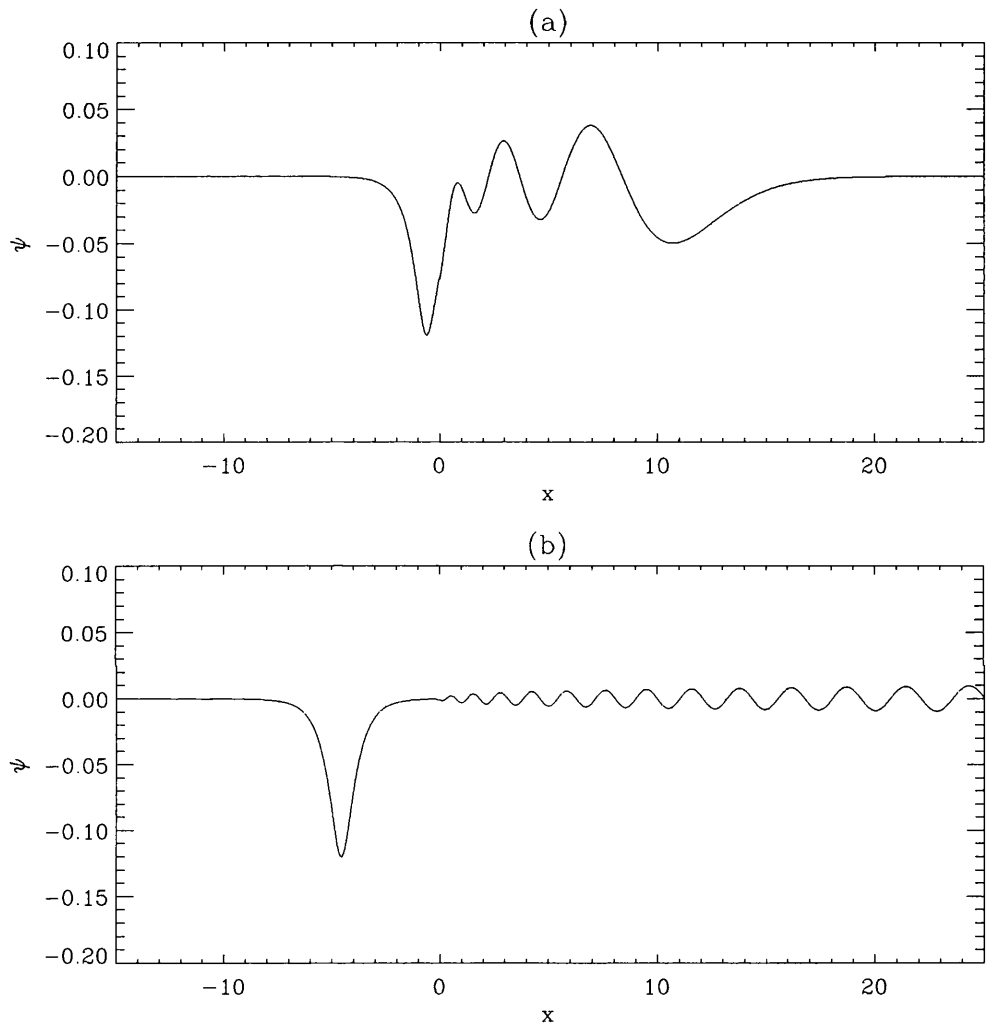
Figure 6.3: FFT evaluation of the solution over $y = W$, for a non-radiating weak vortex. The parameter values used are $\Gamma = +1$, $\epsilon = 0.1$, $W = 0.5$ and $L = 1$. The times are (a) $\tau = 20$ and (b) $\tau = 160$. The dispersive waves, propagating in the opposite direction to the vortex are evident, and the non dispersive disturbance propagating with the vortex is the pseudoimage.
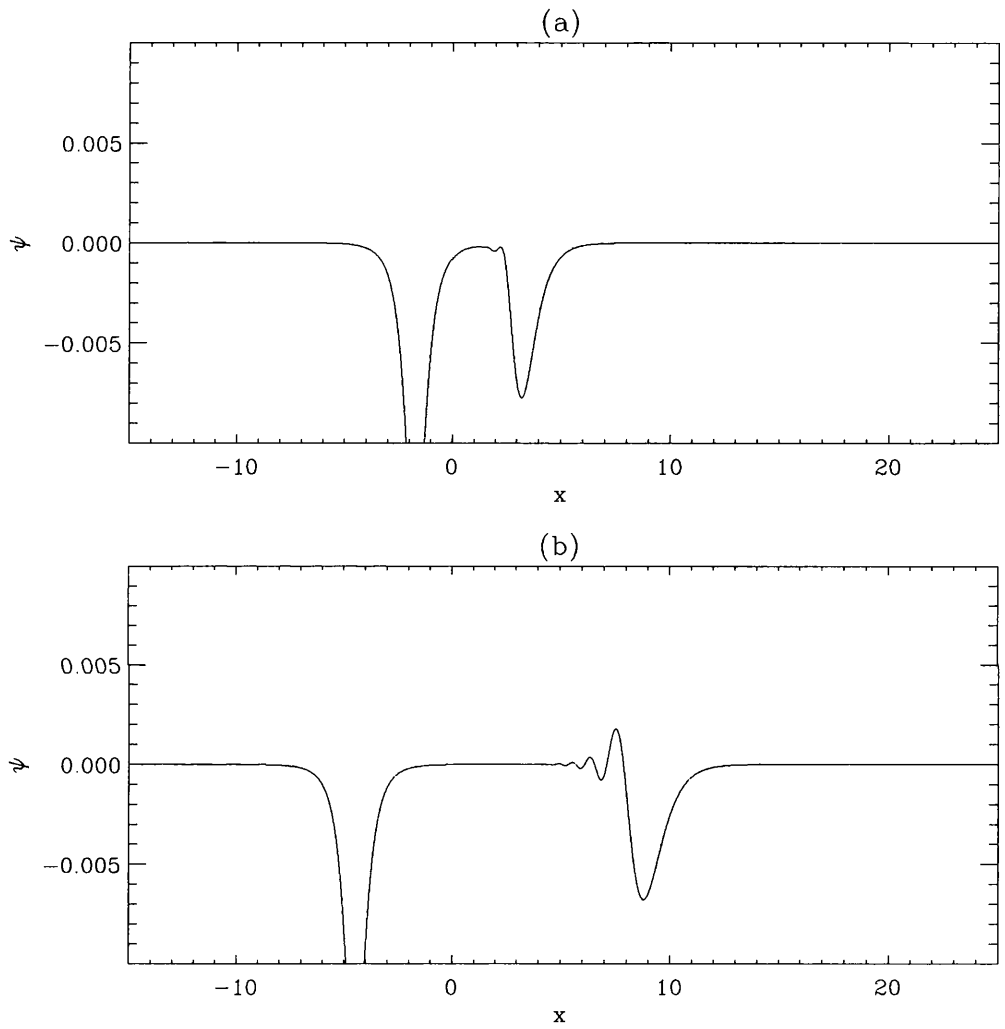
Figure 6.4: FFT evaluation of the solution over $y = W$, for a non-radiating weak vortex. The parameter values used are $\Gamma = +1$, $\epsilon = 0.1$, $W = 0.03$ and $L = 0.6$. The times are (a) $\tau = 60$ and (b) $\tau = 160$. The waves, propagating in the opposite direction to the vortex appear to be almost non dispersive, and the nondispersive disturbance propagating with the vortex is the pseudoimage.

where

$$P(k) = -\frac{1}{(\epsilon u)^2} \frac{(\epsilon u)^2(k^2+1) - (1 - e^{-2W\sqrt{\gamma^2+1}})}{(\epsilon u)^2(k^2+1) - (1 - e^{-2W\sqrt{k^2+1}})} \left(1 - e^{-2W\sqrt{k^2+1}} + \epsilon u\sqrt{k^2+1}\right). \qquad (6.61)$$

Equations (6.59) and (6.60) indicate that the poles are simple. The inversion contour is indented to pass below the poles, (see Figure (4.7) in Chapter 4 for a diagram of the contour). Note that

$$P(\pm\gamma) = -\frac{2}{\epsilon u}\sqrt{\gamma^2+1}. \qquad (6.62)$$

First consider

$$\phi_1^{(s)} = \int_C A_1(k,y)e^{ik(x-\epsilon u\tau)}\, dk. \qquad (6.63)$$

There is no contribution from the semi-circular arcs as $x - \epsilon u\tau \to -\infty$, and the contribution due to the branch cut is also exponentially small as $x - \epsilon u\tau \to \infty$. The residue of the integrand, making use of (6.62), at $k = \gamma$ is

$$\frac{e^{-W\sqrt{\gamma^2+1}}}{\sqrt{\gamma^2+1}} \frac{P(\gamma)}{2\gamma} \tilde\Psi(\gamma)\sinh y\sqrt{\gamma^2+1}e^{i\gamma(x-\epsilon u\tau)}$$

$$= -\frac{1}{(\epsilon u)\gamma}e^{-W\sqrt{\gamma^2+1}}\tilde\Psi(\gamma)\sinh y\sqrt{\gamma^2+1}\; e^{i\gamma(x-\epsilon u\tau)}. \qquad (6.64)$$

Similarly, the residue at $k = -\gamma$ is

$$\frac{1}{(\epsilon u)\gamma}e^{-W\sqrt{\gamma^2+1}}\tilde\Psi(\gamma)\sinh y\sqrt{\gamma^2+1}\; e^{-i\gamma(x-\epsilon u\tau)}. \qquad (6.65)$$

Thus, as $\tau \to \epsilon^{-1}$,

$$\phi_1^{(s)} \approx -\frac{2}{(\epsilon u)\gamma}e^{-W\sqrt{\gamma^2+1}}\; \tilde\Psi(\gamma)\; \sinh y\sqrt{\gamma^2+1}\; \sin\gamma(x-\epsilon u\tau)\, H(x-\epsilon u\tau). \qquad (6.66)$$

The same arguments lead to

$$\phi_2^{(s)} \approx -\frac{2}{(\epsilon u)\gamma}\sinh W\sqrt{\gamma^2+1}\tilde\Psi(\gamma)e^{-y\sqrt{\gamma^2+1}}\; \sin\gamma(x-\epsilon u\tau)\, H(x-\epsilon u\tau). \qquad (6.67)$$

Next consider the wave term, $\phi^{(w)}$. Near the poles $k = \pm\gamma$ a Taylor expansion gives

$$\omega(k) = \pm\gamma\epsilon u + (k \mp \gamma)c_g(\gamma), \qquad (6.68)$$

so near the poles

$$e^{i(kx-\omega t)} \approx e^{ik(x-c_g(\gamma)\tau)}\; e^{\mp i\gamma(c_g(\gamma)-\epsilon u)\tau}. \qquad (6.69)$$

Hence, there is no contribution to the integral as $x - c_g\tau \to -\infty$. Moreover, $\omega(\gamma) = \gamma\epsilon u$, so it is clear that the residues of $\phi^{(w)}$ at $k = \pm\gamma$ are the same as those of $\phi^{(s)}$. Hence, as $t \to \epsilon^{-1}$,

$$\phi(x,y,\tau) \approx g(y)\; \sin\gamma(x-\epsilon u\tau)\; [H(x-\epsilon u\tau) - H(x-c_g(\gamma)\tau)], \qquad (6.70)$$

where

$$g(y) = \begin{cases} -\dfrac{2\Gamma}{(\epsilon u)\gamma} \; e^{-W\sqrt{\gamma^2+1}} \; \tilde{\Psi}(\gamma) \; \sinh y\sqrt{\gamma^2+1}, & 0 < y < W, \\[4mm] -\dfrac{2\Gamma}{(\epsilon u)\gamma} \; \sinh \gamma\sqrt{\gamma^2+1} \; \tilde{\Psi}(\gamma) \; e^{-y\sqrt{\gamma^2+1}}, & y > W. \end{cases} \tag{6.71}$$

Equation (6.70) represents a wavetube growing like the difference between the phase and group velocities of the radiated waves. Figures (6.5) and (6.6) illustrate the process of the wavetube formation. The plots were obtained by FFT of the solution as in Figure (6.3). In Figure (6.5) the parameter values used are $W = 0.5$, $L = 1$ and $\Gamma = -1$ (i.e. a cyclone), and the times shown are $\tau = 20$ and $\tau = 160$. The pseudoimage is the non dispersive disturbance which propagates with the vortex. The waves ahead of the vortex are the dispersive topographic waves which decay with time, whilst the wavetube grows in the wake of the vortex due to radiation. In Figure (6.6) the parameter values used are $W = 0.03$, $L = 0.6$ and $\Gamma = -1$ and the times shown are $\tau = 20$ and $\tau = 200$. In this case the waves ahead of the vortex are of small amplitude and are not resolved in the plot. The wavetube growing due to topographic wave radiation is evident.

Equation (6.70) representing the growth of the wavetube is analogous to the large time response of a weak vortex near an escarpment in Chapter 4. There are, however, some important differences. In the absence of the wall the radiated waves were the *short* waves, with low energy density. This in turn was due to the vortex velocity being an $O(\epsilon)$ quantity, a result of its advection by its pseudoimage occuring on the long timescale $\tau = \epsilon t$. Consequently the momentum loss to the radiated topographic was exponentially small, and the effect on the vortex trajectory was negligible, even for $t \approx \epsilon^{-2}$. In the present case there is no such constraint on the vortex velocity. The longshore velocity of the vortex induced by its true image can take the whole range of values, and for fixed Γ is a function of the distance of the vortex from the wall (and thus the distance from its image). Here then is the possibility of interaction with the long topographic waves, i.e. those with high energy density. The momentum loss through wave radiation may be more significant.

There are two particular limits that are discussed below in detail. First, if $L = O(\epsilon)$ so that ϵu is an $O(1)$ quantity, and if $W \approx O(1)$, then consideration of Figure (6.15) shows that the wavenumber of the radiated waves can take arbitrarily small values. Second, if $W \ll 1$ and if $\epsilon u = O(\epsilon)$ which is possible for $L = O(1)$, then the vortex can travel at the group velocity of the topographic long waves.
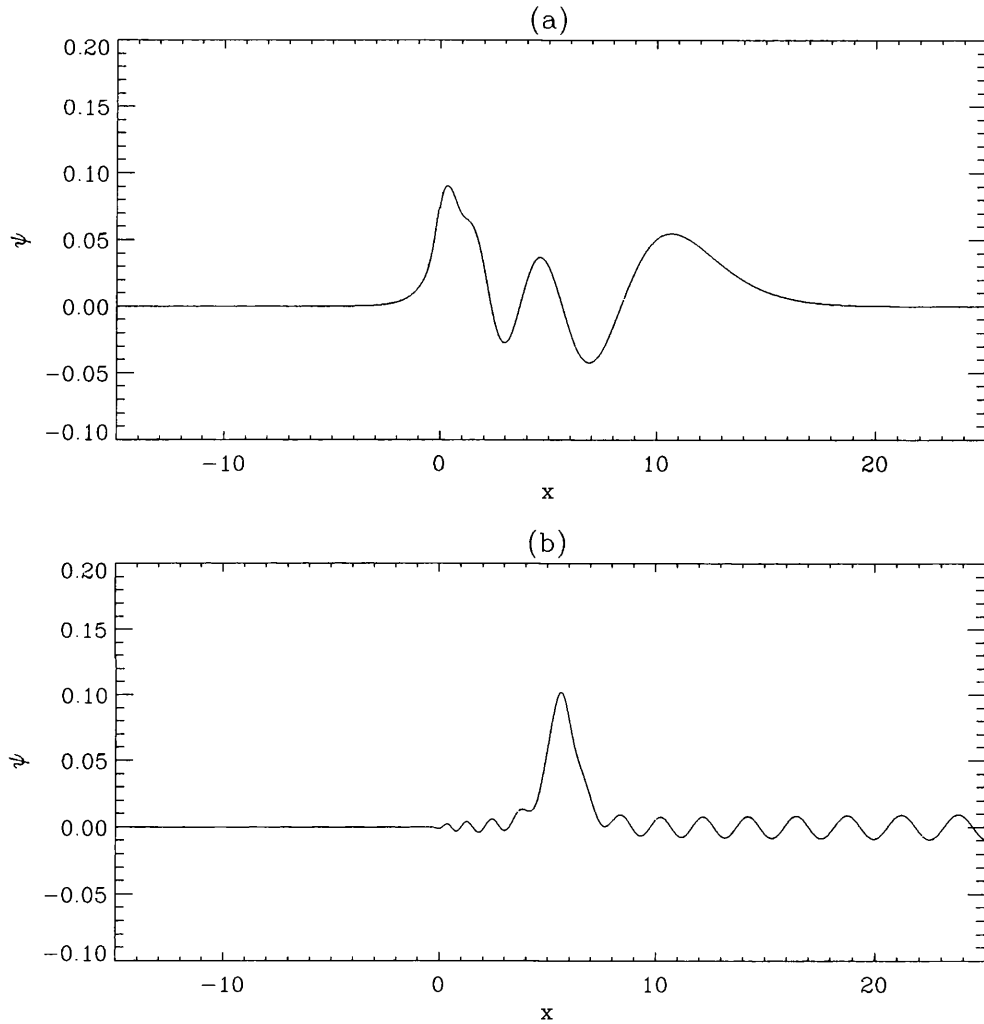
Figure 6.5: FFT evaluation of the solution over $y = W$, for a radiating weak vortex. The parameter values used are $\Gamma = -1$, $\epsilon = 0.1$, $W = 0.5$ and $L = 1$. The times are (a) $\tau = 20$ and (b) $\tau = 160$. Note the dispersive waves ahead of the vortex which decay and the wave tube growing in the wake of the vortex as a result of wave radiation.
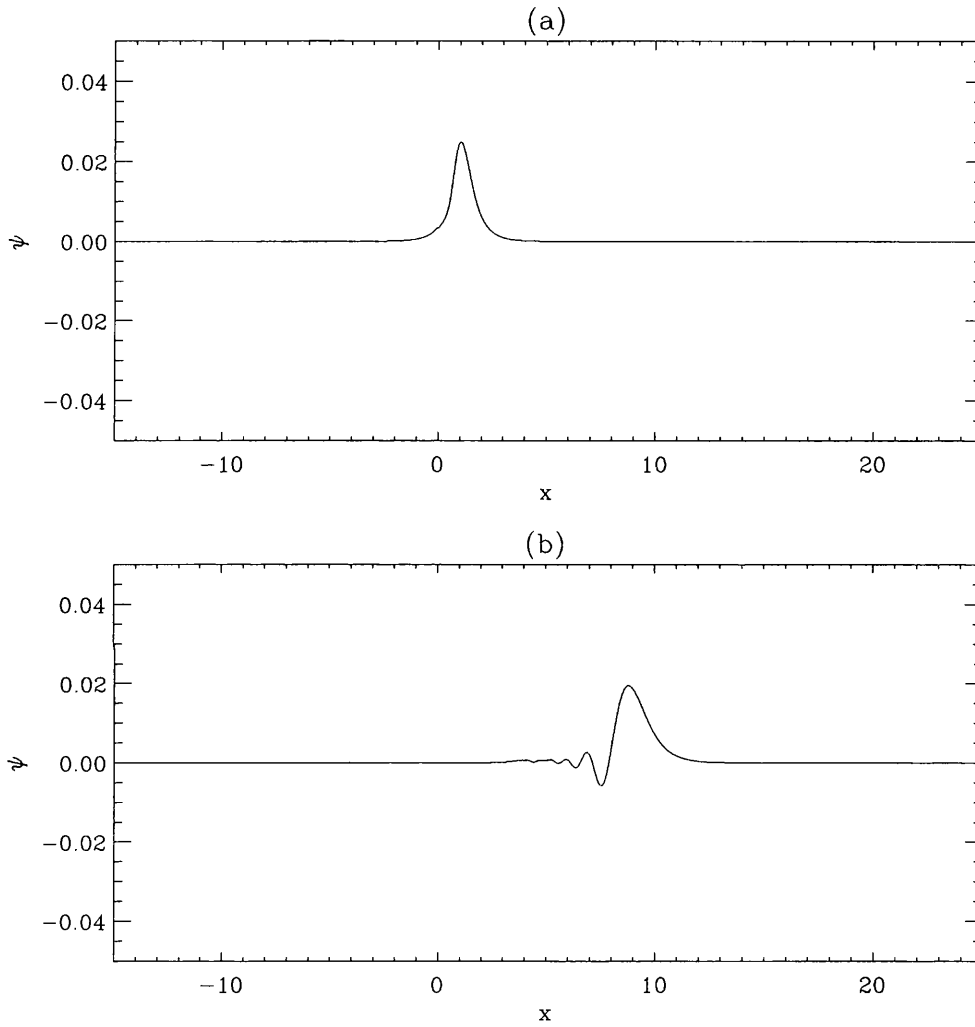
Figure 6.6: FFT evaluation of the solution over $y = W$, for a radiating weak vortex. The parameter values used are $\Gamma = -1$, $\epsilon = 0.1$, $W = 0.03$ and $L = 0.6$. The times are (a) $\tau = 20$ and (b) $\tau = 200$. The topographic wave ahead of the vortex are not resolved in this plot.

Case 3: $\epsilon u = 1 - e^{-2W\sqrt{k^2+1}}$

For a given value of W there is a particular value of L for which a cyclone travels with precisely the velocity of the waves with $k = 0$. In this case the two poles coalesce at $k = 0$ to form a second order pole. Moreover, these are the waves with maximum group velocity (see equation (6.17) and Figure (6.12)), and which therefore correspond to a second order point of stationary phase. McDonald (1996) considered a similar case for a modon travelling at the group velocity of the topographic long waves near an escarpment, and applied the method of Akylas (1984) to the Fourier integral to show that, for a given value of x linear theory predicts that the response becomes unbounded at large times. In particular $\phi \approx \tau^{1/3}$ as $\tau \to \infty$. Figure (6.7) illustrates that this behaviour also occurs in the present case. The plot was obtained by FFT, and for fixed $W = 0.3$ numerically finding the value of L (here $L \approx 1.67$) such that $\epsilon u = 1 - e^{-2W\sqrt{k^2+1}}$, for a vortex off the shelf. The vortex drift velocity was calculated using equation (6.50a). The physical reason for this behaviour is that the large time response is dominated by the waves with vanishing group velocity, so energy can not escape from the vortex. This in turn implies that energy can not escape from the vortex and so the response must eventually become nonlinear.

McDonald (1996) introduces long wave scales into the nonlinear governing equations (6.20) and finds that to leading order the wave amplitude is governed by a forced Kortweg de Vries equation. This procedure is difficult in the present case and the nature of the vortex-wave interaction in the case that the vortex travels at the topographic long wave group velocity is examined by contour dynamics below.

6.2.5   Vortex trajectory

The arguments used in Chapter 4 can be used to equate the momentum flux in the radiated wave tube with the rate of change of the x-momentum of the vortex. The energy density in the wavetube is

$$\rho = \frac{1}{2}\left(\phi_x^2 + \phi_y^2 + \phi^2\right),$$ (6.72)

where ϕ is given by (6.70), and the average value over a wavelength is taken. Denote the on shelf and off shelf components of ρ by

$$\rho = \begin{cases} \rho_1 & 0 < y < W \\ \\ \rho_2 & y > W \end{cases}$$ (6.73)

179
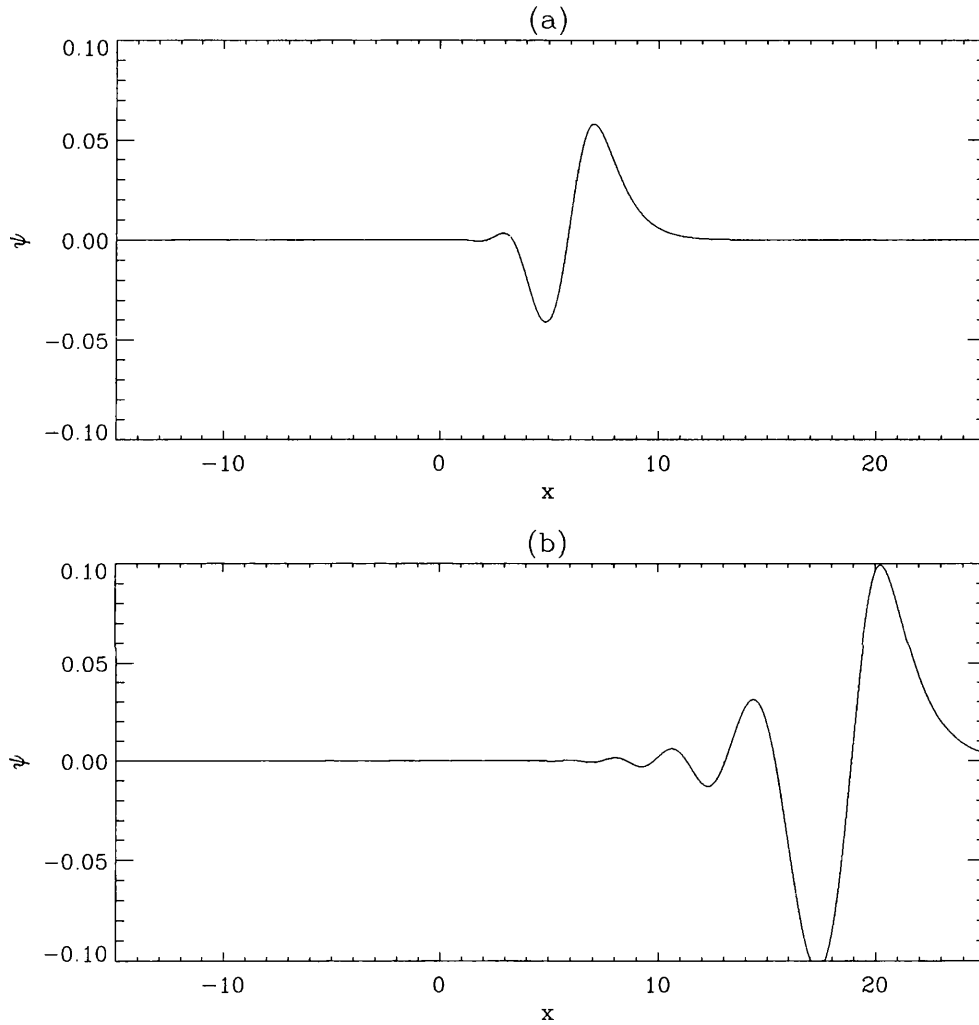
Figure 6.7: FFT evaluation of the solution over $y = W$, for a weak vortex travelling at the topographic long wave speed. The parameter values used are $\Gamma = -1$, $\epsilon = 0.1$, $W = 0.3$ and $L \approx 1.67$. The times are (a) $\tau = 20$ and (b) $\tau = 60$. The amplitude of the waves grows with time.

The required averaged quantities are

$$
\phi_x^2 = \begin{cases} \dfrac{2\Gamma^2}{(\epsilon u)^2}\, e^{-2W\sqrt{\gamma^2+1}}\, \tilde{\Psi}^2(\gamma)\, \sinh^2 y\sqrt{\gamma^2+1} & 0 < y < W \\[3mm] \dfrac{2\Gamma^2}{(\epsilon u)^2}\, \sinh^2 W\sqrt{\gamma^2+1}\, \tilde{\Psi}^2(\gamma)\, e^{-2y\sqrt{\gamma^2+1}} & y > W \end{cases}
\tag{6.74}
$$

$$
\phi_y^2 = \begin{cases} \dfrac{2\Gamma^2(\gamma^2+1)}{(\epsilon u)^2\gamma^2}\, e^{-2W\sqrt{\gamma^2+1}}\, \tilde{\Psi}^2(\gamma)\, \cosh^2 y\sqrt{\gamma^2+1} & 0 < y < W \\[3mm] \dfrac{2\Gamma^2(\gamma^2+1)}{(\epsilon u)^2\gamma^2}\, \sinh^2 W\sqrt{\gamma^2+1}\, \tilde{\Psi}^2(\gamma)\, e^{-2y\sqrt{\gamma^2+1}} & y > W \end{cases}
\tag{6.75}
$$

and

$$
\phi^2 = \begin{cases} \dfrac{2\Gamma^2}{(\epsilon u)^2\gamma^2}\, e^{-2W\sqrt{\gamma^2+1}}\, \tilde{\Psi}^2(\gamma)\, \sinh^2 y\sqrt{\gamma^2+1} & 0 < y < W \\[3mm] \dfrac{2\Gamma^2}{(\epsilon u)^2\gamma^2}\, \sinh^2 W\sqrt{\gamma^2+1}\, \tilde{\Psi}^2(\gamma)\, e^{-2y\sqrt{\gamma^2+1}} & y > W. \end{cases}
\tag{6.76}
$$

These lead to, after some manipulation

$$
\rho_1 \;=\; \frac{\Gamma^2(\gamma^2+1)}{(\epsilon u)^2\gamma^2}\, e^{-2W\sqrt{\gamma^2+1}}\, \tilde{\Psi}^2(\gamma)\, \cosh 2y\sqrt{\gamma^2+1}
\tag{6.77}
$$

$$
\rho_2 \;=\; \frac{\Gamma^2(\gamma^2+1)}{(\epsilon u)^2\gamma^2}\, \sinh^2 W\sqrt{\gamma^2+1}\, \tilde{\Psi}^2(\gamma)\, e^{-2y\sqrt{\gamma^2+1}}.
\tag{6.78}
$$

The wavepower (i.e. the total energy flux), F, is found by integrating ρ over positive y and multiplying the result by the rate of growth of the wavetube (i.e. the group velocity of the radiated waves a frame moving with velocity $c_g(\gamma)$,

$$
F = (\epsilon u - c_g(\gamma)) \int_0^\infty \rho\, dy.
\tag{6.79}
$$

It is straightforward to show

$$
\int_0^W \rho_1\, dy = \frac{1}{2}\frac{\Gamma^2\sqrt{\gamma^2+1}}{(\epsilon u)^2\gamma^2}\, e^{-2W\sqrt{\gamma^2+1}}\, \tilde{\Psi}^2(\gamma)\, \sinh 2W\sqrt{\gamma^2+1},
\tag{6.80}
$$

and

$$
\int_W^\infty \rho_2\, dy = \frac{\Gamma^2\sqrt{\gamma^2+1}}{(\epsilon u)^2\gamma^2}\, e^{-2W\sqrt{\gamma^2+1}}\, \tilde{\Psi}^2(\gamma)\, \sinh^2 W\sqrt{\gamma^2+1},
\tag{6.81}
$$

so that

$$
\begin{aligned}
\int_0^\infty \rho\, dy \;&=\; \frac{\Gamma^2\sqrt{\gamma^2+1}}{(\epsilon u)^2\gamma^2}\, e^{-2W\sqrt{\gamma^2+1}}\, \tilde{\Psi}^2(\gamma)\left[\frac{1}{2}\sinh 2W\sqrt{\gamma^2+1} + \sinh^2 W\sqrt{\gamma^2+1}\right] \\[3mm]
&=\; \frac{1}{2}\frac{\Gamma^2\sqrt{\gamma^2+1}}{(\epsilon u)^2\gamma^2}\, e^{-2W\sqrt{\gamma^2+1}}\, \tilde{\Psi}^2(\gamma)\left[\sinh 2W\sqrt{\gamma^2+1} + \cosh 2W\sqrt{\gamma^2+1} - 1\right]
\end{aligned}
$$

$$= \frac{1}{2} \frac{\Gamma^2 \sqrt{\gamma^2 + 1}}{(\epsilon u)^2 \gamma^2} \, \tilde{\Psi}^2(\gamma) \left[1 - e^{-2W\sqrt{\gamma^2+1}} \right]$$

$$= \frac{1}{2} \frac{\Gamma^2(\gamma^2 + 1)}{(\epsilon u)\gamma^2} \, \tilde{\Psi}^2(\gamma) \tag{6.82}$$

where equation (6.58) has been used to make the final substitution. Thus the wave power in the wavetube is

$$F = \frac{1}{2} \frac{\Gamma^2(\gamma^2 + 1)}{(\epsilon u)\gamma^2} \, \tilde{\Psi}^2(\gamma) \, [\epsilon u - c_g(\gamma)], \tag{6.83}$$

and the rate of change of the wave pseudomomentum is this quantity divided by the phase velocity:

$$M = \frac{F}{\epsilon u} = \frac{1}{2} \frac{\Gamma^2(\gamma^2 + 1)}{(\epsilon u)^2 \gamma^2} \, \tilde{\Psi}^2(\gamma) \, [\epsilon u - c_g(\gamma)]. \tag{6.84}$$

This is also the drag on the vortex, which must therefore respond by losing momentum. The leading order x-momentum of the vortex is, by a generalisation of the result in Batchelor (1967) for barotropic singular vortices

$$\begin{aligned} M_x &= -\int_0^\infty \int_{-\infty}^\infty y \left(\nabla^2 \Psi - \Psi \right) \, dx \, dy \\ &= \Gamma L \end{aligned} \tag{6.85}$$

Finally, equating the rate of change of M_x with M yields the differential equation for L

$$\frac{dL}{d\tau} = \frac{1}{2} \frac{\Gamma(\gamma^2 + 1)}{(\epsilon u)^2 \gamma^2} \, \tilde{\Psi}^2(\gamma) \, (\epsilon u - c_g(\gamma)). \tag{6.86}$$

Figure (6.8) is a plot of $c_p - c_g$ for various values of W. Note that $\epsilon u = c_g(\gamma)$, and so $\epsilon u - c_g(\gamma) > 0$. The maximum occurs for γ near to zero (i.e. the topographic long waves), but if $\gamma = 0$ then $\epsilon u - g_g(\gamma) = 0$ and linear theory predicts that there is no meridional drift due to wave radiation. This is consistent with the fact that since $c_p(0) = c_g(0)$ energy can't escape from the vortex. The response in this case must become nonlinear. There are two cases to consider, and in each case there is a subcase of interest, namely when the vortex travels at a velocity near the topographic long wave group velocity. These subcases are investigated by contour dynamics simulations in the following subsection.

Case 1: Vortex off the shelf

In this case $L > W$ and substitution of (6.33) in (6.86) leads to

$$\frac{dL}{d\tau} = \frac{2\Gamma(\gamma^2 + 1)}{(\epsilon u)^2 \gamma^2} \, e^{-2L\sqrt{\gamma^2+1}} \, \sinh^2 W\sqrt{\gamma^2 + 1} \, (\epsilon u - c_g(\gamma)). \tag{6.87}$$
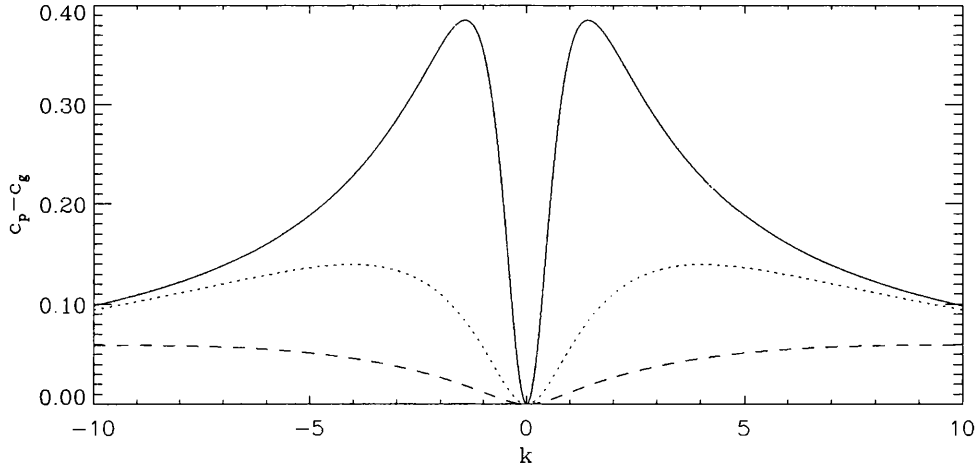
Figure 6.8: A plot of the difference $c_p - c_g$, between the phase and group velocities for $W = 1/4$ (dotted line), $W = 1/10$ (dashed line) and $W \to \infty$. Note that $c_p - c_g > 0$ for all values of W and k.

Note that all of the factors in (6.87) are positive, which in turn implies that $dL/d\tau$ has the same sign as Γ. Here the vortex is a cyclone, so $\Gamma < 0$ and the vortex drifts towards the escarpment as a result of topographic wave radiation.

Case 2: Vortex on the shelf

In this case $L < W$ and substitution of (6.34) in (6.86) leads to

$$\frac{dL}{d\tau} = \frac{2\Gamma(\gamma^2 + 1)}{(\epsilon u)^2 \gamma^2} \, e^{-2W\sqrt{\gamma^2+1}} \, \sinh^2 L\sqrt{\gamma^2 + 1} \, (\epsilon u - c_g(\gamma)). \tag{6.88}$$

Again, all of the factors $\dfrac{dL}{d\tau} = \dfrac{2\Gamma(\gamma^2 + 1)}{(\epsilon u)^2 \gamma^2} \, e^{-2W\sqrt{\gamma^2+1}} \, \sinh^2 L\sqrt{\gamma^2 + 1} \, (\epsilon u - c_g(\gamma))$ s Γ; i.e. the on shelf cyclone migrates towards the wall in response to wave radiation.

6.2.6 Contour dynamics results

To apply the contour dynamics algorithm in the present case the influence of the image of the vortex and the contours in the wall was taken into account. The velocity at the vortex centre is due to its image, the contours and the images of the contours. The velocity at the contour nodes is due to the vortex, the image of the vortex, the deflected contour and the image of the deflected contour.

The results presented here have been selected to illustrate the validity of the linear theory, and to investigate the onset of nonlinearity in the cases where the vortex travels at the group velocity of the topographic long waves. The cases of a vortex off the shelf and a vortex on the shelf are treated

separately.

Off shelf anticyclone

The trajectory of the vortex centre for three different cases is shown in Figure (6.9). Here the shelf width is $W = 1$, 0.5 and 0.1, but the distance of the vortex from the escarpment is fixed at $L - W = 0.5$. Also the value of ϵ is 0.2, i.e. a weak vortex. This was the smallest value that could be used in practice since end effects occur rapidly for smaller values. Figure (6.9a) is a plot of the x location of the vortex centre compared with the linear theory prediction given by (6.50a). The linear theory predicts well the longshore drift velocity for short times. At larger times the velocity in the x-direction begins to retard.

Figure (6.9b) shows the displacement of the vortex centroid from its initial position. The drift in the y-direction is oscillatory but small, and the maximum displacement occurs for the case $(W, L) = (1, 1.5)$.

Figure (6.10) shows the evolution of the contour for $W = 1$ and $L = 1.5$. The topographic waves propagate away from the vortex. Note also the build up of cyclonic relative vorticity in the vicinity of the vortex. This is due to the swirl of the anticyclone competing with the preferred direction of the topographic waves. This process is also apparent in Figure (6.11) which shows the contour evolution for $w = 0.1$ and $L = 0.6$. Note also that in this case the topographic waves appear to be nondispersive. This is consistent with the analytic prediction and, in particular, equation (6.14) which says that the topographic waves are nondispersive to leading order for small W.

Off shelf cyclone

As for the anticyclone the trajectory of the vortex centre for three different cases is shown in Figure (6.12). Here the shelf width $W = 1$, 0.5 and 0.1, but the distance of the vortex from the escarpment is fixed at $L - W = 0.5$. Also the value of ϵ is 0.2. This was the smallest value that could be used in practice since end effects occur rapidly for smaller values. Figure (6.12a) is a plot of the x location of the vortex centre compared with the linear theory prediction given by (6.50a). The linear theory predicts well the longshore drift velocity for short times. Figure (6.12b) shows the displacement of the vortex centroid from its initial position. The drift in the y-direction is oscillatory but small, and the maximum displacement occurs for the case $(W, L) = (0.1, 0.6)$
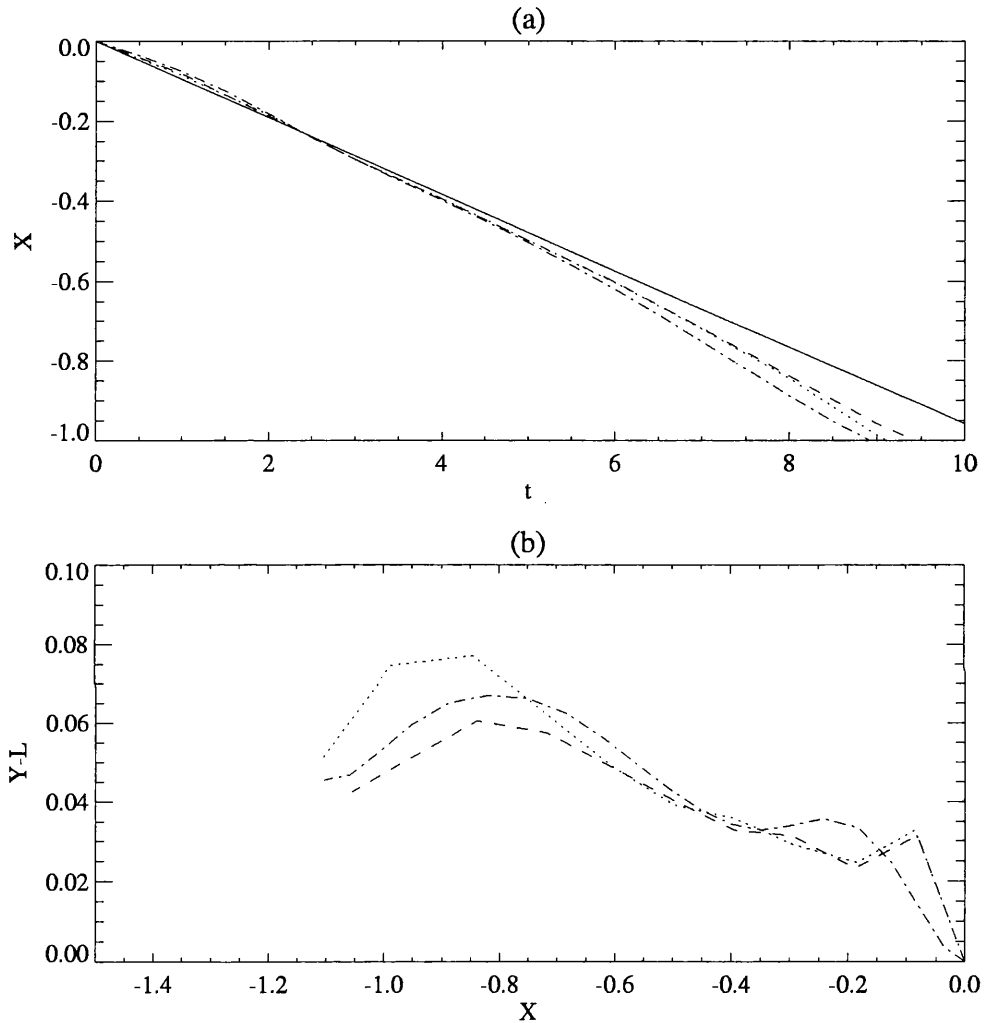
Figure 6.9: A plot of the trajectory of the vortex centre for a weak ($\epsilon = 0.2$) off shelf anticyclone for various pairs (W, L). The dotted line is for $(W, L) = (1, 1.5)$, the dashed line is $(W, L) = (0.5, 1)$ and the dot-dashed line is $(W, L) = (0.1, 0.6)$. The plots are for $0 < t < 10$. (a) is a plot of the x coordinate of the vortex centre compared with the prediction given in (6.50a) (solid line) and (b) shows the displacement of the vortex centre from its initial position.
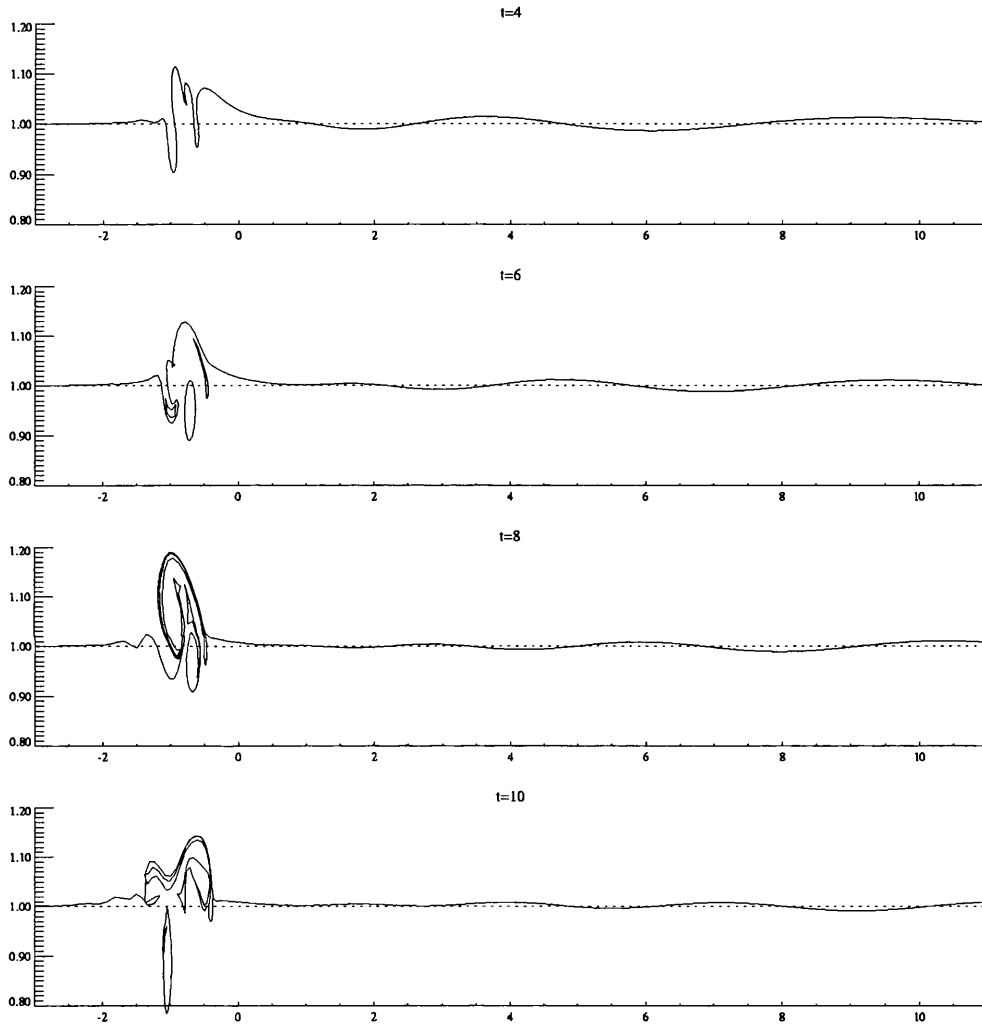
Figure 6.10: The evolution of the contour for a weak ($\epsilon = 0.2$) off shelf anticyclone. The parameter values used are $W = 1$ and $L = 1.5$.
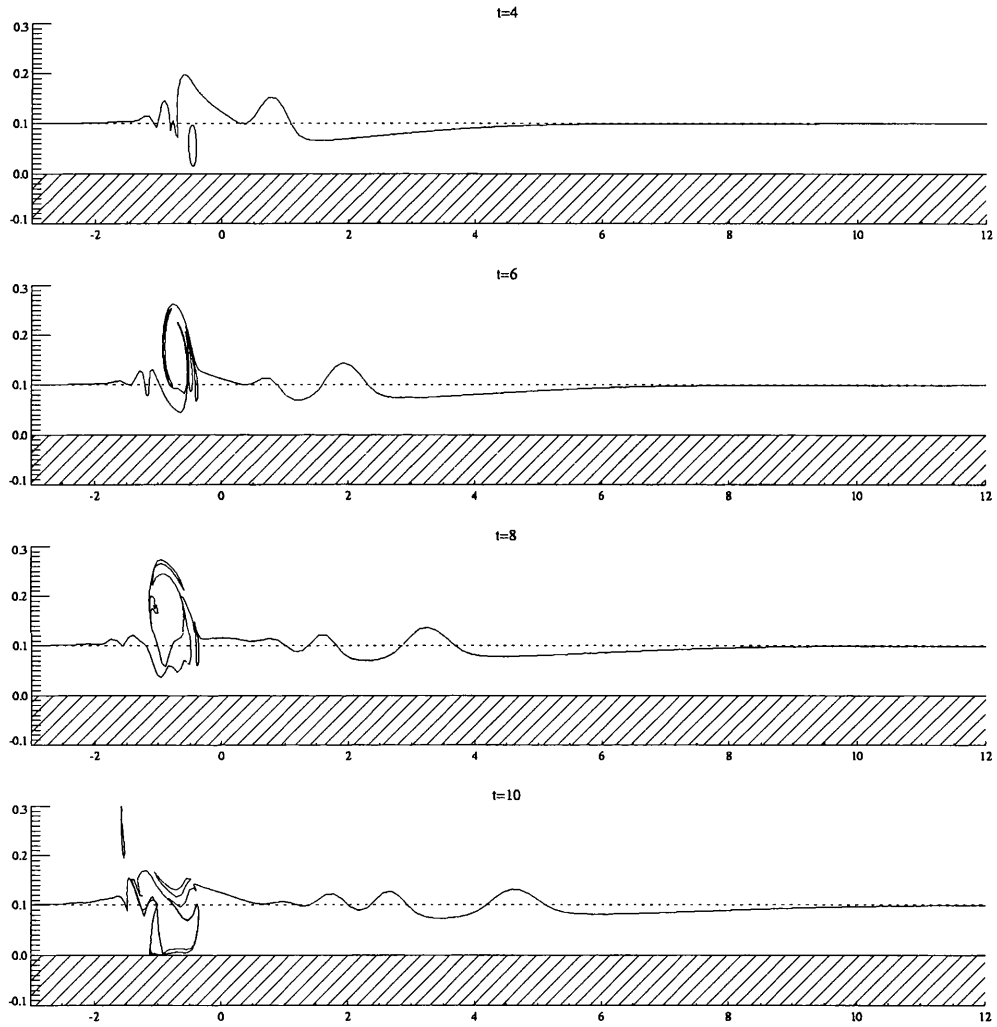
Figure 6.11: The evolution of the contour for a weak ($\epsilon = 0.2$) off shelf anticyclone. The parameter values used are $W = 0.1$ and $L = 0.6$.
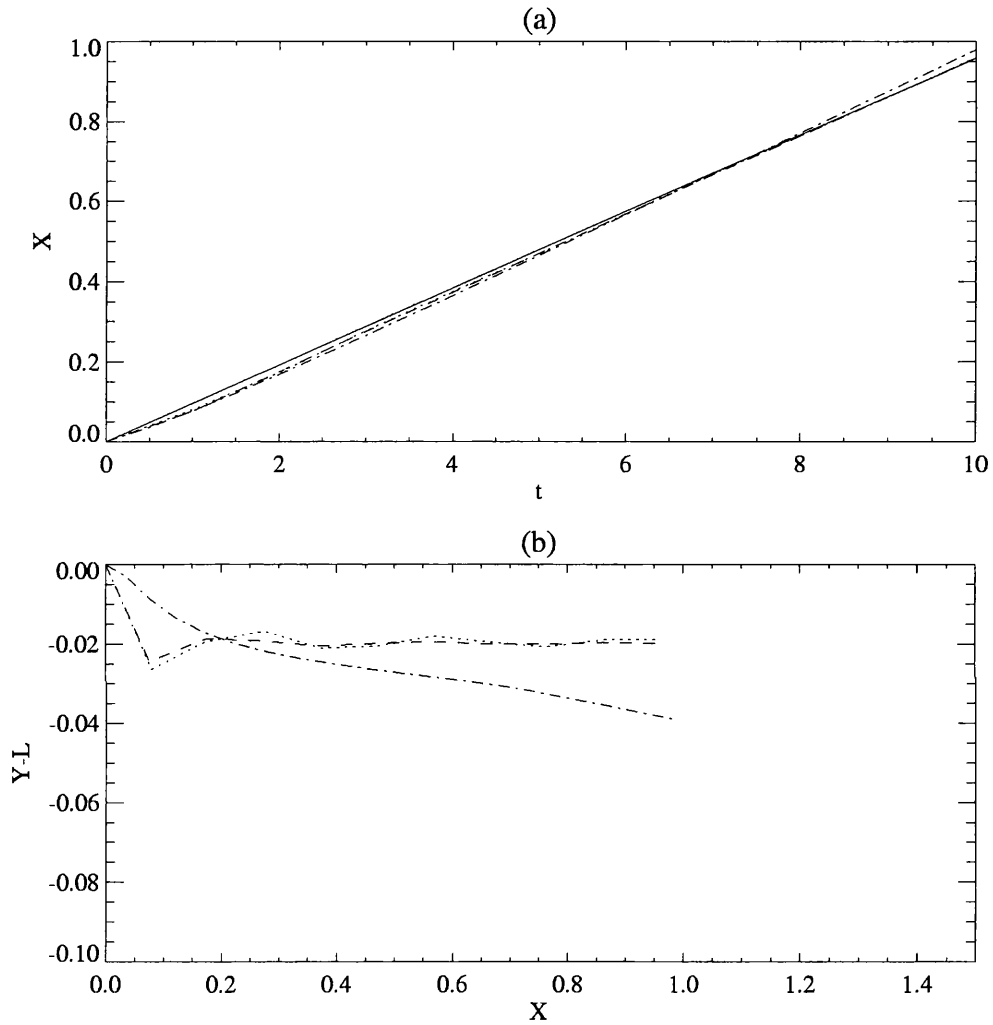
Figure 6.12: A plot of the trajectory of the vortex centre for a weak ($\epsilon = 0.2$) off shelf cyclone for various pairs (W, L). The dotted line is for $(W, L) = (1, 1.5)$, the dashed line is $(W, L) = (0.5, 1)$ and the dot-dashed line is $(W, L) = (0.1, 0.6)$. The plots are for $0 < t < 10$. (a) is a plot of the x coordinate of the vortex centre compared with the prediction given in (6.50a) (solid line) and (b) shows the displacement of the vortex centre form its initial position.

Figure (6.13) shows the evolution of the contour for $W = 1$ and $L = 1.5$. The pseudoimage is apparent as are the topographic waves which propagate away from the vortex. There is no evidence for wave radiation for the times of the runs shown here.

Figure (6.14) shows the contour evolution for the case $W = 0.1$ and $L = 0.6$. As in the case of an anticyclone, the topographic waves appear to be nondispersive. Note also the nonlinear response of the pseudoimage at late times which is evident in the final frame.

Finally consider Figure (6.15) which is an example of an off shelf vortex moving at a speed near the group velocity of the topographic waves. Here $\epsilon = 0.1$, $W = 0.3$ and $L = 1.67$ the same values used to obtain the FFT plot shown in Figure (6.7). The disturbance grows, but is unable to escape from the vicinity of the vortex even at large times. Eventually the response becomes nonlinear. The trajectory of the vortex is shown in Figure (6.16). Note the very slow drift of the vortex in the y-direction.

On shelf vortex

Results are presented here for an on shelf vortex with $W = 1.5$ and $L = 0.5$. Figure (6.17) shows the drift in the x-direction of the vortex centre for an anticyclone and a cyclone. In each case the solid line shows the position predicted by equation (6.54a) and where the calculation has included enough terms of the series to give accuracy to 6 decimal places. Once again the pseudoimage gives an accurate prediction of the vortex drift.

Figure (6.18) shows the contour evolution for the cyclone. Note the pseudoimage and the dispersive waves ahead of it. There is some evidence of wave radiation at later times.
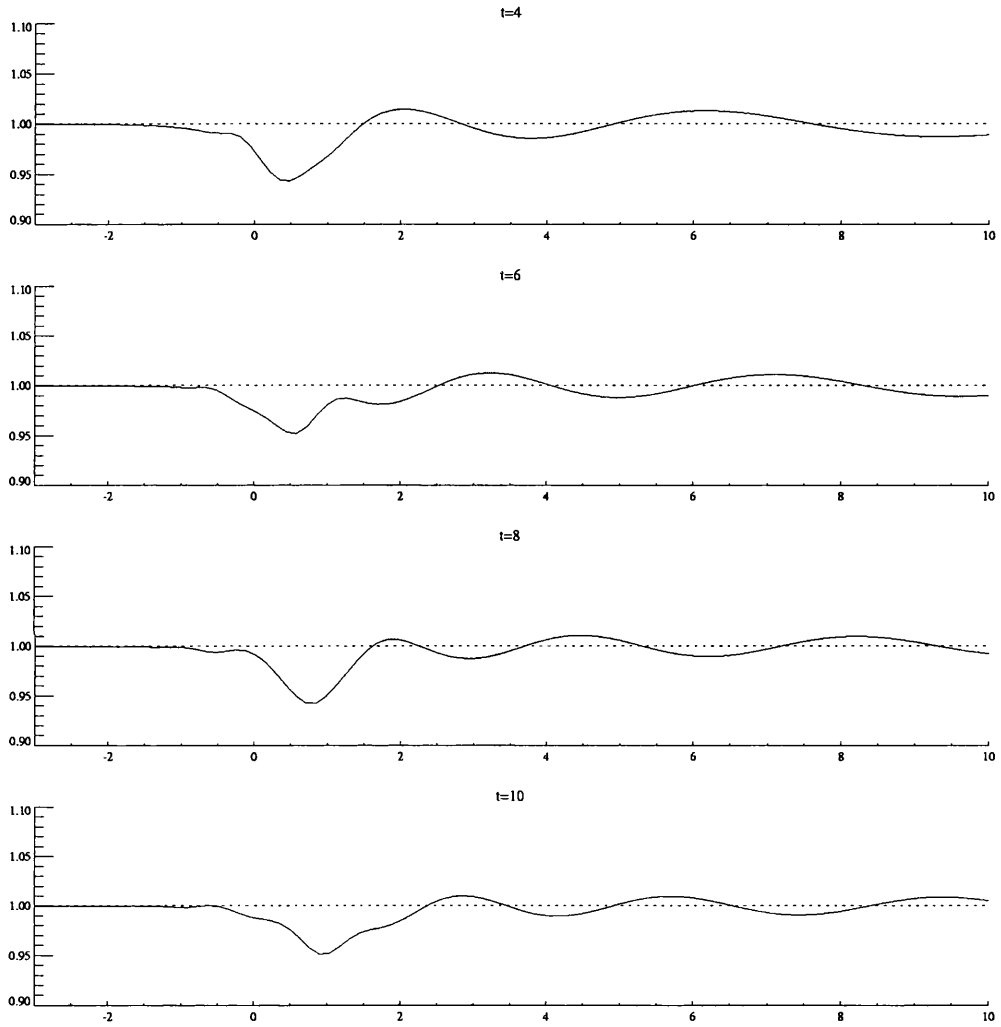
Figure 6.13: The evolution of the contour for a weak ($\epsilon = 0.2$) off shelf cyclone. The parameter values used are $W = 1$ and $L = 1.5$.
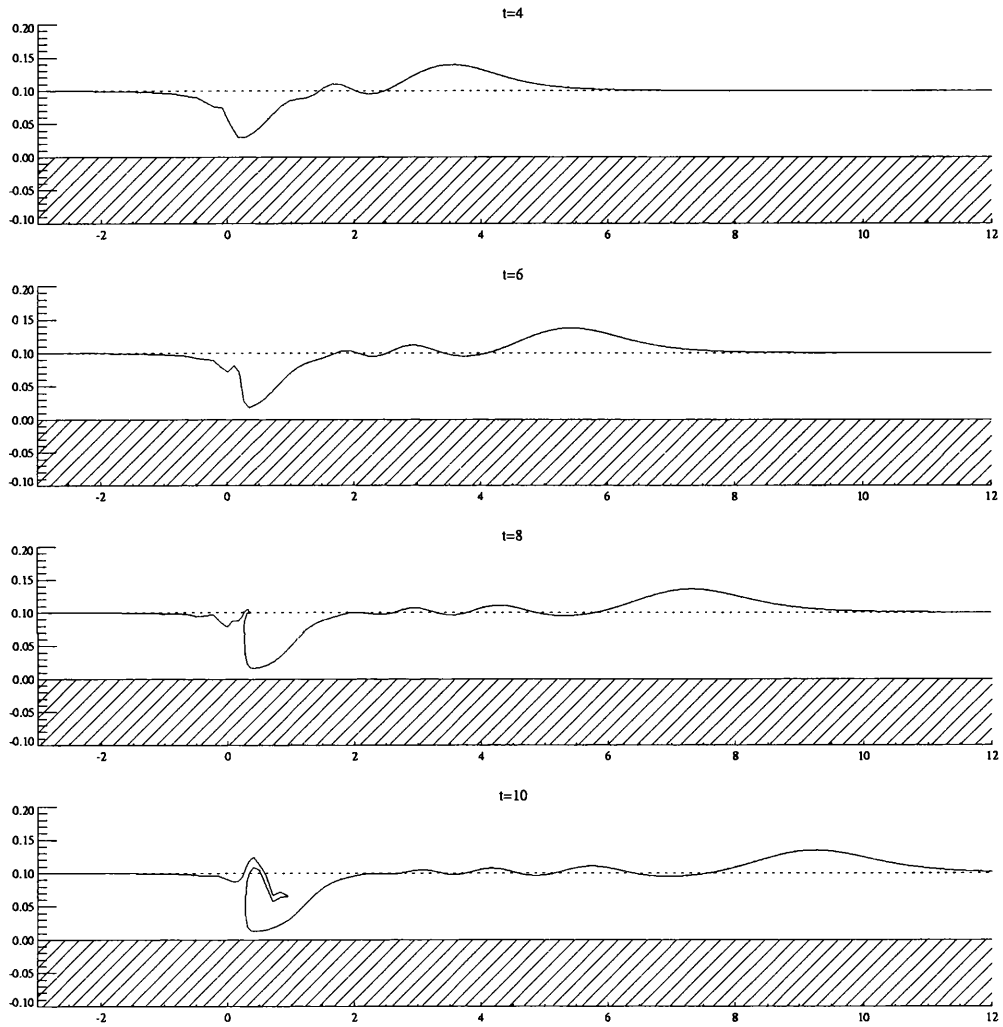
Figure 6.14: The evolution of the contour for a weak ($\epsilon = 0.2$) off shelf anticyclone. The parameter values used are $W = 0.1$ and $L = 0.6$.
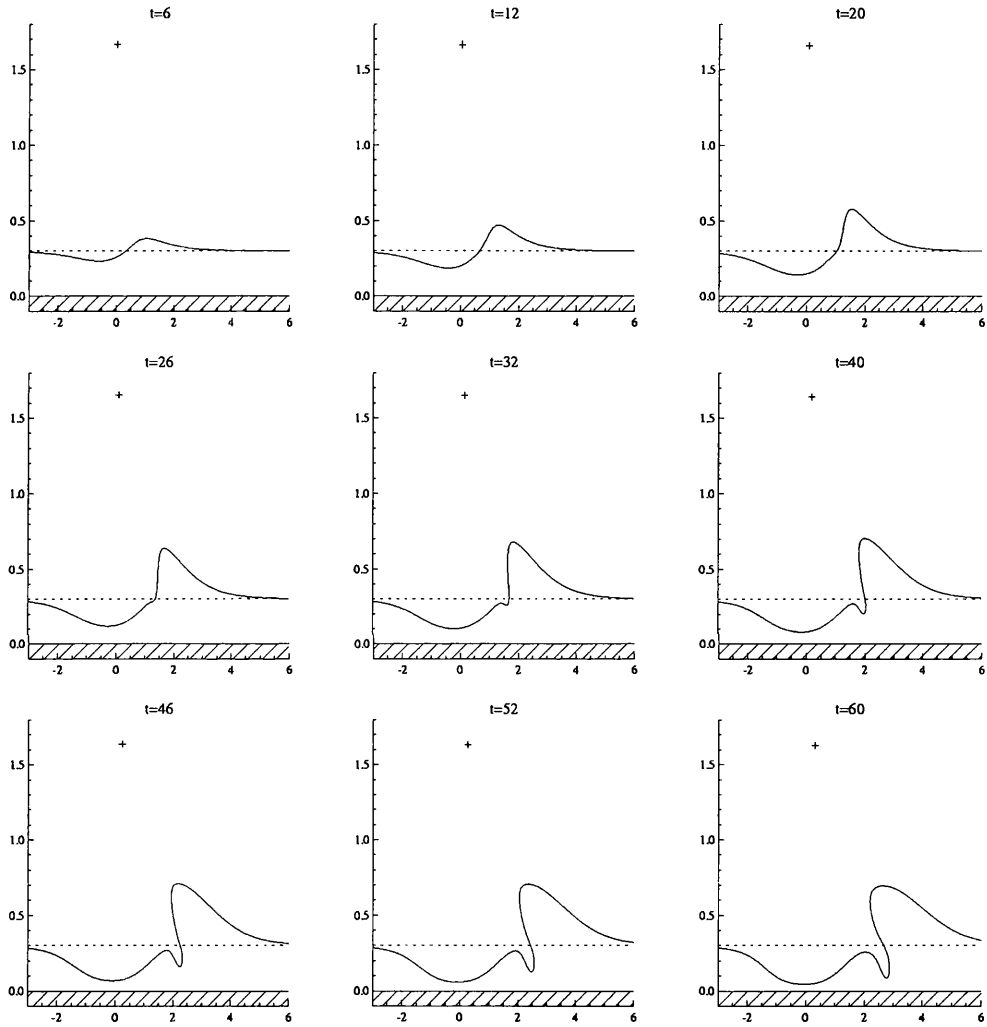
Figure 6.15: The evolution of the contour for a weak ($\epsilon = 0.1$) off shelf cyclone moving at the topographic long wave speed. The parameter values used are $W = 0.3$ and $L = 1.67$.
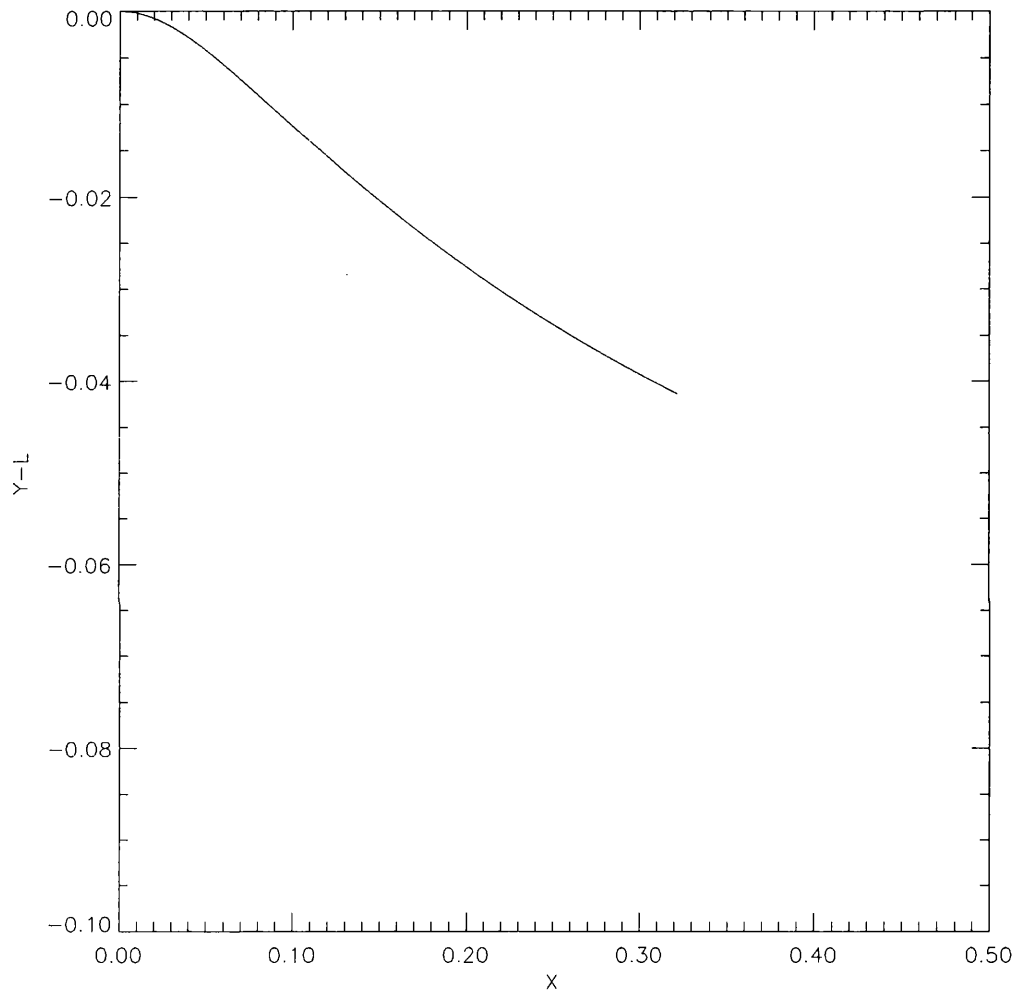
Figure 6.16: The trajectory of the vortex centre for a weak ($\epsilon = 0.1$) off shelf cyclone moving at the topographic long wave speed, for $0 < t < 60$. The parameter values used are $W = 0.3$ and $L = 1.67$.
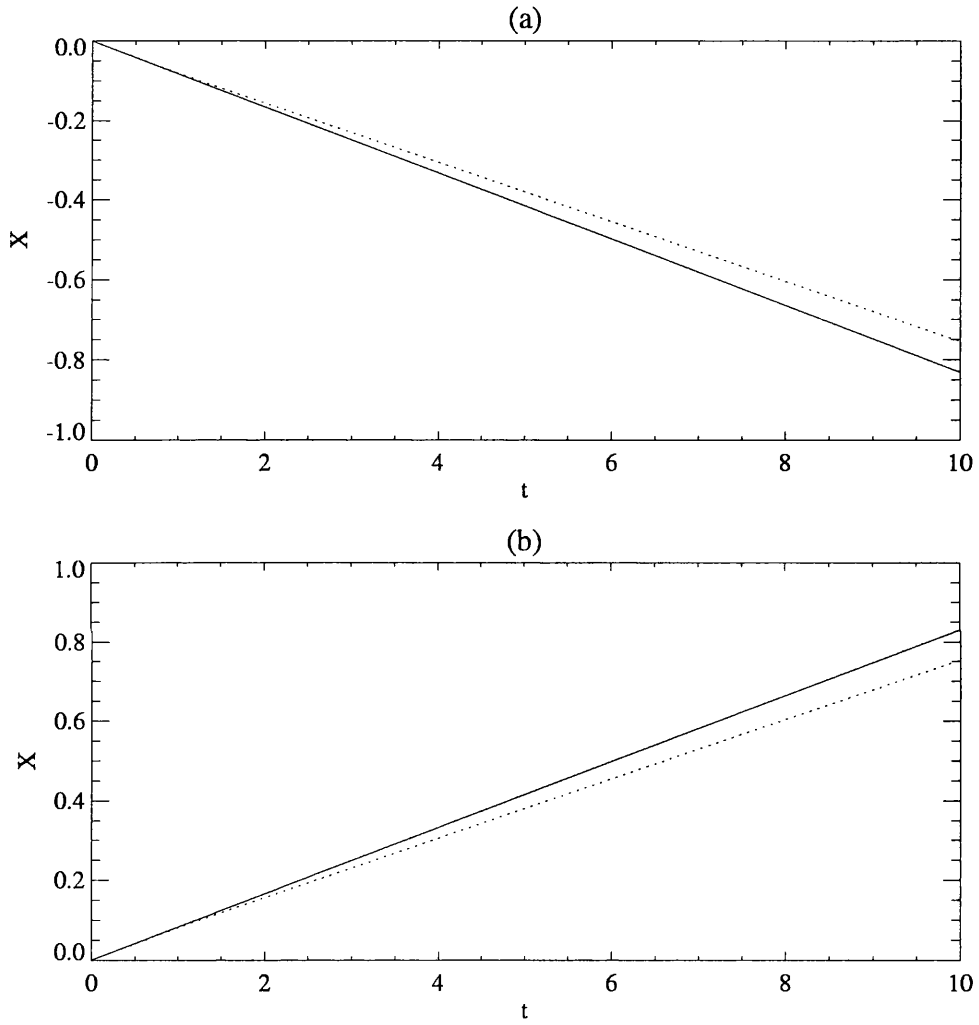
Figure 6.17: The trajectory of the vortex centre for a weak ($\epsilon = 0.2$) on shelf vortex for $0 < t < 10$. The parameter values used are $W = 1$ and $L = 0.5$. (a) anticyclone (b) cyclone.
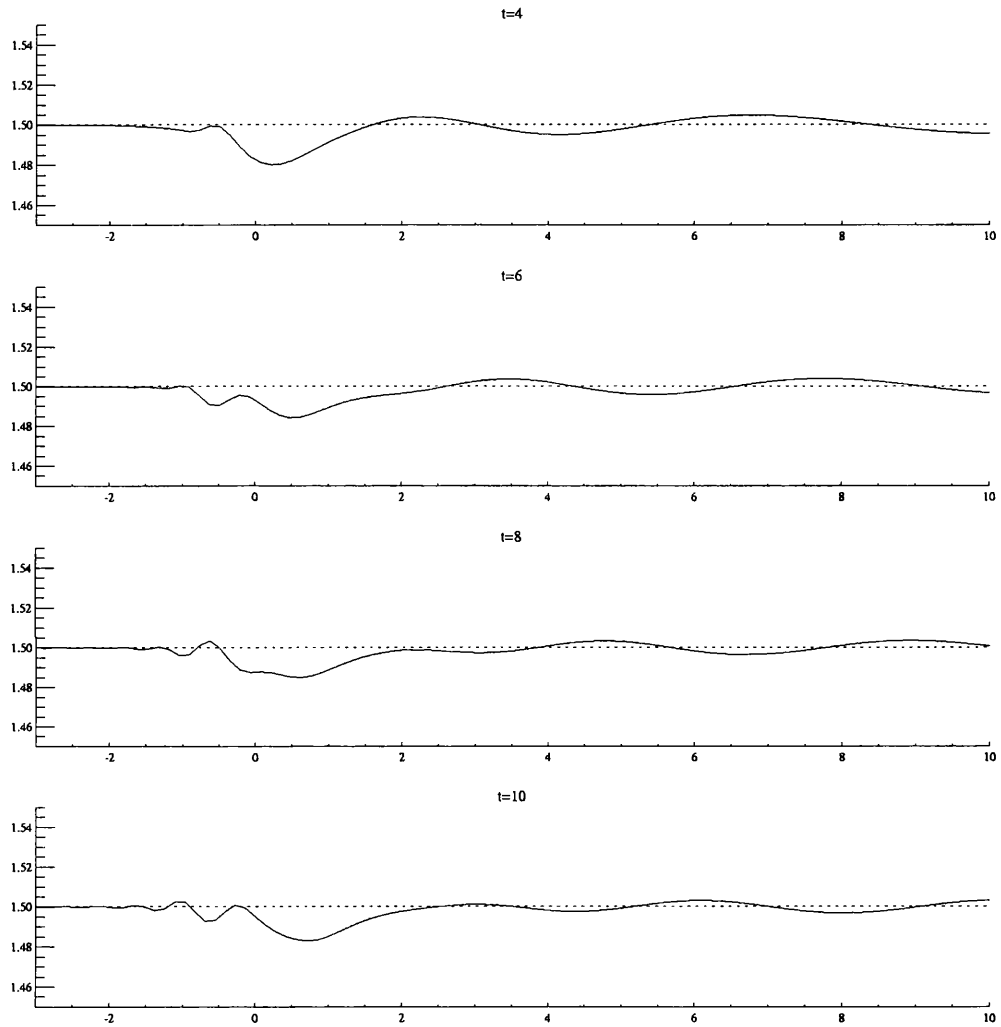
Figure 6.18: The evolution of the contour for a weak on shelf cyclone. The parameter values used are $W = 1.5$, $L = 0.5$ and $\epsilon = 0.2$.

6.3 An intense singular vortex

It is anticipated that some analytical progress is possible in the limit that the vortex is intense, i.e. $S \ll 1$. Here, however, an investigation of the problem is made using only contour dynamics simulations. Some of the important elements of the problem are highlighted.

Before proceeding some comments regarding the general features of the motion may be made. The velocity of the vortex due to its image in the wall is

$$u = -\frac{\Gamma}{2\pi} K_1(2L), \tag{6.89}$$

i.e. the image advects an anticyclone in the direction of decreasing x (hereafter identified as east) and similarly a cyclone is advected in the direction of increasing x (west). On the other hand the velocity induced at the vortex centre due to the deflected topographic contour is such that anticyclones drift southeast and cyclones drift northeast. Hence the secondary circulations enhance the eastward drift of a cyclone and retard the westward drift of an anticyclone. The magnitude of the velocity due to the image is a function of L, and the magnitude of the velocity due to the deflected contour is $O(S)$ and also a function of $|L - W|$, i.e. the distance of the vortex from the escarpment. It is expected that if $L \approx 1$, then the drift of the vortex will be dominated by the image, and if $L \gg 1$ but $|L - W| \approx 1$ then the effect of the image (i.e. the wall) will be weak in comparison with the effect of the deformed contour.

6.3.1 An off shelf vortex

In this subsection results are presented for intense vortices with $L > W$, i.e. vortices located off the shelf. The distance $L - W$ of the vortex from the escarpment is kept fixed at the value 0.5 and the width of the shelf W varies. In all the case given here the value of the parameter S is 0.1. The cases of an anticyclone and a cyclone are treated separately.

Anticyclones

The results of three simulations are given here. The first has $W = 1$ and $L = 1.5$, the second has $W = 0.5$ and $L = 1$ and the third has $W = 0.1$ and $L = 0.6$. Figure (6.19) shows a plot of the trajectories of the vortex centre in each of these cases. The displacement from the initial position $(X, Y - L)$ is plotted for easy comparison, and the solid line shows the analytic prediction of the

trajectory in the absence of the wall, obtained by numerical integration of equations (4.96a,b). For $L = 1.5$ the vortex drift is close to that expected in the absence of the wall, and the eastward drift is only slightly retarded by the image. This is expected since the velocity due to the image vortex decreases exponentially with L, and so in this case the velocity due to the deflected contour dominates the motion. As L is decreased the effect of the image becomes stronger, and for $L = 0.6$ the vortex drift is mainly longshore and the effect of the deflected contour only slightly modifies the velocity due to the image.

Figures (6.20) - (6.22) show the evolution of the contour for the same cases. For $W = 1$ and $L = 1.5$ the contour evolution is very similar to that in the absence of the wall. In Figure (6.21) the contour evolution for the case $W = 0.5$ and $L = 1$ is plotted. Again the flow in the vicinity of the vortex is predominantly axisymmetric. In Figure (6.22), showing the evolution of the contour for $W = 0.1$ and $L = 0.6$, the flow pattern resembles the atmosphere of a singular vortex dipole. This statement is reinforced by considering Figure (6.23) which shows the formation of a singular vortex dipole atmosphere[2]. The plot was obtained by placing a square array of 2500 points over the initial position $(0, \pm 1)$ of the vortex pair. The points were advected by fourth order Runge-Kutta according to the velocity field due to the vortices.

Cyclones

Results are presented for off shelf cyclones for the same parameter values as the case of off shelf intense anticyclones, i.e. $W = 1$ and $L = 1.5$, $W = 0.5$ and $L = 1$ and $W = 0.1$ and $L = 0.6$. Figure (6.24) shows a plot of the trajectories of the vortex centre in each of these cases. The displacement from the initial position $(X, Y - L)$ is plotted and the solid line shows the analytic prediction of the trajectory in the absence of the wall. The same general trends are apparent as for the case of an intense off shelf anticyclone described previously. For $L = 1.5$ the vortex drift is close to that expected in the absence of the wall, and the eastward drift is slightly enhanced by the image. As L is decreased the effect of the image becomes stronger, and for $L = 0.6$ the vortex drift is mainly longshore and the effect of the deflected contour only slightly modifies the velocity due to the image.

Figures (6.25) - (6.27) show the evolution of the contour for the same cases. Exactly the same observations as for the anticyclones may be made. For $W = 1$ and $L = 1.5$ the contour evolution

---

[2]Note that the sense of the circulation of the dipole in Figure (6.23) is opposite to the anticyclones under consideration. The point made here is nonetheless the same. The use of the term 'atmosphere' for a dipole is due to Thomson (1867)
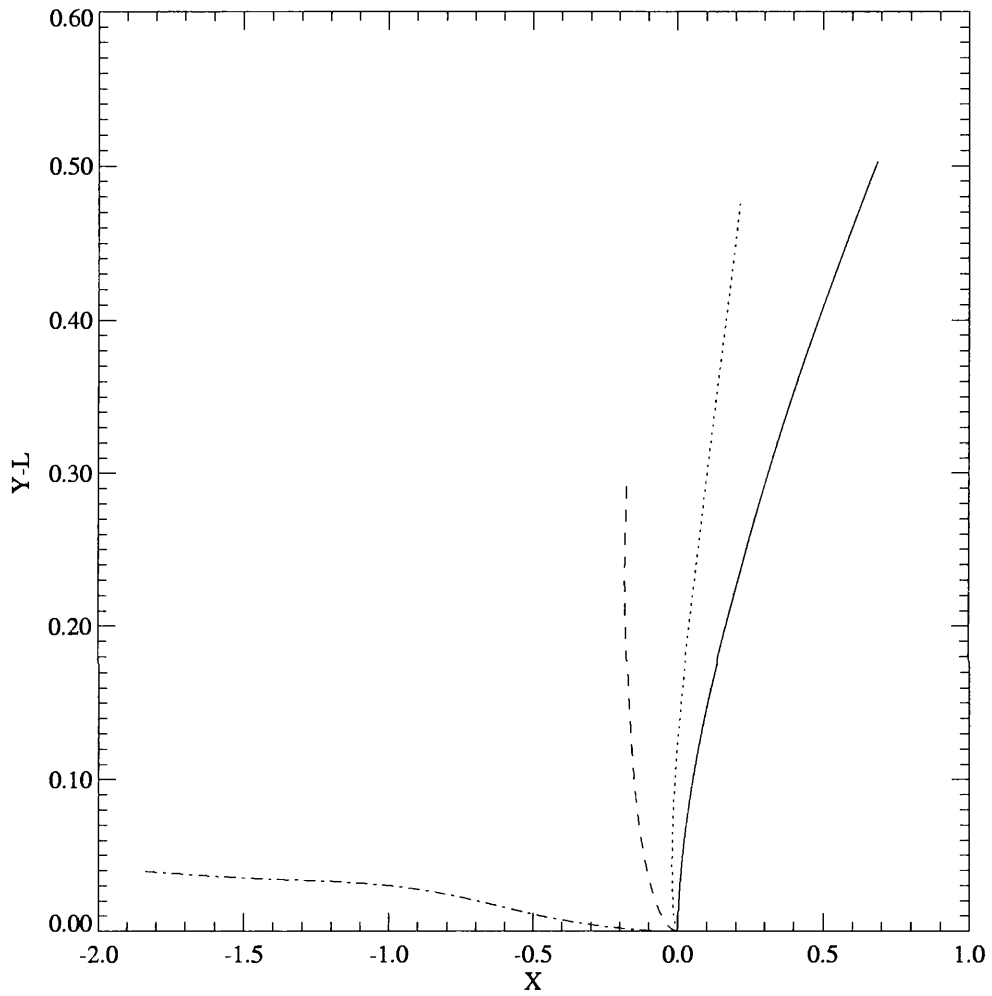
Figure 6.19: A plot of the trajectory of the vortex centroid for various values of L and W for an intense anticyclone. The parameters used are $S = 0.1$ and $\Gamma = 1$ with $L - W = 0.5$ fixed. The solid line shows the analytic prediction for a singular vortex located distance 0.5 from an escarpment in the absence of a wall. The other curves are for $W = 1$, $L = 1.5$ (dotted line), $W = 0.5$ and $L = 1$ (dashed line), $W = 0.1$ and $L = 0.6$ (dot-dashed line). The trajectories are shown for $0 < t < 30$. See text for further comments.
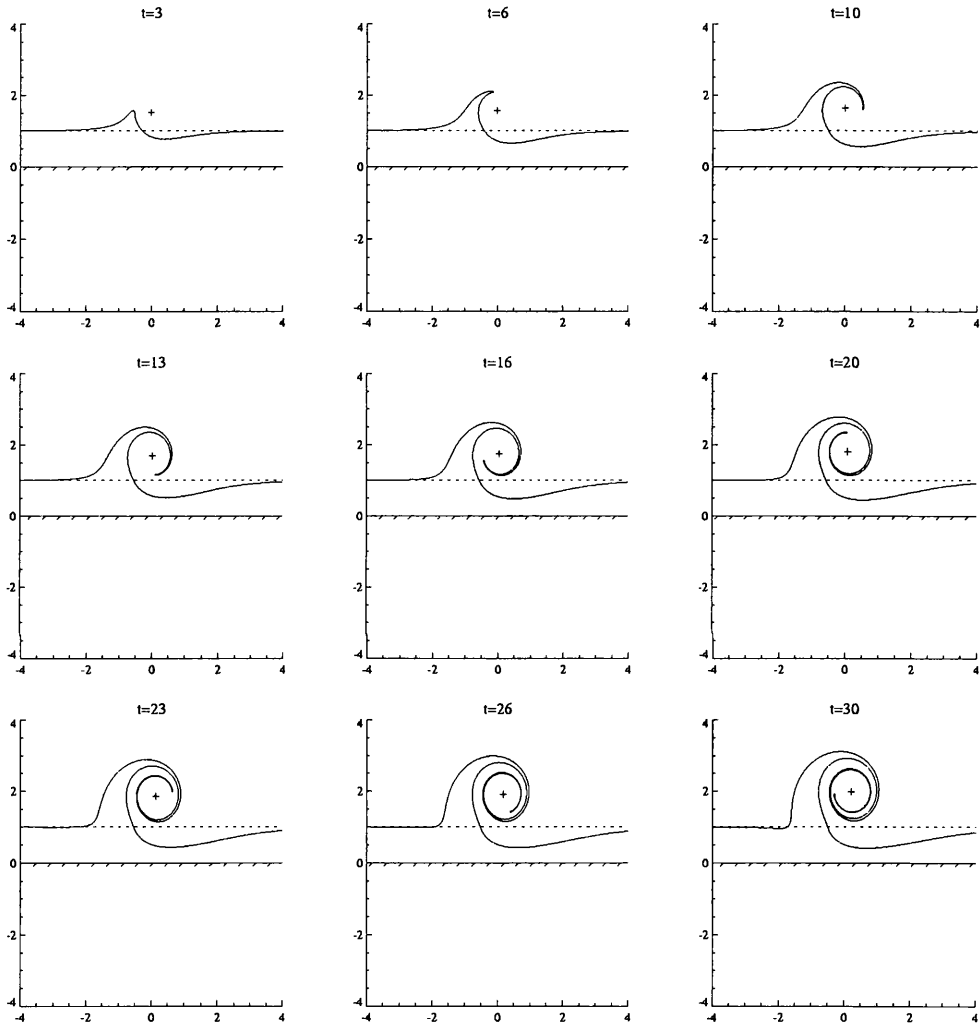
Figure 6.20: The evolution of the contour for an intense off-shelf anticyclone. The parameter values used are $S = 0.1$, $\Gamma = 1$, $W = 1$ and $L = 1.5$.

199
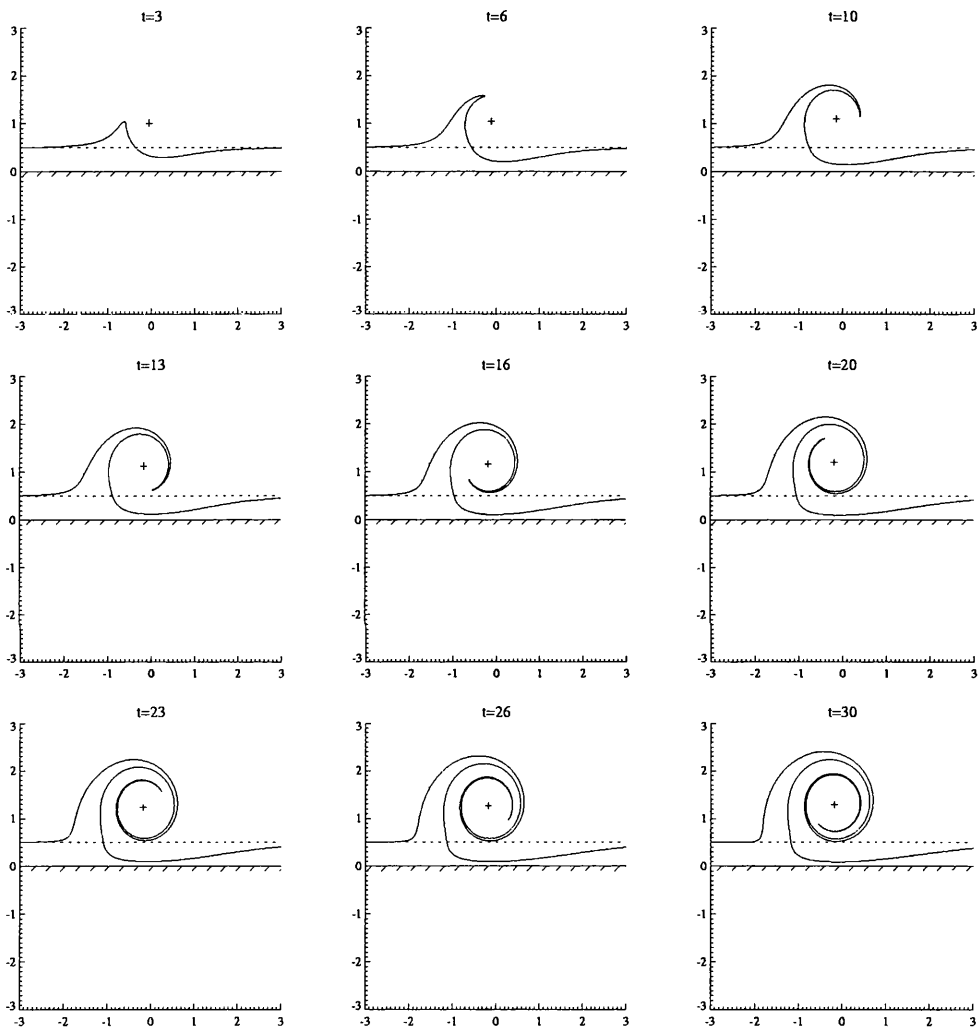
Figure 6.21: As for Figure (6.20) except $W = 0.5$ and $L = 1$.
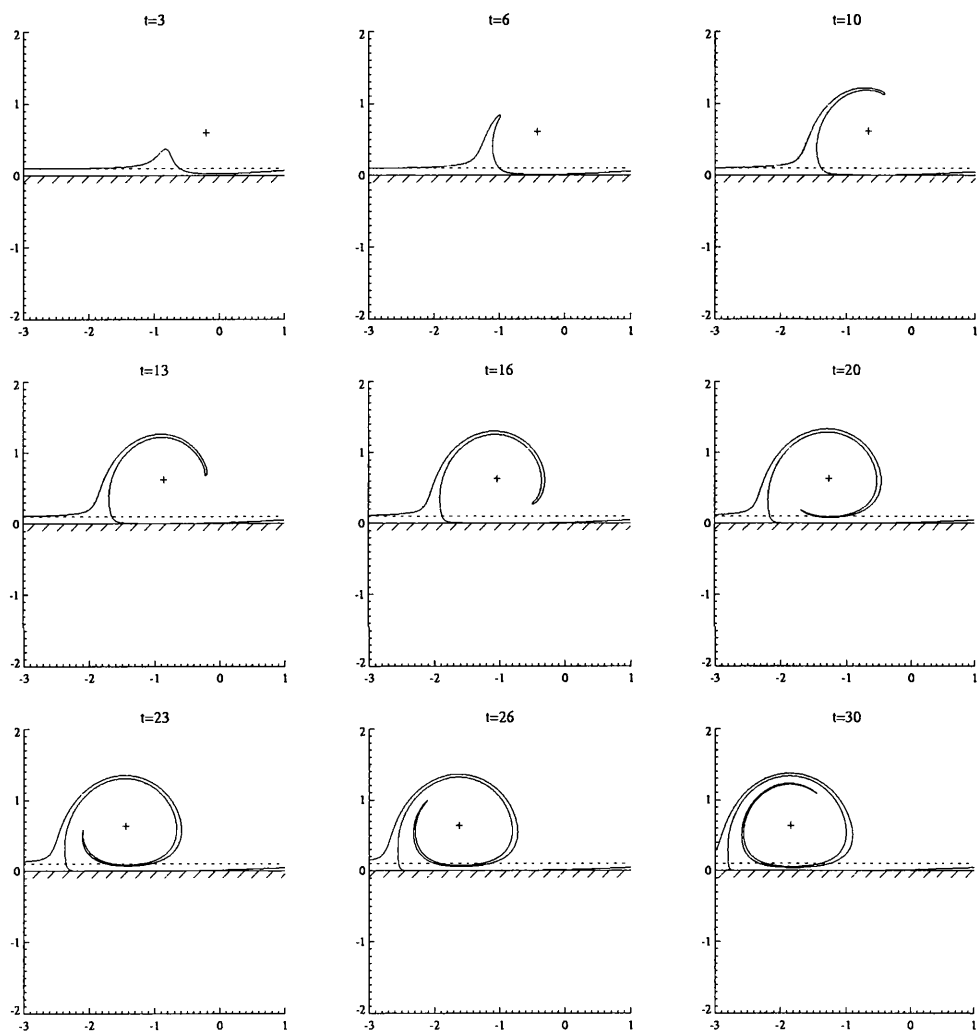
Figure 6.22: As for Figure (6.20) except $W = 0.1$ and $L = 0.6$.
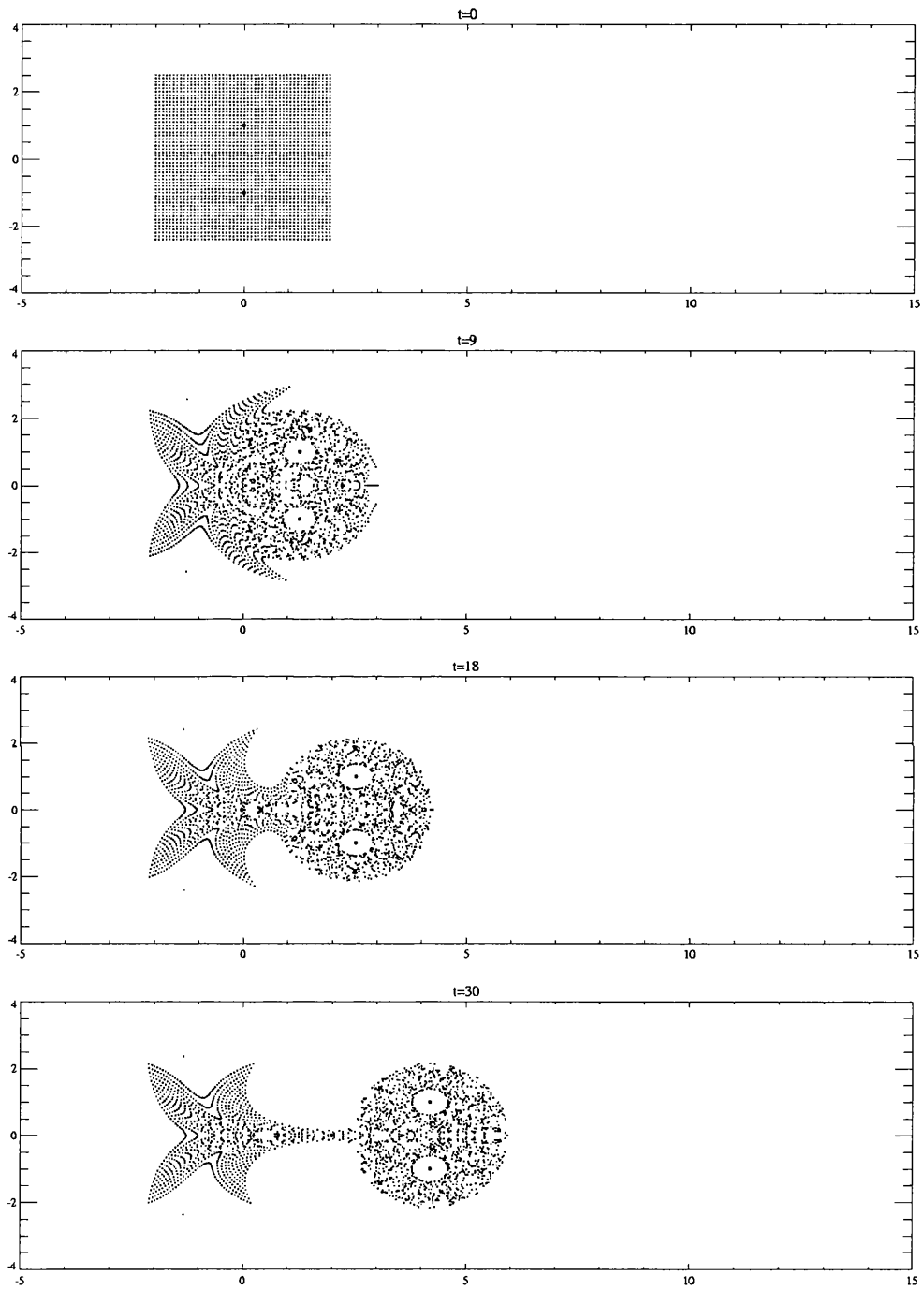
Figure 6.23: The formation of a dipole atmosphere. See text for further comments.
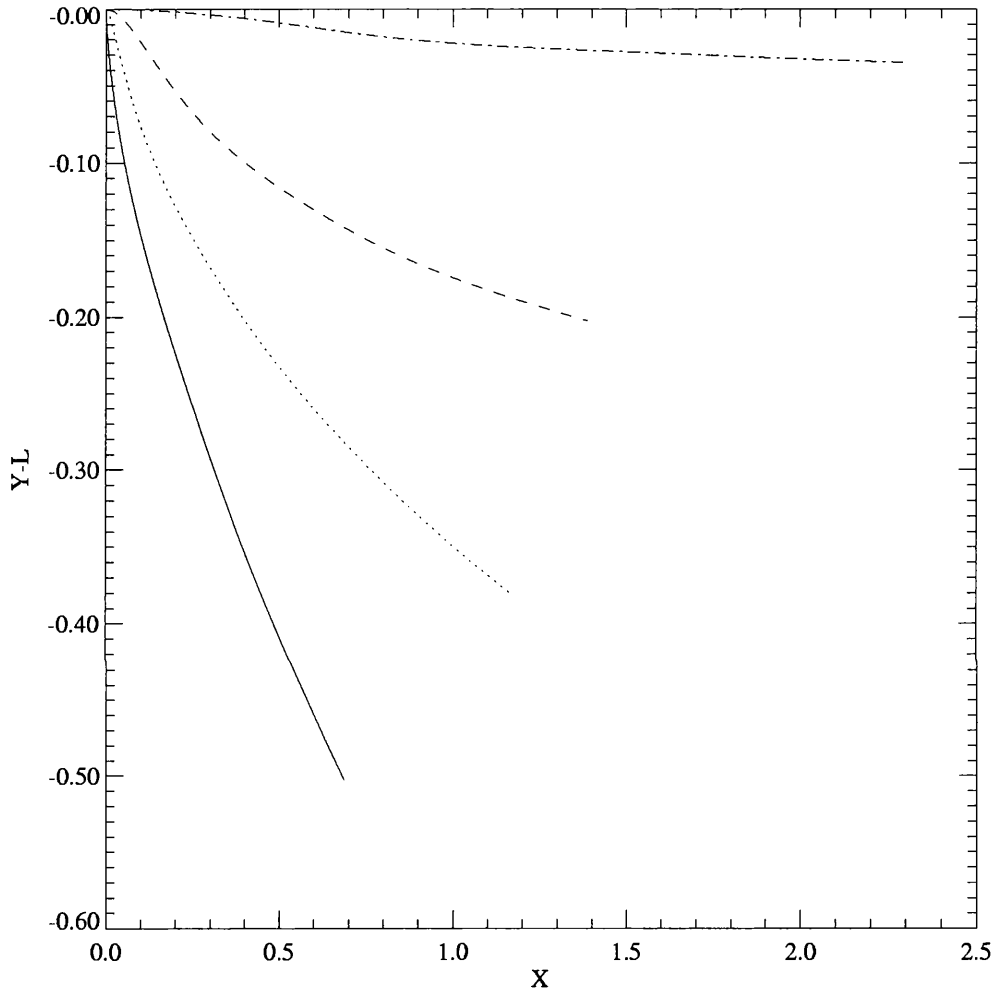
Figure 6.24: A plot of the trajectory of the vortex centroid for various values of L and W for an intense cyclone. The parameters used are $S = 0.1$ and $\Gamma = -1$ with $L - W = 0.5$ fixed. The solid line shows the analytic prediction for a singular vortex located distance 0.5 from an escarpment in the absence of a wall. The other curves are for $W = 1$, $L = 1.5$ (dotted line), $W = 0.5$ and $L = 1$ (dashed line), $W = 0.1$ and $L = 0.6$ (dot-dashed line). The trajectories are shown for $0 < t < 30$. See text for further comments.

is very similar to that in the absence of the wall. In Figure (6.21) the contour evolution for the case $W = 0.5$ and $L = 1$ is plotted. Again the flow in the vicinity of the vortex is predominantly axisymmetric. In Figure (6.22), showing the evolution of the contour for $W = 0.1$ and $L = 0.6$, the flow pattern resembles the atmosphere of a singular vortex dipole, similarly to the case of an anticyclone with the same parameter values. It may be inferred that the leading order effect in the flow is that of the vortex and its image.
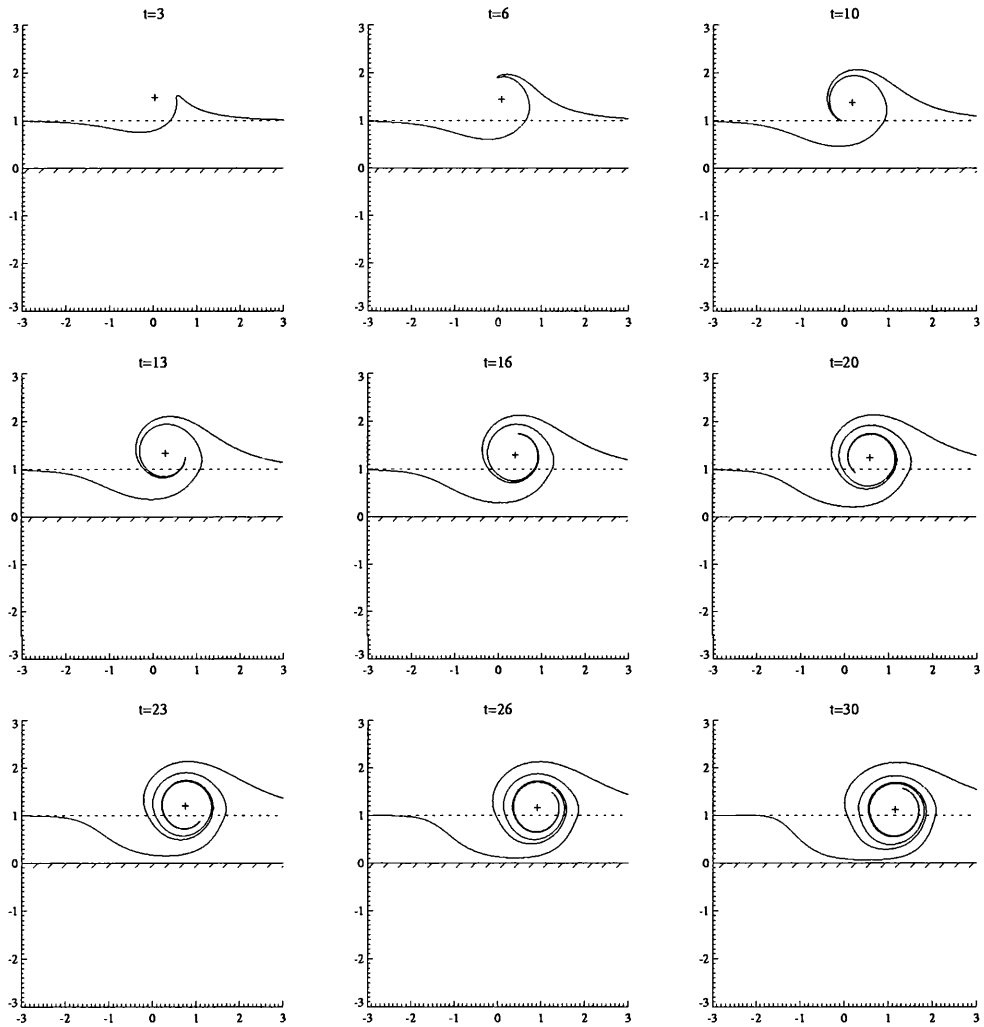
Figure 6.25: The evolution of the contour for an intense off-shelf anticyclone. The parameter values used are $S = 0.1$, $\Gamma = 1$, $W = 1$ and $L = 1.5$.

205
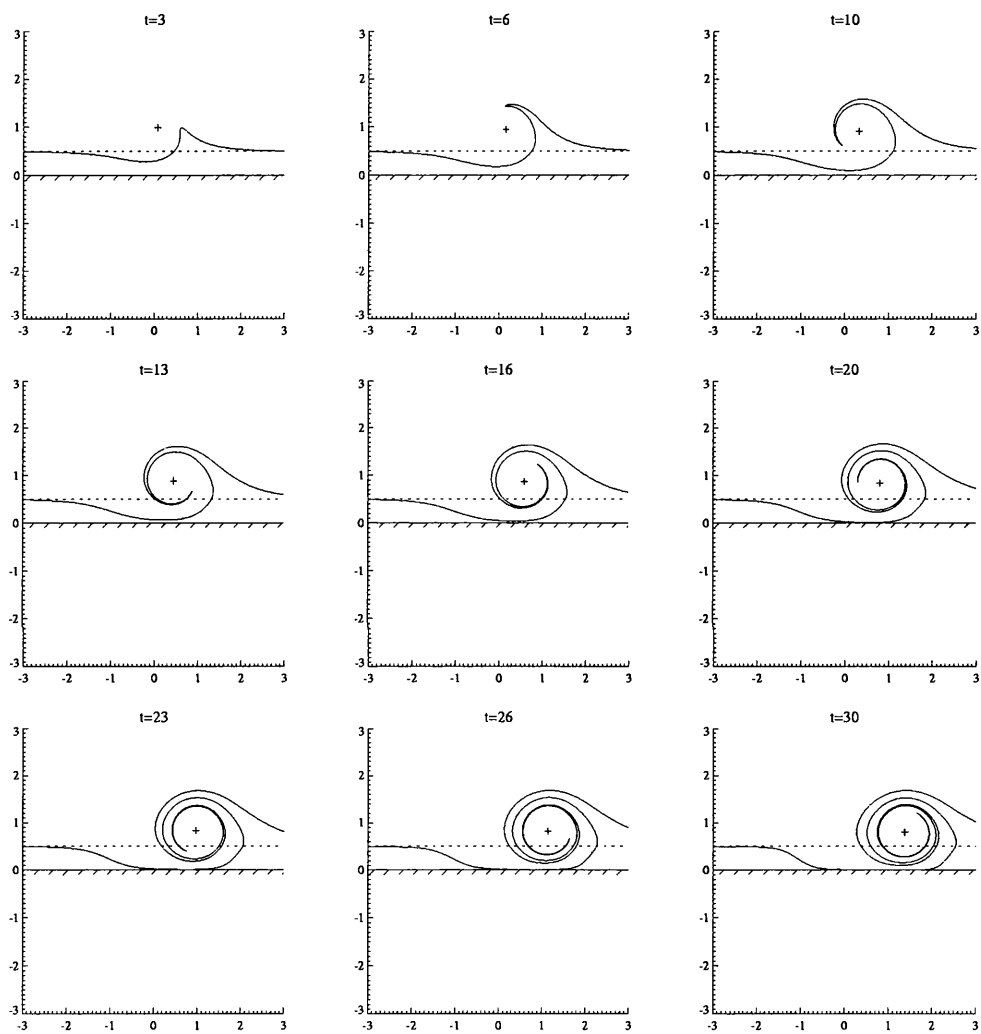
Figure 6.26: As for Figure (6.25) except $W = 0.5$ and $L = 1$.
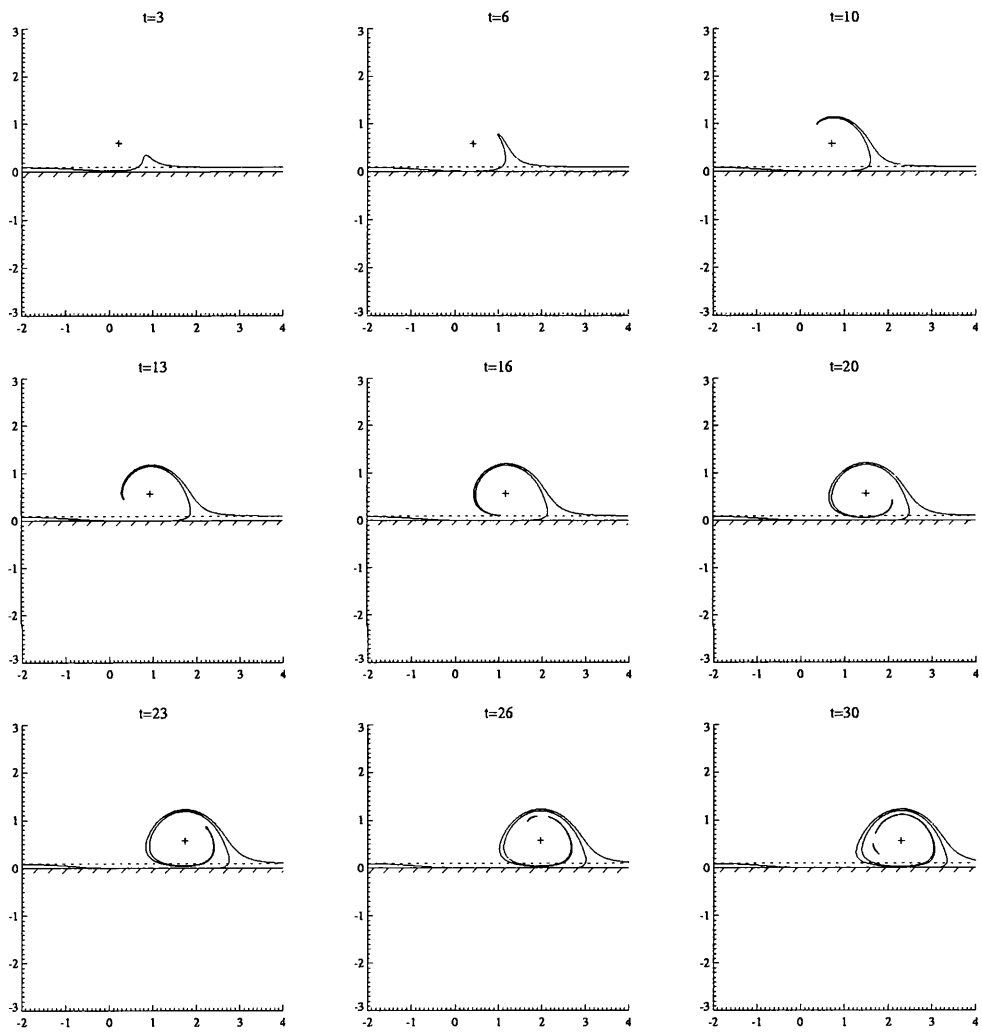
Figure 6.27: As for Figure (6.25) except $W = 0.1$ and $L = 0.6$.

6.3.2 An on shelf vortex

In this section results are presented for just one set of parameters for an intense on shelf vortex. Specifically the case given is $W = 1$ and $L = 0.5$ and for the value $S = 0.1$. The simple conclusion drawn here is that, as expected, the influence of the image on the vortex dominates the motion. Figure (6.28) shows the trajectory of the vortex centres. The drift is primarily long shore, and the deflected contour only induces a slight meridional motion.

The contour evolution for an anticyclone is shown in Figure (6.29) and for a cyclone in Figure (6.30). The anticyclone begins to capture and wrap the contour, but at later times the flow pattern once again resembles that of a dipole. The vortex entrains fluid from both sides of the escarpment and will transport this fluid far along the coast with little influence from the escarpment. The cyclone fails to capture the contour and moves away to the west, only entraining fluid initially located on the shelf. In other words the anticyclones 'collides' with the cross-escarpment fluid whilst the cyclone moves rapidly away from the cross-escarpment fluid.
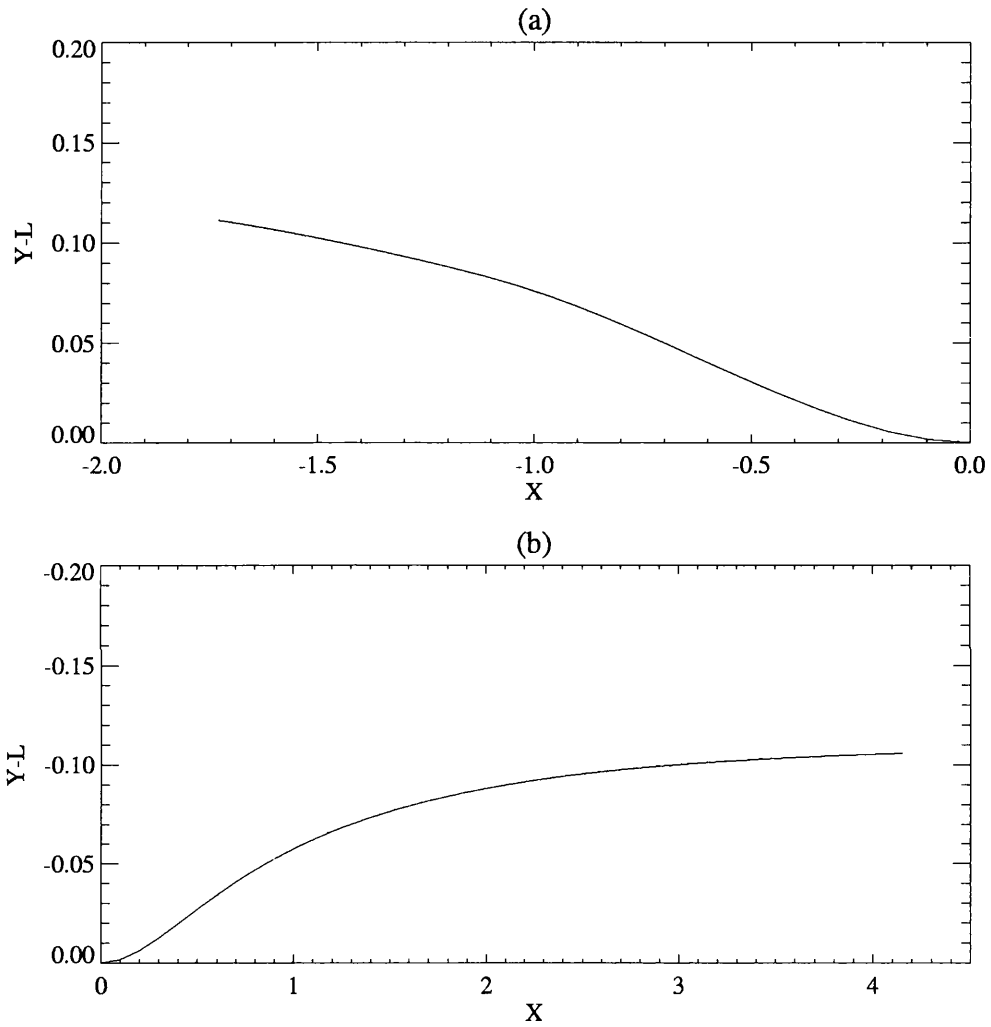
Figure 6.28: The trajectory of the vortex centre for an on shelf intense vortex. The parameter values used are $W = 1$, $L = 0.5$ and $S = 0.1$, for $0 < t < 30$. (a) is the trajectory for an anticyclone ($\Gamma = 1$) and (b) is the trajectory of a cyclone ($\Gamma = -1$).
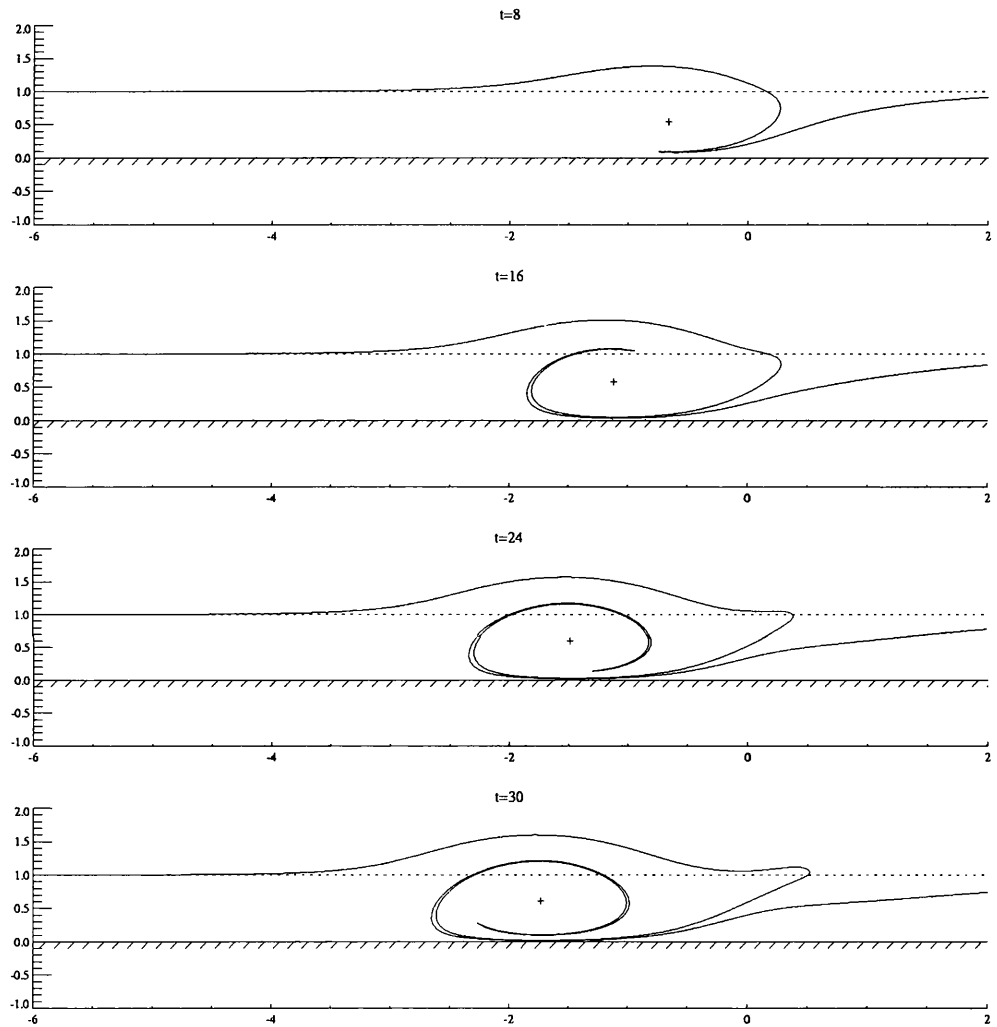
Figure 6.29: The evolution of the contour for an intense on-shelf anticyclone. The parameter values used are $S = 0.1$, $\Gamma = 1$, $W = 1$ and $L = 0.5$.
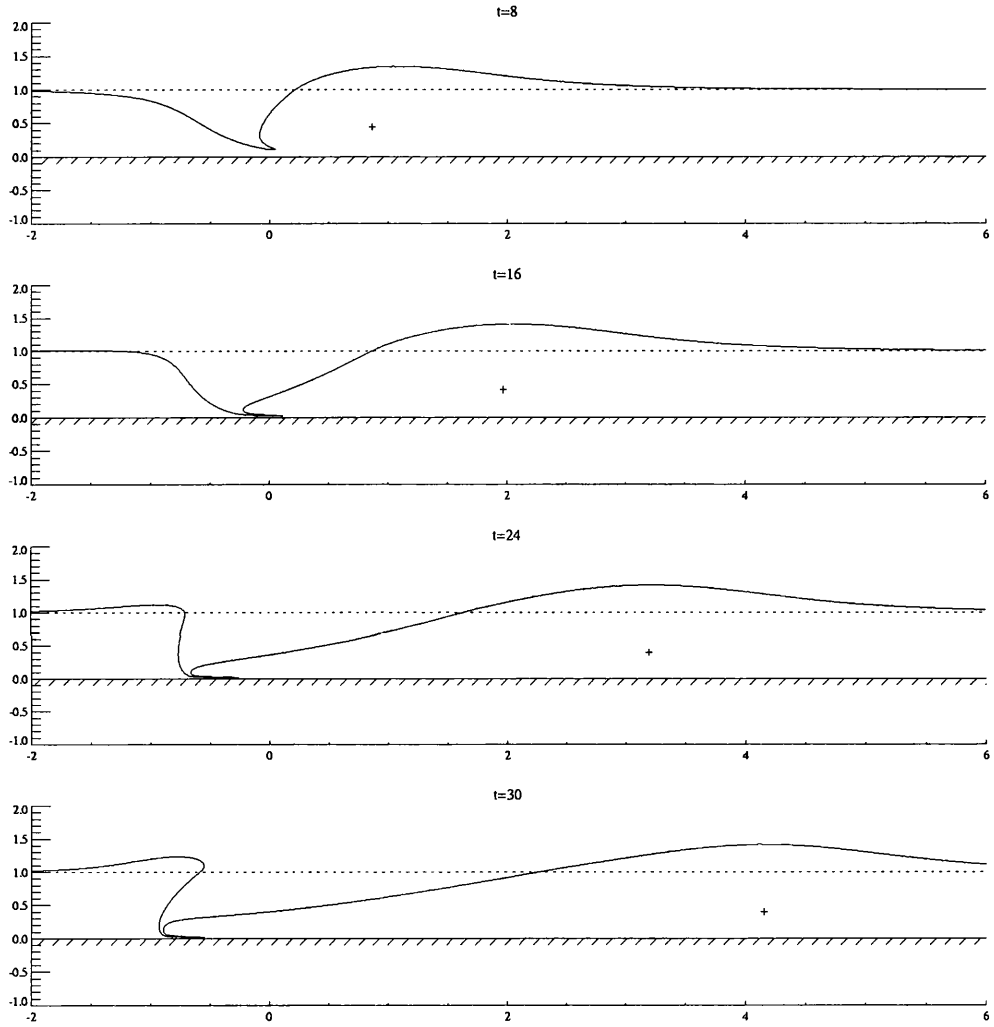
Figure 6.30: The evolution of the contour for an intense on-shelf cyclone. The parameter values used are $S = 0.1$, $\Gamma = 1$, $W = 1$ and $L = 0.5$.

211

6.4 A moderate intensity vortex

In this subsection some preliminary contour dynamics results for the case $S = 1$ of a moderate intensity vortex are given. The values of W and L chosen are the same as those for the intense vortex described in the previous section.

6.4.1 An off shelf vortex

In this subsection results are presented for moderate vortices with $L > W$, i.e. vortices located off the shelf. For consistency with the results presented for the intense vortex limit the distance $L - W$ of the vortex from the escarpment is kept fixed at the value 0.5 and the width of the shelf W varies. In all the case given here the value of the parameter S is 1. The cases of an anticyclone and a cyclone are treated separately.

Anticyclones

The results of three simulations are given here. The first has $W = 1$ and $L = 1.5$, the second has $W = 0.5$ and $L = 1$ and the third has $W = 0.1$ and $L = 0.6$. Figure (6.31) shows a plot of the trajectories of the vortex centre in each of these cases. The displacement from the initial position $(X, Y - L)$ is plotted for easy comparison. In all cases the anticyclones migrate away from the escarpment in the looping motion characteristic of dipoles with cells of opposite but unequal circulations. The motion is very similar to that of the analogous case of cyclones located on the shallow side of the escarpment in the absence of the wall (see subsection 4.4.2 and figures therein).

The contour evolution in these three cases is shown in Figures (6.32) - (6.34) and confirms that dipoles are indeed formed between the primary vortex and fluid originally located on the shelf which has been advected off the shelf by the vortex and which has gained, via vortex stretching, net cyclonic relative vorticity as a result. The process of dipole formation appears to be the trend for all the values of W presented here. Note however the difference between the present case and the analogous case of a moderate cycloe located on the shallow side of the escarpment in the absence of the wall. In particular, consider Figure (6.24). The cyclonic 'blob' of fluid that pairs up with the primary vortex turns back toward the wall and by $t = 30$ is sufficiently close to the wall that the effect of the images of both the primary vortex and the secondary patch of fluid is likely to dominate the
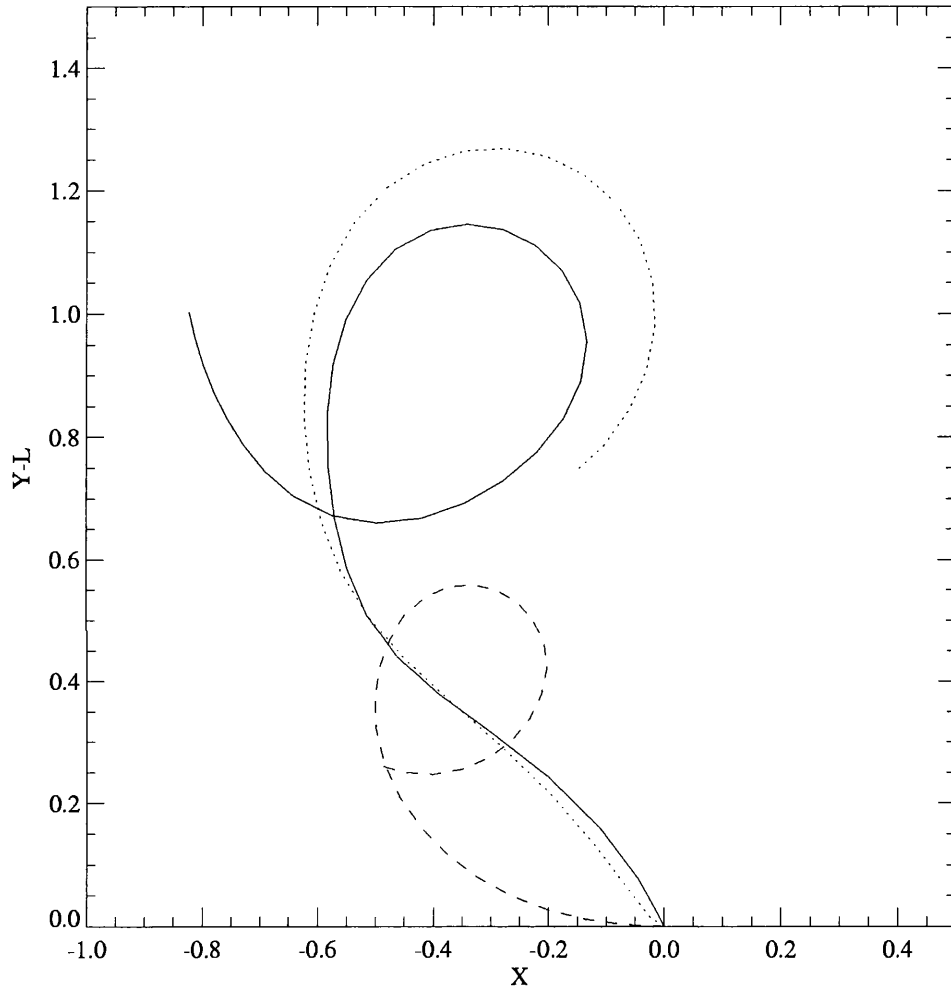
Figure 6.31: A plot of the trajectory of the vortex for various values of L and W for a moderate anticyclone, for $0 < t < 30$. The parameters used are $S = 1$ and $\Gamma = 1$ with $L - W = 0.5$ fixed. The curves are for $W = 1$, $L = 1.5$ (solid line), $W = 0.5$ and $L = 1$ (dotted line), $W = 0.1$ and $L = 0.6$ (dashed line). See text for further comments.

influence of the primary vortex.

Cyclones

The results of three simulations are given here for the same parameter values as presented for the case of an off shelf moderate anticyclone. Figure (6.35) shows a plot of the trajectories of the vortex centre in each of these cases. The displacement from the initial position $(X, Y - L)$ is plotted for easy comparison. In all cases the cyclones migrate towards the wall and climb on to the shelf. Once on the shelf the image of the vortex becomes highly influential and the cyclones move parallel to the wall to the west.

The contour evolution in these three cases is shown in Figures (6.36) - (6.38). The general trend is for the vortices to move toward the escarpment. In doing so they come under the influence of the image which then carries them far away from the initial disturbance in the contour.
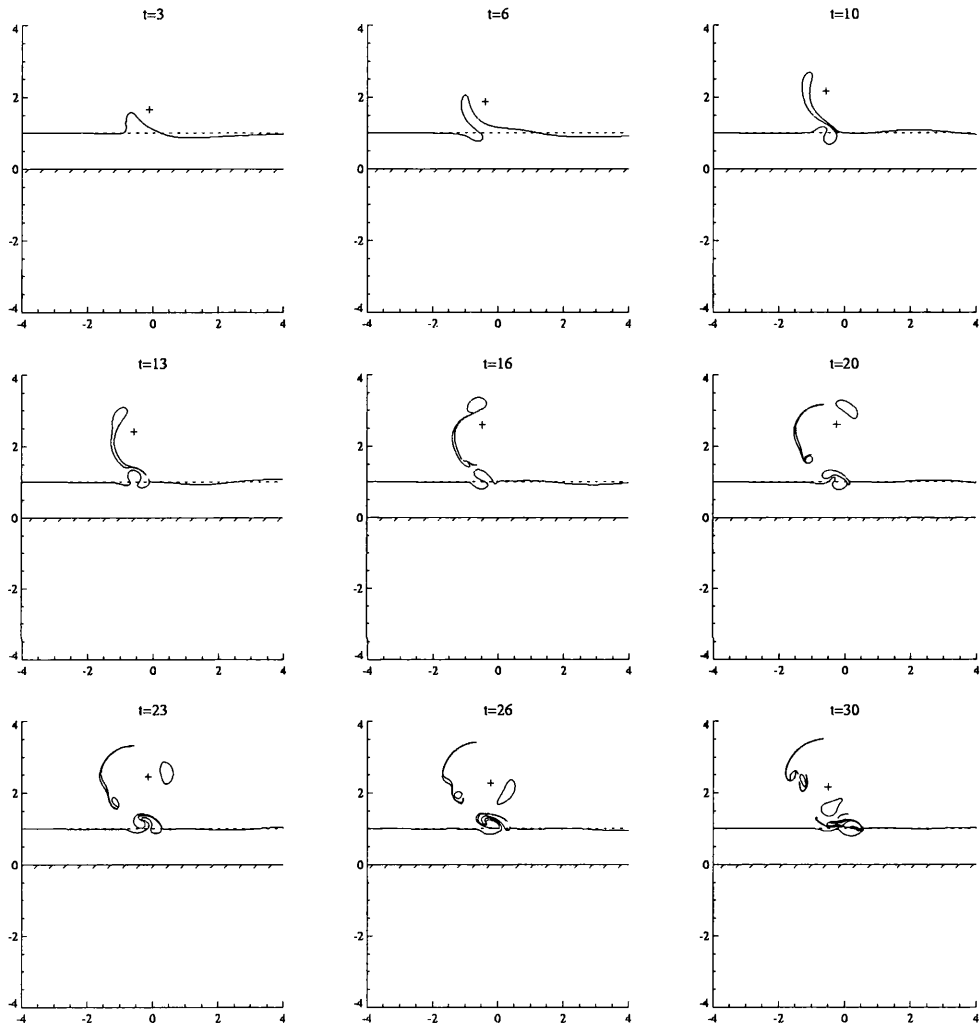
Figure 6.32: The evolution of the contour for a moderate off-shelf anticyclone. The parameter values used are $\S = 1$, $\Gamma = 1$, $W = 1$ and $L = 1.5$.

215
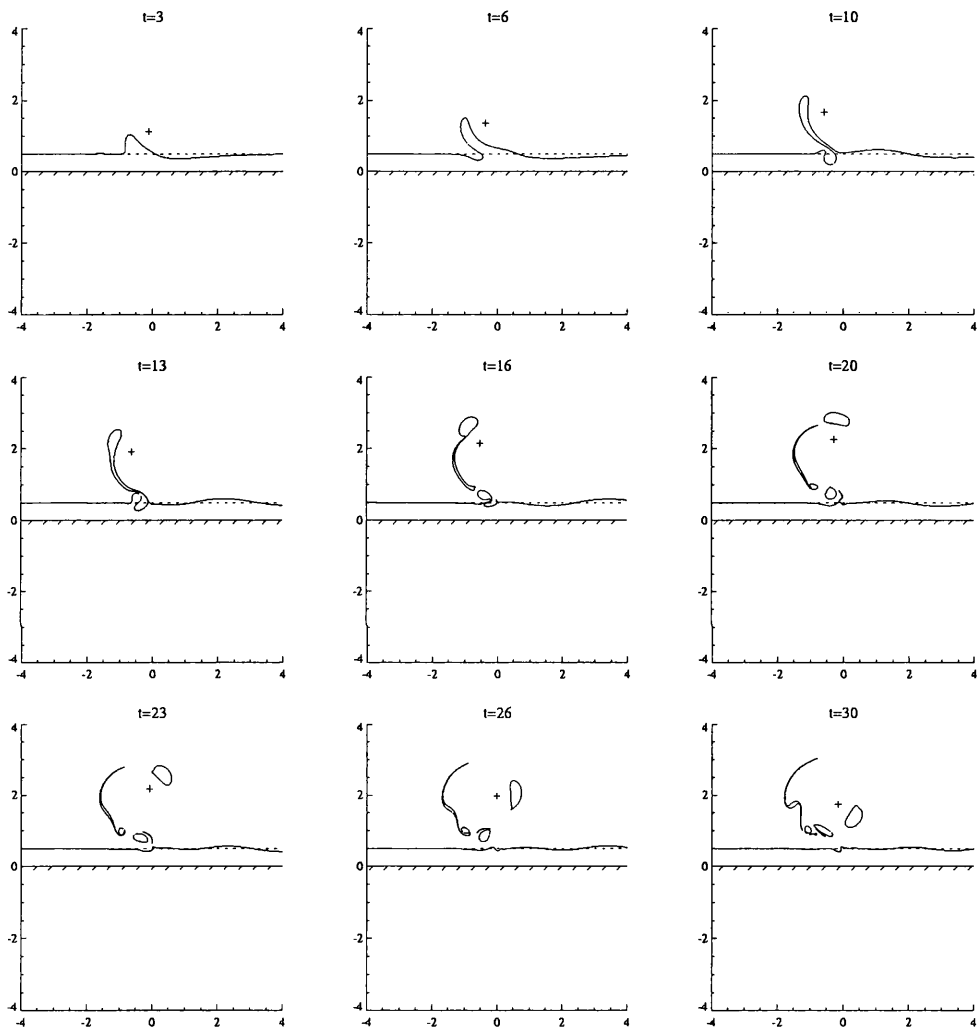
Figure 6.33: As for Figure (6.32) except $W = 0.5$ and $L = 1$.

216
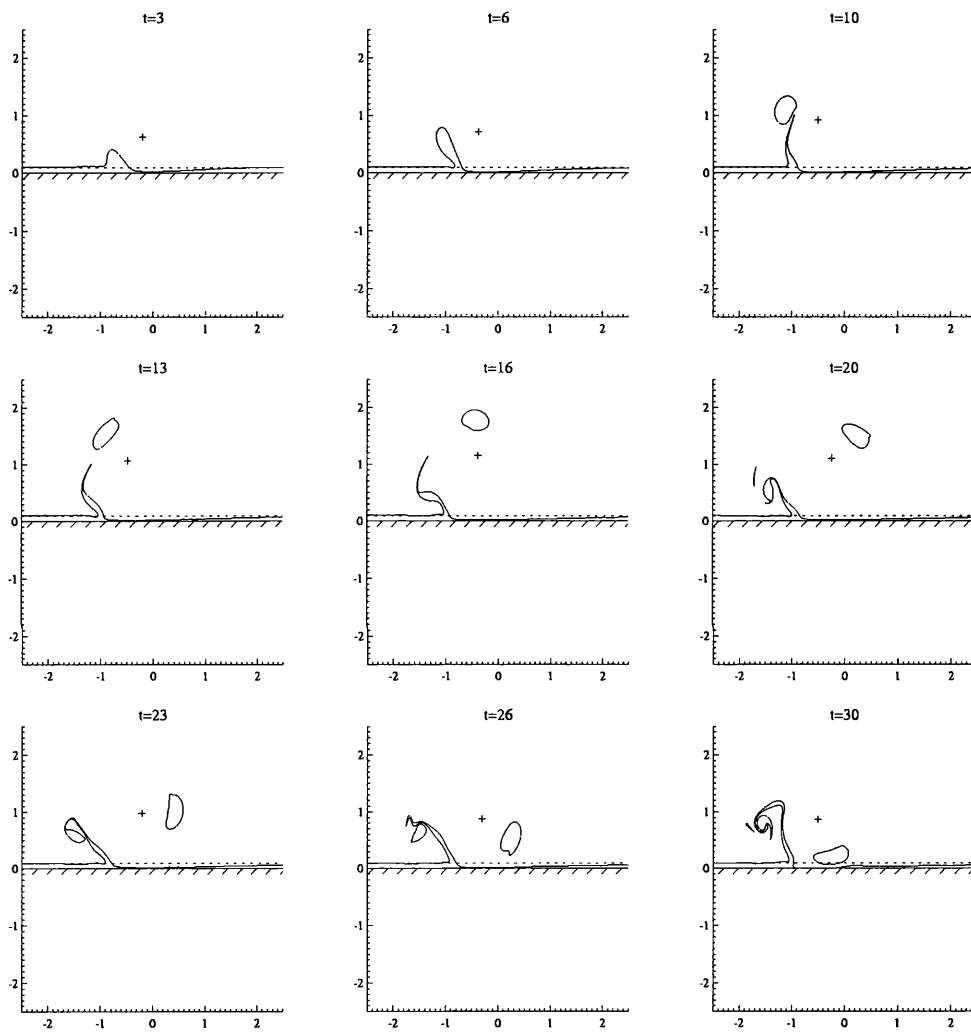
Figure 6.34: As for Figure (6.32) except $W = 0.1$ and $L = 0.6$.
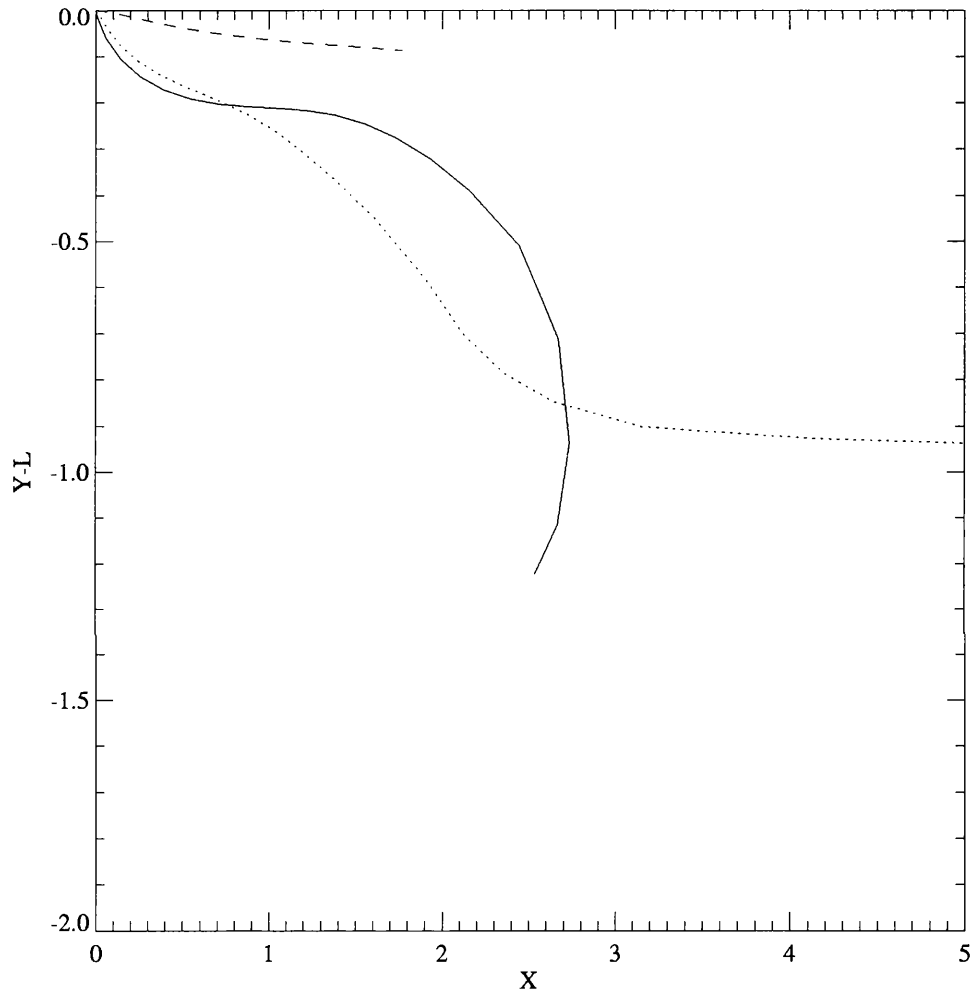
Figure 6.35: A plot of the trajectory of the vortex for various values of L and W for a moderate cyclone. The parameters used are $S = 1$ and $\Gamma = 1$ with $L - W = 0.5$ fixed. The curves are for $W = 1$, $L = 1.5$ (solid line), $W = 0.5$ and $L = 1$ (dotted line), $W = 0.1$ and $L = 0.6$ (dashed line). The times shown in these plots are $0 < t < 20$.
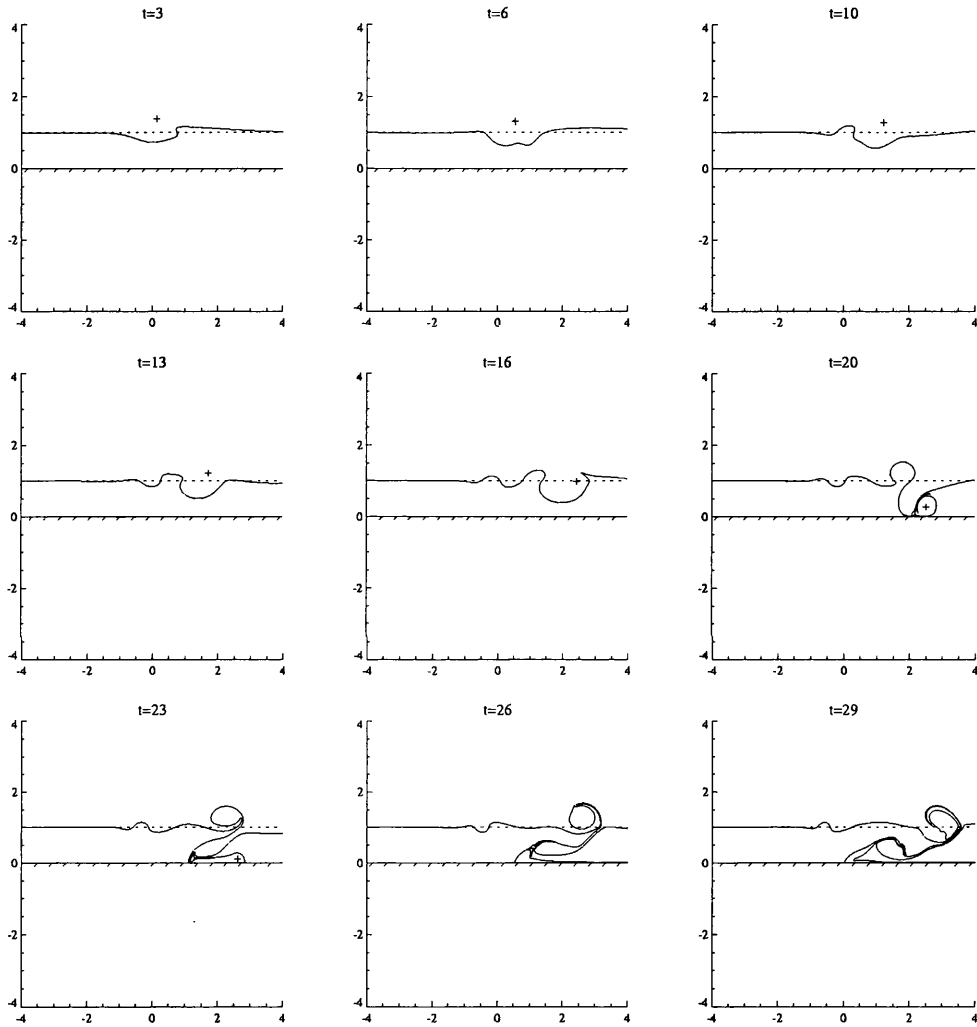
Figure 6.36: The evolution of the contour for a moderate off-shelf cyclone. The parameter values used are $S = 1$, $\Gamma = 1$, $W = 1$ and $L = 1.5$.
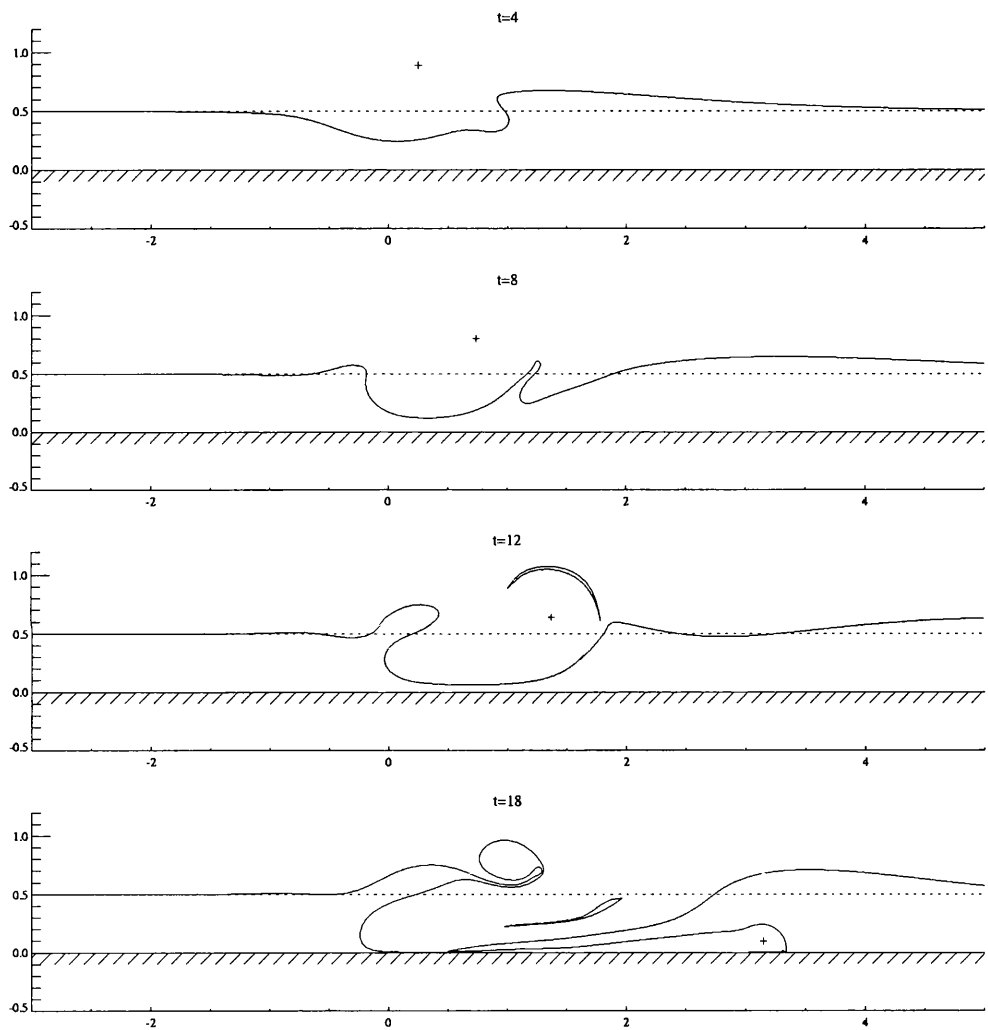
Figure 6.37: As for Figure (6.36) except $W = 0.5$ and $L = 1$.
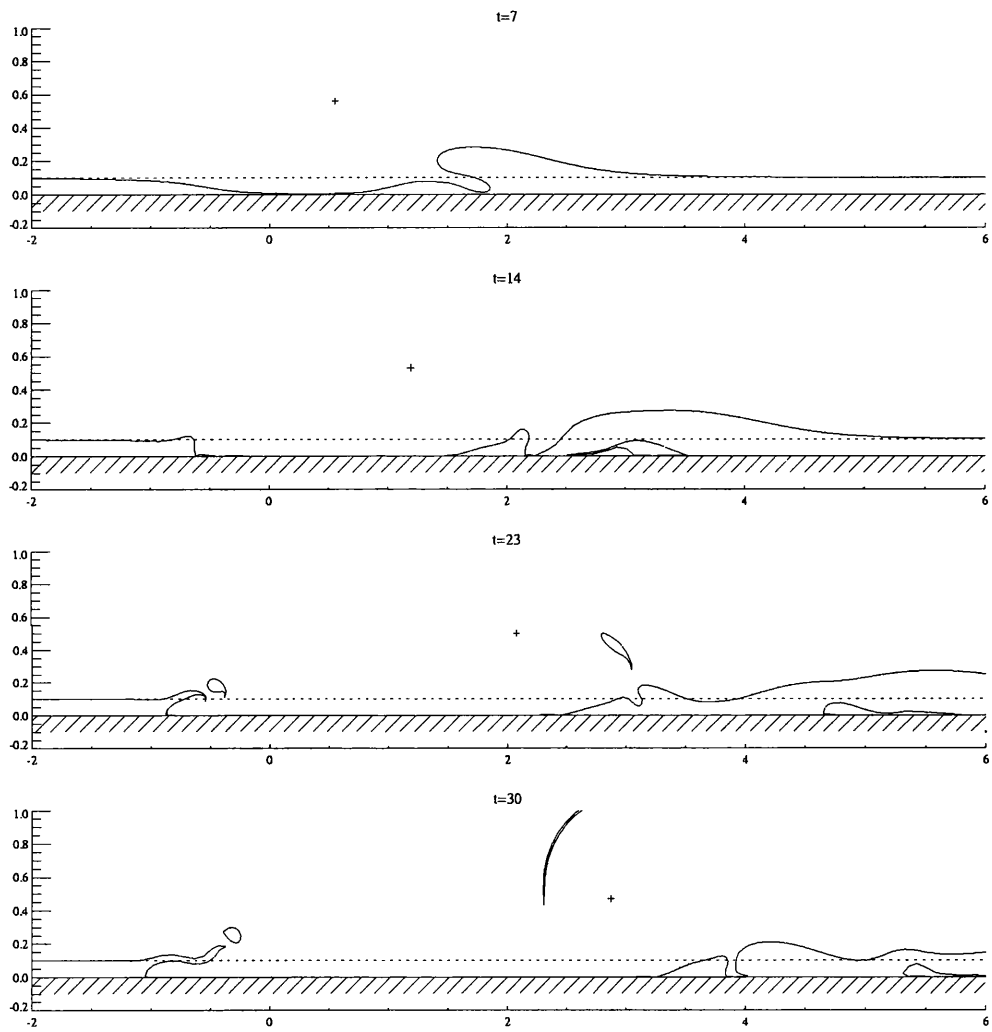
Figure 6.38: As for Figure (6.36) except $W = 0.1$ and $L = 0.6$.

6.4.2 An on shelf vortex

In this section results are presented for just one set of parameters for a moderate on shelf vortex. The case described is $W = 1$ and $L = 0.5$ and for the value $S = 0.1$. Figure (6.39) shows the trajectory of the vortex centres. The anticyclone initially moves northeast but then turns to move to the west. The cyclone rapidly approaches the wall where it comes under the influence of its image and it propagates rapidly to the west.

The contour evolution for an anticyclone is shown in Figure (6.40) and for a cyclone in Figure (6.41). The anticyclone pushes some of the fluid off the shelf, where it gains cyclonic relative vorticity. This then turns the anticyclone to the east, and resembles the pseudoimage. On the other hand the cyclone pulls fluid from the deep water on to the shelf where it gains anticyclonic relative vorticity. This then forces the primary cyclone towards the wall. The image dominates the motion at later times and the cyclone is carried to the west and away from the deflected contour.

6.5 Conclusions

A simple model of vortex motion near coastal topography has been studied for the full range of vortex intensities. Linear theory has been used to calculate the vortex drift velocity in the limit that the vortex is weak. In the intense and moderate vortex regimes some of the principle features of the motion have been identified in a contour dynamics study.

The main result from the linear theory is that, once again, the escarpment acts like a plane wall in the weak vortex limit. This is true for vortices located both on and off the shelf. Contour dynamics results confirm that linear theory describes well the motion for times larger than when it is formally applicable.

Although no theory has been presented for the intense vortex the key feature of the motion has been identified. The secondary circulations that arise due to the deflected contour compete with the influence of the image of the vortex. If the vortex is sufficiently far from the wall then the flow evolves as if the wall were not present. On the other hand if the vortex is sufficiently close to the wall then the vortex motion is dominated by the influence of the image and the secondary circulations only slightly modify the vortex drift. Both of these limits could be tackled analytically.
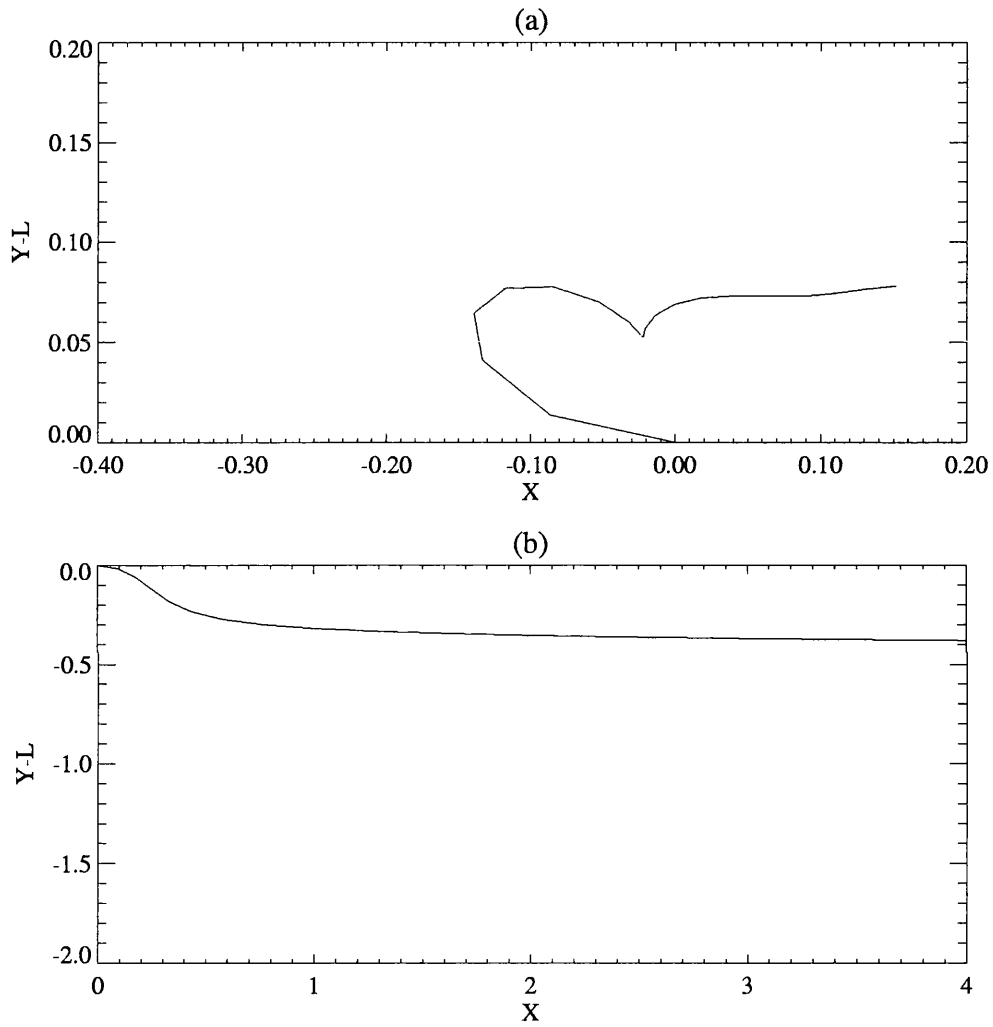
Figure 6.39: The trajectory of the vortex centre for an on shelf moderate intensity vortex. The parameter values used are $W = 1$, $L = 0.5$ and $S = 1$, for $0 < t < 20$. (a) is the trajectory for an anticyclone ($\Gamma = 1$) and (b) is the trajectory of a cyclone ($\Gamma = -1$)
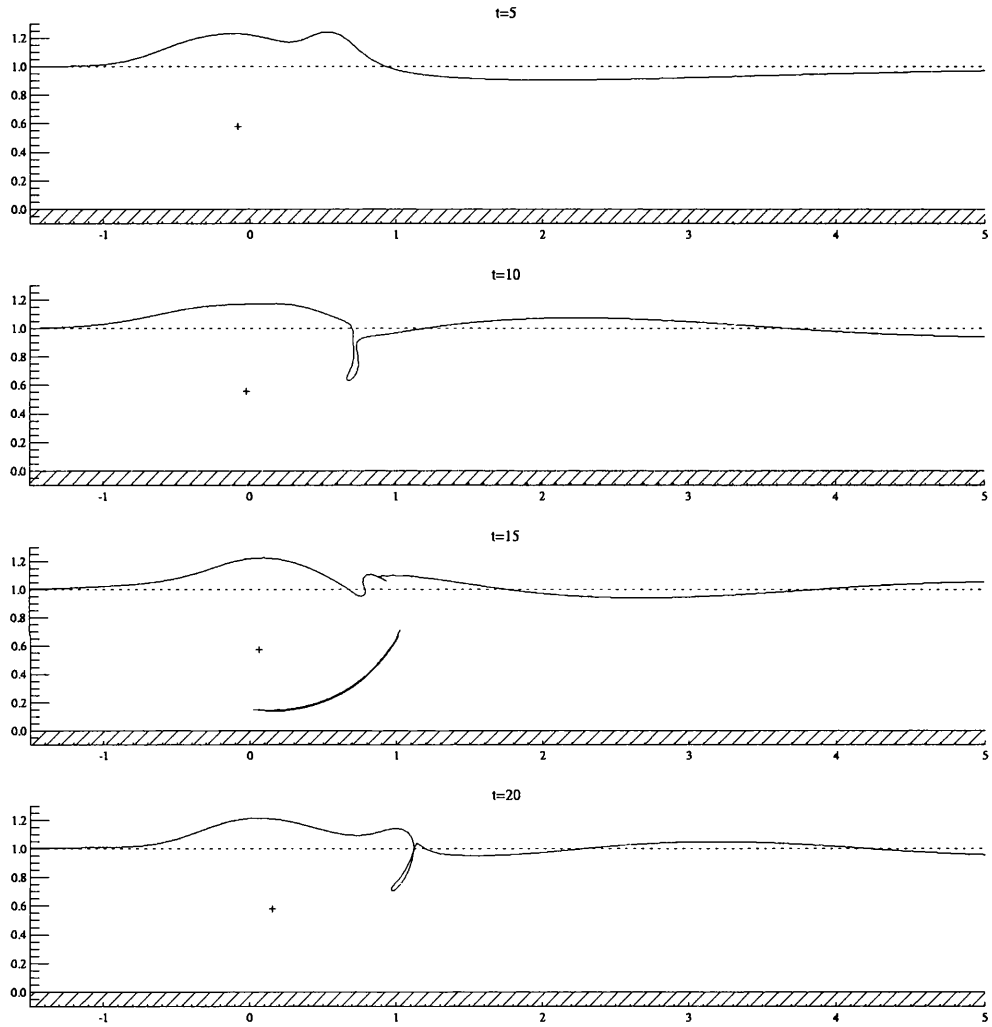
Figure 6.40: The evolution of the contour for a moderate on-shelf anticyclone. The parameter values used are $S = 0.1$, $\Gamma = 1$, $W = 1$ and $L = 0.5$.

224
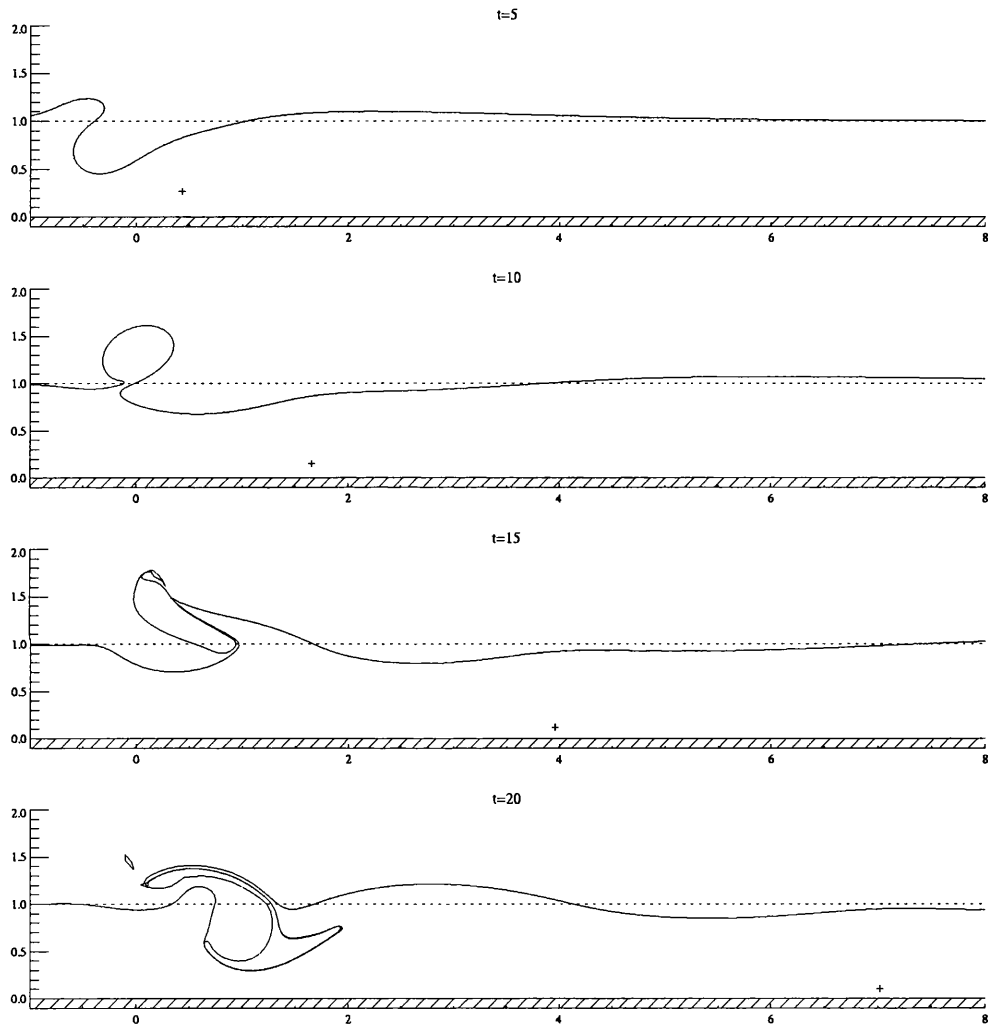
Figure 6.41: The evolution of the contour for a moderate on-shelf cyclone. The parameter values used are $S = 0.1$, $\Gamma = 1$, $W = 1$ and $L = 0.5$.

225

The interesting case is when the secondary circulations and the image have comparable influence on the vortex. This issue is not pursued here.

In the case of a moderate intensity vortex some results have also been presented. It appears that for moderate anticyclones located off the shelf the dipole formation witnessed in the previous two chapters is generic. The dipole moves away from the escarpment, the wall loses its influence and the vortex evolves as in Chapter 4. On the other had the initial dipole formation for the cyclone takes place, but the sense of the secondary circulation is such as to cause coastward motion of the cyclone. At later times the image of the cyclone takes over and the vortex moves far away from the influence of the deflected contour. For moderate intensity anticyclones located on the shelf the dipole formation is such as to compete with the image. For the parameter values shown here the anticyclone moves east at large times. On the other hand the dipole formation for the cyclone is such as to force the vortex closer to the influence of its image. The study of the moderate intensity vortices merits further consideration. Indeed, it should be emphasised that the study in this chapter is incomplete both numerically and analytically. A more extensive and quatitative study of the parameter space should be undertaken.

Appendix A: Derivation of the Fourier transform for a singular vortex pair in a channel.

Consider a singular vortex dipole, located in the middle of a channel of width $2W$, and where the walls are aligned along $y = \pm W$. The vortices have y-coordinates $\pm L$ and strengths $\pm \Gamma$ respectively. See Figure (6.42). The images of the vortices comprise an infinite set of vortices, with the same x-coordinate $X(t)$, and constant y-coordinates. The streamfunction for the flow is

$$\psi = \frac{\Gamma}{2\pi} \sum_{n=-\infty}^{\infty} \left(K_0(r_{n+}) - K_0(r_{n-}) \right), \tag{6.A1}$$

where

$$r_{n+}^2 = (x - X)^2 + (y - (2nW + L))^2, \tag{6.A2}$$

$$r_{n-}^2 = (x - X)^2 + (y - (2nW - L))^2. \tag{6.A3}$$

To obtain the Fourier transform of (6.A1) in the required form rewrite ψ as

$$\psi = \Psi + \Psi_{images}, \tag{6.A4}$$

where Ψ is the vortex pair given by (6.18), and

$$\Psi_{images} = \frac{\Gamma}{2\pi} \sum_{n=1}^{\infty} \left(K_0(r_{n1}) - K_0(r_{n2}) + K_0(r_{n3}) - K_0(r_{n4}) \right), \tag{6.A5}$$

226

$$\oplus \; y=4W+L$$
$$- y=4W$$
$$\ominus \; y=4W-L$$

$$\oplus \; y=2W+L$$
$$- y=2W$$
$$\ominus \; y=2W-L$$

$$///y=W$$

$$\oplus \; y=L$$
$$- y=0$$
$$\ominus \; y=-L$$

$$///y=-W$$

$$\oplus \; y=-2W+L$$
$$- y=-2W$$
$$\ominus \; y=-2W-L$$

$$\oplus \; y=-4W+L$$
$$- y=-4W$$
$$\ominus \; y=-4W-L$$
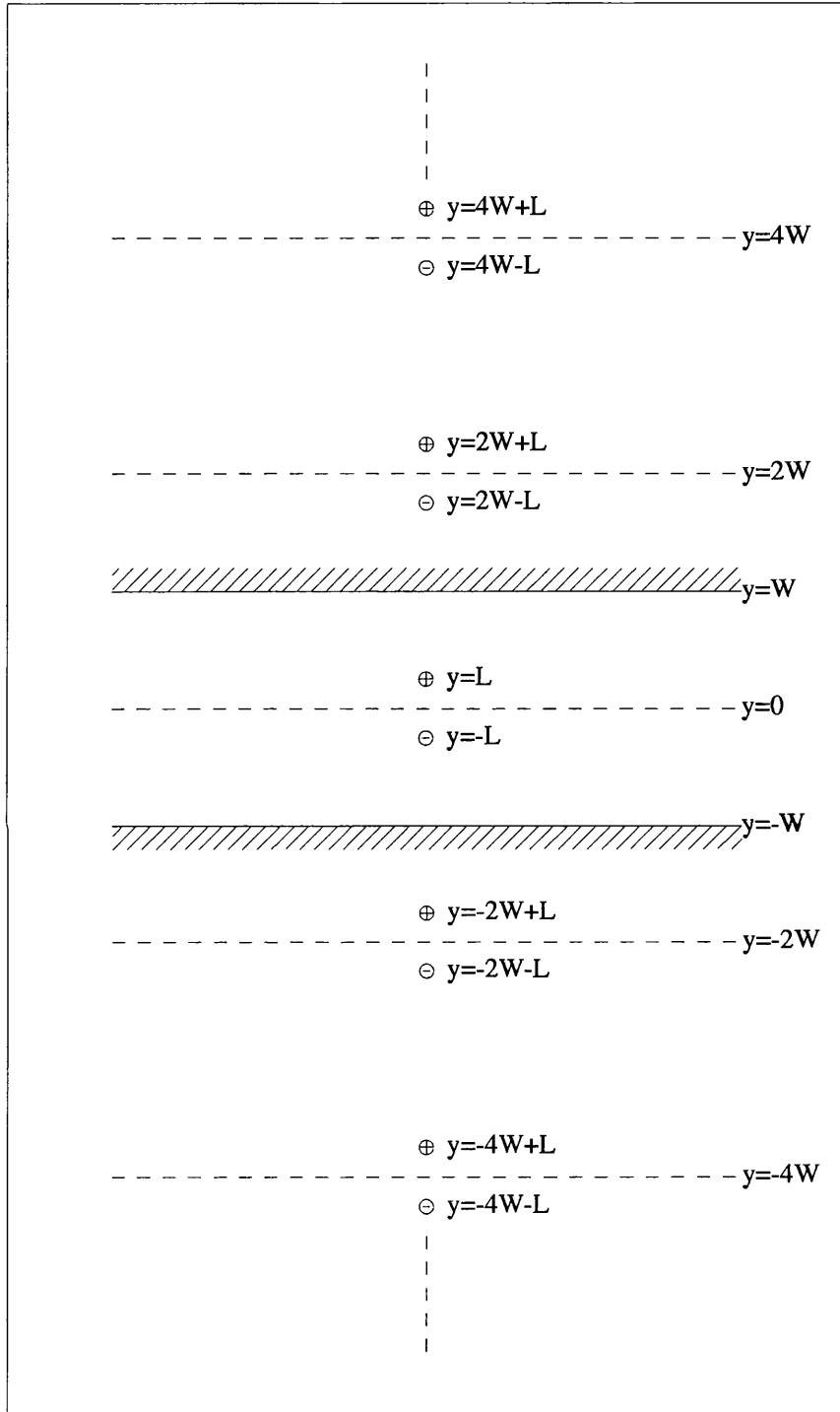
Figure 6.42: The system of images for a singular vortex pair in a channel of width $2W$.

is the system of images. Here

$$r_{n1}^2 = ((x-X)^2 + (y - (2nW + L))^2, \tag{6.A6}$$

$$r_{n2}^2 = ((x-X)^2 + (y - (2nW - L))^2, \tag{6.A7}$$

$$r_{n3}^2 = ((x-X)^2 + (y + (2nW - L))^2, \tag{6.A8}$$

$$r_{n4}^2 = ((x-X)^2 + (y + (2nW + L))^2. \tag{6.A9}$$

Making use of identity (4.26), the Fourier transform of the image term is

$$\hat{\Psi}_{images} = \frac{\Gamma}{2\sqrt{k^2+1}} e^{-ikX} \sum_{n=1}^{\infty} \left(e^{-|(y-(2nW+L)|\sqrt{k^2+1}} - e^{-|y-(2nW-L)|\sqrt{k^2+1}} \right. \tag{6.A10}$$

$$\left. + e^{-|y+(2nW-L)|\sqrt{k^2+1}} - e^{-|y+(2nW+L)|\sqrt{k^2+1}} \right). \tag{6.A11}$$

In the weak coastward vortex problem the transform is required for $y < W$ for which

$$-|y - (2nW \pm L)| = y - (2nW \pm L). \tag{6.A12}$$

It is straightforward to show that the Fourier transform of the image term can then be rewritten,

$$\hat{\Psi}_{images} = \frac{\Gamma}{2\sqrt{k^2+1}} \left(e^{(y-L)\sqrt{k^2+1}} - e^{(y+L)\sqrt{k^2+1}} + e^{(-y+L)\sqrt{k^2+1}} - e^{(-y-L)\sqrt{k^2+1}} \right)$$

$$\times e^{-ikX} \sum_{n=1}^{\infty} e^{-2nW\sqrt{k^2+1}} \tag{6.A13}$$

The term in brackets is

$$2\cosh(y-L)\sqrt{k^2+1} - 2\cosh(y+L)\sqrt{k^2+1} = 4\sinh y\sqrt{k^2+1}\sinh L\sqrt{k^2+1} \tag{6.A14}$$

Moreover, note that

$$\frac{1}{\sinh\eta} = \frac{2}{e^\eta - e^{-\eta}} = \frac{2e^{-\eta}}{1 - e^{-2\eta}} = 2e^{-\eta} \sum_{n=0}^{\infty} e^{-2n\eta} \tag{6.A15}$$

by the Binomial Theorem. Hence

$$\sum_{n=1}^{\infty} e^{-2n\eta} = \frac{1}{1 - e^{-2\eta}} - 1 = \frac{e^{-\eta}}{2\sinh\eta}. \tag{6.A16}$$

Use of (6.A14) and (6.A16), with $\eta = W\sqrt{k^2+1}$ in (6.A13) leads to

$$\hat{\Psi}_{images} = -\frac{\Gamma}{\sqrt{k^2+1}} \frac{\sinh y\sqrt{k^2+1}\sinh L\sqrt{k^2+1}}{\sinh W\sqrt{k^2+1}} e^{-W\sqrt{k^2+1}} e^{-ikX}. \tag{6.A17}$$

This term is even in k so finally, for $0 < y < W$,

$$\Psi_{images} = -\frac{\Gamma}{2\pi} \int_0^\infty \frac{e^{-W\sqrt{k^2+1}}}{\sqrt{k^2+1}} \frac{\sinh L\sqrt{k^2+1}}{\sinh W\sqrt{k^2+1}} \sinh y\sqrt{k^2+1}\cos k(x-X)\, dk, \tag{6.A18}$$

which is the coastward term in equation (6.51) with $X = \epsilon u\tau$.

Chapter 7

Conclusions

Several models of the interaction of a vortex with a topographic escarpment have been studied. The models are simplistic approximations to real geophysical vortices. Nonetheless it is anticipated that these models could offer insights into vortex behaviour in more realistic situations.

One the most important tenets of this thesis is the concept of the pseudoimage for weak vortices. In all cases studied here the linear theory for a weak vortex predicted that the escarpment will act as a plane wall. The pseudoimage description is very robust and in all of the cases studied contour dynamics solutions to the nonlinear equations show that the pseudoimage describes the vortex motion well for many eddy turnover times, i.e. well beyond the formal time for which linear theory is valid. It is expected that the pseudoimage description will be useful in other weak vortex interactions with sharp potential vorticity gradients. For example the study of a vortex near a seamount might begin with the image of a vortex in a cylinder to predict the motion. Stern and Flierl (1987) and Bell (1989) have noted the pseudoimage effect previously for a singular vortex moving near a potential vorticity interface. The phenomenon seems to be generic in weak vortex interactions with potential vorticity gradients and so it seems apt to name it the "pseudoimage", as has been done throughout this thesis. It should be noted that the pseudoimage concept is unique to problems involving discontinuous potential vorticity gradient. On the β-plane a weak vortex decays rapidly due to Rossby wave radiation. A weak vortex travelling parallel to an escarpment is a relatively long lived structure. Indeed vortices travelling in the opposite direction to the topographic waves will continue to do so until they meet another obstacle.

The pseudoimage also presents an interesting question in relation to the initialisation of vortex-

escarpment interactions. In the f-plane models presented in this thesis, the initial condition is the presence of a vortex near un undeflected topographic contour. However a more physical situation is that of a vortex approaching an escaprment from infinity. If the vortex moves towards the escarpment on a time scale which is much slower the both the eddy-turnover time and the topographic wave time, then the contour will adjust to the pseudoimage whatever the strength of the vortex. It would be informative to investigate the range of values of the vortex strength for which this adjustment is stable, i.e. to seek equilibria of vortex shape and topographic contour adjustment, and assess the stability of such solutions.

In addition the contour dynamics results for the interaction of moderate vortices with sharp topography indicates that dipole formation may be a generic feature of the motion, and in keeping with the work of Zavala Sanson *et al* (1999) described previously. This process is not unique to discontinuous background potential vorticity gradients, having been rather well described for moderate β-plane vortices by Lam and Dritschel (1998). It appears that dipole formation for moderate intensity vortices is the primary source of motion perpendicular to the gradient of potential vorticity. If this is a sharp gradient then the possibility arises that the vortex can cross the discontinuity and interact strongly with it, or else move away from the discontinuity as a dipole.

Further work in this area is plentiful. Recent studies of vortex motion on a multilayer β-plane have indicated that the vertical structure of the vortex has important consequences on its evolution (see e.g. Sutyrin and Morel (1997)). It is believed that the Agulhas rings have a barotropic and a baroclinic component, so a more realistic model should take the effects of stratification into account. A good starting point would be a contour dynamics investigation of the motion of a heton (see Hogg and Stommel (1985)) near an escarpment. Modification of the quasigeostrophic contour dynamics scheme is straightforward for a 2-layer fluid and its implication is outlined in Davey *et. al.* (1993)

The quasigeostrophic assumption made throughout this thesis requires both Ro and the amplitude of the interfacial disturbance compared to the layer depth to be small parameters. It is the latter assumption that is too restrictive. For example, as mentioned in Chapter 3, an Agulhas Ring has $Ro \approx 0.1$, but they can undergo interfacial disturbances which is of the same order of magnitude as the layer depth. Furthermore, there are regions in the ocean where the variation in topography is large enough to invalidate quasigeostrophic theory. For example the Walvis Ridge, which is known to greatly affect the trajectories of Agulhas Rings, and which lies in the southern Atlantic off the

east coast of Africa, rises up to 2000 km above the abyssal plain at 4000 km depth. Also, coastal surf zone vortices have large Rossby number and large topographic variations over the range of lengthscales of interest. Relaxing the quasigeostrophic assumption is of importance in developing a study of the interaction of vortices with topographic gradients.

The contour advective semi-Lagrangian algorithm of Dritschel and Ambaum (1998) is suited to a non-quasigeostrophic study. A barotropic, non-divergent (i.e. rigid lid) scheme also allows for both arbitrary Rossby number and O(1) variations in topography. However, for the barotropic, non divergent flow, Ro and δ can not be combined into a single parameter S as in the present problem. Hence the dependence of the vortex dynamics on both the Rossby number and the height of the topography needs to be investigated to cover the whole parameter space. More realistic topography could also be considered. For example, an exponentially varying shelf abutting a flat ocean, where the step height could be O(1) is a better model of a continental shelf than the quasigeostrophic model presented in Chapter 6. Also the effect of varing Ro and the topographic gradient over a linearly sloping bottom, could also be investigated.

It would also be desirable to use a shallow water code to investigate the effect of vortex stretching, absent in the non-divergent model, on the dynamics of vortices. A comparison with the non-divergent case is of interest. Finally a multi-layer shallow water code could be used to investigate the effects of vertical structure on the motion of the vortex.

Acknowledgements

Bibliography

Akylas, T.R. On the excitation of long nonlinear water waves by a moving pressure distribution. *J.Fluid Mech.*, 141:455–466, 1984.

Ambramowitz, M and Stegun, I.A. (eds). *Handbook of mathematical functions.* Dover, 1972.

Aref, H. Motion of three vortices. *Phys. Fluids*, 22:393–400, 1979.

Aref, H. Integrable, chaotic and turbulent vortex motion in two-dimensional flows. *Ann.Rev.Fluid.Mech.*, 15:345–89, 1983.

Aref, H. and Pomphrey, N. Integrable and chaotic motions of four vortices. I.the case of identical vortices. *Proc.R.Soc.Lond.*, 380:359–387, 1982.

Aref, H., Kadtke, J.B, Zawadski, I. *et. al.* Point vortex dynamics:recent results and open problems. *Fluid.Dyn.Res.*, 3:63–74, 1988.

Aref, H., Rott, N. and Thomann,H. Grobli's solution of the three vortex problem. *Ann. Rev. Flu. Mech.*, 24:1–20, 1992.

Batchelor, G.K. *Introduction to Fluid Dynamics.* Cam. Univ. Press, 1967.

Bell, G.I. Interaction between vortices and waves in a simple model of geophysical flow. *Phys.Fluid.A*, 2:575–586, 1989.

Bender, C.M. and Orszag, S.A. *Advanced mathematical methods for scientists and engineers.* McGraw-Hill, 1978.

Davey, M.K., Hurst, R.G.A. and Johnson, E.R. Topographic eddies in multilayer flow. *Dyn. Atmos. Ocean.*, 18:1–27, 1993.

233

Davis, C. S., and P. H. Weibe. Macrozooplankton biomass in a warm-core ring: Time series changes in size structure, taxonomic caomposition, and vertical distribution. *J. Geophys. Res.*, 90:8871–8884, 1985.

Dritschel, D.G. The stability and energetics of corotating uniform vortices. *J. Fluid Mech.*, 157: 95–134, 1985.

Dritschel, D.G. Contour surgery: a topological reconnection scheme for extended integrations using contour dynamics. *J. Comput. Phys.*, 77:240–266, 1988.

Dritschel, D.G. and Ambaum, M.H.P. A contour-advective semi-lagrangian numerical algorithm for simulating fine-scale conservative dynamical fields. *Q.J.R. Met. Soc.*, 123:1097–1130, 1998.

Eckhardt, B. and Aref, H. Integrable and chaotic motions of four vortices.II.collision dynamics of vortex pairs. *Phil.Trans.R.Soc.Lond.*, 326:655–696, 1988.

Fiorino, M. and Elsberry, R.L. Some aspects of vortex structure related to tropical cyclone motion. *J. Atmos. Sci.*, 46:975–990, 1989.

Firing, E and Beardsley, R. The behaviour of a barotropic eddy on a β-plane. *J. Phys. Ocean.*, 6: 57–65, 1976.

Flierl, G.R. The application of linear quasi-geostrophic dynamics to gulf stream rings. *J. Phys. Oceanogr.*, 7:365–379, 1977.

Flierl, G.R. Rossby wave radiation from a strongly nonlinear warm eddy. *J. Phys. Ocean.*, 14:47–58, 1984.

Gill, A.E. *Atmosphere-Ocean Dynamics.* Academic Press, 1982.

Gradshteyn, I.S. and Rhyzik, I.M. *Tables of Integrals Series and Products.* Academic Press, 1980.

Helmholtz, H. On integrals of the hydrodynamical equations which express vortex-motion. *Phil.Mag.*, 33:485–512, 1867.
(translation by P.G.Tait of a paper of 1858).

Herman, A.J. and Rhines, P.B. and Johnson, E.R. Nonlinear Rossby adjustment in a channel:beyond Kelvin waves. *J. Fluid Mech.*, 205:469–502, 1989.

Hide, R. Origin of Jupiter's Great Red Spot. *Nature*, 190:895–896, 1961.

Hogg, N. and Stommel, H. The heton: an elementary interaction between discrete barolclinic geostrophic vortices, and it implications concerning eddy heat-flow. *Proc. Roy. Soc. A*, 397:1–20, 1985.

Johnson, E.R. Starting flow for an obstacle moving transversely in a rapidly rotating fluid. *J. Fluid Mech.*, 149:71–89, 1984.

Johnson, E.R. and Davey, M.K. Free-surface adjustment and topographic waves in coastal currents. *J. Fluid Mech.*, 219:273–289, 1990.

Katok, A. and Hasselblatt,B. *Introduction to the modern theory of dynamical systems.* Cambridge University Press, 1995.

Lam, J.S-L. and Dritschel, D.G. On the beta-drift of an initially circular vortex patch. *J. Fluid Mech.*, (submitted), 1998.

Lamb, H. *Hydrodynamics.* Dover, 6th edition, 1945.

Lighthill, Sir M.J. *Waves in fluids.* Cambridge Unversity Press, 1974.

Longuet-Higgins, M.S. On the trapping of waves along a discontinuity of depth in a rotating ocean. *J. Fluid. Mech.*, 31:417–434, 1968.

McDonald, N.R. Topographic dispersal of bottom water. *J. Phys. Ocean.*, 23:954–969, 1992.

McDonald, N.R. Topographic wave radiation and modon decay. *Geophys. Astrophys. Fluid Dynamics*, 83:51–77, 1996.

McDonald, N.R. Motion of an intense vortex near topography. *J.Fluid Mech.*, 367:359–377, 1998.

McDonald, N.R. The motion of geophysical vortices. *Phil. Trans. Roy. Soc.*, (to appear), 1999.

McDonald, N.R. and Dunn, D.C. Some interactions of a vortex with a seamount. *Il Nuovo Cimento*, (to appear), 1999.

McIntyre, M.E. On the wave momentum myth. *J. Fluid Mech.*, 106:331–347, 1981.

McIntyre, M.E. The stratospheric polar vortex and sub-vortex: fluid dynamics and mid-latitude ozone loss. *Phil. Trans. Roy. Soc. London*, 352:227–240, 1995.

McWilliams, J.C. and Flierl, G.R. On the evolution of isolated, nonlinear vortices. *J. Phys. Oceanogr.*, 9:1155–1182, 1979.

Meleshko, V.V. et al. Advection of a vortex pair atmosphere in a velocity field of point vortices. *Phys. Fluids A*, 4:2779–2797, 1992.

Meleshko, V.V. and van Heijst, G.J.F. On Chaplygin's investigations of two-dimensional vortex structures in an inviscid fluid. *J.Fluid Mech.*, 272:157–82, 1994.

Mied, R.SP. and Lindeman, G.J. The propagation and evolution of cyclonic gulf stream rings. *J. Phys. Oceanogr.*, 9:1183–1206, 1979.

Morikawa, G.K. Geostrophic vortex motion. *J.Meteorol.*, 17:148–54, 1960.

Morikawa, G.K. and Swenson, E.V. Interacting motion of rectilinear geostrophic vortices. *Phys.Fluids*, 14:1058–67, 1973.

Nof, D. Modons and monopoles on a γ-plane. *Geophys.Astrophys.Fluid Dyn.*, 52:71–87, 1990.

Ottino, J.M. Mixing, chaotic advection and turbulence. *Ann.Rev.Fluid Mech.*, 22:207–53, 1990.

Pedlosky, J. *Geophysical Fluid Dynamics*. Springer, 1979.

Pierrhumbert, R.T. A family of steady, translating vortex pairs with distributed vorticity. *J. Fluid Mech.*, 99:129–144, 1980.

Reznik, G.M. Dynamics of singular vortices on a beta-plane. *J.Fluid Mech.*, 240:405–432, 1992.

Reznik, G.M. and Dewar, W.K. An analytical theory of distributed axisymmetric barotropic vortices on the β-plane. *J.Fluid Mech.*, 269:301–322, 1994.

Reznik,G.M. and Grimshaw, R. On the long term evolution of an intense localised divergent vortex on the β-plane. *J.Fluid Mech.*, (Submitted), 1998.

Rossby, C.G., *et al.* Relation between variations in the intensity of the zonal circulation of the atmosphere and the displacements of the semi-permanent centers of action. *J. Marine Res.*, 2: 38–55, 1939.

Rott, N. Constrained three and four vortex problems. *Phys.Fluids A*, 2:1477–1480, 1990.

Salmon, R. Practical use of Hamilton's principle. *J.Fluid Mech.*, 132:431–444, 1983.

Spiegel, M. *Theory and Problems of Theoretical mechanics*. McGraw-Hill, 1967.

Stern, M.E. and Flierl, G.R. On the interaction of a vortex with a shear flow. *J.Geo.Res.*, 92: 10733–10744, 1987.

Sutyrin, G.G. and Flierl, G.R. Intense vortex motion on the beta plane: development of the beta gyres. *J. Atmos. Sci.*, 51:773–790, 1994.

Sutyrin, G.G. and Morel, Y.G. Intense vortex motion in a stratified fluid on the beta-plane: an analytical theory and its validation. *J. Fluid Mech.*, 336:203–220, 1997.

Sutyrin, G.G., Hesthaven, J.S., Lynov, J.P. and Rasmussen, J.J. Dynamical properties of vortical structures on the beta-plane. *J. Fluid Mech.*, 268:103–131, 1994.

Taylor, G.I. Experiments on the motion of solid bodies in rotating fluids. *Proc. Roy. Soc. Lond.*, A 104:213–218, 1923.

Thomson, Sir W. On the motion of vortex atoms. *Proc.R.Soc.Edin.*, 6:94–105, 1867.

Velasco Fuentes, O.U. Propagation and transport properties of dipolar vortices on a γ -plane. *Phys.Fluids*, 6:3341–3352, 1867.

Velasco Fuentes, O.U. and van Heijst, G.J.F. Experimental study of dipolar vortices on a topotgraphic β -plane. *J.Fluid Mech.*, 259:79–106, 1994.

Velasco Fuentes, O.U., van Heijst, G.J.F. and Cremers, B.E. Chaotic advection by dipolar vortices on a β -plane. *J.Fluid Mech.*, 291:139–61, 1995.

Velasco Fuentes, O.U.,van Heist, G.J.F. and van Lipzig, N.P.M.,. Unsteady behaviour of a topography modulated tripole. *J.Fluid Mech.*, 307:11–41, 1996.

Whitham, G.B. *Linear and nonlinear waves.* Wiley, 1974.

Wiggins, S. *Chaotic Transport in Dynamical Systems.* Springer, 1992.

Zabusky, N.J. and McWilliams, J.C. A modulated point-vortex model for geostrophic, β -plane dynamics. *Phys.Fluids*, 25:2175–2182, 1982.

Zavala Sanson, I., van Heijst, G.J.F and Doorschoot, J.J.J. Reflection of barotropic vortices from a step-like topography. *Il Nuovo Cimento*, (submitted), 1999.